POLYELECTROLYTE COMPLEXES: THE EFFECTS OF CHARGE DISTRIBUTION AND CHARGE DENSITY

BY

DERRICK E. HASTINGS, B.Sc.

A THESIS SUBMITTED TO THE SCHOOL OF GRADUATE STUDIES OF MCMASTER UNIVERSITY IN PARTIAL FULFILMENT OF THE REQUIREMENTS FOR THE DEGREE OF DOCTOR OF PHILOSOPHY IN CHEMISTRY

Doctor of Philosophy, Chemistry

McMaster University, Hamilton, Ontario, Canada

Title:	Polyelectrolyte Complexes: The Effects of Charge Distribution and Charge Density
Author:	Derrick E. Hastings, B.Sc. (McMaster University)
Supervisor:	Professor Harald D. H. Stöver
Number of Pages:	XXVI, 304

Abstract

Polyelectrolytes are widely used as components in biomaterial applications. This thesis focuses on the design, synthesis, and investigation of polyelectrolyte complexes and their respective properties based on charge arrangement and charge density. The tunability of ionic interactions in polyelectrolyte complexes was then demonstrated in applications including alginate-based polyelectrolyte complexation for microcapsules and in strong polyampholyte hydrogels.

Polyelectrolytes comprising methacrylic acid (MAA) and *N*-(3-aminopropyl)methacrylamide hydrochloride (APM) in different ratios were prepared and used to explore the interactions of different single- and multicomponent PECs with different charge arrangements using turbidimetric/potentiometric titration, UV-vis spectroscopy, microscopy, and isothermal titration calorimetry. The complexes were shown to have isoelectric points (pH(*I*)) at which macroscopic phase separation is induced that are highly dependent on the polymer composition as well polymer mixing ratio for multi-component PECs. Additionally, these complexes have sensitivity to [NaCl] shielding effects that are dependent on charge separation, improving with charge compensation and shifting from solid precipitates to liquid coacervates in strong complexes. The PECs exhibit cloud point temperatures indicative of lower critical solution temperature behaviours. These polyelectrolytes were then used to bind model ionic dyes and were crosslinked using naturally occurring genipin, indicating their potential as drug delivery materials.

The system of MAA-APM polyelectrolytes was further explored as betaines were introduced to the individual polymers for three distinct coacervates: charge-balanced polyampholytes, pairs of complementary, nonstoichiometric polyampholytes, and pairs of pure polyanion-polycations. 2-methacryloyloxyethyl phosphorylcholine (MPC) was introduced into the different polyelectrolytes and drastically increased the responsiveness of complexes to pH, [NaCl], and temperature. MPC notably enhances complex hydration in single-component polyampholyte coacervates, while complex coacervates are less effectively destabilized with greater coacervate stability by charge separation.

The exploration of structure-property relationships in polyelectrolytes was then extended to alginate-based complexation for applications in cell encapsulation, as compositional distribution and charge dilution influence the formation and stability of the complexed polyanion-polycation surface coatings. A semi-batch approach was employed to limit compositional variability in the copolymerization of APM and MPC. Different copolymers were then explored as potential low-fouling, cationic shell formers capable of covalent crosslinking with different reagents, including naturally occurring genipin. The crosslinked capsules show good mechanical and low protein adsorption.

Finally, the underlying principles of charge density effects were demonstrated in strong polyampholyte hydrogels. Using a styrenic system of charged monomers, a near-alternating copolymerization was achieved and generated physical hydrogels with stimuli-responsive properties and high mechanical strength. Both the physical and mechanical properties are highly dependent on monomer loading during gel preparation. To tune the hydrogel properties, charge-neutral termonomers were incorporated to reduce charge

density but show that termonomer selection has significant impacts on the responsive and mechanical properties. These polyampholyte hydrogels appear capable of stimuli-responsive self-healing.

Acknowledgements

First and foremost, I would like to express my deepest gratitude to my supervisor Prof. Harald Stöver for the chance to contribute to such interesting work with the guidance, support, and trust of an exemplary mentor. I was lucky enough to meet Dr. Stöver in 2012, at which time the research in the Department of Chemistry and Chemical Biology caught my interest. This greatly swayed my decision both to pursue a Bachelor's degree in chemistry at McMaster and to join his group years later. His enthusiasm, optimism, and patience as a supervisor made for a wonderful experience during my graduate studies, allowing me to explore my own interests and set my own goals. My development as a researcher would not have been as successful nor as enjoyable were it not for Dr. Stöver, and I am thankful to have had the opportunity to be part of his research legacy.

I would also like to thank my group members (past and present) Jing Zhao, Alison Stewart, Samantha Ros, Mitchell Johnson, and Sheilan Sinjari as well as former undergraduate students Aleks Redžić and Sean Curtis for their help and support during my studies. Thank you to Nick Burke for his expertise and insight in nearly every area of polymer chemistry. Also, thank you to Carl Ellis, who was pivotal in the repair and resurrection of lab equipment, without which I would not be able to complete my research. Collectively, the expertise of my group members was incredibly beneficial in overcoming various challenges through the years. Thank you also to Cody Gale, Rob Bui, Nick Serniuck, and my fellow department members for their companionship.

I would like to give special thanks to my research committee members, Dr. Todd Hoare and Dr. Ryan Wylie for their helpful feedback and guidance throughout my work. A

special thank you to Dr. José Bozelli Jr. and Dr. Richard Epand for a wonderfully positive collaboration and for the chance to expand our understanding of the systems in our lab. I am also grateful for the assistance of Dr. Bob Berno and Dr. Hilary Jenkins in the NMR facility as their expertise and patience were crucial to our group's investigations. Thank you to Heera Marway and Dr. Michael Thompson for their guidance in mechanical testing and the use of their facilities. I would like to also thank the Department of Chemistry and Chemical Biology, including the administrative staff and the faculty of the department, for both an enjoyable undergraduate and graduate school experience. Although in-person interactions were limited for a portion of my graduate studies, I cannot thank everyone enough for making my time in the department as simple as possible.

Finally, this work is dedicated to my parents, Dave and Kim Hastings, who have been pillars in my life and were an unwavering source of encouragement, comfort, love, and support throughout my education. Thank you also to my brothers, Tyler and Carter, for being two of my best friends growing up, for regularly teaching me things I could not have learned in school, and for being there to make my time away from work enjoyable. I would like to give special thanks to Bob Hastings, for all the guidance and support that made my education possible. Last, but not least, this endeavour would not be possible if not for Libby Furtado and the never-ending care, encouragement, and optimism that she provided throughout and beyond the duration of my studies. Thank you, also, to the Furtado family for their support and to my best buddy Louie for being there whenever I needed a hug or a smile. Words cannot express fully my gratitude for everyone who helped me on my journey.

TABLE OF CONTENTS

List of Abbreviations and Symbols

Acrif.	Acriflavine
APM	*N*-(3-aminopropyl)methacrylamide hydrochloride
APS	Ammonium persulfate
BBG	Brilliant Blue G
BSA	Bovine serum albumin
CPT	Cloud point temperature
CTA	Chain transfer agent
$Đ$	Polydispersity
D_2O	Deuterium oxide
Da	Dalton
DCl	Deuterium chloride
DMF	Dimethylformamide
DP	Degree of polymerization
FITC	Fluorescein isothiocyanate isomer I
GPC	Gel permeation chromatography
HCl	Hydrochloric acid
HEMA	2-hydroxyethyl methacrylate
HEPES	(4-(2-hydroxyethyl)-1-piperazineethanesulfonic acid)
KBr	Potassium bromide
KHP	Potassium hydrogen phthalate
kDa	Kilodalton
LCST	Lower critical solution temperature
MAA	Methacrylic acid
MeOH	Methanol
MPC	2-methacryloyloxyethyl phosphorylcholine
MW	Molecular weight
M_n	Number average molecular weight
M_p	Peak molecular weight

M_w	Weighted average molecular weight
NaOD	Sodium deuteroxide
NaOH	Sodium hydroxide
NaCl	Sodium chloride
NaMAA	Sodium methacrylate
NaSS	Sodium *p*-styrenesulfonate
NMR	Nuclear magnetic resonance
PAM^{b}_{x}	Poly(APM-*co*-MPC)$_x$, *x* = mol % APM in polymer; batch copolymer
PAM^{sb}_{x}	Poly(APM-*co*-MPC)$_x$, *x* = mol % APM in polymer; semibatch copolymer
P(APM)	Poly(*N*-(3-aminopropyl)methacrylamide hydrochloride)
PBS	Phosphate-buffered saline
$PC^{a/b}$	Polyelectrolyte complex (multi-component), *a* = mol % APM in polyanion, *b* = mol % APM in polycation
$PC^{a/b}M_y$	Polyelectrolyte complex (multi-component), *a* = mol % APM in polyanion, *b* = mol % APM in polycation, *y* = mol % MPC in complex
PEC	Polyelectrolyte complex
PLL	Poly(L-lysine)
PMAA	Poly(methacrylic acid)
PMA_x	Poly(methacrylic acid-*co*-APM), *x* = mol % APM in polymer
PMA_xM_y	Poly(methacrylic acid-*co*-APM), *x* = mol % APM in polymer, *y* = mol % MPC in polymer
PM-*a*-M_{50}	Poly(methyl vinyl ether-*alt*-maleic anhydride) 50% hydrolyzed
PMM_y	Poly(methacrylic acid-*co*-MPC), *x* = mol % MPC in polymer
P(NaMAA)	Poly(sodium methacrylate)
PNV_x	Poly(sodium *p*-styrenesulfonate-*co*-vinylbenzyl trimethylammonium chloride), *x* = mol % VBTA
PNV_xH_y	Poly(sodium *p*-styrenesulfonate-*co*-vinylbenzyl trimethylammonium chloride), *x* = mol % VBTA, *y* = mol % HEMA

PNV_xM_y	Poly(sodium *p*-styrenesulfonate-*co*-vinylbenzyl trimethylammonium chloride), *x* = mol % VBTA, *y* = mol % MPC
Q_v	Volumetric swelling ratio
Rhod B	Rhodamine B
TB	Trypan Blue
TEMED	Tetramethylethylenediamine
THPC	Tetrakis (hydroxymethyl) phosphonium chloride
UCST	Upper critical solution temperature
UV-vis	Ultraviolet-visible
Vazo-56	2,2'-azobis(2-methylpropionamidine) dihydrochloride
VBTA	Vinylbenzyl trimethylammonium chloride

List of Figures

Chapter 1

Chapter 2

Chapter 3

Chapter 4

Chapter 5

List of Schemes

Chapter 1

Chapter 2

Chapter 3

Chapter 4

Chapter 5

List of Tables

Chapter 2

Chapter 3

Chapter 4

Chapter 5

Declaration of Academic Achievement

Chapter 2

I designed and performed all of the experiments with guidance from Dr. Stöver, with the exception of several ITC experiments conducted by Dr. Bozelli. ITC experiments were designed by Dr. Bozelli, Dr. Epand, Dr. Stöver, and myself. GPC experiments of acid-rich polymers were performed with the assistance of Alex Jesmer. I wrote the manuscript with edits and guidance from Dr. Stöver, Dr. Bozelli, and Dr. Epand.

Chapter 3

I designed and performed all of the experiments with guidance from Dr. Stöver. I wrote the manuscript with edits and feedback from Dr. Stöver. GPC experiments of acid-rich polymers were performed with the assistance of Alex Jesmer. Temperature-controlled UV-vis experiments were performed with the assistance of Dialia Ritaine.

Chapter 4

I designed and performed all experiments with guidance from Dr. Stöver, Dr. Ros, Dr. Zhao, and Dr. Stewart. I wrote the manuscript with edits and feedback from Dr. Stöver.

Chapter 5

I designed and performed all experiments with guidance from Heera Marway, Robert Bui, Dr. Thompson, Dr. Abrishamkar, and Dr. Hoare. I wrote the manuscript with edits and feedback from Dr. Stöver.

Chapter 1. Introduction

1.1. Polyelectrolytes

Charged macromolecules bearing ionizable repeat units constitute a category of polymers known as polyelectrolytes.[1] These can comprise positive charges, negative charges, or a combination of charges and are known, respectively, as polycations, polyanions, polyampholytes[2,3], and polyzwitterions[4] (Scheme 1.1). Many polyelectrolytes can be found in nature including charged polysaccharides such as alginate, nucleic acids such as deoxyribonucleic acid (DNA), and polyampholytes such as proteins; polyelectrolytes of specific blueprints provide unique properties that offer themselves to highly specialized functions including macromolecular interactions and assembly.[5-8] Because of their relevance and abundance in biology, polyelectrolytes are considered to have played crucial roles in the origin of life.[9] Consequently, there is great interest in exploring and adapting polyelectrolytes for biomaterial applications.

Modern polymer chemistry allows for the precise design of polyelectrolytes comprising different ionizable groups in different ratios and polymer architectures. These include strong acid/base groups (i.e., sulfonate and quaternary ammonium groups, respectively) that are permanently charged or weak acid/base groups that are ionizable under varying pH conditions in solution such as carboxylates and amines[10] By incorporating different monomers into polyanions, polycation, and polyampholytes, the comprised charges facilitate ionic interactions with other charges in solution, offering unique behaviours that make polyelectrolytes advantageous. The ability of polyelectrolytes

to interact with other charged species by associative ionic interactions, coupled with their solubility in water and bio-relevance,[11] make these polymers very interesting on both a fundamental and an applied level. However, the isolation of naturally-derived polymers at a suitable scale for widespread use can be expensive and time intensive, and subject to batch-to-batch variations. In addition, while structural variations are often accessible by modern bioengineering methods, scale-up is relatively limited. As a result, scalable and highly specific synthetic polyelectrolytes are attractive as cost-effective and controlled analogues with near limitless structural designs.

Scheme 1.1. Synthetic polyelectrolytes of different compositions can be made to mimic naturally occurring functional macromolecules.

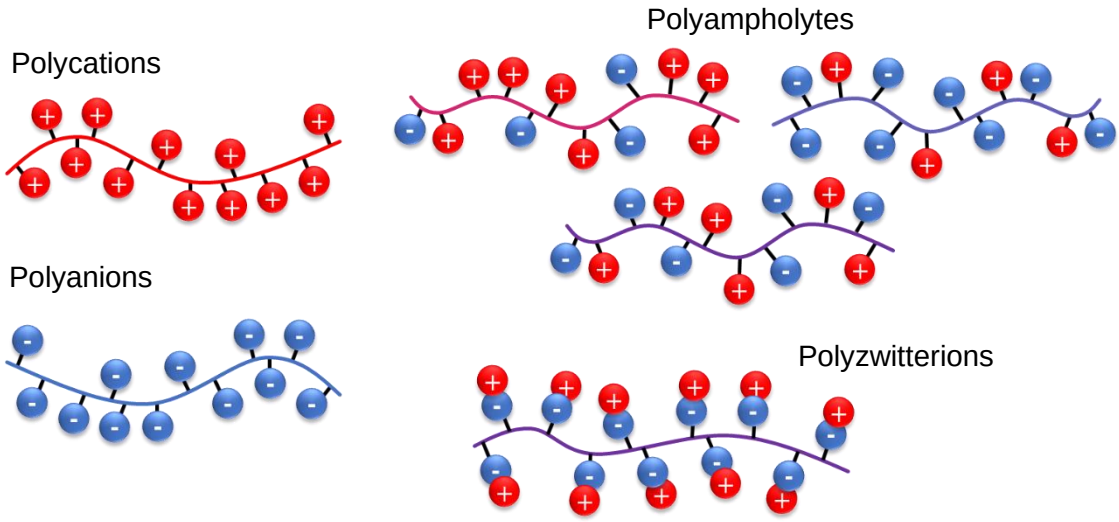

Synthetic polymers offer countless variations of compositions and architectures that can be generated. Common methods such as conventional free-radical (co)-polymerization are useful in large scale generation of polyelectrolytes from a pool of commercially available functional monomers.[12] For specific polyelectrolyte designs, controlled free-radical polymerizations such as reversible addition-fragmentation chain transfer (RAFT)

and atom transfer radical polymerization (ATRP) offer careful control over molecular weight and can be used to generate different architectures such as block, gradient, and graft copolymers. Furthermore, various sequence-controlled polymerization techniques[13] and peptide synthesis methods have been developed to give precise control over the arrangement of functional monomers.[14,15] Post-polymerization modification has also been used to generate polyelectrolytes by hydrolysis of anhydride groups[16,17], deacetylation of chitin to yield water-soluble chitosan[18,19] or active installation of small molecule functionality to achieve particular compositions.[20-22] Hence, the near limitless options for polymer architectures have given rise to materials capable of supporting[23,24], improving on[25,26], or providing biological function.[27-29]

1.2. Polyelectrolyte Complexation - Theoretical Modeling

A key characteristic of polyelectrolytes is their ability to interact with other charged species.[30,31] When oppositely charged polymers interact strongly in aqueous solution, associative phase separation can take place, giving rise to polymer-rich and polymer-poor phases; this is known as polyelectrolyte complexation.[32] As water molecules and salt ions solvating the polymers are displaced by polymeric charged species, the polyelectrolytes collapse into polymer-rich domains ranging from solid precipitates to viscous liquids, known as coacervates. This spontaneous process is fundamental to many biological processes such as DNA compaction around histones in eukaryotic cells[5] and is exploited industrially in the formation of polymer-based surface coatings, layer-by-layer complexes, polyplexes, hydrogels, etc.

First efforts to explore these interactions were conducted by Bungenberg de Jong in the 20th century, reporting the coacervation of two natural polyampholytes, gelatin and gum arabic.[33] These studies laid the groundwork for an early theoretical description of the spontaneous complexation phenomena of polyelectrolytes and the free energy of the system, known as the mean-field theory by Voorn and Overbeek (VO theory).[34] This model is based primarily on the Flory-Huggins expression, the entropy of mixing, and a Debye-Hückel term, with the free energy per unit lattice site (k_BT units) in the system described according to equation 1.1, from Srivastava and Tirrell.[32]

$$f_{total} = -\alpha[\sum_i \sigma_i \phi_i]^{\frac{3}{2}} + \sum_i \frac{\phi_i}{N_i} \ln\phi_i \qquad \textbf{(1.1)}$$

VO theory uses several assumptions to simplify the modeling of PECs that can be substantiated experimentally, such as: salt concentration is always slightly greater in the PEC than the dilute phase, polymers with a higher degree of polymerization (DP) result in a greater tendency for phase separation, increased polymer concentration leads to an increase in complex volume and decreased complex concentration (observed as positive tie lines in VO diagrams, Figure 1.1.), and the addition of salt counterions impedes complexation and phase separation.

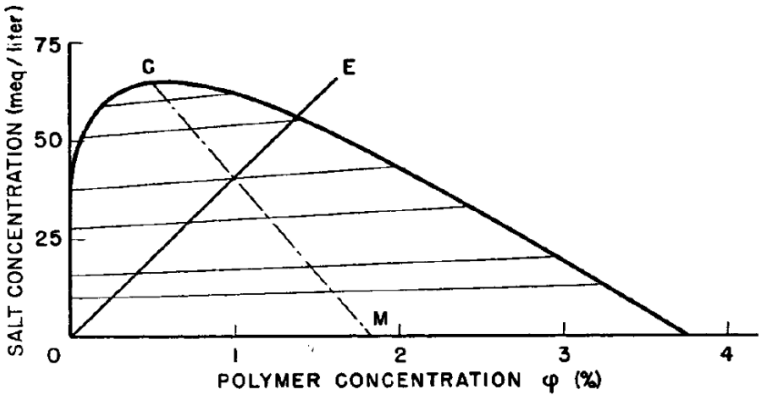

Figure 1.1. Voorn-Overbeek theory predicted binodal phase diagram for polyelectrolyte complex coacervates. Reprinted (adapted) from Overbeek, J. T. G.; Voorn, M. J. Phase Separation in Polyelectrolyte Solutions. Theory of Complex Coacervation. *J. Cell. Comp. Physiol.* **1957**, *49*, 7−26. Copyright (1957) John Wiley and Sons (Lic. 5411991025594).

Although the simplicity of this model is attractive, several limitations are present. For example, VO theory does not account for high linear charge density or consider charge connectivity in polyelectrolytes.[35,36] The noted limitations set in motion a push for more elegant and descriptive models of PECs. Random phase approximation (RPA or the loop expansion) was proposed to better incorporate the charge connectivity and size in polyelectrolytes into the modeling of underlying interactions[37-40], using discrete charge distribution to yield better correlation in the charges and polymer-dense phases.[41] Further development in field-theoretic simulations worked toward solving the limitations of weak charge and low charge density approximations of RPA.[32,42,43] More recently, liquid-state theory and consequent simulations have been developed, describing the interactions of connected charges as cooperative electrostatic interactions which diminish the correlations of counterions and polyelectrolyte during complexation.[44,45] This results in predicted phase behaviours consistent with VO theory while simultaneously predicting a loss of salt counterions in the polymer-dense phase due to excluded volume effects, as shown in RPA.

Alongside the models of simple PECs and nonstoichiometric PEC systems with mismatched polymer charge ratios and chain lengths, reported to a lesser extent,[46-49] empirical research aims to supplement and expand on the existing models for an improved description of the physical principles. While the modelling and theoretical approaches facilitate an understanding of these systems and provide a foundation on which to build, this thesis focuses on the empirical exploration of polyelectrolyte complexation and structure-property relationships.

1.3. Stimuli-Responsiveness in Polyelectrolyte Complexes

1.3.1. Salt Effects

Polyelectrolyte complexation is a thermodynamically driven process dependent on the free energy of the system comprising enthalpic and entropic contributions. While electrostatic (Coulombic) attractions between oppositely charged groups propose an enthalpic contribution toward complexation, these relatively are small and can be easily offset by secondary interactions in individual polymer chains or between pairs of polymers; it has been proposed that enthalpic contributions to ΔG_{PEC} are attributed to changes in perturbation of water by point source electric fields rather than Coulombic attractions and that complexation is almost solely an entropic process.[51] The charged groups of the polymers facilitate interactions with various ionic species in solution such as other polymeric charges and salts. Polyelectrolytes are solvated by bound salt ions and water molecules in aqueous solution, which are displaced by polymeric charges during complexation between oppositely charged chains. This leads to a substantial gain in net

entropy of the system, orders of magnitude larger than the loss of chain mobility in polymer-rich phases. Accordingly, it has been proposed and supported empirically, using two-step modeling of isothermal titration calorimetry, that this entropic contribution is the primary driving force of complexation.[50-53]

While the release of salt counterions is key in driving complexation, salts are also capable of impeding or ultimately preventing polyelectrolyte association, as predicted by VO theory. Substitution of intrinsic polymer-polymer ionic interactions by extrinsic ion pairs with salt counterions allows the solvation of individual polymer chains.[54] The competition for polymeric charges with added salts reduces the favourability of counterion release and complexation, effectively destabilizing the complexes. This "charge shielding" effect of salts on polyelectrolytes facilitates chain plasticization, correlated to the Hofmeister series of salting-in or salting-out ability of different salt ions.[51,55] In general, charge shielding results in weakened associative interactions, which manifest as swollen or fully dissociated PECs.

The impact of salts in complex coacervates was systematically demonstrated by Cohen Stuart and van der Gucht.[35] Using synthetic poly(acrylic acid) and poly(*N*,*N*-dimethylamino ethyl methacrylate) polymers, a binodal phase diagram for the polymer-dense and polymer-poor phases was generated to describe the physical effects of ionic strength on coacervate behaviour according to VO theory. As salt concentration is increased, associative interactions are weakened and the concentration of polymer in coacervates decreases due to an increased volume; this continues toward a critical salt concentration (C_s) at which point coacervates are fully dissociated and the system reaches

a single-phase region. This mapping of the phase behavior of polyelectrolyte coacervates enables further empirical exploration into polyelectrolyte complexation.

Scheme 1.2. Counterion release drives polyelectrolyte complexation, while higher ionic strength facilitates salt screening of charges leading to dissociation of ionic associations.

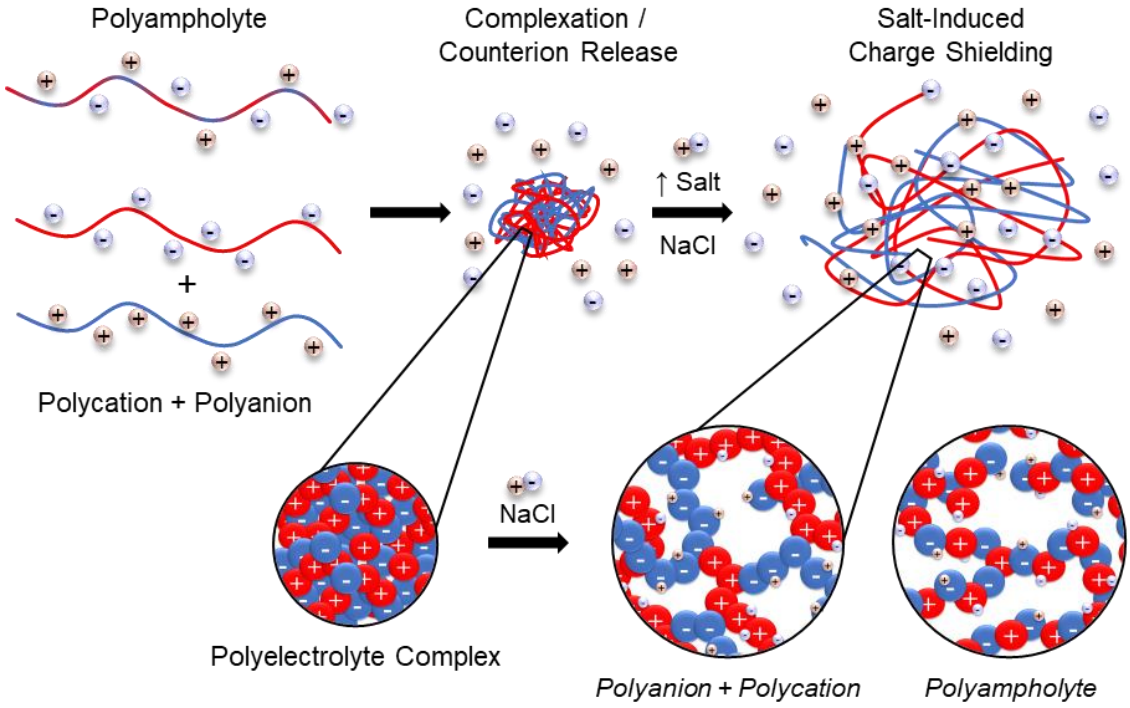

Several studies by Tirrell and others pertaining to salt effects confirm that increases in salt concentration prevent polyelectrolyte complexation.[56-58] Interestingly, at low ionic strength (0-2 M NaBr), salts can plasticize chains and help release kinetically trapped domains, which can enhance the strength of the interactions in complexes and increase the modulus of complexes formed. At higher [NaBr] the complexes transitioned to liquid coacervates and the system resumed the expected salt-dependent behaviour via counterion charge shielding.[59] Wang and Schlenoff further demonstrate the effect of salt in the description of a phase continuum between solid precipitates and liquid coacervates based

on charge shielding and solvation[60]; this was further explored by Perry, using frequency invariant measurements of the complex phase rheology to describe the liquid-solid phase transition which is dictated by interaction strength and salt screening.[61] However, salt ions can also act to bind water in their hydration shells, which hinders the ability of water to act as a plasticizer in PECs and convolutes the net effect of various salts[62]; hence, salts play many intricate roles in polyelectrolyte complex behaviours.

Interestingly, salt partitioning in coacervates has been shown to favour the supernatant phases, by both theoretical[45] and empirical studies[63], and is credited to the presence of excluded volumes in formed complexes. Further investigation demonstrates that salt partitioning in coacervate and solution phases is dependent on the polyelectrolyte compositions, including considerations of hydrophobicity, polarity, charged groups, and monomer structures.[64,65] Researchers also found that the environment inside complexes was comparable to a semi-dilute polymer solution or a polymer melt due to high polymer concentration and that chains do not lose Gaussian conformations or stiffen.[66]

Notably, charge shielding effects are also present in single polyelectrolyte solutions and non-neutral polyampholytes[67], referring to the reduced viscosity of a polyelectrolyte solution increasing with polymer dilution.[68] This also predicts that with increasing salt, the hydrodynamic radius of the polyelectrolyte and, consequently, the viscosity of the solution decreases as the shielding of like-charges allows chains to assume a smaller, collapsed conformation.[69] However, in charge-balanced polyampholytes and polyzwitterions in which oppositely charged groups are introduced causing self-neutralization between charged groups in the polymer or within the monomer structure, an “anti-polyelectrolyte”

behaviour is noted and polymers are increasingly solubilized with greater salt, similar to that observed PECs. Hence, the manifestation of the charge shielding effects depends on the composition of both the individual polyelectrolytes and the system as a whole.

1.3.2. Temperature Effects

For the reason that complexation is a thermodynamic process, solution temperature also has a notable impact on polyelectrolyte physical interactions. As noted, salt ions in adequate concentration inhibit ionic associations and prevent complexation. At high salt concentration, excessive charge shielding permits the solvation of individual chains, while the relative entropic gain through the release of salt counterions during complexation is diminished. However, according to Gibbs free energy of the system, the entropic contribution has a temperature-dependent factor. Therefore, the magnitude of the entropic gain of complexation increases with elevated temperatures, making polymer-polymer association and counterion release more thermodynamically favourable, ultimately leading to spontaneous macroscopic phase separation.

$$\Delta G^0 = \Delta H^0 - T\Delta S^0 \quad \textbf{(1.2)}$$

In this case, the temperature at which the polymer is no longer miscible in solution, or the θ temperature, is defined as the lower critical solution temperature (LCST). LCSTs have been widely demonstrated by non-ionic polymers such as poly(*N*-isopropylacrylamide) (PNIPAM),[70,71] although recent studies have demonstrated that polyelectrolytes[72], polyampholytes,[73,74] and PECs[75,76] can also exhibit LCSTs. In these systems, the LCST of a given mixed polyelectrolyte solution is tunable by changing the ionic strength; higher salt concentration leads to greater charge shielding and less favourable entropy of

complexation, which can be overcome at increasingly higher temperatures to induce spontaneous PEC formation.

In the case of some hydrophobic polyelectrolytes and polyampholytes which form strong phase-separated complexes in solution, increasing the temperature of the system weakens polymer-polymer interactions and the initially insoluble PEC-rich phase becomes miscible in solution. This is representative of an upper critical solution temperature (UCST), which is also susceptible to salt effects, as recently demonstrated in styrenic polyampholytes.[77,78] UCSTs have been primarily demonstrated in polyzwitterions composed of repeat units bearing both positive and negative charges[79,80], although polypeptides have recently expressed this type of temperature response.[64,81]

1.3.3. pH Effects

In addition to salt- and temperature-dependent behaviour, when polyelectrolytes comprise ionizable weak acid/base groups, the polymers become pH-responsive. The pH-dependence in polyelectrolyte solutions gives rise to an isoelectric point (pH(*I*)), classically observed in different proteins and mixed-charged polyampholytes.[82,83] The pH(*I*) is the pH value at which the number of available positive and negative charges are equivalent, and the net charge of the polymer is neutral. At the point of charge balance in solution, ionic associations facilitate chain aggregation and conformational collapse, which can lead to macroscopic phase separation.

Synthetic polyampholyte structures are much simpler than proteins and natural polypeptides, making them more easily modeled. Theoretical predictions of isoelectric

points can be determined according to equation (**1.3**), based on the relevant pK_a and pK_b of the incorporated acid and base groups.[84]

$$pH(I) = pK_a - \log\left\{\frac{R}{2} * \left[-\frac{(1-R)}{R} + \sqrt{\left(\frac{1-R}{R}\right)^2 + \frac{4}{R} * 10^{(pK_a - pK_b)}}\right]\right\} \qquad \textbf{(1.3)}$$

where R is the ratio of acid/base groups, pK_a and pK_b are the negative logarithms of the respective dissociation constants. As the solution pH approaches the pH(I), the number of available ionized groups and, hence, complementary ionic associations increase, leading to favourable polyelectrolyte complexation and macroscopic phase separation via the release of salt counterions at a neutral net charge balance. Consequently, anti-polyelectrolyte effects persist at the isoelectric point, as collapsed neutral polyampholytes become increasingly soluble with increased salt-induced screening.[73,74,85] Solubility is also enhanced by deviation of the solution pH from the isoelectric point, decreasing the degree of ionization of particular charged groups; this leads to a reduction in the charge density of the polymer, resulting in fewer and weaker associative interactions.

This type of pH-dependent behaviour is also present in multicomponent polyelectrolyte solutions. In this case, polyelectrolytes can be homopolymers of single charges with varying charge densities or mixed-charged polyampholytes of varying charge ratios. As seen in polyampholytes, the pH at which complexation is most favourable depends on the charge ratio of the system; however, in mixed solutions comprising multiple components the charge ratio is dictated by the composition of the different polyelectrolytes and by the ratio of the combined polymers, or the mixing ratio. Several studies have demonstrated the impact of mixing ratios on complexation, including for synthetic

polyelectrolytes[35,56,86-88] and complexation of proteins with polyelectrolytes.[89,90] Furthermore, the degree of ionization of weak acid/base groups in the polyelectrolytes is dictated by solution pH, providing another controllable parameter for achieving favourable, balanced charge stoichiometry. Hence, the multifaceted and intricate control over the inherent self-assembly of these polymers makes these systems highly advantageous in bio-relevant applications.[91,92]

1.4. Polymer Architecture and Charge Sequence

Different polymer design elements are key in the elucidation of polyelectrolyte complexation, leading to the description of various structure-property relationships of PECs; for example, the degree of polymerization has notable impacts on physical interactions, as predicted by theoretical models.[34,35,60] Another simple way of altering the underlying interactions in complexation involves employing different functional monomers.[52,93,94] The effects of monomer structure were recently described, showing that charge type strongly impacts the complex binding strength and that hydrophobicity can enhance polyelectrolyte complexation.[95,96] These monomer structure impacts in multicomponent PECs extend to individual polyampholytes[97], exemplified in studies tough, self-healing polyampholyte hydrogels with a range of mechanical properties.[98,99] Furthermore, structure effects extend to variations of zwitterionic monomers containing both positive and negative charges in the same repeat unit. These monomers offer different functional properties including associative zwitterionic interactions[100-103] or significant

hydration properties preventing ionic or hydrophobic associations,[104-106] depending on the spacer length and charge type.[107,108]

Scheme 1.3. Available polymer architectures include statistical and block copolymers. Different copolymer designs can be further tuned by varying charge density.

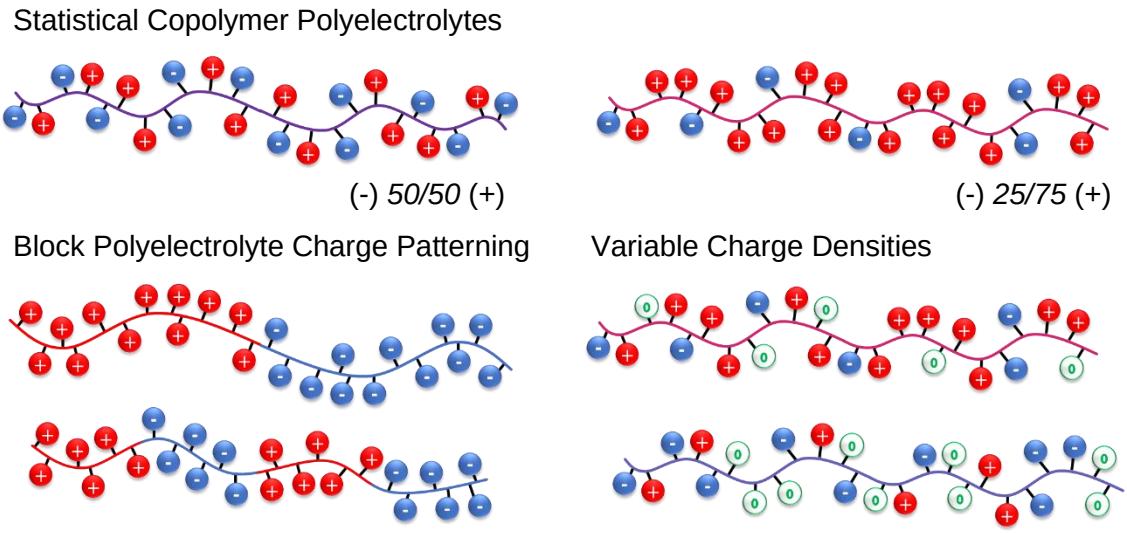

In addition to a diverse library of monomer structures, numerous accessible and highly specific polymer architectures/compositions offer enhanced control of complex properties with several advantages. Different polyelectrolyte charge patterns can be achieved including statistical, alternating, gradient, and block copolymers that offer distinct properties (Scheme 1.3.). Early work by Patrickios, Hertler, and Hatton explored the impact of polymer architecture in random and block copolymer polyampholytes,[109,110] showing that polymers with random charge sequences bind proteins less effectively than polymers with more localized charged segments which behave more as homopolymer polyelectrolytes.[111] This type of block segregation also improves the complexation of polycations incorporating zwitterions with DNA for gene transfection.[112] Molecular simulations confirm that charge separation leads to enhanced polarization and greater

interaction strength, while complexes of alternating polyampholytes with polyelectrolytes possess the lowest stability.[48,113,114] Modelling simulations of polyampholytes also demonstrated the importance of charge sequence and conformational behavior in models for intrinsically disordered proteins[115] and plays a notable role in intracellular compartmentalization in membraneless organelles.[116] Furthermore, charge distribution in the development of strong hydrogels show that as charge localization increases the strength of the physical interactions comprising the integrity of the material.[117]

More recently, sequence-defined polyelectrolytes and polyampholytes have been used to model this specific structure-property relationship. Using controlled polypeptide synthesis to prepare specific block segments and lengths, Perry showed that increasing blockiness ($\boldsymbol{\tau}$) of charged species leads to more favourable ionic interactions and stronger complexation in coacervates.[118,119] These findings describe the increased localization and condensation of salt counterions along larger charge block segments to prevent electrostatic repulsions and the resulting on the impact on resulting coacervate stability. Greater confinement of counterions in larger block segments leads to a greater net gain in translational entropy during coacervation, and hence leads to more stable complexes. This work was then extended to block polyampholytes, confirming that increased charge localization along a chain facilitates greater entropic gain during complexation, leading to stronger complexes with increased salt resistance in single-component PECs.[120] Molecular simulations of intrinsically disordered proteins corroborate the empirical findings that coacervation windows expand with larger blocks and more separated charge distribution.[121]

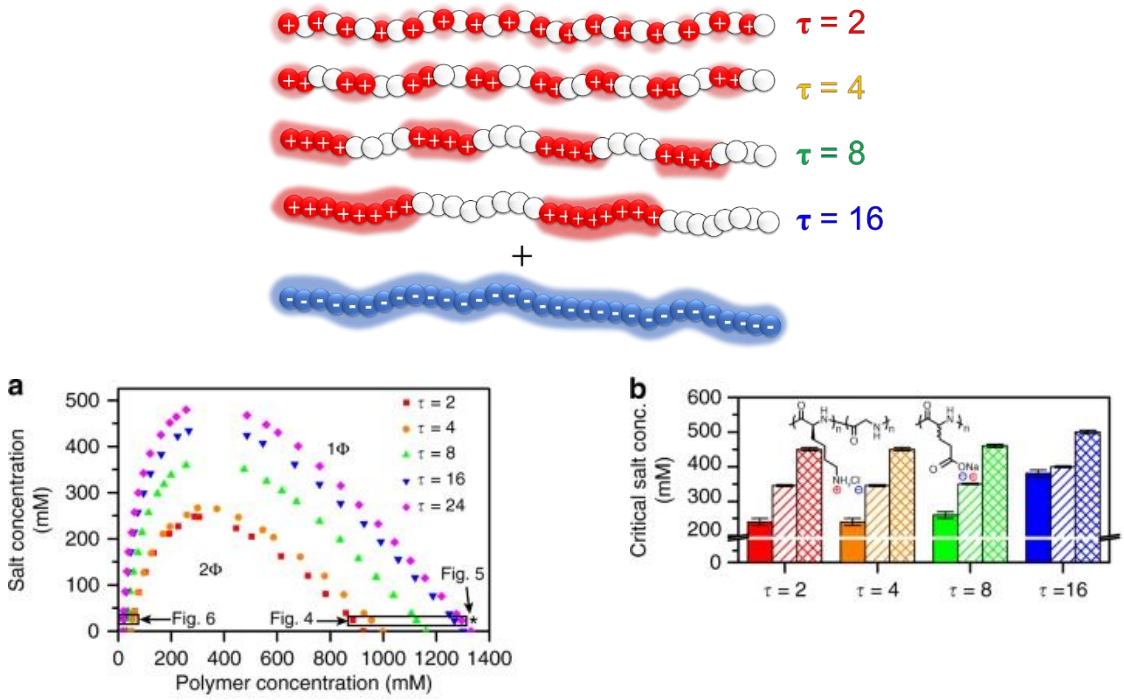

Figure 1.2. Illustration of the effect of blockiness (**τ**) of sequence-defined polyelectrolytes on phase separation. As charge separation increases, (A) the two-phase region or coacervation window of the binodal phase diagram and (B) the critical salt concentration are raised. (A and B) Reprinted (adapted) with permission from Chang, L.-W., *et al. Nat. Commun.* **2017**, *8*, 1273. Copyright (2017) The Authors, published by Springer Nature.

While sequence-specific polyelectrolytes offer the ability to study associative interactions, the effect of increased blockiness and charge separation are also noted in models of random polyelectrolytes, leading to coacervates with greater salt resistance and a larger coacervation window.[122,123] Therefore, the trends and phenomena observed in these sequence-controlled copolymers translate to more scalable polymers, offering the ability to further explore different polyelectrolyte compositions and PEC designs. As mentioned, polyelectrolytes vary in composition to incorporate different monomers and charge ratios, and can be used to form PECs with other polyelectrolytes or, in some cases, themselves.[48] From stoichiometric mixtures of homopolymer polyelectrolytes to a single charge-balanced

polyampholyte solution, the arrangement of charges has been shown to play a key role in the stability of PECs. This presents the opportunity to study different PEC compositions systematically using polyelectrolytes that span from homopolymers to stoichiometric polyampholytes.

Other architectural variations include comb polyelectrolytes that offer a means of spatial separation of, for example, hydrating zwitterionic functional groups from charged blocks. This allows for more favourable coacervation in the presence of hydrating betaines.[124,125] Other structures explored include branched[126] or dendrimer-type polyelectrolytes[127], while additional factors influencing complexation include varying the polymer tacticity[128,129] and stiffness.[130-132]

1.5. Charge Density Tuning of Polyelectrolytes

Though the distribution of charges and polymer structure are crucial in dictating ionic interactions in PECs, the charge density of the polyelectrolyte components is also a key parameter in controlling complex properties. Given that associative interactions occur between oppositely charged species, lower charge density leads to fewer associative inter-chain interactions for complexation and a reduced net entropic gain for complexation.[113,132] In pH-responsive polyelectrolytes, charge density can be altered by varying solution pH toward or away from an optimal isoelectric point to achieve different degrees of ionization in weak acid/base groups. Charge density can also be altered by substitution of charged groups with neutral moieties that disrupt charge runs.[54]

In general, as the number of charges in a polyelectrolyte is reduced, so too is the number of localized counterions. This leads to less favourable entropy of mixing during complexation and, hence, reduces the strength of ionic associations, manifested in complex salt resistance. The effect of charge density in PECs was recently demonstrated using post-polymerization functionalization to develop a library of polyelectrolytes.[133,134] The viscoelasticity of the polymer-dense coacervate phase showed that relaxation dynamics occur faster with decreased charge density, where higher charge density yields stronger associative interactions and enlarges the phase window for coacervation. Interestingly, as charge neutral termonomer is introduced, this work indicates that termonomer hydrophobicity has no notable effects on coacervation; in contrast, others show increased termonomer hydrophobicity can enhance polyelectrolyte complexation at lower charge density.[64,65] These conflicting observations indicate that exploring different termonomers and functional groups is necessary in understanding the effects in tandem with reducing charge density.

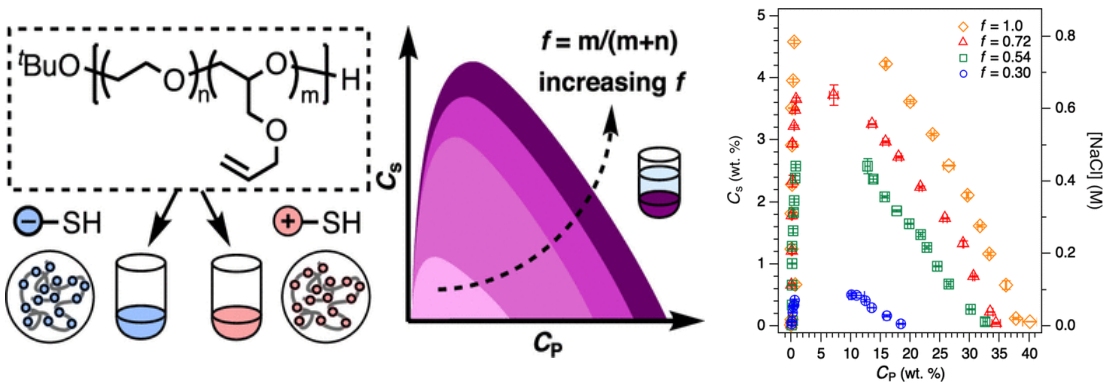

Figure 1.3. Illustration of the use of post-polymerization thiol-ene functionalization to develop a range of polyelectrolyte charge densities; as the charged density (*f*) is increased, the coacervation window widens. Reprinted, (adapted) with permission from Neitzel et al. *Macromolecules* **2021**, *54*, 6878-6890. Copyright (2021) The Authors, published by American Chemical Society.

As in multicomponent PECs, polyampholytes are also susceptible to charge density effects. Addition of a neutral termonomer enhances the sensitivity of coacervates to various stimuli and has been used to shift the responsive properties toward useful physiological conditions.[74,135,136] This was recently demonstrated in polyampholyte terpolymer hydrogels; a reduction in mechanical resilience accompanied improved skin adhesion due to weakened ionic interactions and the liberation of charged groups through the addition of neutral termonomer.[137] Another elegant way to reduce charge density or alter the net charge in polyelectrolytes involves charge-shifting groups based on solution pH, light, or other triggers.[138,139] This has led to the design of degradable PECs for, i.a., DNA binding/release during transfection[140,141] and in antimicrobial wound dressings.[142] In general, tuning the ionic interactions underlying the physical properties of PECs can be achieved by modifying monomer composition and polymer architecture as well as by altering the charge density of the complex components.[143]

1.6. Applications of Polyelectrolytes

Using functional examples of PECs in nature as a guide (i.e., the undersea glue of sandcastle worms,[6] the Humboldt squid beak modulus,[144] and so-called membraneless organelles[145]), many innovative technologies take advantage of synthetic polyelectrolytes that can be used to mimic or improve on the properties of natural polymers. Multifaceted control of the ionic associations in PECs has largely driven the application of polyelectrolytes and PECs in tissue engineering,[146] low-fouling materials,[104-107,147] DNA transfection,[112,140,141] water purification,[148-150] etc. PECs have been extensively studied in

drug delivery as hydrogels,[151] amphiphilic complexes for polymer micelles due to their versatile associative properties,[152,153] and as responsive nanoparticles[154,155] including those used in photothermal ablation therapy of cancerous tissue.[156]

The control over ionic interactions in PECs is specifically important in the design of calcium-alginate (Ca-Alg) microcapsules used in, i.e., the immunoisolation of pancreatic islets cells for insulin delivery in diabetics.[157] Here, polycations are used to complex with the anionic surface of calcium alginate beads, forming a polymer shell that provides improved longevity and mechanical stability. A key challenge is to design functional polymers that do not elicit an undesirable immune response from the host, a common problem accompanying cationic surfaces or materials. Previous work includes the use of charge-shifting polycations,[138] self-deactivating polymeric crosslinking,[16] and reduced charge density polycations[158] including the use of non-fouling moieties such as poly(ethylene glycol)[159] (PEG) and zwitterions.[160,161] Hence, balancing ionic interactions with additional functionality is critical in Ca-Alg based cell encapsulation, requiring careful polymer design and optimization.

High-load bearing, responsive hydrogels are another category of materials that take advantage of polyelectrolyte complexation using natural polymers[162,163] and, more recently, synthetic polyelectrolytes and polyampholytes.[98,117] This has led to the development of numerous materials with impressive tensile strengths and fatigue recovery, and materials that can bind ionic species including drug molecules[164,165] or water contaminants.[148-150,166] Due to the PEC-based nature of these physical hydrogels, the materials are sensitive to salt, temperature, pH, and polymer architecture effects.[99,117,137,167] The dynamic nature of the

ionic cross-links present in PEC-based materials is very attractive, as this can be exploited in stimuli-responsive self-healing.[98,168] Hence, the study and development of new PEC hydrogels as potential biomaterials, such as artificial tissues or implantable devices, is a pertinent area of research that can harness and implement the physical principles of polyelectrolytes.

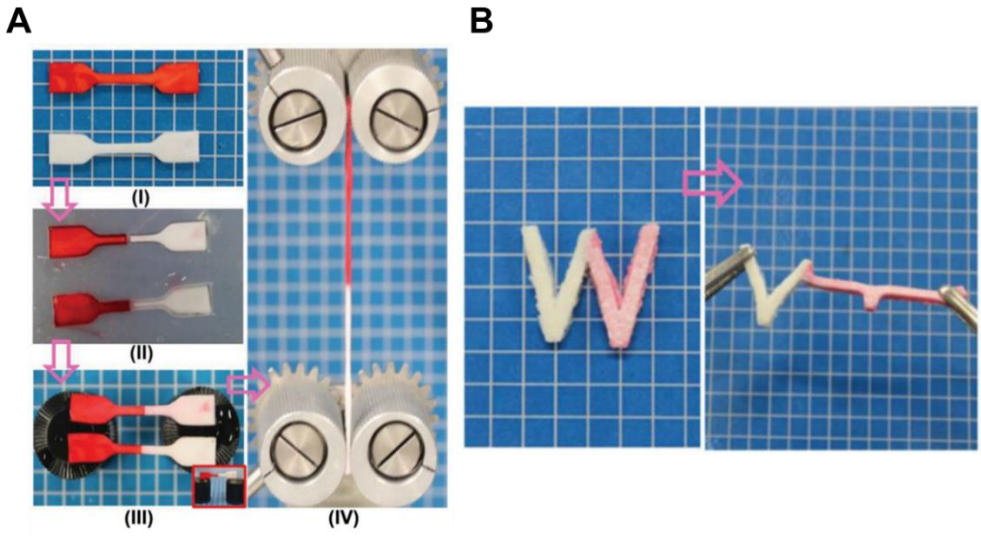

Figure 1.4. (A) Polyion complex hydrogels (PMPTC/PNaSS) are capable of stimuli-responsive self-healing after cutting, dipping in 3 M NaCl, and healing for 12 hours. Healed hydrogels can undergo large deformations. **(B)** Self-glued polyion complex gels (*white, left*) show higher mechanical strength and stiffness compared to polyampholyte hydrogels (*pink, right*). Reprinted (adapted) with permission from Luo, F. *et al.*, *Adv. Mater.* **2015**, *27*, 2722-2727. Copyright (2015) John Wiley and Sons (Lic. 5325380227476).

1.7. Thesis Objectives

Polyelectrolytes can be designed using near-limitless macromolecular structures to express many desirable properties, including several responsive properties that can be exploited in biomedicine. Using specific polyelectrolyte compositions and architectures offers the opportunity to design and explore PECs with a range of responsive properties.

Polyelectrolyte complexation processes and the consequent stimuli-responsive complex properties are remarkably reliant on the charge distribution and compositions of the polymer(s) involved. This thesis focuses on the effects of PEC composition, including charge arrangement and charge density, on the ionic associations and the physical properties of the PECs, as illustrated in Scheme 1.4. Furthermore, investigation of these principles leads to the development of new materials with potential applications in biomedicine.

The second chapter of this thesis describes the systematic investigation of charge arrangement in a polyelectrolyte system comprising weak acid and base monomers, methacrylic acid (MAA) and *N*-(3-aminopropyl)methacrylamide (APM). Different PECs are prepared with showing different stabilities based strictly on the localization of charged monomers, without the need for sequence-control or the addition of non-ionic monomers. The synthesis of polyampholytes with low compositional drift was achieved using a pH-based tuning of reactivity ratios, according to previous work.[73] The pH(*I*) of various single- and multi-component polyelectrolyte solutions were then determined to illustrate the significance of copolymer composition and (co)polymer mixing ratio on the net charge of the resulting complexes. The physical properties including response to change in pH, ionic strength, and temperature at different molecular weights were explored, demonstrating that the strength of ionic associations is inversely proportional to intramolecular charge compensation, or directly proportional to charge separation. The PECs were then observed by microscopy to develop a basic phase diagram, showing transitions from solid precipitates to liquid coacervates and further to homogeneous solutions. Different

coacervates were also used to bind ionic dyes and were covalently crosslinked, as a proof of concept for potential drug delivery technologies.

Scheme 1.4. Overview of PEC compositions used to explore the structure-property relationships in each chapter, using different monomer building blocks to generate accessible polyelectrolytes and polyampholytes.

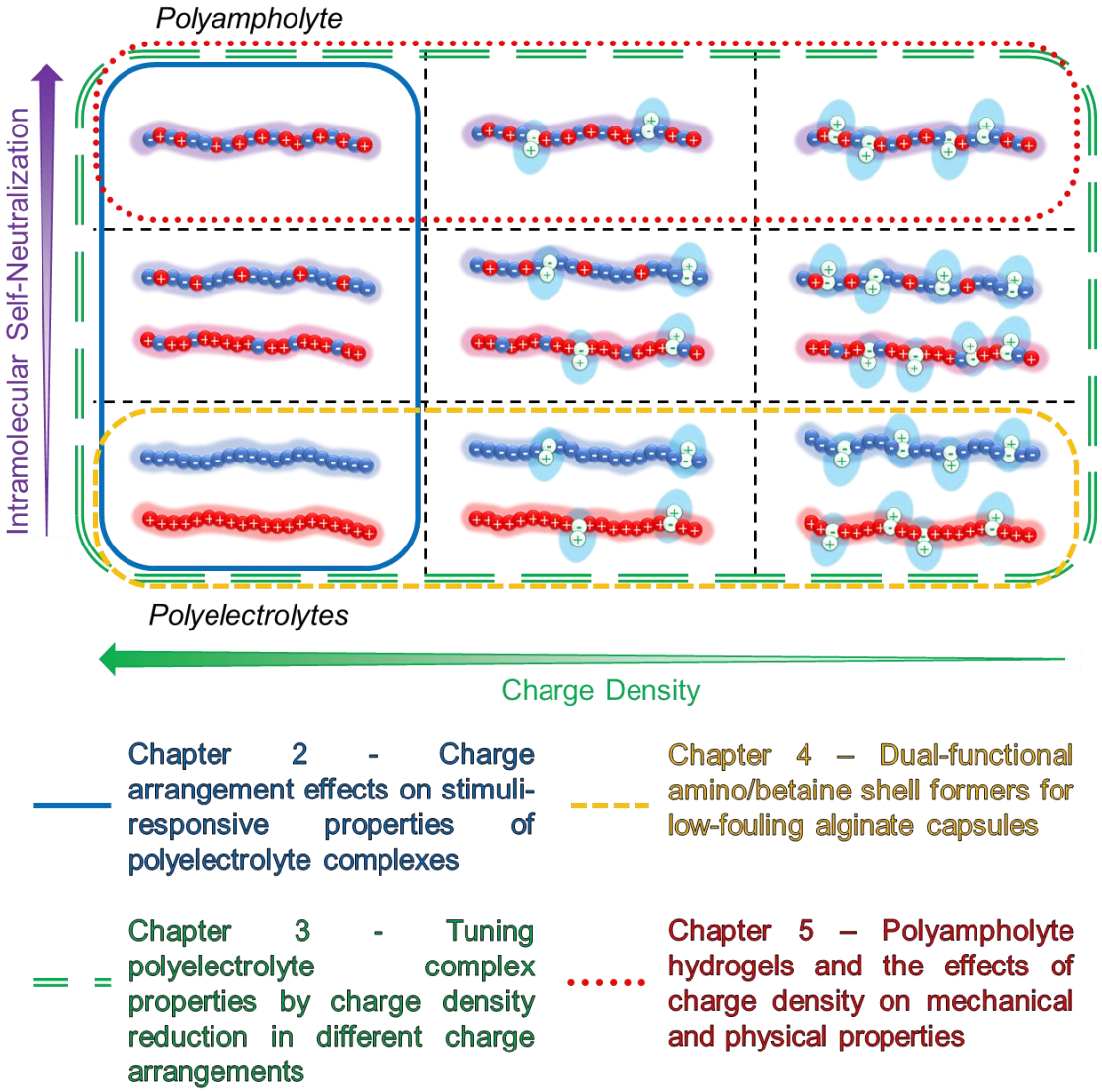

In chapter 3, three distinct charge arrangements were used to explore the impact of charge density in different PECs. The incorporation of zwitterionic 2-methacryloylozyethyl

phosphorylcholine (MPC) during free-radical copolymerization was tracked by ^{1}H NMR spectroscopy in both binary and ternary co-polymerizations. The resulting copolymers were then used to explore the effects of charge dilution in single-component charge-balanced polyampholytes, charge-balanced combinations of complementary nonstoichiometric polyampholytes, and polyanion-polycation combinations. MPC was shown to increase responsiveness to pH, [NaCl], and temperature in all charge arrangements, due to interruption and dilution of ionic associations, but the effects were most significant in self-coacervates. Hydration effects of MPC were most notable in the physical properties and morphologies of single polyampholyte coacervates, in which ionic associations are destabilized by intramolecular self-neutralization and decreased counterion localization. This investigation demonstrates an additional method of tuning ionic associations in different complex compositions and a means of control over stimuli-responsive properties for biomedical applications.

In chapter 4, polycation copolymers were designed to balance ionic associations of APM with calcium alginate hydrogel beads with the low fouling, hydration properties of zwitterionic MPC. Reactivity ratios of the two monomers show a significant compositional drift between the two monomers; hence, a semibatch polymerization method was developed and employed to mitigate compositional drift. Batch and semibatch copolymers were used to form alginate capsules and showed that betaine content could be better confined to the surface using semibatch control. The resulting capsules demonstrate that as MPC is increased, ionic associations at the alginate gel interface are impeded and in-diffusion of the copolymer into the gel leads to thicker, weaker shells. Capsules were then

crosslinked using three different reagents: cationic tetrakis(hydroxymethyl)phosphonium chloride, neutral genipin, and anionic poly(methylvinyl ether-*alt*-maleic anhydride)$_{50}$. The capsules were then used in a binding assay with bovine serum albumin-*f* and showed low fouling with specific MPC content and genipin crosslinking.

In chapter 5, tough polyampholyte hydrogels composed of sodium *p*-styrenesulfonate (NaSS) and (vinylbenzyl)trimethylammonium chloride (VBTA) were explored as responsive materials with high tensile strength. Monomer loading had a notable effect on the morphologies of the hydrogels, as well as the responsive and mechanical properties. Termonomer introduction of MPC and 2-hydroxyethyl methacrylate (HEMA) was used to reduce charge density, impede the underlying associative interactions, and improve the responsive properties. The response to salts such as NaCl and KBr shows that MPC is more effective in weakening the ionic associations for chain plasticization and hydrogel swelling. Additionally, these gels show increased temperature responsiveness with additional termonomer. MPC was more effective in influencing physical properties and can lead to full solubilization during polymerization at just above 8 mol % incorporation., whereas HEMA can be incorporated at up to 50%. Finally, the capacity of the different polyampholyte materials for self-healing illustrates that the addition of termonomer enhances chain plasticization and the ability to reform ionic associations. This work demonstrates the utility of polyampholyte-based physical hydrogels as potential responsive, high load-bearing materials.

1.8. References

1. Fuoss, R. M. Polyelectrolytes. *Science.* **1948**, *108*, 545-550.

2. Katchalsky, A.; Miller, I. R. Polyampholytes. *J. Polym. Sci.* **1954**, *13*, 57-68.

3. Dobrynin, A. V.; Colby, R. H.; Rubinstein, M. Polyampholytes. *J. Polym. Sci. B: Polym. Phys.* **2004**, *42*, 3513-3538.

4. Hart, R.; Timmerman, D. New Polyampholytes: poly(sulfo betaines). *J. Polym. Sci.* **1958**, *28*, 638-640.

5. Widom, J. Structure, Dynamics, and Function of Chromatin in Vitro. *Annu. Rev. Biophys. Biomol. Struct.* **1998**, *27*, 285-327.

6. Stewart, R. J.; Weaver, J. C.; Morse, D. E.; Waite, J. H. The tube cement of *Phragmatopoma californica*: a solid foam. *J. Exp. Biol.* **2004**, *207*, 4727-4734.

7. Forooshani, P. K.; Lee, B. P. Recent Approaches in Designing Bioadhesive Materials Inspired by Mussel Adhesive Protein. *J. Polym. Sci.* **2017**, *55*, 9-33.

8. Uversky, V. N. Introduction to Intrinsically Disordered Proteins (IDPs). *Chem. Rev.* **2014**, *114*, 6557-6560.

9. Oparin, A. I. *The Origin of Life*. Dover Publications: New York, 1935.

10. Bianchi, E.; Conio, G.; Ciferri, A.; Puett, D.; Rajagh, L. The role of pH, temperature, salt type, and salt concentration on the stability of the crystalline, helical, and randomly coiled forms of collagen. *J. Biol. Chem.* **1967**, *242*, 1361-1369.

11. Rubinstein, M.; Papoian, G. A. Polyelectrolytes in biology and soft matter. *Soft Matter* **2012**, *8*, 9265-9267.

12. Laschewsky, A. Recent trends in the synthesis of polyelectrolytes. *Curr. Opin. Colloid Interface Sci.* **2012**, *17*, 56-63.

13. Lutz, J.-F.; Ouchi, M.; Sawamoto, M. Sequence-Controlled Polymers. *Science* **2013**, *341*, 1238149.

14. Merrifield, R. B.; Solid Phase Peptide Synthesis. I. The Synthesis of a Tetrapeptide. *J. Am. Chem. Soc.* **1963**, *85*, 2149–2154.

15. Bodanszky, M. *Principles of Peptide Synthesis.* Springer-Verlag: Berlin, 1993.

16. Gardner, C. M.; Burke, N. A. D.; Stöver, H. D. H. Cross-linked microcapsules formed from self-deactivating reactive polyelectrolytes. *Langmuir* **2010**, *26*, 4916-4924.

17. Stewart, S. A.; Backholm, M.; Burke, N. A. D.; Stöver, H. D. H. Cross-Linked Hydrogels Formed through Diels-Alder Coupling of Furan- and Maleimide-Modified Poly(methyl vinyl ether-*alt*-maleic acid). *Langmuir* **2016**, *32*, 1863-1870.

18. Kiang, T.; Wen, J.; Lim, H. W.; Leong, K. W. The effect of the degree of chitosan deacetylation on the efficiency of gene transfection. *Biomaterials* **2004**, *25*, 5293-5301.

19. Mima, S.; Miya, M.; Iwamoto, R.; Yoshikawa, S. Highly Deacetylated Chitosan and Its Properties. *J. Appl. Polym. Sci.* **1983**, *28*, 1909-1917.

20. Sun, J.; Schlaad, H. Thiol-Ene Clickable Polypeptides. *Macromolecules* **2010**, *43*, 4445-4448.

21. Matsumura, K.; Hayashi, F.; Nagashima, T.; Rajan, R.; Hyon, S.-H. Molecular mechanisms of cell cryopreservation with polyampholytes studied by solid-state NMR. *Commun. Mater.* **2021**, *2*, 15.

22. Matsumura, K.; Hyon, S. H. Polyampholytes as Low Toxic Efficient Cryoprotective Agents with Antifreeze Protein Properties. *Biomaterials* **2009**, *30*, 4842-4849.

23. Tan, H.; Chu, C. R.; Payne, K. A.; Marra, K. G. Injectable *in situ* forming biodegradable chitosan-hyaluronic acid based hydrogels for cartilage tissue engineering. *Biomaterials* **2009**, *30*, 2499-2506.

24. Bhardwaj, N.; Kundu, S. C. Silk fibroin protein and chitosan polyelectrolyte complex porous scaffolds for tissue engineering applications. *Carbohydr. Polym.* **2011**, *85*, 325-333.

25. Lindhoud, S.; Claessens, M. M. A. E. Accumulation of small protein molecules in a macroscopic complex coacervate. *Soft Matter* **2016**, *12*, 408-413.

26. Harada, A.; Kataoka, K. Switching by Pulse Electric Field of the Elevated Enzymatic Reaction in the Core of Polyion Complex Micelles. *J. Am. Chem. Soc.* **2003**, *125*, 15306-15307.

27. Wagner, E.; Cotton, M.; Foisner, R.; Birnstiel, M. L. Transferrin-polycation-DNA complexes: The effect of polycations on the structure of the complex and DNA delivery to cells. *Proc. Natl. Acad. Sci. USA* **1991**, *88*, 4255-4259.

28. Jung, K.; Corrigan, N.; Wong, E. H. H.; Boyer, C. Bioactive Synthetic Polymers. *Adv. Mater.* **2022**, *34*, 2105063.

29. Muthukumar, M. *50th Anniversary Perspective*: A Perspective on Polyelectrolyte Solutions. *Macromolecules* **2017**, *50*, 9528-9560.

30. Fuoss, R. M.; Sadek, H. Mutual Interaction of Polyelectrolytes. *Science* **1949**, *110*, 552-554.

31. Michaels, A. S. Polyelectrolyte Complexes. *Ind. Eng. Chem.* **1965**, *57*, 32-40.

32. Srivastava, S.; Tirrell, M. V. Polyelectrolyte Complexation. *Adv. Chem. Phys.* **2016**, *161*, 499-543.

33. Bundenberg de Jong, H. G.; Kruyt, H. R. Coacervation (Partial miscibility in colloid systems) *Proc. Sect. Sci. K. Ned. Akad. Wet.* **1929**, *32*, 849-859.

34. Overbeek, J. T. G.; Voorn, M. J. Phase separation in polyelectrolyte solutions. Theory of complex coacervation. *J. Cell. Comp. Physiol.* **1957**, *49*, 7.

35. Spruijt, E.; Westphal, A. H.; Borst, J. W.; Cohen Stuart, M. A.; van der Gucht, J. Binodal Compositions of Polyelectrolyte Complexes. *Macromolecules* **2010**, *43*, 6476-6484.

36. Sing, C. E.; Perry, S. L. Recent Progress in the Science of Coacervation. *Soft Matter* **2020**, *16*, 2885-2914.

37. Borue, V. Y.; Erukhimovich, I. Y. A statistical theory of weakly charged polyelectrolytes: fluctuations, equation of state and microphase separation. *Macromolecules* **1988**, *21*, 3240-3249.

38. Borue, V. Y.; Erukhimovich, I. Y. A statistical theory of globular polyelectrolyte complexes. *Macromolecules* **1990**, *23*, 3625-3632.

39. Kudlay, A.; Ermoshkin, A. V.; Olvera de La Cruz, M. Complexation of oppositely charged polyelectrolytes: effect of ion pair formation. *Macromolecules* **2004**, *37*, 9231-9241.

40. Castelnovo, M.; Joanny, J. F. Phase diagram of diblock polyampholyte solutions. *Macromolecules* **2002**, *35*, 4531-4538.

41. Potemkin, I. I.; Palyulin, V. V. Complexation of oppositely charged polyelectrolytes: Effect of discrete charge distribution. *Phys. Rev. E* **2010**, *81*, 041802.

42. Popov, Y. O.; Lee, J.; Fredrickson, G. H. Complex coacervation: A field theoretic simulation study of polyelectrolyte complexation. *J. Chem. Phys.* **2008**, *128*, 224908.

43. Riggleman, R. A.; Kumar, R.; Fredrickson, G. H. Investigation of the interfacial tension of complex coacervates using field-theoretic simulations. *J. Chem. Phys.* **2012**, *136*, 024903.

44. Perry, S. L.; Sing, C. E.; PRISM-Based theory of complex coacervation: Excluded volume versus chain correlation. *Macromolecules* **2015**, *48*, 5040-5053.

45. Zhang, P.; Shen, K.; Alsaifi, N. M.; Wang, Z. G. Salt partitioning in complex coacervation of symmetric polyelectrolytes. *Macromolecules* **2018**, *51*, 5586-5593.

46. Oskolkov, N. N.; Potemkin, I. I. Complexation in asymmetric solutions of oppositely charged polyelectrolytes: Phase diagram. *Macromolecules* **2007**, *40*, 8423-8429.

47. Zhang, R.; Shklovkii, B. I. Phase diagram of solution of oppositely charged polyelectrolytes. *Physica A* **2005**, *352*, 216-238.

48. Jeon, J.; Dobrynin, A. V. Molecular Dynamics Simulations of Polyampholyte-Polyelectrolyte Complexes in Solutions. *Macromolecules* **2005**, *38*, 5300-5312.

49. Wang, F.; Xu, X.; Zhao, S. Complex Coacervation in Asymmetric Solutions of Polycation and Polyanion. *Langmuir* **2019**, *35*, 15267-15274.

50. Ou, Z.; Muthukumar, M. Entropy and enthalpy of polyelectrolyte complexation: Langevin dynamics simulations. *J. Chem. Phys.* **2006**, *124*, 154902.

51. Fu, J.; Schlenoff, J. B. Driving forces for oppositely charged polyion association in aqueous solutions: enthalpic, entropic, but not electrostatic. *J. Am. Chem. Soc.* **2016**, *138*, 980-990.

52. Priftis, D.; Laugel, N.; Tirrell, M. Thermodynamic Characterization of Polypeptide Complex Coacervation. *Langmuir* **2012**, *28*, 15947-15957.

53. Priftis, D.; Megley, K.; Laugel, N.; Tirrell, M. Complex coacervation of poly(ethylene-imine)/polypeptide aqueous solutions: Thermodynamic and rheological characterization. *J. Colloid Interface Sci.* **2013**, *398*, 39-50.

54. Neitzel, A. E.; De Hoe, G. X.; Tirrell, M. V. Expanding the structural diversity of polyelectrolyte complexes and polyzwitterions. *Curr. Opin. Solid State Mater. Sci.* **2021**, *25*, 100897.

55. Salomäki, M.; Tervasmäki, P.; Areva, S.; Kankare, J. The Hofmeister anion effect and the growth of polyelectrolyte multilayers. *Langmuir* **2004**, *20*, 3679-3683.

56. Chollakup, R.; Smitthipong, W.; Eisenbach, C. D.; Tirrell, M. Phase Behavior and Coacervation of Aqueous Poly(acrylic acid)-Poly(allylamine) Solutions. **2010**, *43*, 2518-2528.

57. Chollakup, R.; Beck, J. B.; Dirnberger, K.; Tirrell, M.; Eisenbach, C. D. Polyelectrolyte Molecular Weight and Salt Effects on the Phase Behavior and Coacervation of Aqueous

Solutions of Poly(acrylic acid) Sodium Salt and Poly(allylamine) Hydrochloride. *Macromolecules* **2013**, *46*, 2376-2390.

58. Priftis, D.; Xia, X.; Margossian, K. O.; Perry, S. L.; Leon, L.; Qin, J.; de Pablo, J. J.; Tirrell, M. Ternary, Tunable Polyelectrolyte Complex Fluids Driven by Complex Coacervation. *Macromolecules* **2014**, *47*, 3076-3085.

59. Meng, S.; Ting, J. M.; Wu, H.; Tirrell, M. V. Solid-to-Liquid Phase Transition in Polyelectrolyte Complexes. *Macromolecules* **2020**, *53*, 7944-7953.

60. Wang, Q.; Schlenoff, J. B. The Polyelectrolyte Complex/Coacervate Continuum. *Macromolecules* **2014**, *47*, 3108-3116.

61. Liu, Y.; Momani, B.; Henning Winter, H.; Perry, S. L. Rheological characterization of liquid-to-solid transitions in bulk polyelectrolyte complexes. *Soft Matter* **2017**, *13*, 7338.

62. Zhang, R.; Zhang, Y.; Antila, H. S.; Lutkenhaus, J. L.; Sammalkorpi, M. Role of Salt and Water in the Plasticization of PDAC/PSS Polyelectrolyte Assemblies. *J. Phys. Chem. B* **2017**, *121*, 322-333.

63. Radhakrishna, M.; Basu, K.; Liu, Y.; Shamsi, R.; Perry, S. L.; Sing, C. E. Molecular connectivity and correlation effects on polymer coacervation. *Macromolecules* **2017**, *50*, 3030-3037.

64. Tabandeh, S.; Leon, L. Engineering peptide-based polyelectrolyte complexes with increased hydrophobicity. *Molecules* **2019**, *24*, 868-885.

65. Neitzel, A. E.; Fang, Y. N.; Yu, B.; Rumyantsev, A. M.; de Pablo, J. J.; Tirrell, M. V. Polyelectrolyte Complex Coacervation across a Broad Range of Charge Densities. *Macromolecules* **2021**, *54*, 6878-6890.

66. Spruijt, E.; Leermakers, F. A. M.; Fokkink, R.; Schweins, R.; van Well, A. A.; Cohen Stuart, M. A.; van der Gucht, J. Structure and Dynamics of Polyelectrolyte Complex Coacervates Studied by Scattering of Neutrons, X-rays, and Light. *Macromolecules* **2013**, *46*, 4596-4605.

67. McCormick, C. L.; Johnson, C. B. Water-soluble copolymers. 29. Ampholytic copolymers of sodium 2-acrylamido-2-methylpropanesulfonate with (2-acrylamido-2-methylpropyl)dimethylammonium chloride: solution properties. *Macromolecules* **1988**, *21*, 694-699.

68. Fuoss, R. M.; Strauss, U. P. Electrostatic interaction of polyelectrolytes and simple electrolytes. *J. Polym. Sci.* **1948**, *3*, 602-603.

69. Chen, H. W.; Isihara, C. H.; Isihara, A. Intrinsic Viscosity of Polyelectrolytes in Salt Solutions. *Polym. J.* **1976**, *8*, 288-293.

70. Heskins, M.; Guillet, J. E. Solution Properties of Poly(*N*-isopropylacrylamide). *J. Macromol. Sci., Part A: Pure Appl. Chem.* **1968**, *2*, 1441-1455.

71. Pelton, R. Poly(*N*-isopropylacrylamide) (PNIPAM) is never hydrophobic. *J. Coll. Interface Sci.* **2010**, *348*, 673-674.

72. Büntün, V.; Armes, S. P.; Billingham, N. C. Synthesis and aqueous solution properties of near-monodisperse tertiary amine methacrylate homopolymers and diblock copolymers. *Polymer* **2001**, *42*, 5993-6008.

73. Dubey, A.; Burke, N. A. D.; Stöver, H. D. H. Preparation and Characterization of Narrow Compositional Distribution Polyampholytes as Potential Biomaterials: Copolymers of *N*-(3-Aminopropyl)methacrylamide Hydrochloride (APM) and Methacrylic Acid (MAA). *J. Polym. Sci., Part A: Polym. Chem.* **2015**, *53*, 353-365.

74. Abdilla, A.; Shi, S.; Burke, N. A. D.; Stöver, H. D. H. Multistimuli responsive ternary polyampholytes: Formation and crosslinking of coacervates. *J. Polym. Sci., Part A: Polym. Chem.* **2016**, *54*, 2109-2118.

75. Ali, S.; Bleuel, M.; Prabhu, V. M. Lower Critical Solution Temperature in Polyelectrolyte Complex Coacervates. *ACS Macro. Lett.* **2019**, *8*, 289-293.

76. Adhikari, S.; Prabhu, V. M.; Muthukumar, M. Lower Critical Solution Temperature Behavior in Polyelectrolyte Complex Coacervates. *Macromolecules* **2019**, *52*, 6998-7004.

77. Kanta Sharker, K.; Ohara, Y.; Shigeta, Y.; Ozoe, S.; Yusa, S. Upper critical solution temperature (UCST) behavior of polystyrene-based polyampholytes in aqueous solution. *Polymers* **2019**, *11*, 265.

78. Kanta Sharker, K.; Shigeta, Y.; Ozoe, S.; Damsongsang, P.; Hoven, V. P.; Yusa, S. Upper Critical Solution Temperature Behavior of pH-responsive Amphoteric Statistical Copolymers in Aqueous Solutions. *ACS Omega* **2021**, *6*, 9153-9163.

79. Lowe, A. B.; McCormick, C. L. Synthesis and Solution Properties of Zwitterionic Polymers. *Chem. Rev.* **2002**, *102*, 4177-4190.

80. Lewoczko, E. M.; Wang, N.; Lundberg, C. E.; Kelly, M. T.; Kent, E. W.; Wu, T.; Chen, M.-L.; Wang, J.-H.; Zhao, B. Effects of *N*-Substituents on the Solution Behavior of Poly(sulfobetaine methacrylate)s in Water: Upper and Lower Critical Solution Temperature Transitions. *ACS Appl. Polym. Mater.* **2021**, *3*, 867-878.

81. Deng, Y.; Xu, Y. Wang, X.; Yuan, Q.; Ling, Y.; Tang, H. Water-Soluble Thermoresponsive α-Helical Polypeptide with an Upper Critical Solution Temperature: Synthesis, Characterization, and Thermoresponsive Phase Transition Behaviors. *Macromol. Rapid. Commun.* **2015**, *36*, 453-458.

82. Strege, M. A.; Dubin, P. L.; West, J. S.; Flinta, C. D. Protein separation via polyelectrolyte complexation. *ACS Symp. Ser.* **1990**, *427*, 66-79.

83. Park, J. M.; Muhoberac, B. B.; Dubin, P. L.; Xia, J. Effects of protein charge heterogeneity in protein-polyelectrolyte complexation. *Macromolecules* **1992**, *25*, 290-295.

84. Patrickios, C. S. Polypeptide amino acid composition and isoelectric point: 1. A closed-form approximation. *J. Colloid Interface Sci.* **1995**, *175*, 256-260.

85. Masuda, S.; Minagawa, K.; Tsuda, M.; Tanaka, M. Spontaneous copolymerization of acrylic acid with 4-vinylpyridine and microscopic acid dissociation of the alternating copolymer. *Euro. Polym. J.* **2001**, *37*, 705-710.

86. Perry, S.; Li, Y.; Priftis, D.; Leon, L.; Tirrell, M. The Effect of Salt on the Complex Coacervation of Vinyl Polyelectrolytes. *Polymers* **2014**, *6*, 1756-1772.

87. Shovsky, A.; Varga, I.; Makuška, R.; Claesson, P. M. Formation and Stability of Water-Soluble, Molecular Polyelectrolyte Complexes: Effects of Charge Density, Mixing Ratio, and Polyelectrolyte Concentration. *Langmuir* **2009**, *25*, 6113-6121.

88. Chen, Y.; Yang, M.; Shaheen, S. A.; Schlenoff, J. B. Influence of Nonstoichiometry on the Viscoelastic Properties of a Polyelectrolyte Complex. *Macromolecules* **2021**, *54*, 7890-7899.

89. Cooper, C. L.; Dubin, P. L.; Kayitmazer, A. B.; Turksen, S. Polyelectrolyte-protein complexes. *Curr. Opin. Colloid Interface Sci.* **2005**, *10*, 52-78.

90. Mattison, K. W.; Dubin, P. L.; Brittain, I. J. Complex Formation between Bovine Serum Albumin and Strong Polyelectrolytes: Effect of Polymer Charge Density. *J. Phys. Chem. B.* **1998**, *102*, 3830-3836.

91. Zhuo, S.; Zhang, F.; Yu, J.; Zhang, X.; Yang, G.; Liu, X. pH-Sensitive Biomaterials for Drug Delivery. *Molecules* **2020**, *25*, 5649.

92. Kanamala, M.; Wilson, W. R.; Yang, M.; Palmer, B. D.; Wu, Z. Mechanisms and biomaterials in pH-responsive tumour targeted drug delivery: A review. *Biomaterials* **2016**, *85*, 152-167.

93. Izumrudov, V. A.; Zhiryakova, M. V.; Kudaibergenov, S. E. Controllable stability of DNA-containing polyelectrolyte complexes in water-salt solutions. *Biopolymers* **1999**, *52*, 94-108.

94. Marras, A. E.; Vieregg, J. R.; Ting, J. M.; Rubien, J. D.; Tirrell, M. V. Polyelectrolyte Complexation of Oligonucleotides by Charged Hydrophobic-Neutral Hydrophilic Block Copolymers. *Polymers* **2019**, *11*, 83.

95. Fu, J.; Fares, H. M.; Schlenoff, J. B. Ion-Pairing Strength in Polyelectrolyte Complexes. *Macromolecules* **2017**, *50*, 1066-1074.

96. Sadman, K.; Wang, Q.; Chen, Y.; Keshavarz, B.; Jiang, Z.; Shull, K. R. Influence of Hydrophobicity on Polyelectrolyte Complexation. *Macromolecules* **2017**, *50*, 9417-9426.

97. Zhao, J. Synthesis and Properties of Polyampholyte and Their Application to Cell Cryoprotection. Ph.D. Dissertation, McMaster University, Hamilton, ON, **2018**.

98. Sun, T. L.; Kurokawa, T.; Kuroda, S.; Ihsan, A. B.; Akasaki, T.; Sato, K.; Haque, A.; Nakajima, T.; Gong, J. P. Physical hydrogels composed of polyampholytes demonstrate high toughness and viscoelasticity. *Nat. Mater.* **2013**, *12*, 932-937.

99. Luo, F.; Sun, T.-L.; Nakajima, T.; Kurokawa, T.; Li, X.; Guo, H.; Huang, Y.; Zhang, H.; Gong, J. P. Tough polyion-complex hydrogels from soft to stiff controlled by monomer structure. *Polymer* **2017**, *116*, 487-497.

100. Bia, T.; Liu, S.; Sun, F.; Sinclair, A.; Zhang, L.; Shao, Q.; Jiang, S. Zwitterionic fusion in hydrogels and spontaneous and time-dependent self-healing under physiological conditions. *Biomaterials* **2014**, *35*, 3926-3933.

101. Wang, L.; Gao, G.; Zhou, Y.; Xu, T.; Chen, J.; Wang, R.; Zhang, R.; Fu, J. Tough, Adhesive, Self-Healable, and Transparent Ionically Conductive Zwitterionic

Nanocomposite Hydrogels as Skin Strain Sensors. *ACS Appl. Mater. Interfaces* **2019**, *11*, 3506-3515.

102. Ning, J.; Li, G.; Haraguchi, K. Synthesis of Highly Stretchable, Mechanically Tough, Zwitterionic Sulfobetaine Nanocomposite Gels with Controlled Thermosensitivities. *Macromolecules* **2013**, *46*, 5317-5328.

103. Zheng, S. Y.; Mao, S.; Yuan, J.; Wang, S.; He, X.; Zhang, X.; Du, C.; Zhang, D.; Wu, Z. L.; Yang, J. Molecularly Engineered Zwitterionic Hydrogels with High Toughness and Self-Healing Capacity for Soft Electronic Applications. *Chem. Mater.* **2021**, *33*, 8418-8429.

104. Shao, Q.; Jiang, S. Influence of Charged Groups on the Properties of Zwitterionic Moieties: A Molecular Simulation Study. *J. Phys. Chem. B* **2014**, *118*, 7630-7637.

105. Shao, Q.; Jiang, S. Molecular Understanding and Design of Zwitterionic Materials. *Adv. Mater.* **2015**, *27*, 15-26.

106. Zhao, W.; Zhu, Y.; Zhang, J.; Xu, T.; Li, Q.; Guo, H.; Zhang, J.; Lin, C.; Zhang, L. A comprehensive study and comparison of four types of zwitterionic hydrogels. *J. Mater. Sci.* **2018**, *53*, 13813-13825.

107. Sinclair, A.; O'Kelly, M. B.; Bai, T.; Hung, H.-C.; Jain, P.; Jiang, S. Self-Healing Zwitterionic Microgels as a Versatile Platform for Malleable Cell Constructs and Injectable Therapies. *Adv. Mater.* **2018**, *30*, 1803087.

108. Laschewsky, A.; Rosenhahn, A. Molecular Design of Zwitterionic Polymer Interfaces: Searching for the Difference. *Langmuir* **2019**, *35*, 1056-1071.

109. Patrickios, C. S.; Jang, C. J.; Hertler, W. R.; Hatton, T.A. Interaction of proteins with acrylic polyampholytes. *ACS Symposium Ser.* **1994**, *548*, 257-267.

110. Patrickios, C. S.; Hertler, W. R.; Hatton, T. A. Protein complexation with acrylic polyampholytes. *Biotechnol. Bioeng.* **1994**, *44*, 1031-1039.

111. Chen, W.-Y.; Alexandridis, P.; Su, C.-K.; Patrickios, C. S. ; Hertler, W. R.; Hatton, T. A. Effect of Block Size and Sequence on the Micellization of ABS Triblock Methacrylic Polyampholytes. *Macromolecules* **1995**, *28*, 8604-8611.

112. Ahmed, M.; Bhuchar, N.; Ishihara, K.; Narain, R. Well-Controlled Cationic Water-Soluble Phospholipid Polymer-DNA Nanocomplexes for Gene Delivery. *Bioconj. Chem.* **2011**, *22*, 1228-1238.

113. Dobrynin, A. V.; Rubinstein, M.; Joanny, J. F. Adsorption of Polyampholyte Chain on a Charged Surface. *Macromolecules* **1997**, *30*, 4332-4341.

114. Chang, O.; Jiang, J. Sequence Effects on the Salt-Enhancement Behavior of Polyelectrolytes Adsorption. *Macromolecules* **2022**, *55*, 897-905.

115. Das, R. K.; Pappu, R. V. Conformations of Intrinsically Disordered Proteins are Influenced by Linear Sequence Distributions of Oppositely Charged Residues. *Proc. Natl Acad. Sci. USA* **2013**, *110*, 13392-13397.

116. Pak, C. W.; Kosno, M.; Holehouse, A. S.; Padrick, S. B.; Mittal, A.; Ali, R.; Yunus, A. A.; Liu, D. R.; Pappu, R. V.; Rosen, M. K. Sequence Determinants of Intracellular Phase Separation by Complex Coacervation of a Disordered Protein. *Mol. Cell* **2016**, *63*, 72-85.

117. Luo, F.; Sun, T. L.; Nakajima, T.; Kurokawa, T.; Zhao, Y.; Sato, K.; Ihsan, A. B.; Li, X.; Guo, H.; Gong, J. P. Oppositely Charged Polyelectrolytes Form Tough, Self-Healing, and Rebuildable Hydrogels. *Adv. Mater.* **2015**, *27*, 2722-2727.

118. Chang, L.-W.; Lytle, T. K.; Radhakrishna, M.; Madinya, J. J.; Vélez, J.; Sing, C. E.; Perry, S. L. Sequence and entropy-based control of complex coacervates. *Nat. Commun.* **2017**, *8*, 1273.

119. Lytle, T. K.; Chang, L.-W.; Markiewicz, N.; Perry, S. L. Sing, C. E. Designing Electrostatic Interactions via Polyelectrolyte Monomer Sequence. *ACS Cent. Sci.* **2019**, *5*, 709-718.

120. Madinya, J. J.; Chang, L.-W.; Perry, S. L.; Sing, C. E. Sequence-Dependent Self-Coacervation in High-Density Polyampholytes. *Mol. Syst. Des. Eng.* **2020**, *5*, 632-644.

121. McCarty, J.; Delaney, K. T.; Danielsen, S. P. O.; Fredrickson, G. H.; Shea, J.-E. Complete Phase Diagram for Liquid-Liquid Phase Separation of Intrinsically Disordered Proteins. *J. Phys. Chem. Lett.* **2019**, *10*, 1644-1652.

122. Rumyantsev, A. M.; Jackson, N. E.; Yu, B.; Ting, J. M.; Chen, W.; Tirrell, M. V.; de Pablo, J. J. Controlling Complex Coacervation via Random Polyelectrolyte Sequences. *ACS Macro. Lett.* **2019**, *8*, 1296-1302.

123. Hastings, D. E.; Bozelli, J. C.; Epand, R. M.; Stöver, H. D. H. Investigating the Effects of Charge Arrangement in Stimuli-Responsive Polyelectrolytes. *Macromolecules* **2021**, *54*, 11427-11438.

124. Johnston, B. M.; Johnston, C. W.; Letteri, R.; Lytle, T. K.; Sing, C. E.; Emrick, T.; Perry, S. L. The effect of comb architecture on complex coacervation. *Org. Biomol. Chem.* **2017**, *15*, 7630-7642.

125. Parelkar, S. S.; Letteri, R.; Chan-Seng, D.; Zolochevska, O.; Ellis, J.; Figueiredo, M.; Emrick, T. Polymer-Peptide Delivery Platforms: Effect of Oligopeptide Orientation on Polymer-Based DNA Delivery.

126. Priftis, D.; Xia, X.; Margossian, K. O.; Perry, S. L.; Leon, L.; Qin, J.; de Pablo, J. J.; Tirrell, M. Ternary, Tunable Polyelectrolyte Complex Fluids Driven by Complex Coacervation. *Macromolecules* **2014**, *47*, 3076-3085.

127. Welch, P.; Muthukumar, M. Dendrimer-Polyelectrolyte Complexation: A Model Guest-Host System. *Macromolecules* **2000**, *33*, 6159-6167.

128. Perry, S. L.; Leon, L.; Hoffman, K. Q.; Kade, M. J.; Priftis, D.; Black, K. A.; Wong, D.; Klein, R. A.; Pierce, C. F.; Margossian, K. O.; Whitmer, J. K.; Qin, J.; de Pablo, J. J.; Tirrell, M. Chirality-Selected Phase Behaviour in Ionic Polypeptide Complexes. *Nat. Commun.* **2015**, *6*, 6052.

129. Marciel, A. B.; Srivastava, S.; Tirrell, M. V. Structure and rheology of polyelectrolyte complex coacervates. *Soft Matter* **2018**, *14*, 2454-2464.

130. Elder, R. M.; Emrick, T.; Jayaraman, A. Understanding the effect of polylysine architecture on DNA binding using molecular dynamics simulations. *Biomacromolecules* **2011**, *12*, 3870-3879.

131. Vieregg, J. R.; Lueckheide, M.; Marciel, A. B.; Leon, L.; Bologna, A. J.; Rivera, J. R.; Tirrell, M. V. Oligonucleotide-Peptide Complexes: Phase Control by Hybridization. *J. Am. Chem. Soc.* **2018**, *140*, 1632-1638.

132. Strand, S. P.; Danielsen, S.; Christensen, B. E.; Vârum, K. M. Influence of Chitosan Structure on the Formation and Stability of DNA-Chitosan Polyelectrolyte Complexes. *Biomacromolecules* **2005**, *6*, 3357-3366.

133. Huang, J.; Morin, F. J.; Laaser, J. E. Charge-density-dominated phase behavior and viscoelasticity of polyelectrolyte complex coacervates. *Macromolecules* **2019**, *52*, 4957-4967.

134. Huang, J.; Laaser, J. E. Charge Density and Hydrophobicity-Dominated Regimes in the Phase Behavior of Complex Coacervates. *ACS Macro Lett.* **2021**, *10*, 1029-1034.

135. Das, E.; Matsumura, K. Tunable phase-separation behavior of thermoresponsive polyampholytes through molecular design. *J. Polym. Sci., A: Polym. Chem.* **2017**, *55*, 876-884.

136. Peiffer, D. G.; Lundberg, R. D. Synthesis and viscometric properties of low charge density ampholytic ionomers. *Polymer* **1985**, *26*, 1058–1068.

137. Lee, J. H.; Lee, D. S.; Jung, Y. C.; Oh, J.-W.; Na, Y. H. Development of a Tough, Self-Healing Polyampholyte Terpolymer Hydrogel Patch with Enhanced Skin Adhesion via Tuning the Density and Strength of Ion-Pair Associations. *ACS Appl. Mater. Interfaces* **2021**, *13*, 8889-8900.

138. Ros, S.; Burke, N. A. D.; Stöver, H. D. H. Synthesis and Properties of Charge-Shifting Polycations: Poly[3-aminopropylmethacrylamide-*co*-20(dimethylamino)ethyl acrylate]. *Macromolecules* **2015**, *48*, 8958-8970.

139. Ros, S.; Wang, J.; Burke, N. A. D.; Stöver, H. D. H. A Mechanistic Study of the Hydrolysis of Poly[*N*,*N*-(dimethylamino)ethyl acrylates] as Charge-Shifting Polycations. *Macromolecules* **2020**, *53*, 3514-3523.

140. Ros, S. Freitag, J. S.; Smith, D. M.; Stöver, H. D. H. Charge-Shifting Polycations Based on *N*,*N*-(dimethylamino)ethyl Acrylate for Improving Cytocompatibility During DNA Delivery. *ACS Omega* **2020**, *5*, 9114-9122.

141. Sinclair, A.; Bai, T.; Carr, L. R.; Ella-Menye, J.-R.; Zhang, L.; Jiang, S. Engineering Buffering and Hydrolytic or Photolabile Charge-Shifting in a Polycarboxybetaine Ester Gene Delivery Platform. *Biomacromolecules* **2013**, *14*, 1587-1593.

142. Mi, L.; Xue, H.; Li, Y.; Jiang, S. A Thermoresponsive Antimicrobial Wound Dressing Hydrogel Based on a Cationic Betaine Ester. *Adv. Mater.* **2011**, *21*, 4028-4034.

143. Hastings, D. E.; Stöver, H. D. H. Exploring the Impact of Zwitterions in Discrete Charge Arrangements of Stimuli-Responsive Polyelectrolyte Complexes. *ACS Appl. Polym. Mater.* **2022**, *4*, 5035-5046.

144. Cai, H.; Gabryelczyk, B.; Manimekalai, M. S. S.; Grüber, G.; Salentinig, S.; Miserez, A. Self-coacervation of modular squid beak proteins – a comparative study. *Soft Matter* **2017**, *13*, 7740-7752.

145. Riback, J. A.; Zhu, L.; Ferrolino, M. C.; Tolbert, M.; Mitrea, D. M.; Sanders, D. W.; Wei, M.-T.; Kriwacki, R. W.; Bragwynne, C. P. Composition-dependent thermodynamics of intracellular phase separation. *Nature* **2020**, *581*, 209-214.

146. Coimbra, P.; Ferreira, P.; De Sousa, H. C.; Batista, P.; Rodrigues, M. A.; Correia, I. J.; Gil, M. H. Preparation and chemical and biological characterization of a pectin/chitosan polyelectrolyte *complex* scaffold for possible bone tissue engineering applications. *Int. J. Biol. Macromol.* **2011**, *48*, 112-118.

147. Schroeder, M. E.; Zurick, K. M.; McGrath, D. E.; Bernards, M. T. Multifunctional Polyampholyte Hydrogels with Fouling Resistance and Protein Conjugation Capacity. *Biomacromolecules* **2013**, *14*, 3112-3122.

148. Yu, L.; Liu, X.; Yuan, W.; Brown, L. J.; Wang, D. Confined Flocculation of Ionic Pollutants by Poly(L-dopa)-Based Polyelectrolyte Complexes in Hydrogel Beads for Three-Dimensional, Quantitative, Efficient Water Decontamination. *Langmuir* **2015**, *31*, 6351-6366.

149. Copello, G. J.; Diaz, L. E.; Campo Dall' Orto, V. Adsorption of Cd(II) and Pb(II) onto a one step-synthesized polyampholyte. Kinetics and equilibrium studies. *J. Hazard. Mater.* **2012**, *217*, 374-384.

150. Tripathi, B. P.; Dubey, N. C.; Stamm, M. Functional polyelectrolyte multilayer membranes for water purification applications. *J. Hazard. Mater.* **2013**, *252-253*-401-412.

151. Ishii, S.; Kaneko, J.; Nagasaki, Y. Development of a long-acting, protein-loaded, redox-active, injectable gel formed by a polyion complex for local protein therapeutics. *Biomaterials* **2016**, *84*, 210-218.

152. Ting, J. M.; Wu, H.; Herzog-Arbeitman, A.; Srivastava, S.; Tirrell, M. V. Synthesis and Assembly of Designer Styrenic Diblock Polyelectrolytes. *ACS Macro Lett.* **2018**, *7*, 726-733.

153. Zhou, Z.; Yeh, C.-F.; Mellas, M.; Oh, M.-J.; Zhu, J.; Li, J.; Huang, R.-T. ; Harrison, D. L.; Shentu, T.-P.; Wu, D.; Lueckheide, M.; Carver, L.; Chung, E. J.; Leon, L.; Yang, K.-C.; Tirrell, M. V.; Fang, Y. Targeted polyelectrolyte complex micelles treat vascular complications in vivo. *Proc. Natl. Acad. Sci. U.S.A.* **2021**, *118*, 2114842118.

154. Cheng, W. P.; Gray, A. I.; Tetley, L.; Hang, T. L. B.; Schätzlein, A. G.; Uchegbu, I. F. Polyelectrolyte Nanoparticles with High Drug Loading Enhance the Oral Uptake of Hydrophobic Compounds. *Biomacromolecules* **2006**, *7*, 1509-1520.

155. Sinjari, S.; Freitag, J. S.; Herold, C.; Otto, O.; Smith, D. M.; Stöver, H. D. H. Tunable polymer microgel particles and their study using microscopy and real-time deformability cytometry. *J. Polym. Sci.* **2020**, *58*, 2317-2326.

156. Cheng, L.; Yang, K.; Chen, Q.; Liu, Z. Organic Stealth Nanoparticles for Highly Effective *in Vivo* Near-Infrared Photothermal Therapy of Cancer. *ACS Nano* **2012**, *6*, 5605-5613.

157. Lim, F.; Sun, A. M. Microencapsulated islets as bioartificial endocrine pancreas. *Science* **1980**, *210*, 908-910.

158. Kleinberger, R. M.; Burke, N. A. D.; Zhou, C.; Stöver, H. D. H. Synthetic polycations with controlled charge density and molecular weight as building blocks for biomaterials. *J. Biomater. Sci., Polym. Ed.* **2016**, *27*, 351-369.

159. Sawhney, A. S.; Hubbell, J. A. Poly(ethylene oxide)-graft-poly(L-lysine) copolymers to enhance the biocompatibility of poly(L-lysine)-alginate microcapsule membranes. *Biomaterials* **1992**, *13*, 863-870.

160. Yesilyurt, V.; Veiseh, O.; Doloff, J. C.; Li, J.; Bose, S.; Xie, X.; Bader, A. R.; Chen, M.; Webber, M. J.; Vegas, A. J.; Langer, R.; Anderson, D. G. A Facile and Versatile Method to Endow Biomaterial Devices with Zwitterionic Surface Coatings. *Adv. Healthcare Mater.* **2017**, *6*, 1601091.

161. Hastings, D. E.; Stöver, H. D. H. Crosslinked Hydrogel Capsules for Cell Encapsulation Formed Using Amino/Betaine Dual-Functional Semibatch Copolymers. *ACS Appl. Polym. Mater.* **2019**, *1*, 2055-2067.

162. Swetha, M.; Shithi, K.; Moorthi, A.; Srinivasan, N.; Ramasamy, K.; Selvamurugan, N. Biocomposites containing natural polymers and hydroxyapatite for bone tissue engineering. *Int. J. Biol. Macromol.* **2010**, *47*, 1-4.

163. Fratzl, P. *Collagen: Structure and Mechanics.* Springer: New York, 2008.

164. Chen, L.; Tian, Z.; Du, Y. Synthesis and pH sensitivity of carboxymethyl chitosan-based polyampholyte hydrogels for protein carrier matrices. *Biomaterials* **2004**, *25*, 3725-3732.

165. Jin, S.; Liu, M.; Chen, S.; Gao, C. A drug-loaded gel based on polyelectrolyte complexes of poly(acrylic acid) with poly(vinylpyrrolidone) and chitosan. *Mater. Chem. Phys.* **2010**, *123*, 463-470.

166. Kudaibergenov, S. E.; Tatykhanova, G. S.; Klivenko, A. N. Complexation of macroporous amphoteric cryogels based on *N*,*N*-dimethylaminoethyl methacrylate and methacrylic acid with dyes, surfactant, and protein. *J. Appl. Polym. Sci.* **2016**, *133*, 43784.

167. Hastings, D. E.; Stöver, H. D. H. Physical Polyampholyte Hydrogels and the Effects of Termonomer Charge Density Reduction. *To be submitted*.

168. Ihsan, A. B.; Sun, T. L.; Kurokawa, T.; Karobi, S. N.; Nakajima, T.; Nonoyama, T.; Roy, C. K.; Luo, F.; Gong, J. P. Self-Healing Behaviors of Tough Polyampholyte Hydrogels. *Macromolecules* **2016**, *49*, 4245-4252.

Chapter 2. Investigating the Effects of Charge Arrangement in Stimuli-Responsive Polyelectrolytes

Derrick E. Hastings[1], José C. Bozelli, Jr.[2], Richard M. Epand[2], Harald D. H. Stöver[1*]

[1]Department of Chemistry and Chemical Biology, McMaster University, Hamilton, ON, L8S 4M1, Canada

[2]Department of Biochemistry and Biomedical Sciences, McMaster University, Hamilton, ON, L8S 4M1, Canada

Reprinted (adapted) with permission from Hastings, D. E. *et al.*, *Macromolecules* **2021**, *54*, 11427-11438.

2.1. Abstract

The transition from self-coacervation to complex coacervation of a series of charge-balanced polyampholyte (PA) and polyelectrolyte (PE) pairs based on the copolymers of methacrylic acid and *N*-(3-aminopropyl) methacrylamide hydrochloride is described, with focus on the effects of charge distribution on coacervate properties. Turbidimetric pH titration was used to compare the response of different charge-balanced coacervates to changes in pH. At high molecular weight, resistance to stimuli such as ionic strength and pH increased from the liquid self-coacervate formed from the stoichiometric PA, through complex coacervates formed from complementary nonstoichiometric PAs, to less hydrated

coacervates or precipitates formed from two PE homopolymers. In addition, optical microscopy was used to map the compositional regions as a function of ionic strength corresponding to liquid− liquid phase separation by both self- and complex coacervation and liquid−solid phase separation or precipitation. Coacervates were thermally responsive and showed lower critical solution temperatures that were sensitive to composition and ionic strength. Isothermal titration calorimetry (ITC) was used to explore the energetics of complexation for select complex coacervates, confirming that complexation is dominated by an entropic contribution. Coacervate droplets were shown to reversibly bind ionic dyes and thus have potential use as drug release systems. The coacervate droplets also reacted with genipin to form cross-linked coacervate microgels. The synthetic coacervates used here are easily accessible by free-radical copolymerization and can serve as model systems for phase separation of natural polyampholytes.

2.2. Introduction

Reversible phase separation of polyelectrolytes (PEs) from aqueous solution is a captivating phenomenon with relevance for many biomaterial applications, including high-load-bearing hydrogels,[1,2] drug delivery vehicles,[3] and underwater bioadhesives[4,5] including surgical glues.[6] We recently described the use of low-fouling[7] and charge-shifting polycations[8] in composite hydrogels. Responsive synthetic PEs can serve as model systems for natural analogues, including intrinsically disordered proteins (IDPs) that can reversibly phase-separate within mammalian cells.[9] PEs can be classified as polyanions, polycations, or mixed charged polyampholytes (PAs). PAs composed of weak acid and base groups on

separate repeat units often undergo liquid−solid (precipitation) or liquid−liquid (coacervation) phase separations from aqueous solution at their isoelectric point [pH(*I*)], similar to proteins.[10–16] The polymer-rich aqueous phases formed from a single PA or of two oppositely charged PEs, are called self- and complex coacervates, respectively.[17,18] Several groups have explored the effects of salt, temperature, polymer concentration, mixing ratio, and polymer chain length on the properties of coacervates.[19–26] Classic complex coacervates, such as those observed using gum arabic and gelatin, can involve macromolecules with many different charge distributions along their backbones. Recent work has started to explore the effect of charge distribution on coacervation of synthetic polymers. Perry's group studied self- and complex coacervation of sequence-controlled PEs and PAs,[27–29] and confirmed predictions[30] that grouping charges into blocks increases the complexation strength and widened the coacervation windows.[31,32] A recent theoretical study suggests that charge separation in random, statistical PEs can also impact the strength of their ionic associations and, hence, their physical properties.[33] We here report the effects of charge arrangement on self- and complex coacervates for a series of statistical copolymers and homopolymers of methacrylic acid (MAA) and *N*-(3-aminopropyl) methacrylamide (APM) prepared by low-drift free-radical batch copolymerization. Copolymer compositional drift was minimized through pH-based tuning of reactivity ratios as previously described by our group.[11] Scheme 2.1 illustrates the different charge arrangements from self-coacervation to complex coacervation and the expected interaction strength. We used turbidimetric pH titration, as well as coacervation efficiency as a function of ionic strength and optical microscopy to map the physical properties of the resulting PE

complexes. We also used isothermal titration calorimetry (ITC) to assess thermodynamic information and report the ability of select coacervates to reversibly bind model dyes and to be cross-linked into microgels.

Scheme 2.1. Illustration of five charge-balanced PE complexes based on homopolymer PEs and both nonstoichiometric and stoichiometric PAs, sorted by intramolecular charge separation.[a]

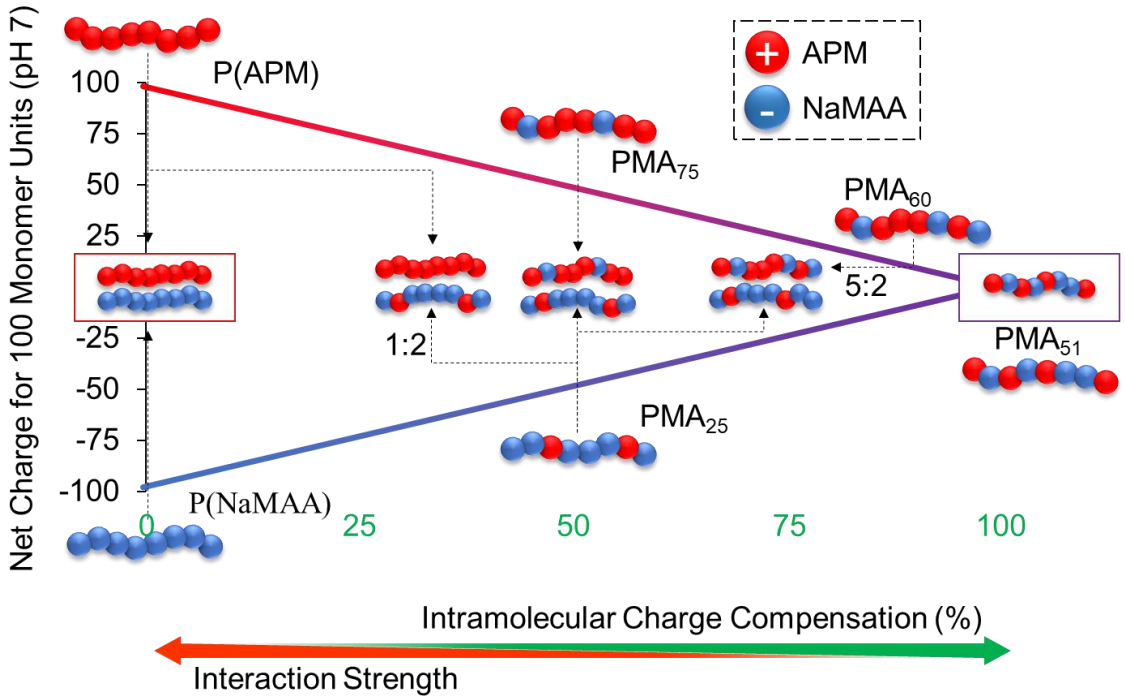

[a]*P(APM) and P(NaMAA) are homopolymers of APM and NaMAA, respectively. Copolymer composition is described as* PMA_{xx}*, where xx stands for the mol % of APM in the copolymer with NaMAA. The complexes* PMA_{25}*-P(APM) and* PMA_{25}*-*PMA_{60} *comprise their cationic and anionic (co)polymer constituents in 1:2 and 5:2 mole ratios, respectively, to ensure charge balance.*

2.3. Experimental

2.3.1. Materials

2,2′-Azobis(2-methylpropionamidine) dihydrochloride (97%, Vazo56), deuterium chloride (99% D), D_2O (>99%), MAA, sodium methacrylate, fluorescein isothiocyanate isomer I (FITC) (>90%), brilliant blue G (BBG), acriflavine, rhodamine B, potassium hydrogen phthalate (>99.95%), *N*-(3-aminopropyl) methacrylamide hydrochloride (APM·HCl, 98%), poly(methacrylic acid) sodium salt (18.5 kDa), and ethylene carbonate (98%) were purchased from Sigma-Aldrich. Trypan blue (0.4% solution) was purchased from Thermo Fischer. APM·HCl (98%) and poly(methacrylic acid) 100 kDa were purchased from PolySciences Inc. APM·HCl from PolySciences was used for most polymerizations unless explicitly stated. Genipin was donated and confirmed using ^{1}H NMR. Cellulose dialysis tubing (3.5 kDa) was purchased from Spectrum Laboratories. All materials were used as received.

2.3.2. Preparation of PAs

Polymers are denoted as poly(MAA-*co*-APM_x) (PMA_x), where x represents the mol % of APM in the copolymer (Scheme 2.2). All polymers were characterized post purification using ^{1}H NMR spectroscopy and gel permeation chromatography (GPC). To generate PAs, previously reported procedures were used as a reference, with respect to altering reactivities using varying NaMAA/MAA ratios.[11]

Scheme 2.2. Copolymerization of NaMAA/MAA with APM using Vazo-56 to generate PMA_x.

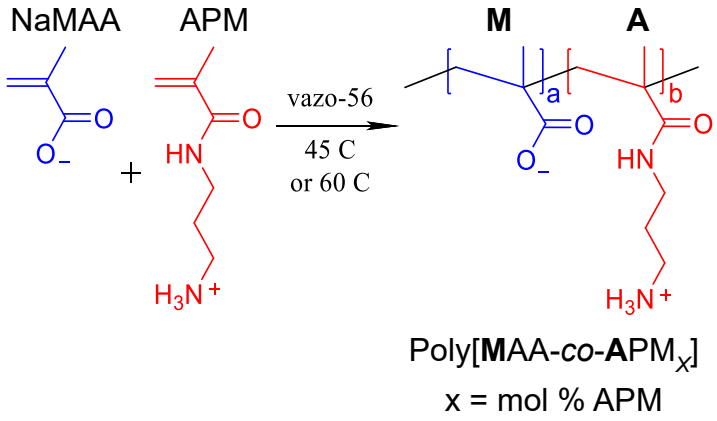

A 3:1 molar ratio of NaMAA/MAA in 1.0 M NaCl was used empirically to equate the reactivities of APM and the (NaMAA/ MAA) pool, and thus give zero-drift 1:1 incorporation of MAA and APM. Likewise, a 1:0 molar ratio of NaMAA/MAA was used in copolymerization with APM to generate PMA_{75}, a 7:1 molar ratio of NaMAA/MAA was used to generate PMA_{60}, and a 3:2 molar ratio of NaMAA/MAA was used to form PMA_{25}, all with very little compositional drift. Conversions were limited to 50−75% to avoid residual compositional drift toward the end of polymerization. P(APM) was prepared by homopolymerization, while P(MAA) was purchased from Sigma-Aldrich.

Polymers with predicted pH(*I*) above 6 (amine-rich) were analyzed using a Waters GPC consisting of a 717Plus autosampler, a 515 HPLC pump, Ultrahydrogel (120, 250, and 500) columns (30 cm × 7.8 mm i.d.; 6 μm particles), and a 2414 refractive index detector, using a 1 M acetate buffer (pH 4.76) with a flow rate of 0.8 mL/min at 30 °C as the mobile phase. This GPC system was calibrated with poly(ethylene glycol) (PEG) standards (Waters Inc.) ranging in molecular weights (MWs) (106 Da to 881 kDa).

Polymers with pH(*I*) below 6 (acid-rich) were analyzed using an Agilent 1260 infinity II GPC system equipped with an Agilent 1260 infinity RI detector, and a GE Healthcare Superose 6 Increase 10/300 GL with a 100 mM borate running buffer (pH 9.4). The column was calibrated using PEG standards (M_n of 3000 to 60,000 Da).

2.3.2.1. 1:1 Charge-Balanced PMA_{51}

A 1:1 charge-balanced PA was prepared at a 1 g scale as follows: to a 20 mL screw cap vial, NaMAA (288 mg, 2.67 mmol), MAA (77 mg, 0.895 mmol), APM (635 mg, 3.55 mmol), and Vazo-56 (19.3 mg, 0.0712 mmol) were added and dissolved in 10 mL of 1 M NaCl. The vial was purged with nitrogen and subsequently submerged in a 45 °C water bath, and the polymerization followed by ^{1}H NMR spectroscopy using a 600 MHz Bruker Avance spectrometer by diluting aliquots of the reaction solution in D_2O. The polymerization was halted at roughly 50% conversion to ensure minimal monomer drift. The copolymer was isolated by dialysis using 3.5 kDa MW cutoff cellulose tubing against 1 M NaCl for 1 day and against deionized water, adjusted to pH 3 with aq. HCl, for 3 days. PMA_{51} was then freeze-dried to yield a solid white polymer (>90% yield). Lower MW polymer was prepared using the described procedure with the addition of 0.5 mol % cysteamine chain transfer agent relative to total monomer

2.3.2.2. PMA_{25}

NaMAA (140 mg, 1.30 mmol), MAA (167 mg, 1.94 mmol), APM (193 mg, 1.08 mmol), Vazo-56 (12 mg, 0.044 mmol), and ethylene carbonate (internal standard, 20 mg, 0.227 mmol) were added to an 8 mL screw cap vial and dissolved in 5 mL of a 1:1 mixture of dimethylformamide (DMF) and water (10% w/v total monomer loading). The vial was then

placed in a UVP Laboratory Products HB-1000 hybridizer oven at 60 °C. As precipitation of insoluble polymer was observed, the vials were centrifuged at intervals for sampling aliquots of the supernatant, which were diluted in D_2O and used to track comonomer consumption. Polymerizations were halted at roughly 65% conversion after roughly 1.5 h of cumulative heating. The polymerization mixture was then combined with 5 mL of 1 M NaOH to dissolve the precipitated polymer, before purification by dialysis against 1 M NaCl at pH 11 for 1 day and against deionized water for 3 days. The polymer was lyophilized to yield a solid white polymer (>90% yield). Lower MW polymer was prepared using the described procedure with the addition of 1 mol % cysteamine chain transfer agent.

2.3.2.3. PMA_{60}

Using an 8 mL screw cap vial, NaMAA (112.6 mg, 1.04 mmol), MAA (15 mg, 0.174 mmol), APM (372.5 mg, 2.08 mmol), and Vazo-56 (8.96 mg, 0.033 mmol) were dissolved in 5 mL of deionized water (10% w/v total monomer loading). The vial was submerged in a 45 °C water bath and monitored using ^{1}H NMR spectroscopy at 30 min intervals by using aliquots as described above, before halting at about 60% conversion after 4 h of cumulative heating. The polymer was then dialyzed against 1 M NaCl for 1 day, followed by deionized water for 3 days before lyophilization (>90% yield).

2.3.2.4. PMA_{75}

Using an 8 mL screw cap vial, NaMAA (84 mg, 0.778 mmol), APM (416 mg, 2.33 mmol), and Vazo-56 (8.4 mg, 0.031 mmol) were dissolved in 5 mL of deionized water (10% w/v total monomer loading). The vial was submerged in a 45 °C water bath and monitored using ^{1}H NMR spectroscopy at 30 min intervals, before halting at about 60% conversion after

about 3 h of cumulative heating. The polymer was then dialyzed against 1 M NaCl for 1 day, followed by deionized water for 3 days before lyophilization (>90% yield). Lower MW polymer was prepared using the described procedure with the addition of 0.75 mol % cysteamine chain transfer agent.

2.3.2.5. P(APM)

Polycation homopolymer was prepared using 500 mg of APM (Sigma-Aldrich) with a 1 mol % Vazo-56 initiator at a 10% w/v total monomer loading in deionized water. The polymerization was heated using a 45 °C water bath and monitored using ^{1}H NMR at 30 min intervals as described above until it exceeded 65% conversion. The polymer was dialyzed against 1 M NaCl for 1 day, followed by deionized water for 3 days and lyophilized to yield a solid white polymer. Lower MW polymer was prepared using the described procedure with the addition of 1 mol % cysteamine chain transfer agent.

2.3.2.6. P(NaMAA)

P(NaMAA) at 100 kDa was prepared by dissolving 1 g of PMAA in 50 mL of deionized water, adjusting pH to 7 with 1 M NaOH and dialyzing in 1 M NaCl for 1 day and distilled water for 3 days, changing diazylate every 24 h. Lower MW P(NaMAA) at 18.5 kDa was purchased from Sigma-Aldrich and used as received.

2.3.3. Fluorescent Labelling of Copolymers

50−60 mg of amine-rich copolymers (PMA_{51}, PMA_{60}, PMA_{75}, and P(APM)) were separately dissolved in 6 mL of deionized water and the solution pH was raised to 8.8−9.0 (9.5−10 for PMA_{60}) using 1 M NaOH. While stirring, appropriate volumes of 10 mg/mL FITC dissolved in DMF were added to each solution to target a 0.1% labeling relative to

total monomer. The reactions were stirred for 1 h in the absence of light before the pH was decreased to 3 for PMA_{51} or 7 for PMA_{60}, PMA_{75}, and P(APM), respectively. Polymers were then dialyzed against deionized water for 3 days (pH 3 for PMA_{51}), filtered, and lyophilized to yield a yellow-orange solid polymer in >85% yield.

2.3.4. Turbidimetric Titration

2.3.4.1. PAs

Turbidimetric titrations of individual PAs were carried out at 22 °C on 25 mL solutions of 0.1 mg/mL polymer total in deionized water. This was chosen to decrease the hysteresis due to slow redissolution after passing the pH(*I*) and to minimize macroscopic precipitation. All polymer solutions were adjusted to pH 2−3 with HCl prior to titration to ensure all polymers were dissolved. The solution was then stirred continuously while titrating to pH 10, by manually adding 25 μL aliquots of 5 mM to 1 M NaOH with a micropipette. The pH and turbidity of the solution were monitored after 30 s of stabilization following each addition, using a VWR SympHony pH probe and a Mitsubishi GT-LD photometric detector equipped with an optical fiber turbidity probe (λ > 620 nm). The concentration of NaOH aliquots added were selected to achieve pH changes of roughly 0.05−0.15 pH units per injection. The same solutions were subsequently titrated from high pH to low pH using 25 μL aliquots of 5 mM to 1 M HCl, while again monitoring the pH and turbidity. Because of the significant peak shoulders following phase separation at pH(*I*), the pH(*I*) was determined as the midpoint between the leading edges of the forward and backward titration curves at the half-minimum transmittance detected.

2.3.4.2. PE Complexation Between (Co)polymers with Complementary Net Charges

A naming system of $PC^{a/b}$ is used to describe complex coacervates, where *a* represents the mol % APM in the MAA-rich (co)polymer, and *b* represents the mol % APM in the APM-rich (co)polymer, as estimated using ^{1}H NMR. The titration of $PC^{25/75}$ (PMA_{25}-PMA_{75}) is given as an example: 1.07 mL of PMA_{25} solution (1 mg/mL) at pH 3 was diluted into 22.5 mL of deionized water in a 30 mL beaker. The solution was adjusted to pH 3 before 1.43 mL of PMA_{75} solution (1 mg/mL) at pH 3 was added to achieve 0.1 mg/mL total polymer loading. The charge-balanced mixture was then titrated as described above up to pH 11. For homopolymer complexes ($PC^{0/100}$), 0.94 mL of P(NaMAA) at pH 3 (1 mg/mL) was diluted into 22.5 mL of deionized water. The solution was adjusted to pH 3 before 1.56 mL of P(APM) solution (0.1% w/v) at pH 3 was added to yield a solution of 0.1 mg/mL total polymer loading. The mixture was then titrated as described above up to pH 11.5. Complexes between PAs and homopolymers were similarly probed at stoichiometric, 1:1 overall charge ratios and 0.1 mg/mL total polymer loading. To investigate the coacervate properties of nonstoichiometric overall charge ratios, titrations of mixtures with varying ratios of $PC^{0/100}$, P(NaMAA)-PMA_{75} ($PC^{0/75}$), and PMA_{25}-P(APM) ($PC^{25/100}$) were carried out as described above. Finally, a ternary mixture of P(NaMAA)-PMA_{25}-PMA_{75} polymers ($PC^{0/25/75}$) was prepared using 0.5:1:2 mole ratios and titrated as described. Procedures were repeated for low-MW polymer solutions.

2.3.5. Phase Separation Efficiency

2.3.5.1. PMA_{51}

In separate screw cap vials, 4 mg samples of FITC-labeled PMA_{51} were dissolved at 1 mg/mL in deionized water containing different amounts of NaCl. The pH of the solutions was briefly raised to 10 using 0.1 M NaOH to fully solubilize the copolymer. The pH was then adjusted to induce phase separation at its pH(*I*) (7.0−7.4) by the addition of 0.1−0.01 M HCl, and the cloudy polymer suspension centrifuged at 2360 *g* for 5 min. The supernatant was removed, adjusted to pH 10, and analyzed using UV−visible spectrophotometry (Varian Cary 50 Bio Spectrophotometer) in 10 mm glass cuvettes to determine the concentration of polymer remaining. Efficiency was determined according to equation **2.1**.

$$\%\, Efficiency = \frac{A(initial) - A(final)}{A(initial)} \times 100\% \qquad (\mathbf{2.1})$$

2.3.5.2. Complementary PAs and PEs

In a screw cap vial, 2−3 mg samples of polyanion and 2−3 mg samples of fluorescently labeled polycation, were separately dissolved at 1 mg/mL in deionized water containing different amounts of NaCl, and each solution pH was adjusted to 7.0. For complementary complexes $PC^{25/75\text{-}f}$, 1.29 mL of PMA_{25} solution and 1.71 mL of PMA_{75}-*f* solution were mixed in a separate vial. For homopolymer complex coacervates $PC^{0/100\text{-}f}$, 1.20 mL of P(NaMAA) solution and 2.00 mL of P(APM)-*f* solution were mixed in a separate vial. The pH of the mixed solutions was re-adjusted to pH 7.0, centrifuged, the supernatant removed, and its pH was adjusted to 11 for analysis using UV−visible spectrophotometry as

mentioned above. The complex supernatants were compared with standard solutions of fluorescent polycation (FITC) in deionized water at pH 11 (0.56 mg/ mL for PMA_{75}-*f* and 0.62 mg/mL for P(APM)-*f*). Abovementioned procedures were repeated for $PC^{25/100\text{-}f}$ (1.81 mL of PMA_{25} and 1.4 mL of P(APM)-*f*) and $PC^{25/60\text{-}f}$ (0.97 mL of PMA_{25} and 2.23 mL of PMA_{60}-*f*) at varying [NaCl].

2.3.5.3. ^{1}H NMR

Composition of 10 mg of scale phase separation mixtures were determined using ^{1}H NMR. Polymers were dissolved separately in 35 mM HEPES buffered saline with additional NaCl, to achieve roughly 50% of the required ionic strength to prevent complexation for each respective combination. Separate polyanion and polycation solutions were mixed in a 15 mL polypropylene centrifuge tube. For example, to form $PC^{25/75}$, 4.31 mL of polyanion and 5.69 mL of polycation were combined. The resulting PECs were then sedimented by centrifugation at 2360 *g* for 5 min and the resulting polymer-rich phases were then isolated, lyophilized, and redissolved in D_2O containing DCl for ^{1}H NMR spectroscopy. NMR experiments were repeated at pH 7 without buffer to avoid residual HEPES signals in the polymer dense phase.

2.3.6. Temperature Response of Aqueous Solutions of PE Complexes

Cloud point measurements were carried out using a Varian 3E spectrophotometer with a temperature-controlled 12-sample holder. Using low-MW polymers 1 mg/mL solutions were heated at 1 °C/min from 23 to 87 °C, and the transmittance at 500 nm was measured at 0.5 °C intervals. Charge-balanced complex solutions were formed from stock solutions as described above for the phase separation efficiency of $PC^{25/75}$ and $PC^{0/100}$. Polymer

solutions of different ionic strengths were used to study the effect of salt on the temperature-induced phase separation. The solution pH was adjusted to pH 7.0 for each PA/PC combination. Cloud point temperatures corresponding to the lower critical solution temperatures (LCST) were defined at a value that was halfway between 100% transmittance and the minima value for the curve with the lowest [NaCl]. For example, PMA_{50} showed a minimum transmittance value of 10%, therefore, the cloud point temperature was determined as the temperature at which the transmittance reached 55%.

2.3.7. Optical Microscopy of Phase-Separated Polymer Complexes at pH(I)

Polymer complexes in suspension were imaged with a Nikon Eclipse Ti optical microscope equipped with a pco.panda 4.2 monochrome sCMOS camera. Copolymer solutions at 10 mg/mL were prepared using solutions of varying [NaCl]. PMA_{51} solutions were adjusted to pH 7.0 to induce phase separation. The pH of premixed polyanion/polycation solutions were adjusted to pH 7.0 before mixing. A drop of the resulting mixture was placed on a clean glass microscope slide for imaging. After initial imaging, a copper wire was gently dragged across the glass surface to disturb the settled polymer dense phase, and the subsequent trail was imaged to illustrate the liquid or gel nature of the polymer dense phases.

2.3.8. ITC

Thermodynamic parameters and binding constants of PE complexes with different charge arrangements were estimated using ITC according to Bozelli et al.[34] Briefly, polymer solutions prepared in a HEPES buffer (35 mM HEPES, 215 mM NaCl, pH 7.4) were degassed under vacuum at 15 °C with continuous stirring for 10 min before each ITC run.

The heat flow resulting from the interaction between polymers was measured using a Nano ITC (TA Instruments, New Castle, DE) by titrating 2 μL of anionic polymer into a cationic polymer solution every 300 s at 20 °C. [Anionic] = 2.5−10 mM and [cationic] = 0.5−2.5 mM. Each injection produced a heat of reaction which was determined by integration of the heat flow tracings after subtraction of the heat of dilution of buffer into cationic polymer peak-by-peak. This model can provide both the binding isotherm and the total binding enthalpy. Binding isotherms were fitted using an independent binding model present in NanoAnalyze software (TA Instruments, New Castle, DE), which yielded the thermodynamic parameters and binding constants for each polymer−polymer pair. Three independent trials were run per polymer pair. Statistical analysis was done by performing a one-way ANOVA test on each data set. Statistical significance was assumed for *p*-values < 0.01.

2.3.9. Complex Binding of Ionic Dyes

Phase separation of different polymer solutions was induced at ionic strength corresponding to roughly 50% of the [NaCl] required to prevent phase separation. For PMA_{51} self-coacervates, procedures from the phase separation efficiency were repeated to induce phase separation. For complex coacervates, mixing of calculated volumes of polyanion and polycation solutions at pH 7.0 was used to induce coacervation. To separate 3 mL aliquots of each coacervate suspension (1 mg/mL) in 15 mL centrifuge tubes were added 30 μL of dye solutions containing either BBG (1 mg/mL, 1.3 μmol/mL), acriflavine (1 mg/mL, 2.1 μmol/mL), rhodamine B (1 mg/mL, 2.1 μmol/mL), or trypan blue (1 mg/ mL, 1.1 μmol/mL).The samples were mixed using a wrist shaker for 10 min before centrifugation

at 2360g for 5 min. Supernatant dye concentrations were measured using UV−Vis spectrophotometry in 1 cm square quartz cuvettes on a Cary 50Bio UV−Vis spectrophotometer. The absorption maxima of the supernatants were compared to reference solutions prepared by adding 30 μL (or 60 μL) of dye solution to 3 mL of deionized water. Binding experiments BBG and trypan blue were then repeated at 300 mM NaCl and at polymer concentrations of 0.1 mg/mL for lower polymer loading. All dye binding complexations were repeated in triplicate (n = 3).

2.3.10. Covalent Cross-linking

Coacervate suspensions formed at 1 mg/mL and at different [NaCl] were exposed to different amounts of genipin solution (5 mg/mL) to target 10 and 25 mol % genipin relative to total APM units in solution. Solutions were left for 30 min and 1 h to allow full consumption of genipin before imaging using optical microscopy. The resulting cross-linked microgels were then challenged with NaCl (2.5 M for both PA and $PC^{25/75}$ and 4 M for $PC^{0/100}$) and 1 M HCl, separately, to assess covalent cross-linking.

2.4. Results and Discussion

This work describes the formation and properties of overall charge-balanced self- and complex coacervates based on MAA and APM homo- and copolymers, as a function of charge distribution over the polymer chains in the system. Specifically, we are exploring to what extent intrachain charge balancing in coacervates formed from stoichiometric and nonstoichiometric PAs will reduce responsiveness to changes in ionic strength, pH, and temperature, compared to PECs formed from a pair of oppositely charged PEs.

2.4.1. Preparation of Polymers

Copolymerizations of MAA and APM at different molar ratios were carried out in aqueous solution using a water soluble Vazo-56 initiator. To minimize copolymer compositional drift during copolymerization, we tuned the reactivity of the MAA monomer by adjusting its degree of ionization. In practice, this involved replacing empirically determined fractions of MAA with NaMAA.11,14 1 M NaCl was used in 1:1 MAA/APM copolymerizations to ensure solubility of the forming copolymer.

Previous work has shown that chain lengths of polyanions and polycations impact the mechanism of complexation.[23,35,36] We explore the PEC properties at both low (18−30 kDa) and high (>100 kDa) MW. Coacervation at sufficiently high MW (>500 DP) shows no significant effect of MW.[24,37] Polymers of 18−30 kDa were prepared separately to explore the effects of charge arrangement at lower MW, below the renal clearance limit.[38,39]

The properties of the homo- and copolymers used are listed in Table 2.1. Compositions of the isolated copolymers were estimated using ^{1}H NMR, comparing the areas under the peaks for backbone and sidechain groups of the two monomers. Analogous lower MW copolymers are described. Only M_p is given for the high-MW copolymers (MW > 100 kDa) as they elute at the exclusion limit of the SEC columns (Figure 2A.1).

Table 2.1. Homo- and copolymers of MAA and APM.

MAA: NaMAA	Polymer	^{1}H NMR Composition (MAA:APM)	$^b M_p$ (kDa)	M_n (kDa)	Excess Charge Ratio (pH 7)	Polymerization Conditions
N/A	**P[NaMAA] (PMA_0)**	100:0	412	--	-100	Lyoph. (pH 7)
N/A	**P[NaMAA]** ***low MW***	100:0	28	19	-100	N/A
3:2	**PMA_{25}**	24:76	448	--	-52	1:1 DMF:H_2O (60 C)
3:2	**PMA_{25}** ***low MW***	25:75	37	27	-50	1:1 DMF:H_2O (60 C)
1:3	**PMA_{51}** [a]	49:51	307	--	0	1 M NaCl
1:3	**PMA_{52}** [a] ***low MW***	48:52	39	28	0	1 M NaCl
1:7	**PMA_{60}** [a]	41:59	271	--	+18	D.I. H_2O
0:1	**PMA_{75}** [a]	76:24	332	--	+52	D.I. H_2O
0:1	**PMA_{75}** [a] ***low MW***	75:25	26	19	+50	D.I. H_2O
N/A	**P[APM]** [a] **(PMA_{100})**	0:100	187	--	+100	D.I. H_2O
N/A	**P[APM]** [a] ***low MW***	0:100	38	26	+100	D.I. H_2O

[a]FITC labelled post-polymerization, [b]M_p values are given as the MW of the high MW polymers exceed the column exclusion limit.

2.4.2. Turbidimetric pH Titrations: Response to pH

Coacervates and PE complexes are formed in an entropically driven process in which small, mobile counterions are displaced by charged groups attached to the same or to another polymer chain, known as intra- and intermolecular interactions, respectively.[40] Both

interactions exist in PAs comprising anionic and cationic groups, and cause the formation of self-coacervates. Conversely, complementary pairs of homopolymer PEs interact exclusively by intermolecular ionic attraction, leading to complex coacervates.[41,42] PECs can be formed by mixing PEs, diluting concentrated solutions of polyanion/polycation mixtures to lower ionic strength, adjusting temperature, or by adjusting pH to achieve a balance of anionic and cationic groups in weak acids/bases.

We used turbidimetric/potentiometric titrations to study the pH-induced phase separation of dilute, charge-balanced polymer solutions near their pH(*I*).[16,30,43] Figure 2.1 shows the forward (low pH to high pH) titration curves for three different charge-balanced polymer systems.

The PA PMA_{51}, the pair of off-stoichiometric PAs PMA_{25} and PMA_{75} ($PC^{25/75}$) and the pair of homopolymers P(NaMAA) and P(APM) ($PC^{0/100}$) all show phase separation near their pH(*I*), between about pH 7.0−7.4. All curves show significant hysteresis visible as a high pH shoulder. This hysteresis is attributed to slow redissolution of the complexes formed and extends to higher pH with the increasing degree of charge separation. Experimental pH(*I*) values were, hence, determined as the midpoint between the two pH values for the half-maximum turbidity of the leading edges of forward and backward titrations (Figure 2A.3).

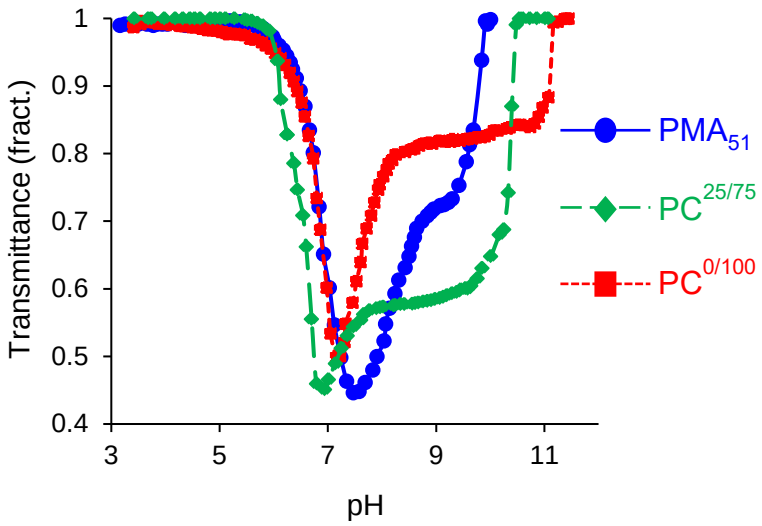

Figure 2.1. Forward (pH-rising) turbidimetric pH titrations of high MW PMA_{51}, $PC^{25/75}$, and $PC^{0/100}$ in charge-balanced solutions.

The observed pH(*I*) for PMA_{51} of 7.50 is very close to its theoretical pH(*I*) of 7.58, estimated using eq **2.2**.[43] Titration plots of the individual, nonstoichiometric PAs PMA_{25}, PMA_{60}, and PMA_{75} (Figure 2A.2) closely resemble previously reported titration curves plots for these compositions.[11]

$$pH(I) = pK_a - \log\left\{\frac{R}{2} * \left[-\frac{(1-R)}{R} + \sqrt{\left(\frac{1-R}{R}\right)^2 + \frac{4}{R} * 10^{(pK_a - pK_b)}}\right]\right\} \qquad \textbf{(2.2)}$$

A precisely 1:1 PA, PMA_{50}, has a theoretical pH(*I*) of 6.9, reflecting the strong dependence of on very small changes in composition.[14] The experimental pH(*I*) of $PC^{25/75}$, $PC^{0/100}$ and all other charge-balanced polymer complexes studied here are close to their theoretical value of 6.9 (Figure 2A.4).

The pH range over which complexes are formed and remain insoluble during titration is a distinct feature of each set of curves. First-derivative plots of turbidity versus pH were used to identify drastic reductions in turbidity following the main onset of

complexation to indicate pH levels required for dissociation at high (forward) and low pH (backward). The difference between the two pH values is indicative of the sensitivity to pH change and, hence, relative strength of associative interactions. These results demonstrate increasing insoluble pH ranges with decreasing intramolecular charge compensation* (PA < $PC^{25/75}$ < $PC^{0/100}$). These trends also hold for other combinations of PAs and homopolymer PEs. First-derivative plots can be found in the Supporting Information.

Interesting features in the titration of the different high MW complexes can likely be attributed to the strength of complexes based on charge distribution. In the single-component PA, coacervation is induced resulting in an onset in turbidity, followed by slow re-dissolution, and finally full miscibility and transmittance at large deviations from the isoelectric pH. However, in stronger, two-component $PC^{25/75}$ and $PC^{0/100}$, adjusting pH induces complexation to yield stronger complexes; the enhanced stability leads to a plateau in transmittance over a range of pH before redissolution at a higher pH value than PA coacervates. In $PC^{0/100}$ forward titrations and $PC^{25/75}$ reverse titrations, curves show a rapid increase in transmittance after onset of complexation before expressing a plateau, which we attribute to the formation of complex that adhere to the beaker walls, hence reducing the amount of suspended complex measured. As pH is further changed, the complexes remain stable before dissociation at extreme pH deviations. These features require greater investigation to determine the exact origin as it pertains to charge distribution, however,

**In this work, charge compensation is used to define charges which can be neutralized via intramolecular interactions of opposite charges along the polymer chain, i.e., the percentage of ionizable groups balanced with an oppositely charged unit along the polymer chain (i.e., PMA_{50} has 100%compensated charges; PMA_{60} = 80% compensated charges; PMA_{75} = 50% compensated charges; P(APM) = 0% compensated charges). This terminology helps to describe the copolymer charge arrangements and, hence, the underlying interactions in different polyelectrolyte mixtures.*

we expect that charge ratio and phase behaviour may underlie these phenomena. We also note that these features do not persist in lower MW complexes, in which all polyelectrolytes form coacervates (Figure 2.2 (A)).

Both the shielding of interchain attraction due to neighbouring charges along the backbone, and the increased intramolecular association due to oppositely charged neighbouring units should destabilize the complex and increase its pH responsiveness. Complexes between PEs with fewer oppositely charged units along their respective chains will, therefore, be more resistant to changes in pH. Lower MW (co)polymer electrolytes (Figure 2.2) of 18−30 kDa also show phase separation over a wider pH range with increased charge separations. These (co)polymer titrations show fewer features in their transmittance curves compared to their higher MW analogues, reflecting their liquid coacervate nature which are more colloidally stable in the stirred beaker and do not adhere during stirring.

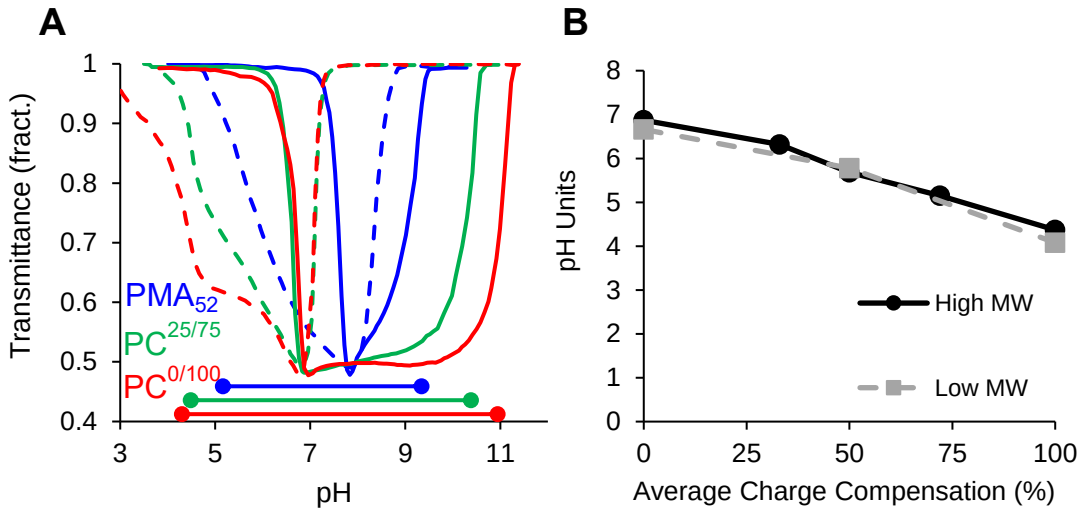

Figure 2.2. (A) Turbidimetric titrations of low-MW coacervates (forward – solid; backward – dash) with insoluble ranges superimposed. **2.2. (B)** pH ranges of insolubility for high- and low-MW complexes as a function of charge arrangement, as determined from first-derivative plots.

We also demonstrate that the polyanion/polycation mixing ratios within different PE charge arrangements can be used to tune the pH(*I*).[44] The effects of mixing ratio have been widely demonstrated in food chemistry, including biopolymers and proteins,[45–47] and in a variety of polymer architectures;[30] for example, varying the block copolymer length or composition offers the ability to control the pH(*I*) while block separation of charges increases the favourability phase separation over random PAs.[48] In the current study, we demonstrate this by varying the copolymer ratio and, hence, the complex charge ratio (Figure 2.3). Different pH(*I*) and pH sensitivities that may be more accessible by the mixing ratio of two or more polymers than by PA composition. The pH(*I*) of PECs depends on the overall charge ratio and can, thus, be controlled by combining stoichiometric and nonstoichiometric polyanions and polycations in different ratios.

Figure 2.3 shows the potentiometric/turbidimetric titrations of PECs with nonstoichiometric charge ratios of 50:50, 58.4:41.6, and 68.2:31.8 of MAA/APM, formed by combining polymers with 0 and 75% APM, and complexes of 50.4:49.6 to 46:54 MAA/APM by combining polymers with 25 and 100% APM. In agreement with eq. **2.2**, the pH(*I*) increases with greater APM and decreases with greater MAA. At 68% MAA, the curve shape and pH(*I*) resemble that of the PMA_{25} PA; similarly, at 54% APM, the curve is comparable to PMA_{60}. This illustrates that regardless of the charge arrangement, the pH(*I*) of different PECs are tunable by the charge ratio. It is noted that plateaus and in some cases small secondary minima in transmittance, are observed for high-MW coacervate titrations past the pH(*I*). The plateaus are again attributed to partial aggregation of

coacervate particles, while the secondary minima are attributed to dissociation of these aggregates just prior to complete dissolution at high pH.

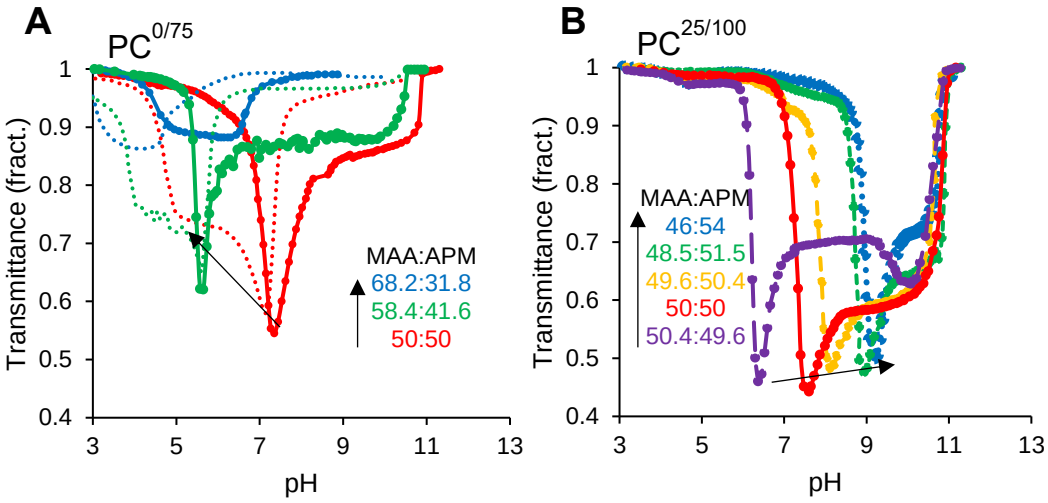

Figure 2.3. Different mixing ratios offer different pH(*I*) for homopolymer/nonstoichiometric PA combinations of (A) $PC^{0/75}$ and (B) $PC^{25/100}$.

2.4.3. Phase Separation Efficiency: Response to Ionic Strength

Phase separation efficiencies of coacervates at their pH(*I*) as a function of independent experimental variables offer another view into the strength of the associative interactions and complex stability. The phase separation efficiencies of PMA_{51} and of overall charge-balanced polymer pairs are plotted in Figure 2.4, as a function of [NaCl]. Phase separation was induced for single PA (PMA_{51}) by adjusting pH to the pH(*I*), and by mixing complementary (co)polymers at pH 7.0 in ratios that correspond to overall charge balance,

in the presence of increasing [NaCl]. Polymers with ≥ 50 mol % APM were labeled with FITC to allow quantitation of soluble polymer in the supernatant phase after sedimentation.

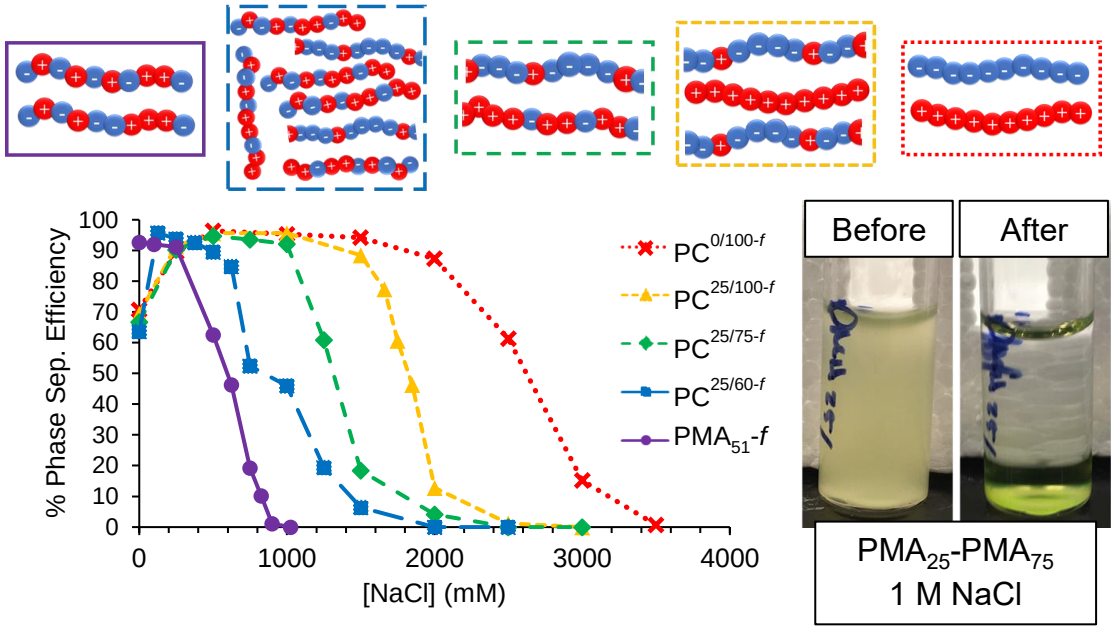

Figure 2.4. (A) Phase separation efficiency graph as a function of [NaCl] for different charge-balances PECs. **2.4. (B)** Images of vials containing PMA_{25}-$PMA_{75\text{-}f}$ phase separations in 750 mM NaCl, before and after centrifugation.

All coacervates except PMA_{51} require small amounts of salt (50−100 mM NaCl) to shield residual net charges and allow effective sedimentation of the coacervates by centrifugation, however it is noted that prior to adjusting toward the pH(*I*) PA solutions are adjusted to pH 10; such additional pH adjustments introduce small amounts (< 50 mM) of salt to each prepared PA solution. Complex coacervates show lower phase separation efficiency at 0 M NaCl; we attribute this to a small percentage of small, strong PEC particles that are colloidally stable due to residual net surface charges, and thus not effectively sedimented by centrifugation. The associated supernatants are slightly turbid and the suspended PEC particles are solubilized upon increasing pH for UV−Vis analysis,

which artificially decreases the measured complexation efficiency. This phenomenon has been previously reported and can be overcome by adding small amounts of salt to screen surface charges and enhance aggregation sedimentation.[22,37,43,49–51]

Figure 2.4 shows that coacervation efficiencies were quantitative (90−95%) up to 250 mM NaCl, and then started to decrease, with PMA_{51} reaching 60% at 500 mM NaCl, and becoming fully soluble at 1 M. The copolymer mixtures $PC^{25/60\text{-}f}$, $PC^{25/75\text{-}f}$, and $PC^{25/100\text{-}f}$ have progressively less intramolecular charge compensation and, hence, dissolve only at correspondingly higher [NaCl], with the homopolymer complex $PC^{0/100\text{-}f}$ requiring 3.5 M NaCl for dissolution. The increase of coacervate resistance to [NaCl] from PMA_{51} to $PC^{0/100}$ shown in Figure 2.4 corresponds to their increasing charge separation into separate chains.

These results support previous reports indicating that increased charge localization in PEs and PAs improves the coacervation efficiency and strength of PECs by minimizing repulsive effects and intramolecular charge balancing from nearby complementary charges.[27,28,30] Where previous reports use block separation and sequence control to carefully localize charges, we use statistical copolymers of various charge ratios to separate charges to different degrees both along the polymer chains and between two oppositely charged species. The coacervation efficiencies of lower MW PECs follow the same trends (Figure 2A.11). Although the sensitivity to [NaCl] increases for all complexes in agreement with previous reports on coacervates with lower MW,[52] the PMA_{51} self-coacervates are more affected by the change in MW than the complex coacervates of $PC^{25/75\text{-}f}$ and $PC^{0/100\text{-}f}$ (Figure 2A.11).

2.4.4. Temperature Response of Aqueous Solution

The PMA_{51} PA solution show cloud point temperatures that increase with increasing [NaCl] (Figure 2.5) reflecting the lower entropy gain obtained by liberating small counterions at higher [NaCl], in line with observations for the closely related PMA_{48} [11] and analogous PAs.[14,15,53] The steepness of the transmittance curves increases from $PC^{25/75}$ over PMA_{51} to $PC^{0/100}$, reflecting the decreasing variation of composition along the backbones. Cloud point temperatures, obtained here as halfway points between 100% T and the minimum transmittance achieved, were plotted (Figure 2A.12) against [NaCl] and show slopes (ΔCPT/Δ[NaCl]) that decrease with charge separation (PA > $PC^{25/75}$ > $PC^{0/100}$), further demonstrating the increased resistance to NaCl as charges are separated.

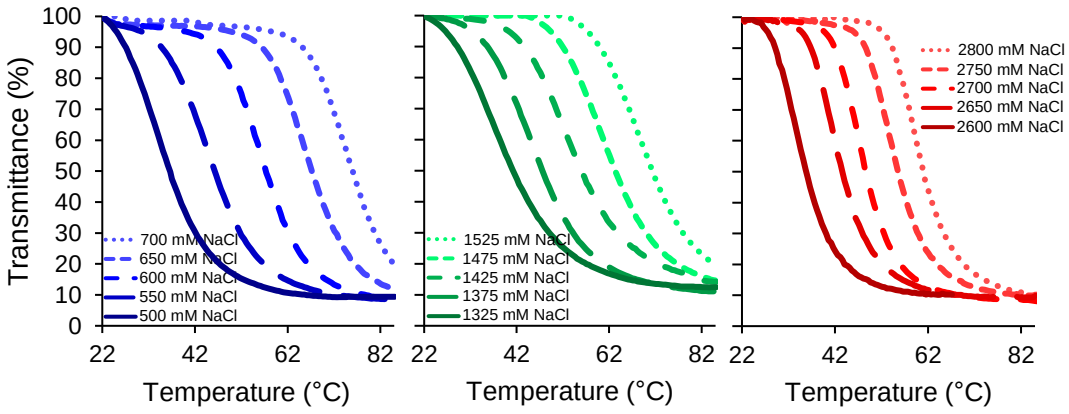

Figure 2.5. Optical transmittance curves of PMA_{51} (left), $PC^{25/75}$ (centre), and $PC^{0/100}$ (right) show cloud point temperatures increasing with [NaCl].

2.4.5. Microscopy of Phase-Separated PE Complexes

We used optical microscopy to study the macroscopic properties of the present complexes at pH(*I*), in particular liquid−liquid versus liquid−solid phase separations. We explored coacervates formed from both high- and low-MW PMA_{51}, and high-MW $PC^{25/60}$, $PC^{25/75}$,

$PC^{25/100}$, and $PC^{0/100}$ complexes, at 1 wt % loading and at three different [NaCl]: 0 mM [NaCl] corresponding to >90% phase separation, and [NaCl] corresponding to the coacervation efficiency of about 60%. Microscope images of PMA_{51}, $PC^{25/75}$ and $PC^{0/100}$ at particular ionic strengths are shown in Figure 2.6. The phase separation efficiency data of each complex are superimposed on the image series, with highlighted points indicative of each different [NaCl].

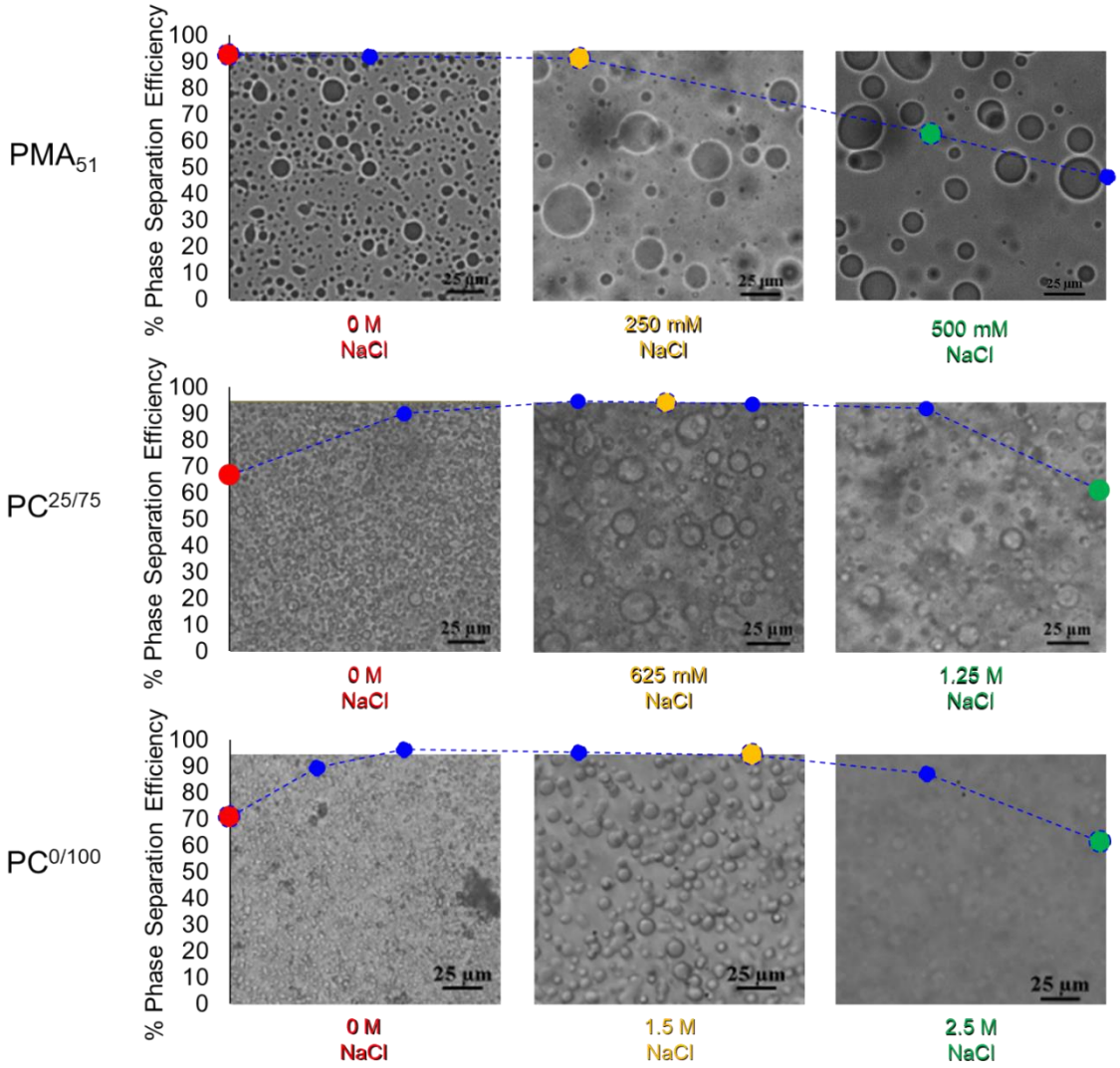

Figure 2.6. Optical microscope images of PMA_{51} (top), $PC^{25/75}$ (middle), and $PC^{0/100}$ (bottom) high-MW complexes at 0 mM [NaCl] and at [NaCl] corresponding to 90% (middle column) and 60% (right column) phase separation efficiency.

At 0 mM NaCl, high-MW PA PMA_{51} initially forms a cloudy solution, with large coacervate droplets that grow by fusion with other droplets (Figure 2A.13). These droplets are confirmed to be viscous liquids, especially at increasing [NaCl], by watching deformation and recovery after dragging a copper wire through them on a microscopy slide

(Figures 2A.16 and 2A.17). $PC^{25/60}$ coacervates show similar behavior but at higher ionic strength.

$PC^{25/75}$ coacervate droplets are significantly smaller as formed. They continue to fuse, and anneal after mechanical disturbance, but require much higher [NaCl] to resemble PA droplets. $PC^{25/100}$ complexes begin to show small amounts of solid precipitate in addition to coacervate when initially formed at low [NaCl] and require greater increases in [NaCl] to form fully liquid coacervate droplets.

At 0 mM [NaCl], $PC^{0/100}$ form clusters of small, dense particles that were displaced rather than smeared by the copper wire test. [NaCl] of about 1.5 M was required to observe liquid−liquid phase separation, with higher [NaCl] showing more fluidity. Figure 2.7 shows a simple phase diagram for these high-MW complexes, mapping the formation of coacervates and precipitates as a function of composition and [NaCl].

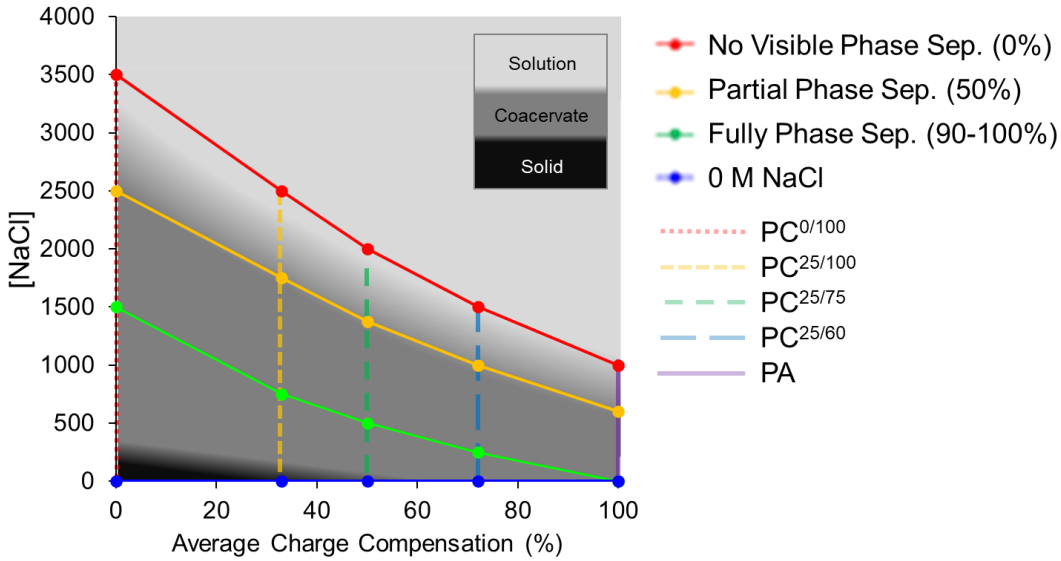

Figure 2.7. Phase diagram of high-MW PECs based on arrangement of charges (PA = 100, PE=0), approximated by the physical characteristics and behaviors observed at different [NaCl].

These experiments were then repeated for low-MW PECs for PA, $PC^{25/75}$, and $PC^{0/100}$ (Figure 2A.15). Here, all coacervates form spherical droplets at 0 M NaCl, reflecting the weaker polymer−polymer interactions at lower MW. The PECs follow similar trends to the high-MW PA, with greater [NaCl] shielding charges and reducing the viscosity. Furthermore, investigation into the effects of MW on these different charge arrangements may offer an improved mapping of the underlying interactions

2.4.6. ITC

Previous reports indicate that the ability to shed counterions and form coacervates depends strongly on charge arrangements.[28] ITC work for these types of systems use a two-step model to analyze the thermodynamics of coacervation,[27,54] separately modeling ion pairing and the coacervation process. However, this two-step modeling assumes anionic and cationic charges located on distinct polyanions and polycations. In the present work, intramolecular charge-balancing is included as the statistical PAs are capable of intrachain compensation. The interaction thermodynamics in PAs comprise the net result of counterion clustering together with competing intermolecular and intramolecular interactions; PAs complicate the interactions due to the self-neutralization of charged groups limiting the required counterion condensation.[55]

We used ITC to investigate the thermodynamics of coacervation for different charge arrangements, with summarized enthalpic and entropic contributions in Figure 2.8. The data confirm that while there is a small increase in enthalpy as charge separation is increased ($PC^{25/60} < PC^{25/75} < PC^{25/100} < PC^{0/100}$), complexation overall is driven by the

entropic dissociation of small counterions and water molecules, in accordance with the literature. Coacervation is an endothermic process,[54] which is confirmed by the positive enthalpy observed in each system during titration. Accordingly, the LCST behaviors exhibited by these PE pairs demonstrate that as energy is put into the system, the coacervation process becomes more favorable and overcomes the charge shielding and chain solvation.

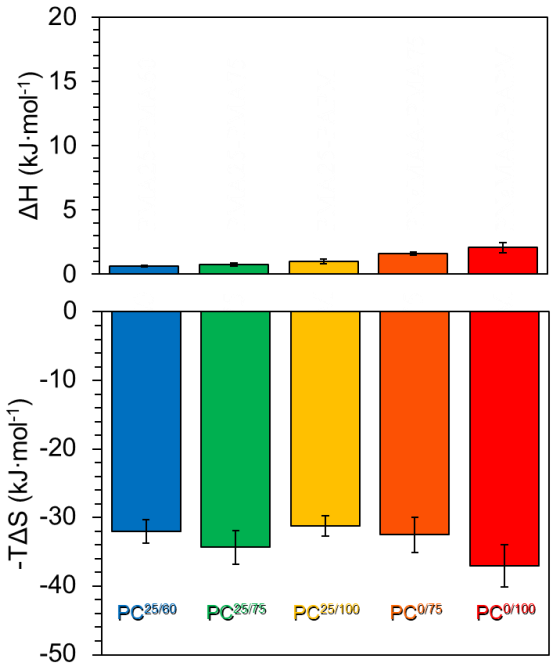

Figure 2.8. Enthalpic and entropic contributions of complex coacervation $PC^{25/60}$ to $PC^{0/100}$, using the model described by Bozelli et al.[34]

Previous work by Perry showed that as block lengths were increased and charges localized to larger segments, the entropic gain of coacervation increases due to counterion localization and release.[27–29] The copolymers prepared in the current work are not specifically designed with block lengths, but rather statistical distributions which generate

random domains of high charge localization as compositions trend from charge balanced PMA_{50} toward homopolymer PAs.

Although the present data are in agreement with previous reports, the reported trends of higher entropic gain during coacervation are not discernible due to greater uncertainties using more accessible, statistical copolymers. ITC investigation by Perry used sequence-controlled copolymers;[27,28] while our copolymers show little overall comonomer drift during copolymerization, there are statistical distributions of composition and MW. Further investigation may reveal comparable trends in entropic contributions of coacervation based on charge arrangement and adequately capture the effects of intramolecular self-neutralization interactions. ITC data can be found in Figures 2A.18 and 2A.19.

2.4.7. Complex Dye-Binding Assays

We next explored ionic dye binding of these coacervates, both to study coacervate properties and to elucidate their potential use in dye removal for textiles, which may further extend into use as controlled binding/release technologies. Dyes were selected to model ionic target molecules with different structures and charge at pH 7. Complexes of $PC^{25/75}$ and $PC^{0/100}$ show high binding affinities for BBG and trypan blue, while acriflavine and rhodamine B were not well bound, which is attributed to the single-charged nature of these molecules (Figures 2A.21−2A.22).[16] Dissociation of coacervates at high pH demonstrates these interactions are reversible (data not shown). Although all coacervates appear to have comparable binding affinity to the different dyes, the slightly lower binding affinity of PA complexes for BBG (Figure 2A.22) corresponds to their slightly lower phase separation

efficiency of roughly 80% at 300 mM NaCl. Although we previously showed that comonomer structure (hydrophobicity and charge type) and selection in PAs has a significant impact on the coacervate dye-binding affinity, loading capacity, and capture/release profiles,[16] this work demonstrates that coacervates of different charge arrangements with the same overall comonomer makeup have comparable binding abilities. Future work will be directed at exploring the ability to adjust selectivity of protein binding by adjusting charge separation.[56]

2.4.8. PMA_{51} and $PC^{25/75}$ Coacervates Cross-linked with Genipin

Freshly formed high-MW coacervates of PMA_{51} and $PC^{25/75}$ were then cross-linked using both 10 and 25 mol % genipin relative to total amine groups of each PEC.[14] The resulting colloidally stable cross-linked microgels were exposed to drastic pH and ionic strength changes to confirm covalent cross-linking (Figure 2A.20). Because of the prolonged reaction times required for genipin cross-linking, many of the coacervate microgels settle and aggregate during cross-linking.

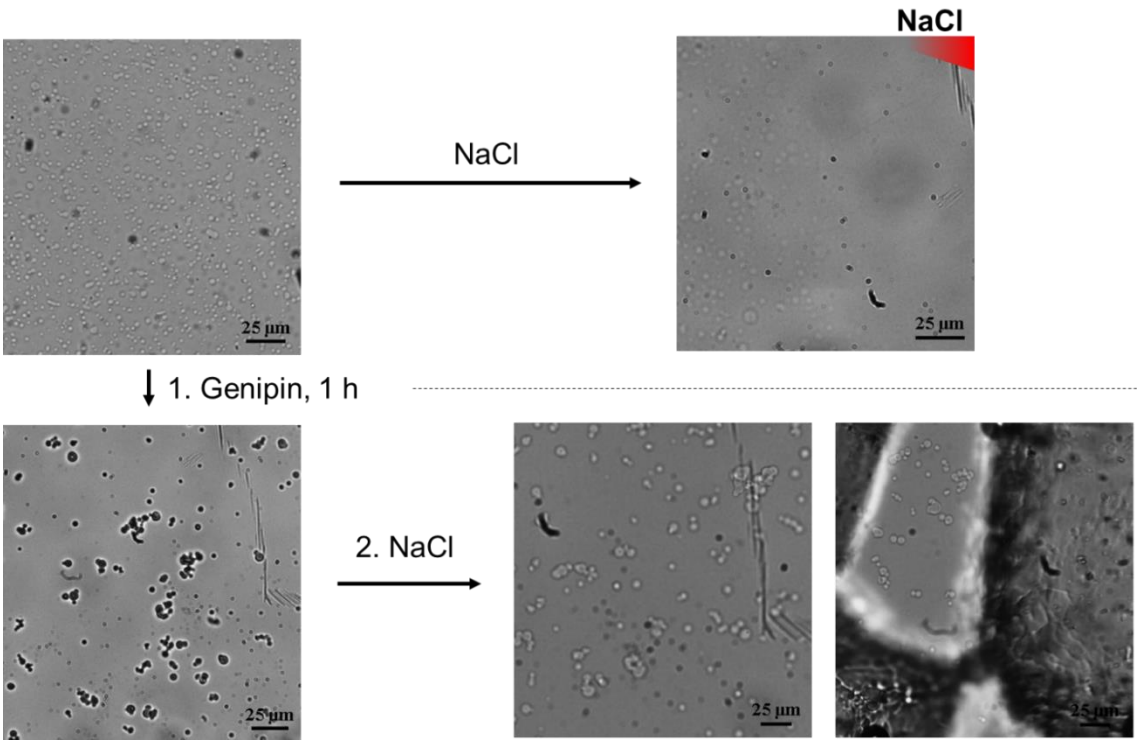

Figure 2.9. Coacervates of $PC^{25/75}$ are dissolved in the presence of an increased [NaCl] (top) but show complete resistance to 2 and 6 M (saturated) [NaCl] between solid NaCl crystals (right) when cross-linked with genipin (bottom).

After 30 min of cross-linking, these microgels can withstand increased ionic strength and presence of 1 M HCl without dissolving or dissociating (Figure 2.9). The degree of swelling and hydration is significantly greater in 10% as compared with 25% genipin cross-linked microgels.

$PC^{0/100}$ coacervates were not successfully cross-linked in the presence of 10 or 25% Genipin, but nearly dissolved at low pH and completely dissociated at higher NaCl. Limiting the presence of cross-linkable primary amines to the homopolymer polycation prevents intermolecular cross-links between strongly interacting polymers (polyanion−polycation); the PEC can only form cross-links between nearby P(APM) chains which proved insufficient to maintain the coacervate. In general, the inherent

binding/release properties of the prepared coacervates and their ability to form cross-linked microgels make these systems interesting candidates for capture/release of target molecules or drug delivery systems.

2.5. Conclusions

This work demonstrates that the arrangement of charges has a significant impact on the strength of PE complexes formed and the stimuli-responsiveness of the resulting PECs. Here, we have investigated the structure−property relationship of PEs using PAs and PEs formed using pH-controlled zero-drift free radical copolymerizations.

Using these PEs, phase-separated (complex) coacervates with a range of different pH(*I*) could be formed easily by mixing complementary nonstoichiometric PAs such as PMA_{25}- PMA_{60}, as an alternate route to coacervates with properties comparable to those of self-coacervates formed by phase separation of individual PAs.

We find that increasing the separation of charges from PA to homopolymer PEs increases the interaction strength and, hence, resistance to both salt and pH. Additionally, we show that liquid coacervates are accessible across the whole compositional space, from single stoichiometric PAs (PMA_{51}) through to homopolymer polyelectrolytes ($PC^{0/100}$), by adjusting [NaCl]. These conditions provide comparable physical characteristics and binding affinity, by freeing charged groups in the PECs through salt-shielding.

We also indicate that when the ionic strength is held constant, the arrangement of charges and consequent physical properties of the complexes have little effect on the ability to bind ionic small molecules, such as ionic dyes. Liquid coacervates formed under optimal

conditions can also be covalently cross-linked to form pH- and NaCl-resistant microgels which may be useful in capture or delivery of drugs or other molecules.

In future work, larger scale polymerizations with more cost-effective cationic monomers would facilitate experiments for salt-polymer phase diagrams for associative phase separation demonstrated by Spruijt et al.[23] Additionally, thermogravimetric analysis would facilitate study of the salt and water content of the individual PECs.[21] We have also identified the need for further exploration into the entropic contributions of complexation with these polymers, which may require more complex modeling to provide better interpretation of ITC data for these highly complex ionic interactions.

Supporting Information

GPC traces of polymers; characterization of low-MW polymers; forward turbidimetric titrations of individual PAs, forward/backward titrations of charge-balanced solutions of PMA_{51}, $PC^{25/60}$, $PC^{25/75}$, $PC^{25/100}$, $PC^{0/75}$, $PC^{0/100}$, and $PC^{0/25/75}$, and forward/backward charge-balanced solutions of low-MW complexes PMA_{52}, $PC^{25/75}$, and $PC^{0/100}$; pH insolubility ranges plotted for low-MW charge-balanced complexes; experimentally determined pH(*I*) plotted with respect to theoretical estimations based on composition; forward/backward turbidimetric titration of $PC^{0/100}$ solutions of different charge ratios; images of potentiometric/turbidimetric titrations through forward titration of $PC^{25/100}$; first-derivative plots of turbidimetric titrations; ^{1}H NMR spectra of polymer-dense phases of PA, $PC^{25/75}$, and $PC^{0/100}$ at optimal [NaCl]; phase separation efficiency for UV−vis absorbance curves of $PC^{0/100}$; image of $PC^{25/60}$ supernatants analyzed by UV−vis

absorbance; phase separation efficiency data for low-MW complexes; lower critical solution temperatures plotted against ionic strength for PA, $PC^{25/75}$, and $PC^{0/100}$; microscope images of coacervate fusion of PMA_{51} at 500 mM NaCl; microscope images of coacervates of low-MW coacervates at increasing NaCl; copper wire drag images; summarized ITC data collected for complex coacervates; genipin-cross-linked coacervates images through the pH change using HCl; and dye binding at 300 mM NaCl for PA, $PC^{25/75}$, and $PC^{0/100}$.

Author Information

Corresponding Author

Email: stoverh@mcmaster.ca, Ph.: 1-905-525-9140 ext. 24983.

Notes:

The authors declare no competing financial interest.

2.6. Acknowledgements

The authors would like to thank the Natural Sciences and Engineering Research Council of Canada for funding this research through its Discovery Grant program (RGPIN89661-11 and RGPIN-2018-05585), and through the PGS-D award held by D. E. Hastings. The authors would like to thank Ryan Wylie for the use of his equipment (Agilent GPC). The authors would also like to thank both Nick Burke and Jing Zhao for their insight and expertise in PE/PA systems, and Alex Jesmer for assisting with Agilent GPC experiments. Finally, the authors would like to thank Carl Ellis for his assistance with general equipment maintenance and operation.

2.7. References

1. Luo, F.; Sun, T. L.; Nakajima, T.; Kurokawa, T.; Zhao, Y.; Sato, K.; Ihsan, A. B.; Li, X.; Guo, H.; Gong, J. P. Oppositely Charged Polyelectrolytes Form Tough, Self-Healing and Rebuildable Hydrogels. *Adv. Mater.* **2015**, *27*, 2722−2727.

2. Sun, T. L.; Kurokawa, T.; Kuroda, S.; Ihsan, A. B.; Akasaki, T.; Sato, K.; Haque, M. A.; Nakajima, T.; Gong, J. P. Physical hydrogels composed of polyampholytes demonstrate high toughness and viscoelasticity. *Nat. Mater.* **2013**, *12*, 932−937.

3. Kabanov, A. V.; Kabanov, V. A. Interpolyelectrolyte and block ionomer complexes for gene delivery: physico-chemical aspects. *Adv. Drug Delivery Rev.* **1998**, *30*, 49−60.

4. Ahn, B. K.; Das, S.; Linstadt, R.; Kaufman, Y.; Martinez-Rodriguez, N. R.; Mirshafian, R.; Kesselman, E.; Talmon, Y.; Lipshutz, B. H.; Israelachvili, J. N.; Waite, J. H. High-performance mussel-inspired adhesives of reduced complexity. *Nat. Commun.* **2015**, *6*, 8663.

5. Shao, H.; Stewart, R. J. Biomimetic Underwater Adhesives with Environmentally Triggered Setting Mechanism. *Adv. Mater.* **2010**, *22*, 729−733.

6. Dompé, M.; Cedano-Serrano, F. J.; Vahdati, M.; Westerveld, L.; Hourdet, D.; Creton, C.; Gucht, J.; Kodger, T.; Kamperman, M. Underwater Adhesion of Multiresponsive Complex Coacervates. *Adv. Mater. Interfaces* **2020**, *7*, 1901785.

7. Hastings, D. E.; Stöver, H. D. H. Crosslinked Hydrogel Capsules for Cell Encapsulation Formed Using Amino/Betaine Dual-Functional Semibatch Copolymers. *ACS Appl. Polym. Mater.* **2019**, *1*, 2055−2067.

8. Ros, S.; Burke, N. A. D.; Stöver, H. D. H. Synthesis and Properties of Charge-Shifting Polycations: Poly[3-aminopropylmethacrylamide-*co*-2-(dimethylamino)ethyl acrylate]. *Macromolecules* **2015**, *48*, 8958−8970.

9. Lin, Y.-H.; Brady, J. P.; Chan, H. S.; Ghosh, K. A unified analytical theory of heteropolymers for sequence-specific phase behaviors of polyelectrolytes and polyampholytes. *J. Chem. Phys.* **2020**, *152*, 045102.

10. Bjellqvist, B.; Basse, B.; Olsen, E.; Celis, J. E. Reference points for comparisons of two-dimensional maps of proteins from different human cell types defined in a pH scale where isoelectric points correlate with polypeptide compositions. *Electrophoresis* **1994**, *15*, 529−539.

11. Dubey, A.; Burke, N. A. D.; Stöver, H. D. H. Preparation and Characterization of Narrow Compositional Distribution Polyampholytes as Potential Biomaterials: Copolymers of *N*-(3-Aminopropyl)-methacrylamide Hydrochloride (APM) and Methacrylic Acid (MAA). *J. Polym. Sci., Part A: Polym. Chem.* **2015**, *53*, 353−365.

12. Edwards, S. F.; King, P. R.; Pincus, P. Phase changes in polyampholytes. *Ferroelectrics* **1980**, *30*, 3−6.

13. Ulrich, S.; Seijo, M.; Stoll, S. A Monte Carlo study of weak polyampholytes: stiffness and primary structure influences on titration curves and chain conformations. *J. Phys. Chem. B* **2007**, *111*, 8459−8467.

14. Abdilla, A.; Shi, S.; Burke, N. A. D.; Stöver, H. D. H. Multistimuli Responsive Ternary Polyampholytes: Formation and Crosslinking of Coacervates. *J. Polym. Sci., Part A: Polym. Chem.* **2016**, *54*, 2109−2118.

15. Zhao, J.; Burke, N. A. D.; Stöver, H. D. H. Preparation and study of multi-responsive polyampholyte copolymers of *N*-(3-aminopropyl)methacrylamide hydrochloride and acrylic acid. *RSC Adv.* **2016**, *6*, 41522−41531.

16. Zhao, J. Synthesis and Properties of Polyampholyte and Their Application to Cell Cryoprotection. Ph.D. Dissertation, McMaster University, Hamilton, ON, 2018.

17. Overbeek, J. T. G.; Voorn, M. J. Phase Separation in Polyelectrolyte Solutions. Theory of Complex Coacervation. *J. Cell. Comp. Physiol.* **1957**, *49*, 7−26.

18. Sing, C. E.; Perry, S. L. Recent Progress in the Science of Complex Coacervation. *Soft Matter* **2020**, *16*, 2885.

19. Chollakup, R.; Smitthipong, W.; Eisenbach, C. D.; Tirrell, M. Phase Behavior and Coacervation of Aqueous Poly(acrylic acid)-Poly(allylamine) Solutions. *Macromolecules* **2010**, *43*, 2518−2528.

20. Perry, S.; Li, Y.; Priftis, D.; Leon, L.; Tirrell, M. The Effect of Salt on the Complex Coacervation of Vinyl Polyelectrolytes. *Polymers* **2014**, *6*, 1756−1772.

21. Meng, S.; Ting, J. M.; Wu, H.; Tirrell, M. V. Solid-to-Liquid Phase Transition in Polyelectrolyte Complexes. *Macromolecules* **2020**, *53*, 7944−7953.

22. Priftis, D.; Xia, X.; Margossian, K. O.; Perry, S. L.; Leon, L.; Qin, J.; de Pablo, J. J.; Tirrell, M. Ternary, Tunable Polyelectrolyte Complex Fluids Driven by Complex Coacervation. *Macromolecules* **2014**, *47*, 3076−3085.

23. Spruijt, E.; Westphal, A. H.; Borst, J. W.; Cohen Stuart, M. A.; van der Gucht, J. Binodal Compositions of Polyelectrolyte Complexes. *Macromolecules* **2010**, *43*, 6476−6484.

24. Wang, Q.; Schlenoff, J. B. The Polyelectrolyte Complex/Coacervate Continuum. *Macromolecules* **2014**, *47*, 3108−3116.

25. Kudaibergenov, S. E.; Bekturov, E. A. Influence of the coil-globule conformational transition in polyampholytes on sorption and desorption of polyelectrolytes and human serum albumin. *Vysokomol. Soedin., Ser. A* **1989**, *31*, 2870−2874.

26. Jeon, J.; Dobrynin, A. V. Molecular Dynamics Simulations of Polyampholyte-Polyelectrolyte Complexes in Solutions. *Macromolecules* **2005**, *38*, 5300−5312.

27. Chang, L.-W.; Lytle, T. K.; Radhakrishna, M.; Madinya, J. J.; Vélez, J.; Sing, C. E.; Perry, S. L. Sequence and entropy-based control of complex coacervates. *Nat. Commun.* **2017**, *8*, 1273.

28. Madinya, J. J.; Chang, L.-W.; Perry, S. L.; Sing, C. E. Sequence-Dependent Self-Coacervation in High Charge-Density Polyampholytes. *Mol. Syst. Des. Eng.* **2020**, *5*, 632−644.

29. Lytle, T. K.; Chang, L.-W.; Markiewicz, N.; Perry, S. L.; Sing, C. E. Designing Electrostatic Interactions via Polyelectrolyte Monomer Sequence. *ACS Cent. Sci.* **2019**, *5*, 709−718.

30. Patrickios, C. S.; Hertler, W. R.; Abbott, N. L.; Hatton, T. A. Diblock, ABC Triblock, and Random Methacrylic Polyampholytes: Synthesis by Group Transfer Polymerization and Solution Behaviour. *Macromolecules* **1994**, *27*, 930−937.

31. McCarty, J.; Delaney, K. T.; Danielsen, S. P. O.; Fredrickson, G. H.; Shea, J.-E. Complete Phase Diagram for Liquid-Liquid Phase Separation of Intrinsically Disordered Proteins. *J. Phys. Chem. Lett.* **2019**, *10*, 1644−1652.

32. Goloub, T.; de Keizer, A.; Cohen Stuart, M. A. Association behavior of ampholytic diblock copolymers. *Macromolecules* **1999**, *32*, 8441−8446.

33. Rumyantsev, A. M.; Jackson, N. E.; Yu, B.; Ting, J. M.; Chen, W.; Tirrell, M. V.; de Pablo, J. J. Controlling Complex Coacervation via Random Polyelectrolyte Sequences. *ACS Macro Lett.* **2019**, *8*, 1296−1302.

34. Bozelli, J. C.; Yune, J.; Dang, X.; Narayana, J. L.; Wang, G.; Epand, R. M. Membrane activity of two short Trp-rich amphipathic peptides. *Biochim. Biophys. Acta, Biomembr.* **2020**, *1862*, 183280.

35. Zhang, R.; Shklovskii, B. I. Phase diagram of solution of oppositely charged polyelectrolytes. *Phys. A* **2005**, *352*, 216−238.

36. Spruijt, E.; Cohen Stuart, M. A.; van der Gucht, J. Linear Viscoelasticity of Polyelectrolyte Complex Coacervates. *Macromolecules* **2013**, *46*, 1633−1641.

37. Priftis, D.; Tirrell, M. Phase behaviour and complex coacervation of aqueous polypeptide solutions. *Soft Matter* **2012**, *8*, 9396−9405.

38. Smeets, N. M. B.; Hoare, T. Designing Responsive Microgels for Drug Delivery Applications. *J. Polym. Sci., Part A: Polym. Chem.* **2013**, *51*, 3027−3043.

39. Asgeirsson, D.; Venturoli, D.; Rippe, B.; Rippe, C. Increased glomerular permeability to negatively charged Ficoll relative to neutral Ficoll in rats. *Am. J. Physiol. Renal Physiol.* **2006**, *291*, F1083−F1089.

40. Neitzel, A. E.; De Hoe, G. X.; Tirrell, M. V. Expanding the structural diversity of polyelectrolyte complexes and polyzwitterions. *Curr. Opin. Solid State Mater. Sci.* **2021**, *25*, 100897.

41. Philipp, B.; Dautzenberg, H.; Linow, K.-J.; Kötz, J.; Dawydoff, W. Polyelectrolyte Complexes − Recent Developments and Open Problems. *Prog. Polym. Sci.* **1989**, *14*, 91−172.

42. Srivastava, S.; Tirrell, M. V. Polyelectrolyte Complexation. *Adv. Chem. Phys.* **2016**, *161*, 499−544.

43. Patrickios, C. S. Polypeptide amino acid composition and isoelectric point: 1. A closed-form approximation. *J. Colloid Interface Sci.* **1995**, *175*, 256−260.

44. Mattison, K. W.; Dubin, P. L.; Brittain, I. J. Complex Formation between Bovine Serum Albumin and Strong Polyelectrolytes: Effect of Polymer Charge Density. *J. Phys. Chem. B* **1998**, *102*, 3830−3836.

45. Weinbreck, F.; de Vries, R.; Schrooyen, P.; de Kruif, C. G. Complex Coacervation of Whey Proteins and Gum Arabic. *Biomacromolecules* **2003**, *4*, 293−303.

46. Patrickios, C. S.; Hertler, W. R.; Hatton, T. A. Protein Complexation with Acrylic Polyampholytes. *Biotechnol. Bioeng.* **1994**, *44*, 1031−1039.

47. Liu, S.; Low, N. H.; Nickerson, M. T. Effect of pH, Salt, and Biopolymer Ratio on the Formation of Pea Protein Isolate-Gum Arabic Complexes. *J. Agric. Food Chem.* **2009**, *57*, 1521−1526.

48. Chen, W.-Y.; Alexandridis, P.; Su, C.-K.; Patrickios, C. S.; Hertler, W. R.; Hatton, T. A. Effect of Block Size and Sequence on the Micellization of ABC Triblock Methacrylic Polyampholytes. *Macromolecules* **1995**, *28*, 8604−8611.

49. Tanaka, M.; Tanaka, T. Clumps of randomly charged polymers: Molecular dynamics simulation of condensation, crystallization, and swelling. *Phys. Rev. E: Stat. Phys., Plasmas, Fluids, Relat. Interdiscip. Top.* **2000**, *62*, 3803−3816.

50. Higgs, P. G.; Joanny, J. F. Theory of polyampholyte solutions. *J. Chem. Phys.* **1991**, *94*, 1543−1554.

51. Dobryin, A. V.; Rubinstein, M. Flory Theory of a Polyampholyte Chain. *J. Phys. II* **1995**, *5*, 677−695.

52. Chollakup, R.; Beck, J. B.; Dirnberger, K.; Tirrell, M.; Eisenbach, C. D. Polyelectrolyte Molecular Weight and Salt Effects on the Phase Behavior and Coacervation of Aqueous Solutions of Poly(acrylic acid) Sodium Salt and Poly(allylamine) Hydrochloride. *Macromolecules* **2013**, *46*, 2376−2390.

53. Das, E.; Matsumura, K. Tunable Phase-Separation Behavior of Thermoresponsive Polyampholytes Through Molecular Design. *J. Polym. Sci., Part A: Polym. Chem.* **2017**, *55*, 876−884.

54. Priftis, D.; Laugel, N.; Tirrell, M. Thermodynamic Characterization of Polypeptide Complex Coacervation. *Langmuir* **2012**, *28*, 15947−15957.

55. Blocher, W. C.; Perry, S. L. Protein Encapsulation Using Complex Coacervates: What Nature Has to Teach Us. *Small* **2020**, *16*, 1907671.

56. Black, K. A.; Priftis, D.; Perry, S. L.; Yip, J.; Byun, W. Y.; Tirrell, M. Protein Encapsulation via Polypeptide Complex Coacervation. *ACS Macro Lett.* **2014**, *3*, 1088−1091.

2.8. Appendix

Figure 2A.1. GPC traces of polyelectrolytes.

I) Normalized GPC traces for PMA_{51}, PMA_{60}, PMA_{75}, P(APM) using Waters GPC (pH 7.4).

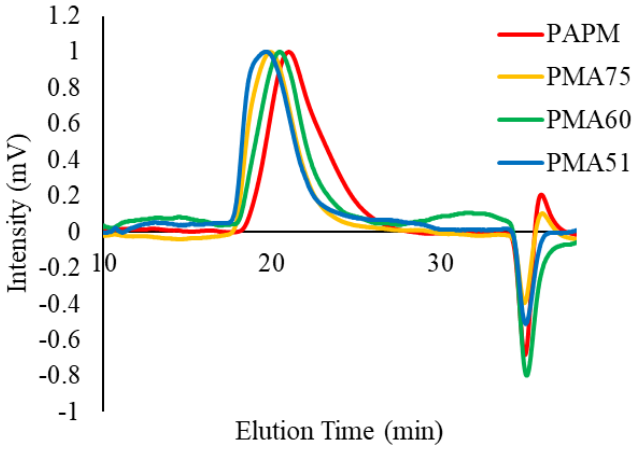

II) Normalized GPC trace for PMA_{25} using Agilent GPC (pH 9.4).

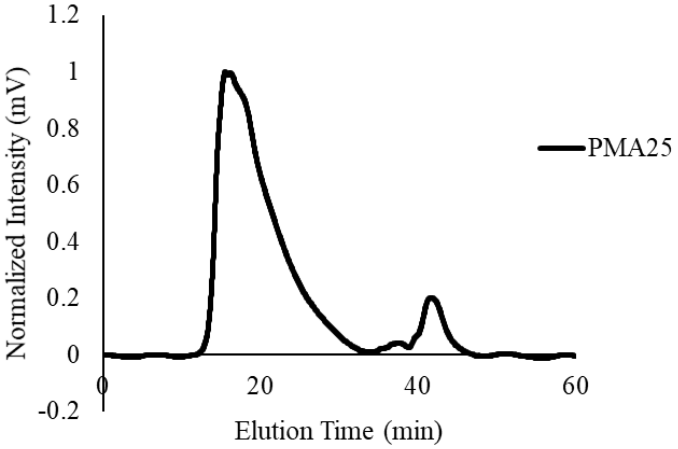

III) Normalized GPC traces for low MW polymers using Waters GPC (pH 4.7).

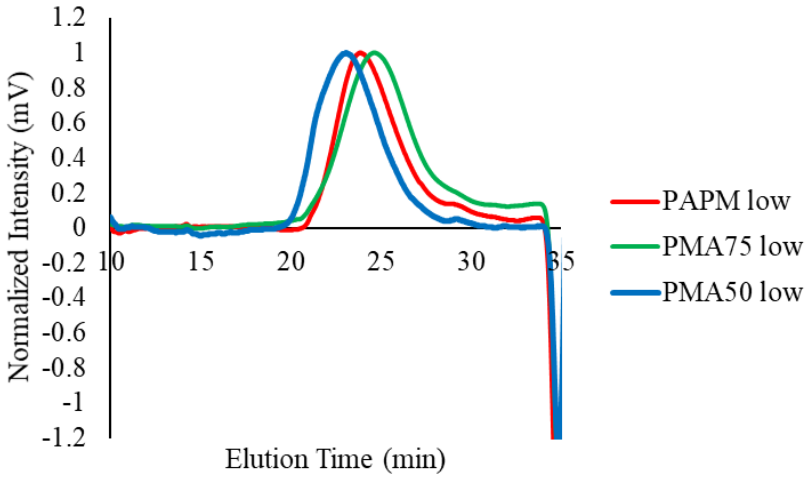

IV) Normalized GPC trace for low MW PMA_{25} using Agilent GPC (pH 9.4).

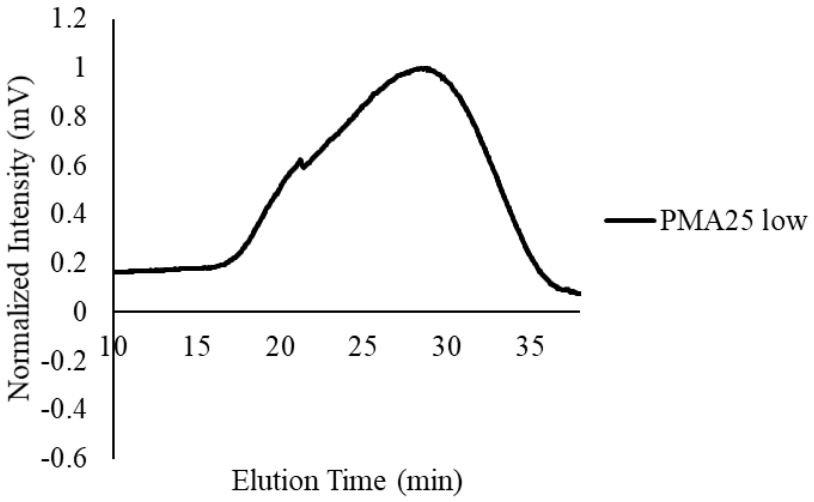

Figure 2A.2. Turbidimetric titration curves – forward titrations of synthesized polyampholytes.

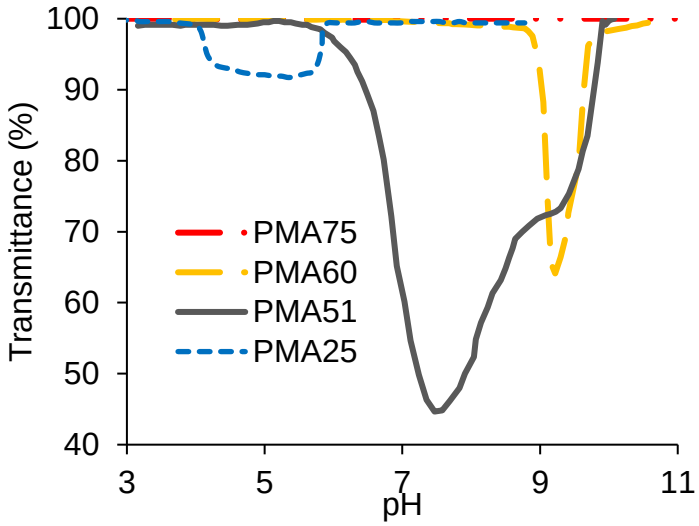

Figure 2A.3. Turbidimetric titration curves – 1:1 charge balanced complexes.

I) PMA_{51}

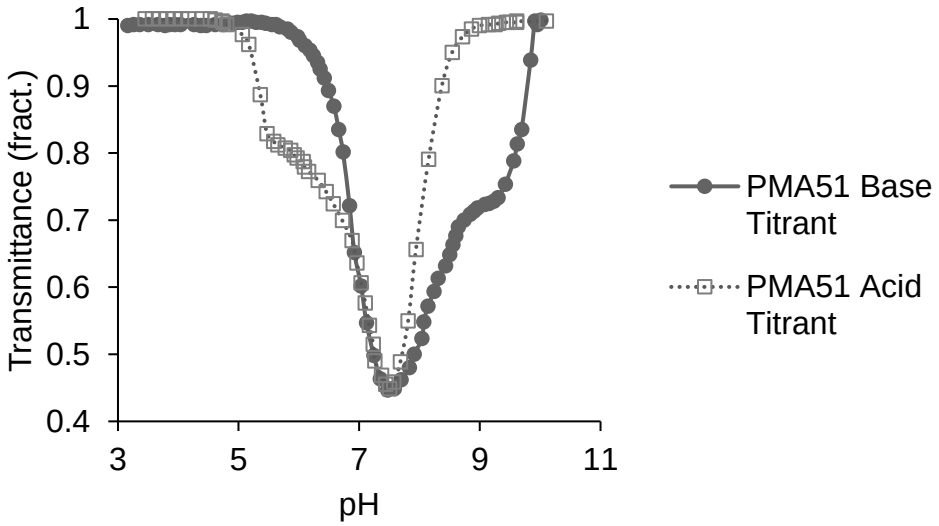

II) PMA_{25}-PMA_{60}

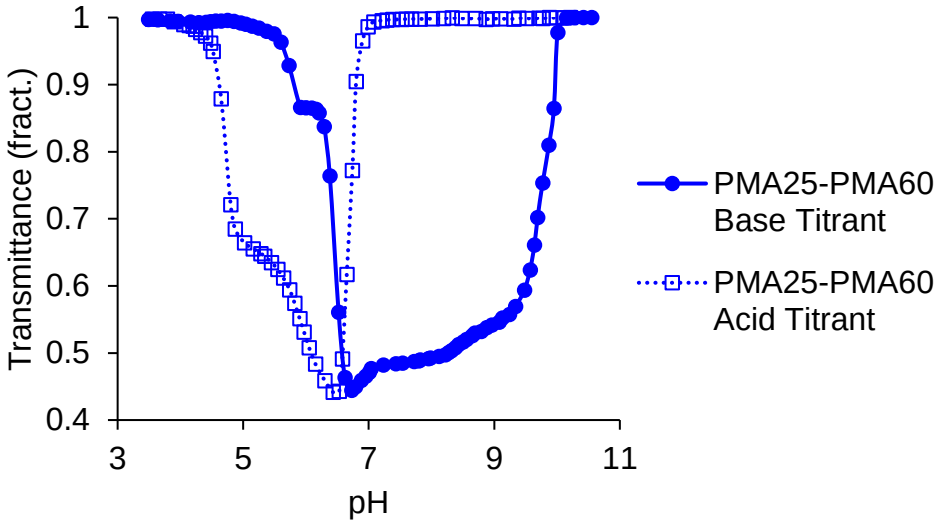

III) PMA_{25}-PMA_{75}

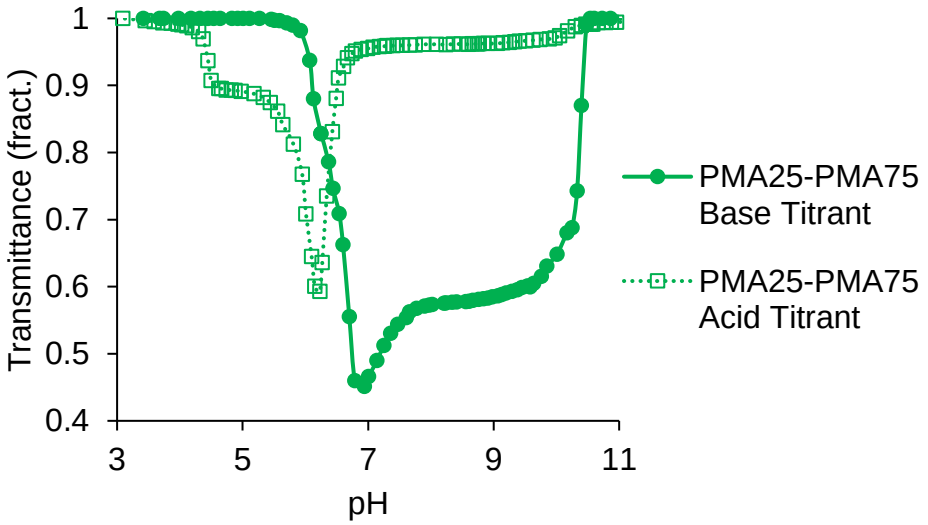

IV) PMA_{25}-P(APM)

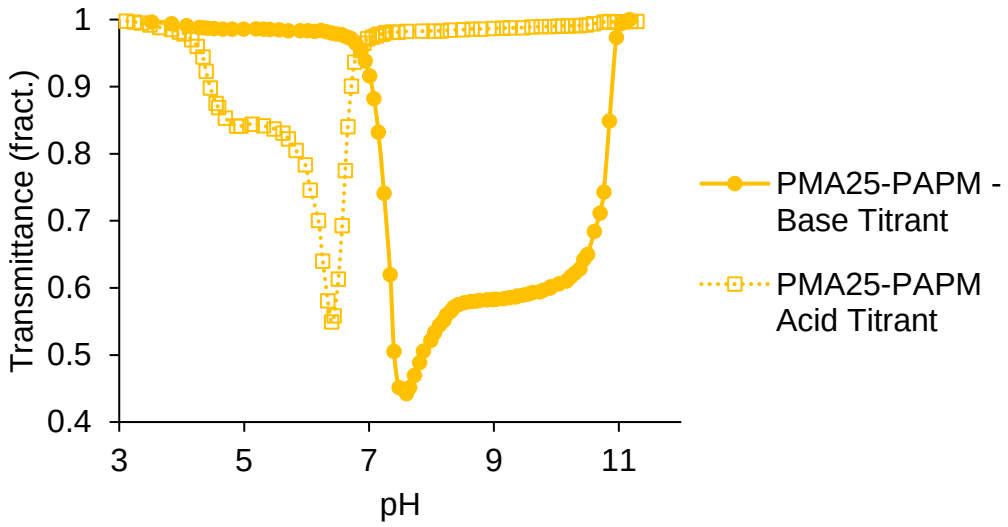

V) P(NaMAA)-PMA_{75}

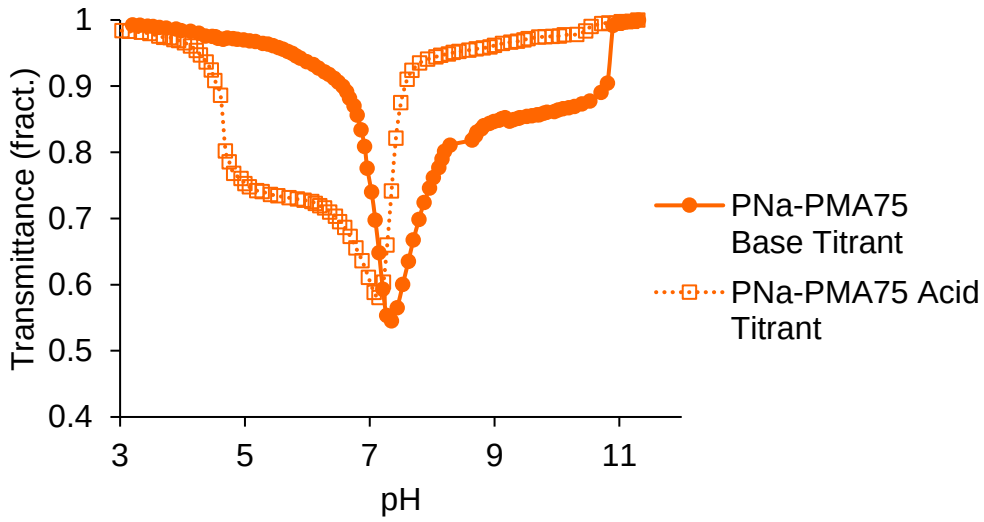

VI) P(NaMAA)-P(APM)

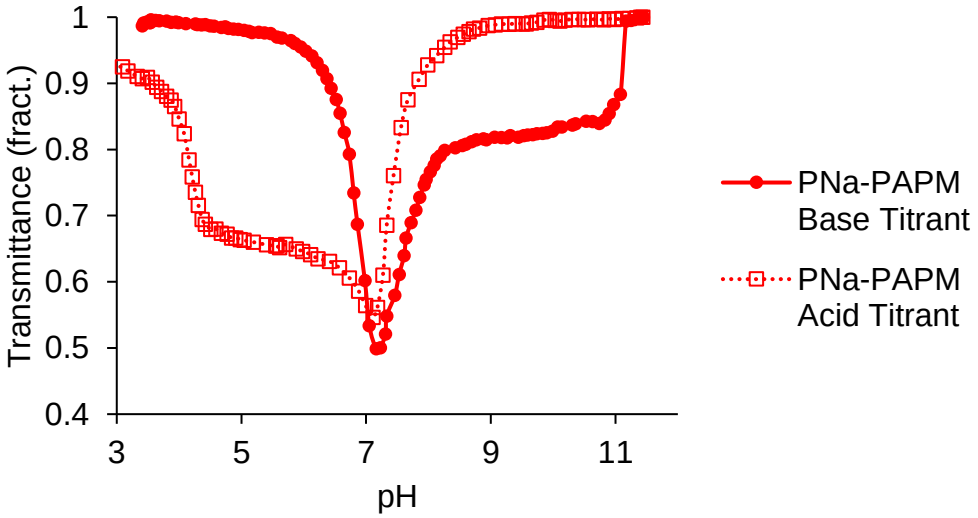

VII) P(NaMAA)-PMA_{25}-PMA_{75}

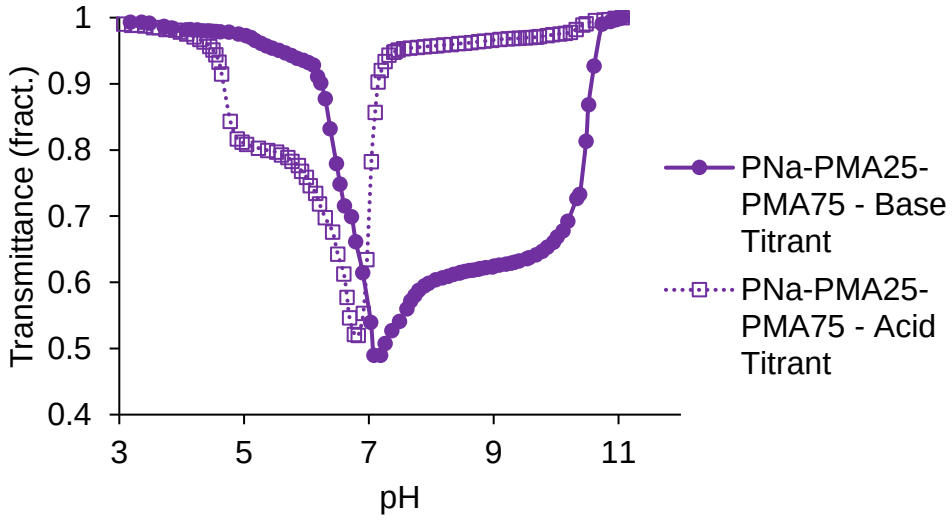

IX) PMA_{52} low MW

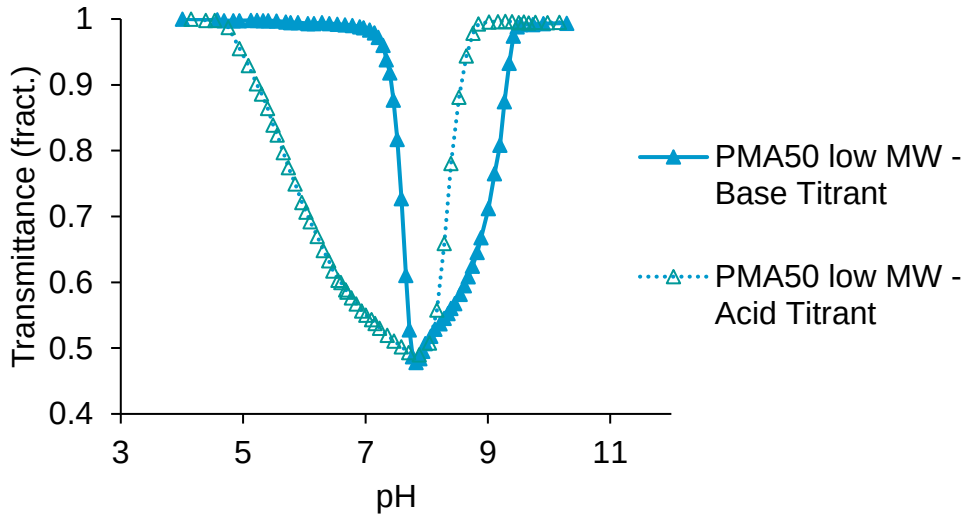

X) PMA_{25}-PMA_{75} low MW

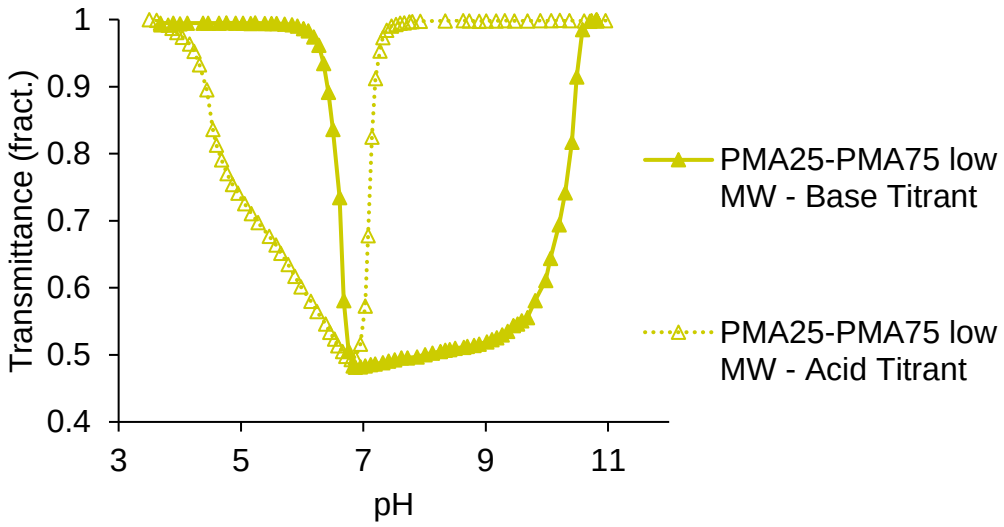

XI) P(NaMAA)-P(APM) low MW

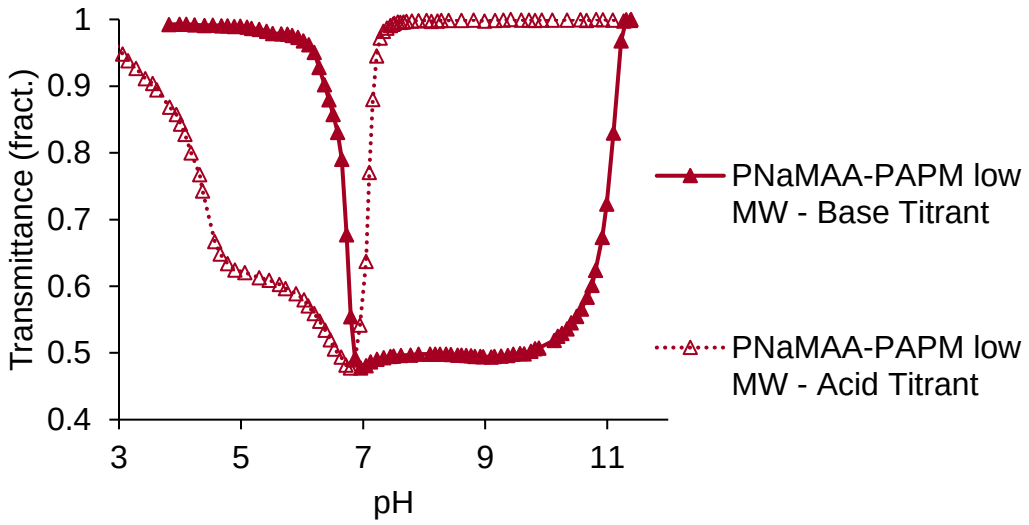

Figure 2A.4. Complex compositions approximated by pH(*I*) in polyampholytes of MAA-APM:

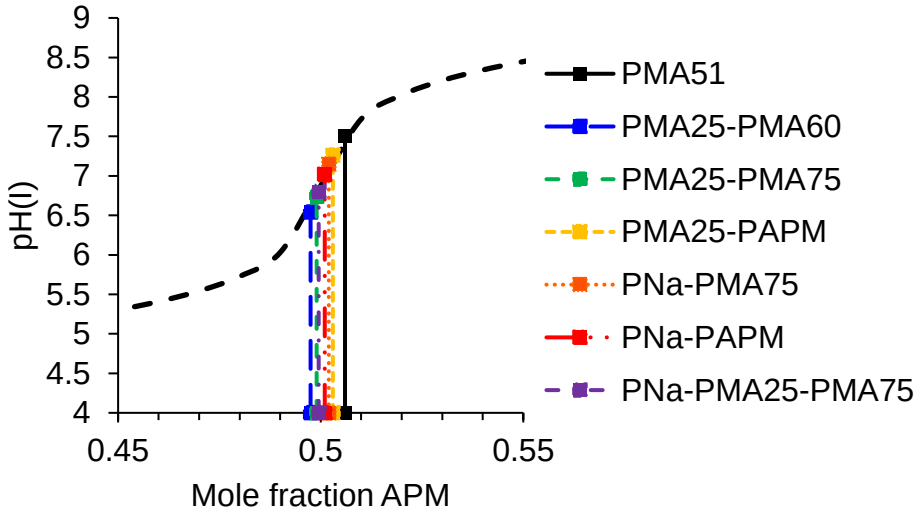

Dashed line represents the approximated isoelectric points of MAA-APM polyampholytes based on compositions and pK_a/pK_b values by equation (**2.2**).

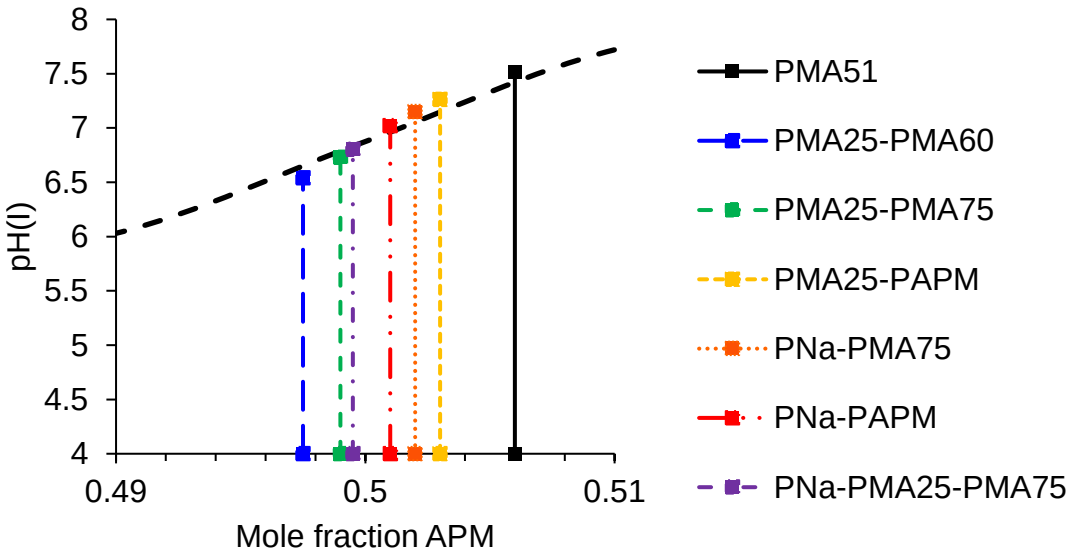

pH(*I*) of complexes are very close to predicted stoichiometric polyampholytes.

Figure 2A.5. Non-stochiometric turbidimetric titrations of P(NaMAA)-P(APM) (forward – solid; backward – dashed).

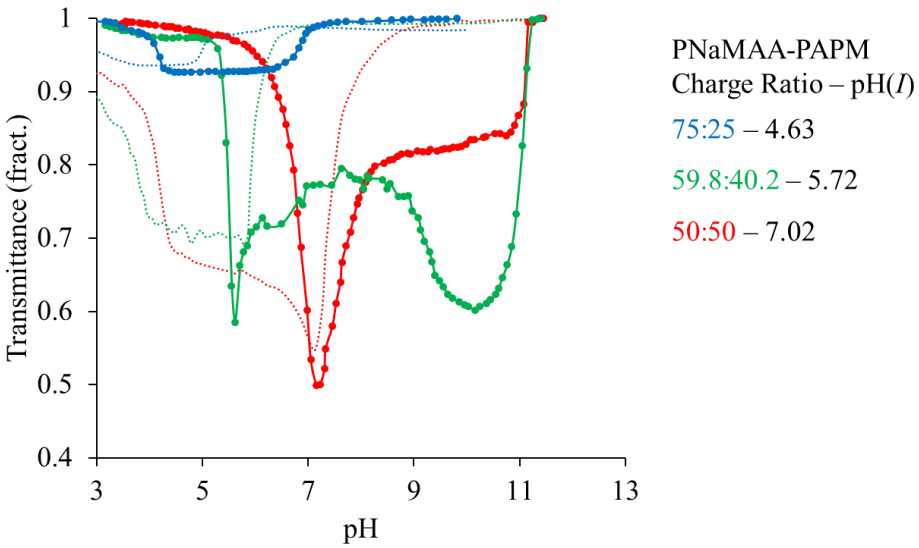

Figure 2A.6. Forward titration of PMA_{25}-P(APM) at a charge ratio of 48.5:51.5 MAA:APM, illustrating clear polymer solution at low pH (**A.**), max. turbidity at pH ~ 8.7 (**B.**), and slow dissolution of complexes (**C., D., E.**) as pH approaches pH 11.

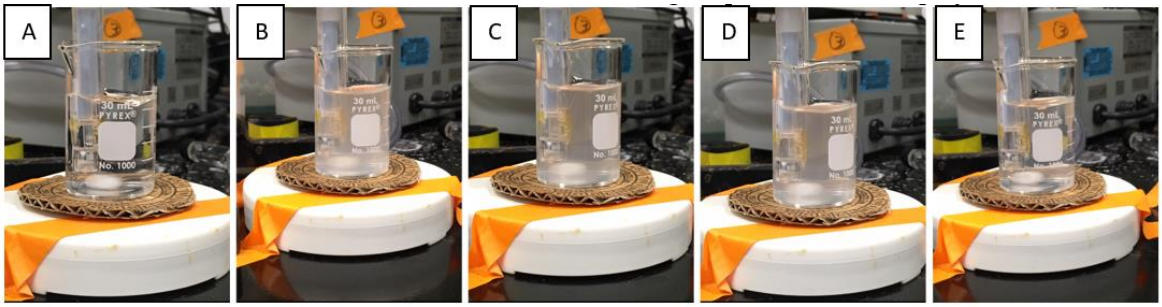

Figure 2A.7. First derivative plots of turbidimetric titrations (forward – blue/solid; backward – orange/dashed).

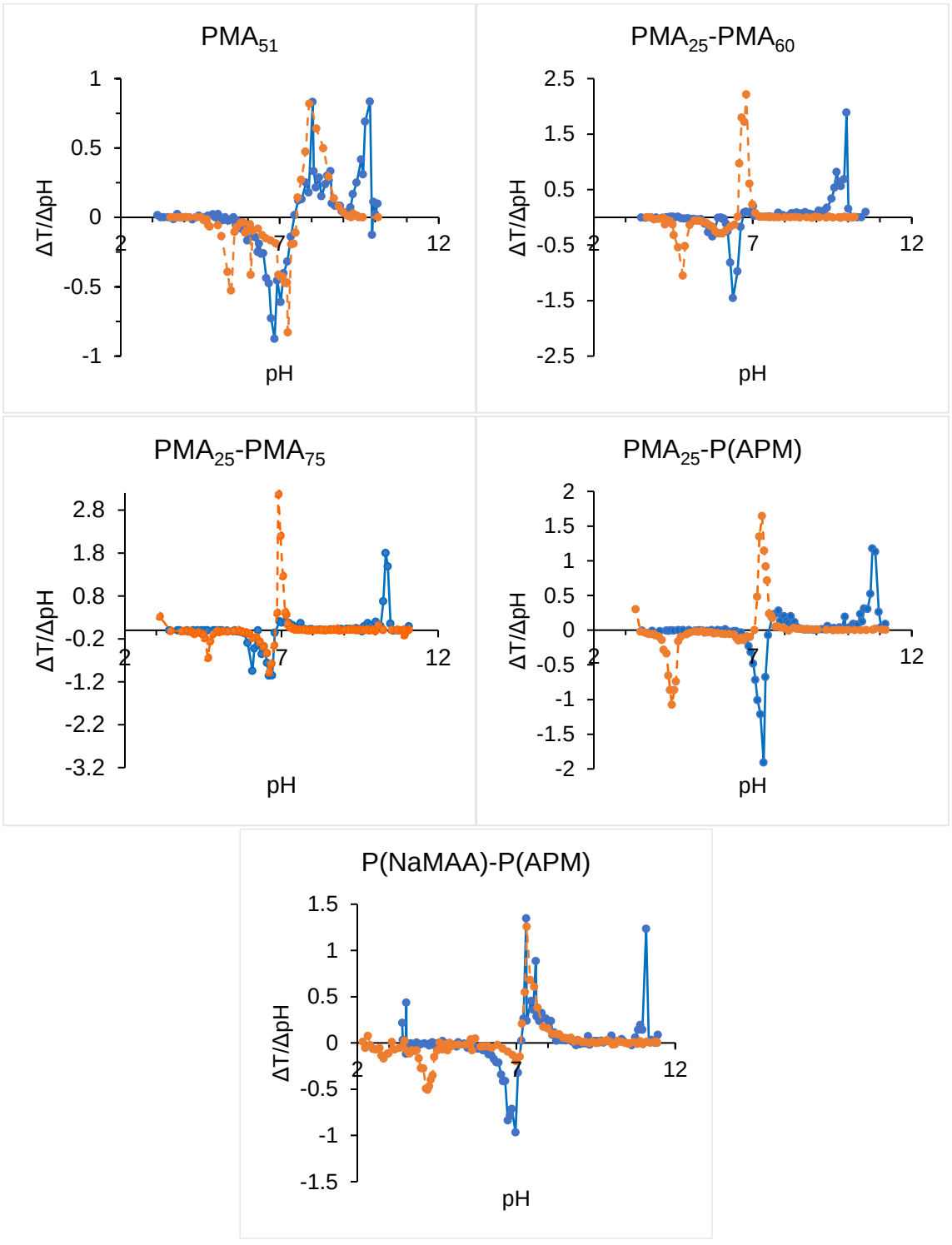

Figure 2A.8. Phase separation – ^{1}H NMR of 1:1 stoichiometric complexes.

I) PMA_{51} in D_2O/DCl

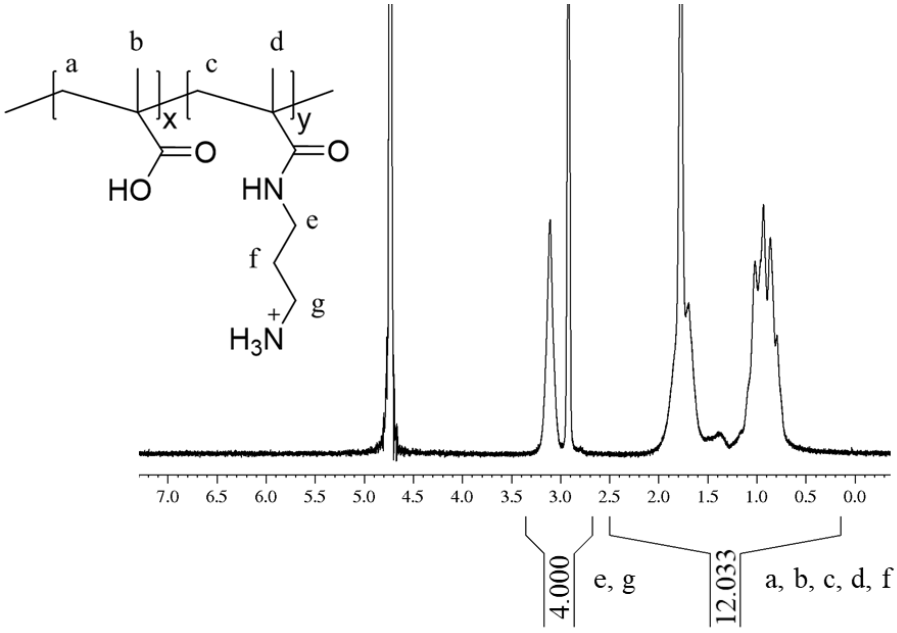

II) PMA_{25}-PMA_{75} complex in D_2O/DCl

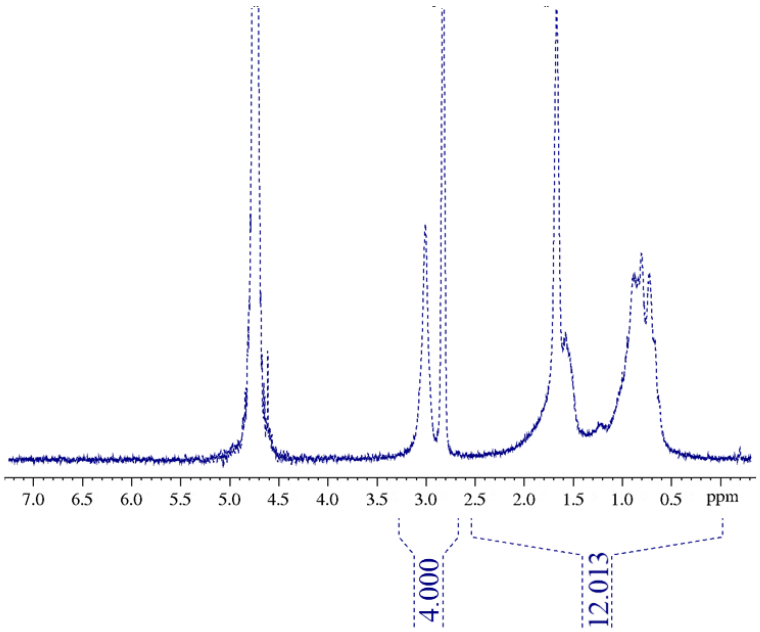

III) P(NaMAA)-P(APM) complex in D_2O/DCl

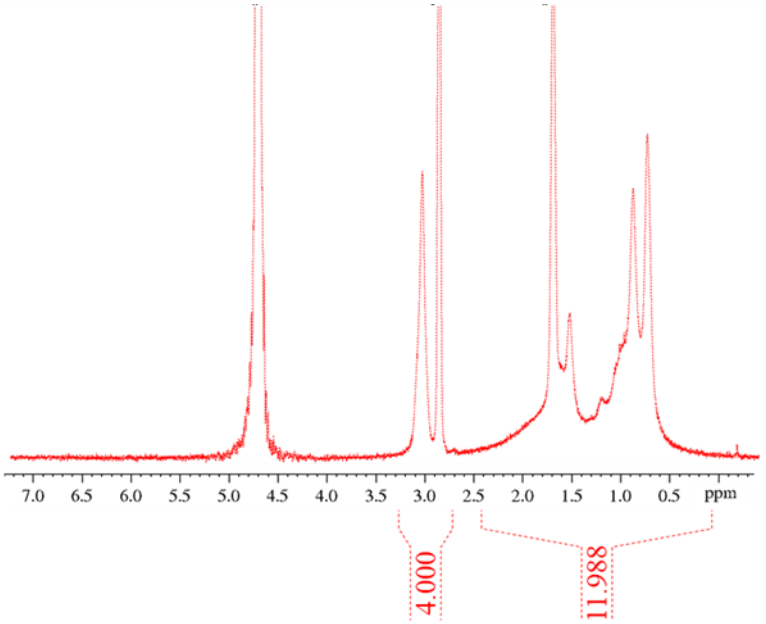

^{1}H NMR spectra of the isolated polymer-rich phases confirm that the complexes are formed at 1:1 charge ratios, by comparing the integrations of polymer sidechain and backbone signals to those of the inherently stoichiometric polyampholyte (PMA_{51}).

Figure 2A.9. Phase Separation Efficiency – UV-vis Data: P(NaMAA)-P(APM)-*f*.

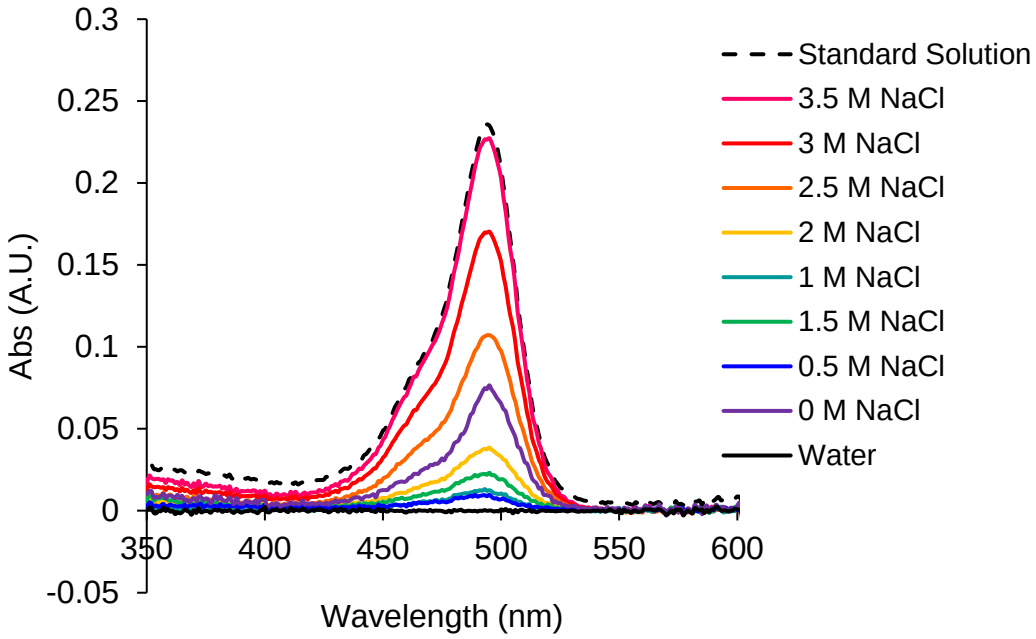

Figure 2A.10. Phase separation efficiency supernatants (PMA_{25}-$PMA_{60\text{-}f}$).

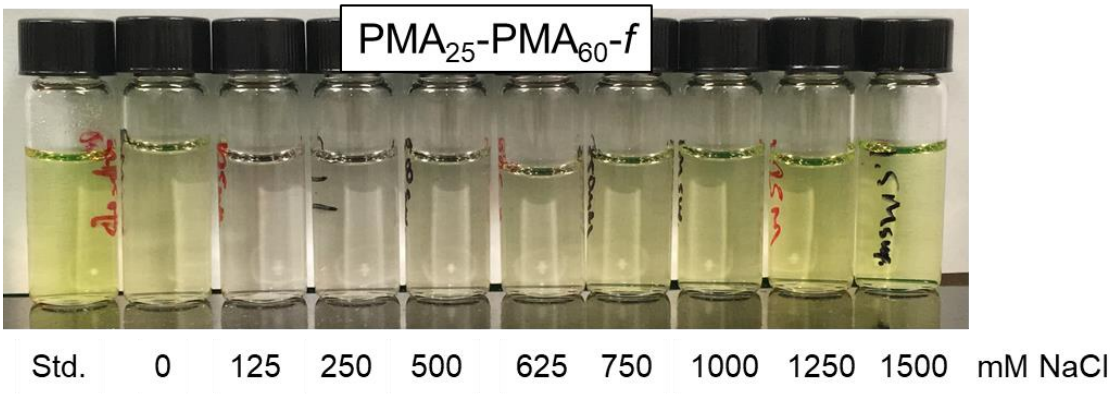

Supernatants show presence (colour) or absence (clear) or PMA_{60}-*f* based on ionic strength after complexation and centrifugation to remove PEC from solution.

Figure 2A.11. Phase separation efficiency of low MW polyelectrolytes.

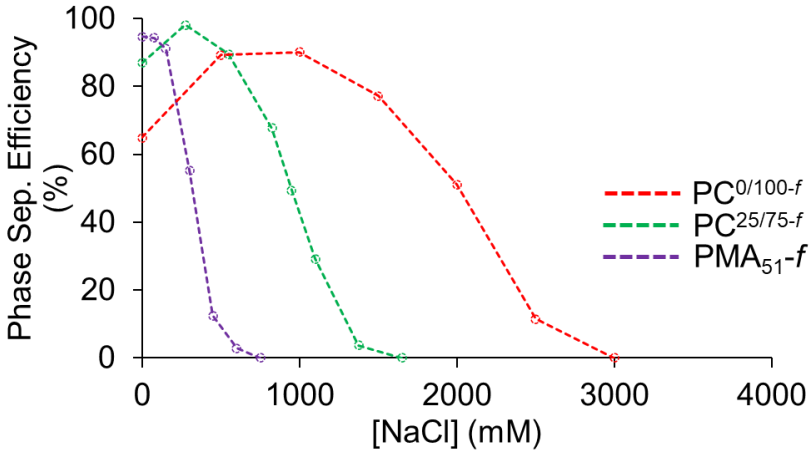

Figure 2A.12. LCST values of PA, $PC^{25/75}$ and $PC^{0/100}$ show reduced sensitivity to increasing [NaCl] with charge separation.

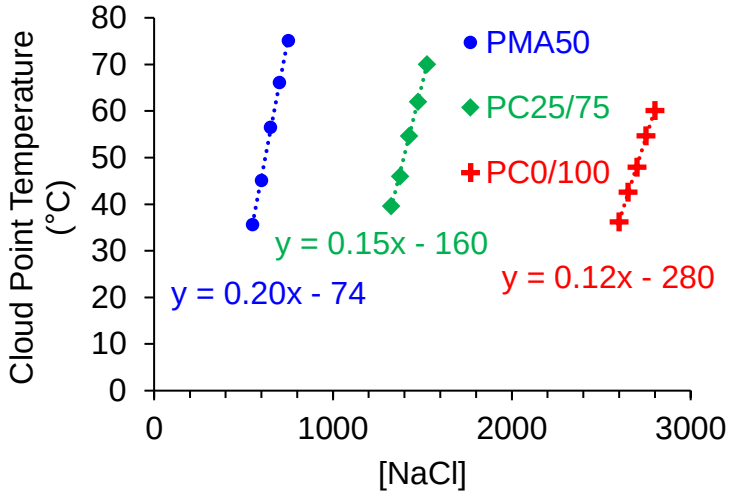

Figure 2A.13. PMA_{51} coacervates at 500 mM NaCl show rapid fusion of droplets

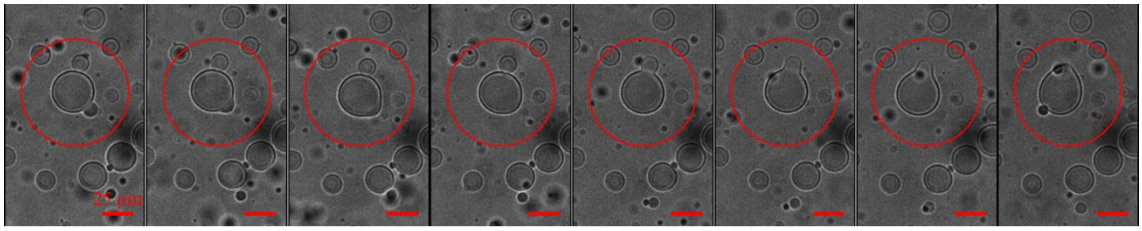

Scale bar – 25 µm

Figure 2A.14. Bright field microscope images of $PC^{25/60}$ and $PC^{25/100}$ with 0 mM NaCl, and at levels corresponding with phase separation data for high (>90%) and moderate coacervation efficiency (60%).

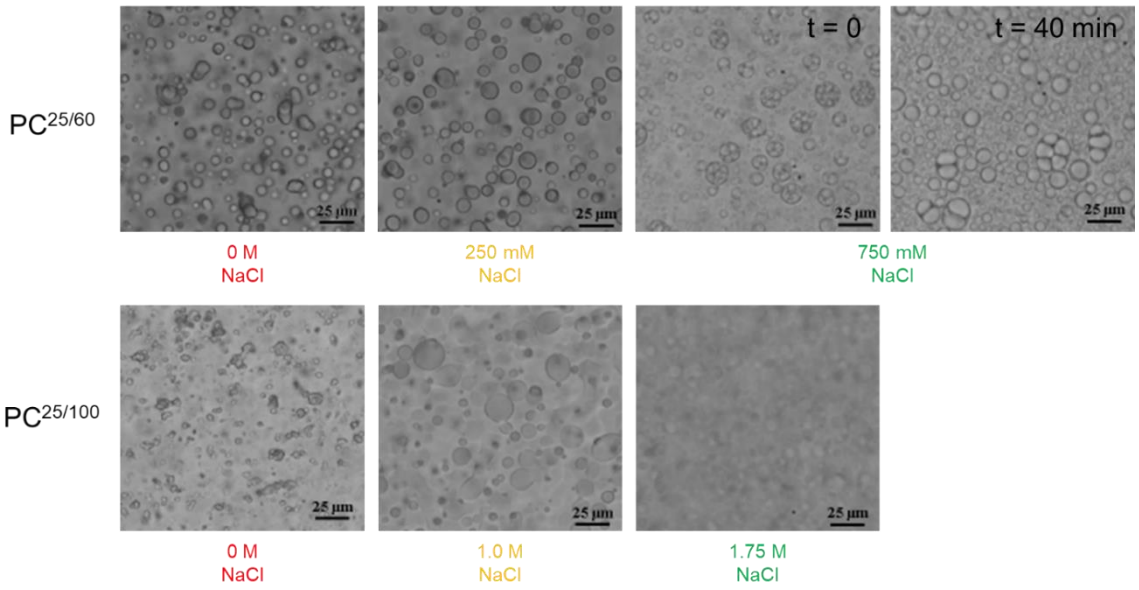

$PC^{25/60}$ exhibit interesting properties at 750 mM NaCl: coacervates appear to be made up of clustered small droplets. The coacervate droplets are also very stable, with well-defined spherical boundaries that do not fuse as readily into free-form fluid layers as seen in 250 mM NaCl. The raspberry-like clusters of coacervate droplets are fairly stable, with smaller coacervate clusters fusing together over the span of 30-60 minutes. It is of note that this is the only PEC explored here comprised of two polyampholytes capable of simple coacervation at a pH(*I*). Further exploration of these types of coacervates may be interesting in forming different coacervate or microgel morphologies. Future work will explore these coacervates with fluorescent labels to identify polymer distribution in different domains, to further elucidate the coacervate compositions.

Figure 2A.15. Bright field microscope images of low MW polyelectrolyte coacervates at 0 mM and intermediate NaCl, for high phase coacervation efficiency, show increasing droplet size due to NaCl charge shielding or potentially enabled Ostwald ripening.

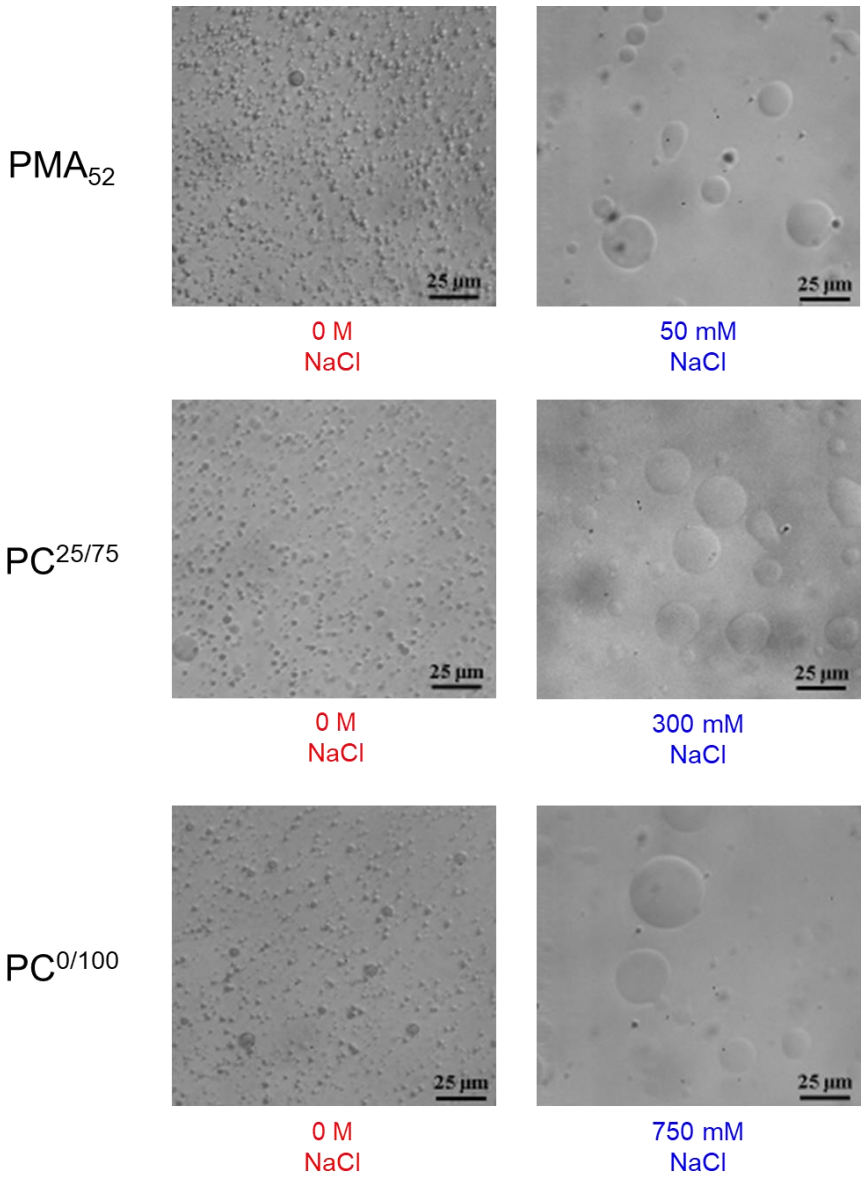

Figure 2A.16. Copper wire drag assay.

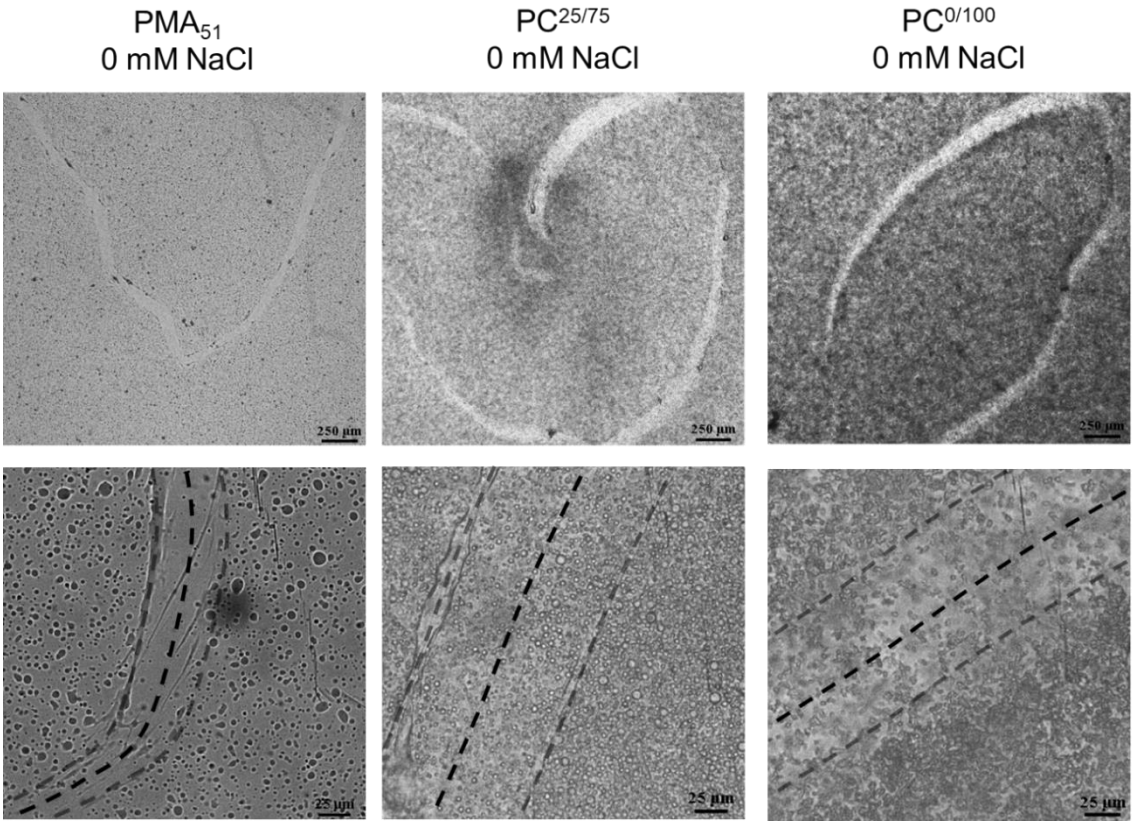

Figure 2A.17. Addition of NaCl to PA and $PC^{0/100}$.

I) Increasing ionic strength increases fluidity of coacervates in images of PA and $PC^{0/100}$ drag paths; more coacervate is smeared and drag paths are more hydrated, with faster rates of fusion and recovery.

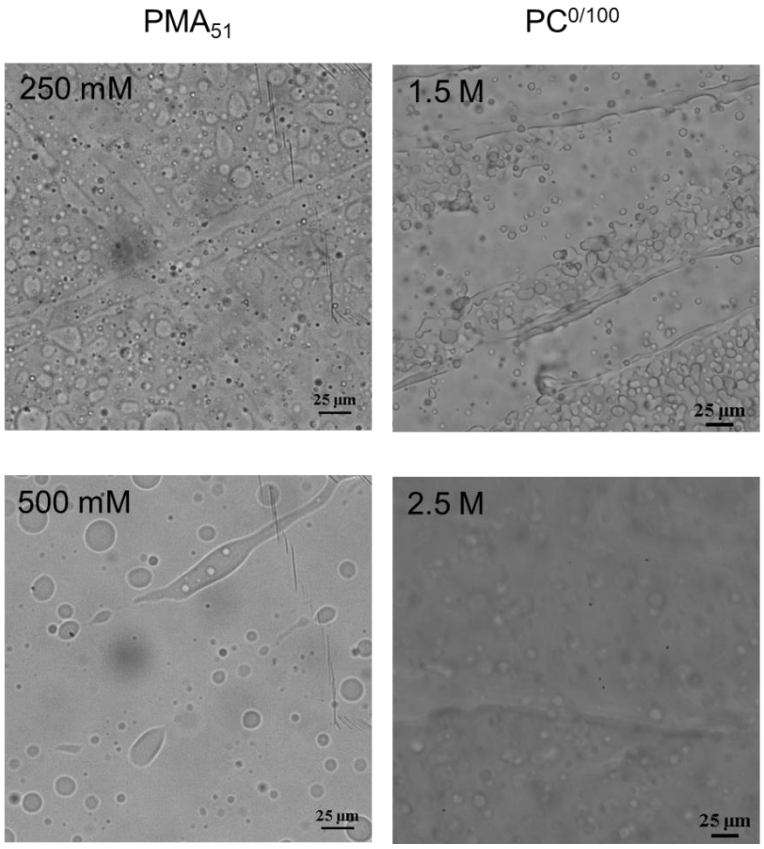

II) Drag path of polymer-dense layer quickly recovers and fuses with settling droplets within 30 s in $PC^{0/100}$ at 2.5 M NaCl.

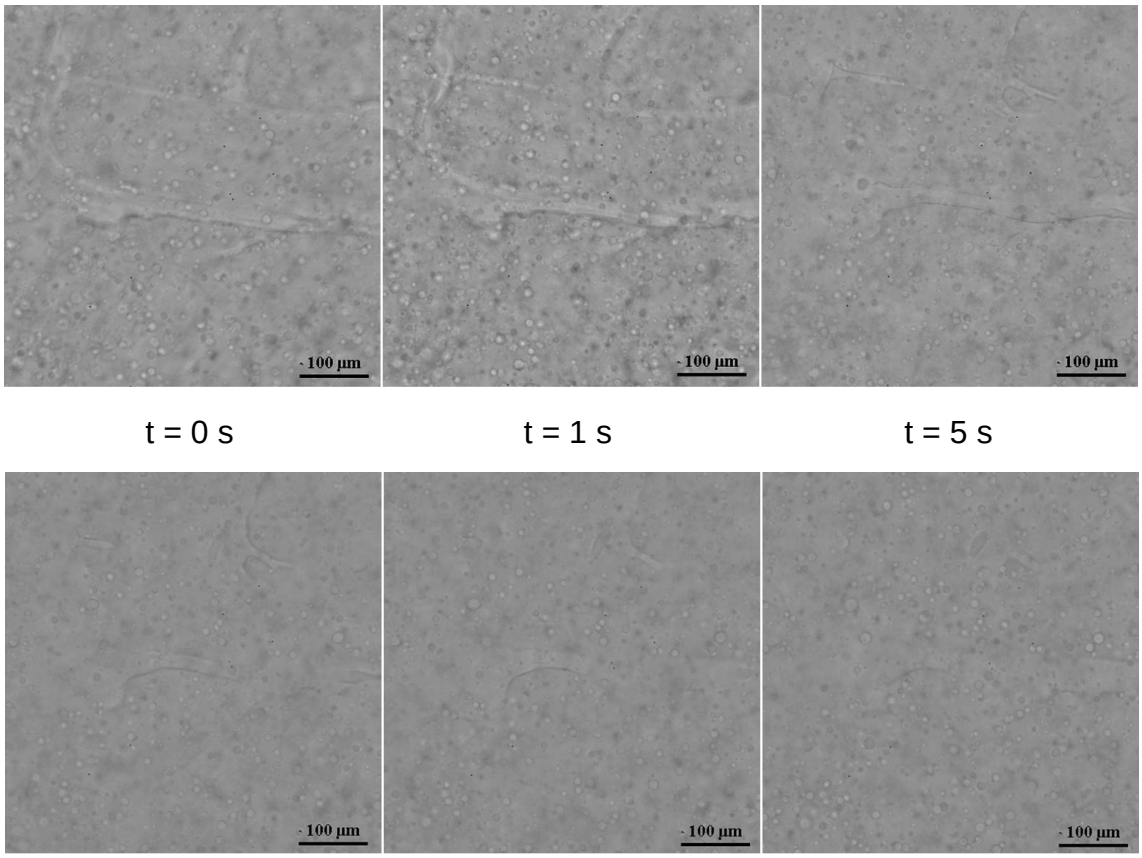

Table 2A.18. Isothermal titration calorimetry data.

Complex Pair	*ΔG* *(kJ/mol)*	*ΔH* *(kJ/mol)*	*TΔS* *(kJ/mol)*	*n*	*n theoretical*	K_D (nM)
$PC^{0/100}$	-35 ± 3	2.1 ± 0.4	-37 ± 3	0.70 ± 0.1	1.0	$9 \pm 8 \times 10^2$
$PC^{0/75}$	-31 ± 3	1.6 ± 0.1	-33 ± 3	0.20 ± 0.1	0.5	$4 \pm 4 \times 10^3$
$PC^{25/100}$	-30 ± 2	1.0 ± 0.2	-31 ± 2	0.50 ± 0.03	2.0	$5 \pm 3 \times 10^3$
$PC^{25/75}$	-34 ± 3	0.7 ± 0.1	-34 ± 3	0.50 ± 0.2	1.0	$2 \pm 2 \times 10^3$
$PC^{25/60}$	-31 ± 2	0.6 ± 0.1	-32 ± 2	0.24 ± 0.4	0.4	$3 \pm 2 \times 10^3$

Figure 2A.19. Raw ITC data of P(NaMAA)-P(APM) (*n=3*) runs (black, dark, and light blue) with buffer (red) injection control.

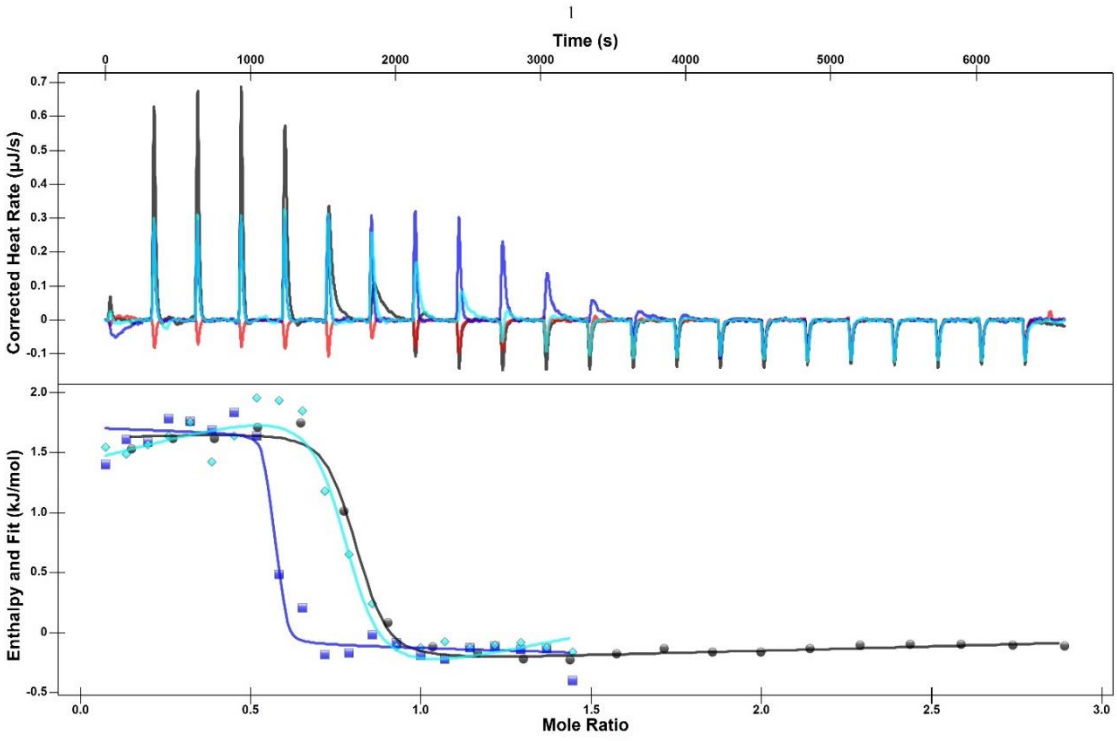

Figure 2A.20. Crosslinked $PC^{25/75}$ microgels survive drastic changes in pH, exposed to 1 M HCl.

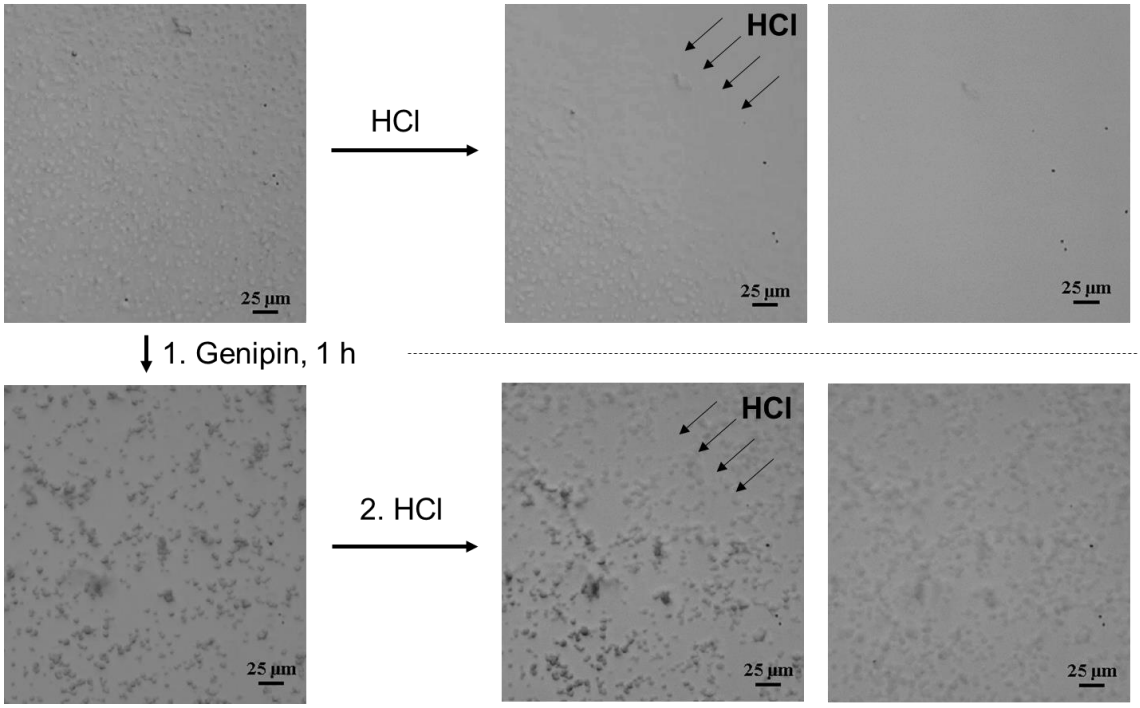

$PC^{25/75}$ coacervates successfully cross-linked (0.25:1 genipin to total amine groups, 60 min).

Figure 2A.21. Dye binding efficiency of different complexes at optimal [NaCl] for coacervation (left) and images of complex solutions with 60 μL of 1 mg/mL BBG upon addition and after 10 minutes of gentle mixing on a wrist shaker (right).

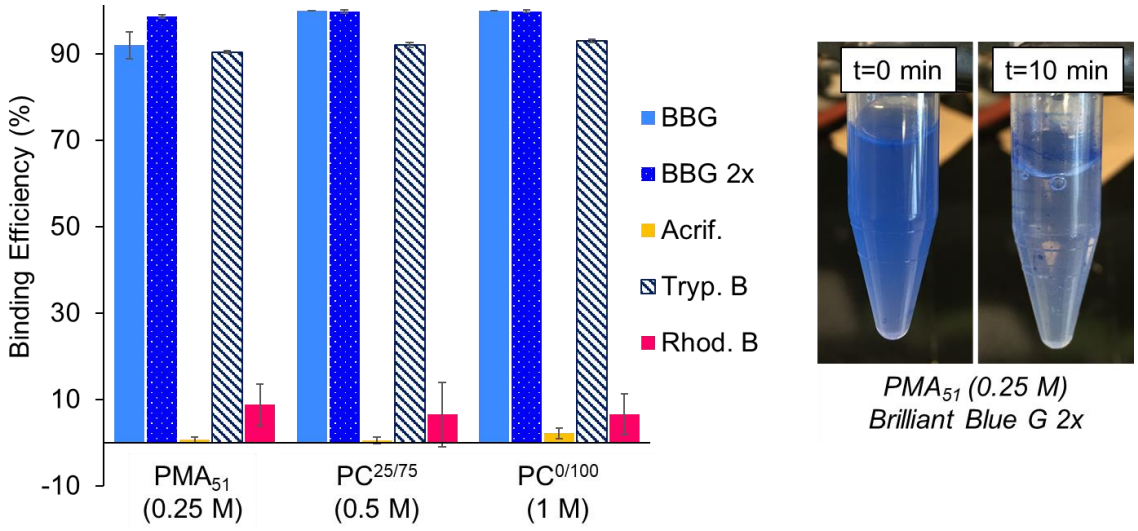

Figure 2A.22. Dye binding efficiency (0.01% w/v PEC loading) in 300 mM NaCl.

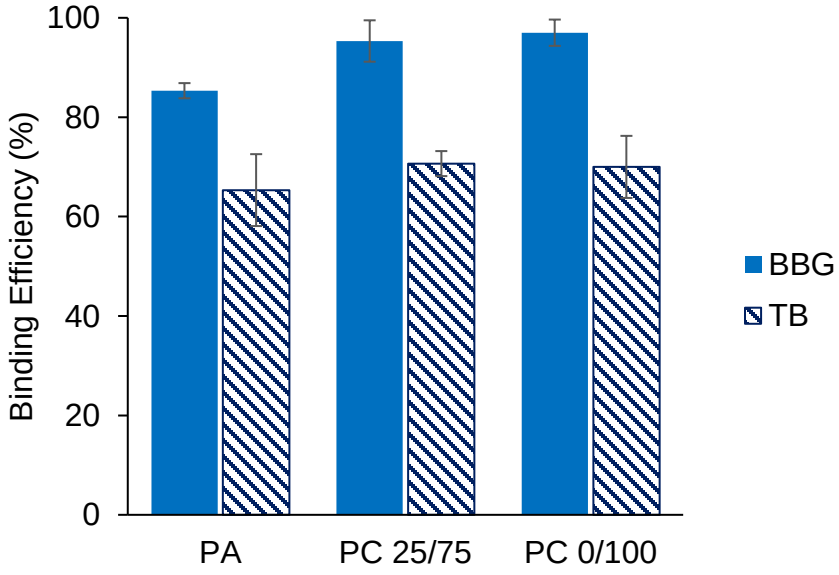

Figure 2A.23. Structures of chosen ionic dyes.

Brilliant Blue G

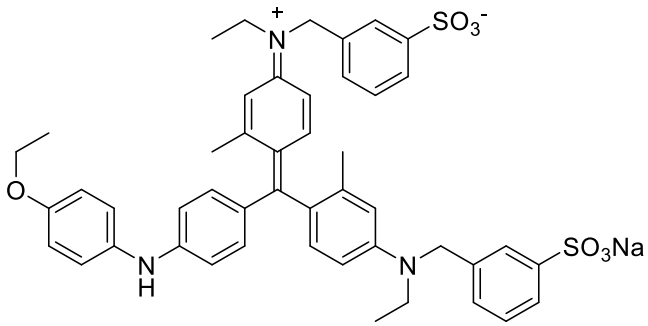

Trypan Blue

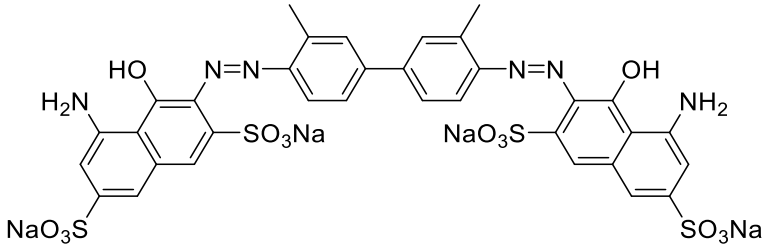

Rhodamine B

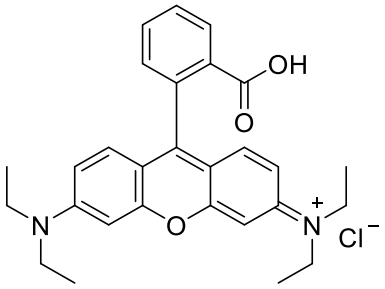

Acriflavine

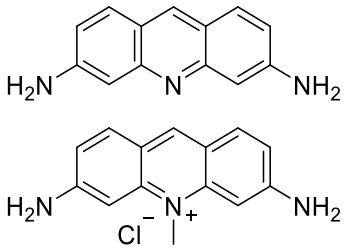

Chapter 3. Exploring the Impact of Zwitterions in Discrete Charge Arrangements of Stimuli-Responsive Polyelectrolyte Complexes

Derrick E. Hastings, Harald D. H. Stöver

Department of Chemistry and Chemical Biology, McMaster University, Hamilton, ON, L8S 4M1, Canada

Reprinted (adapted) with permission from Hastings, D. E. *et al.*, *ACS Appl. Polym. Mater.* **2022**, *4*, 5035-5046.

3.1. Abstract

The effects of introducing zwitterionic 2-methacryloyloxyethyl phosphorylcholine (MPC) into synthetic aqueous coacervates are described. A series of polyampholytes and polyelectrolytes composed of methacrylic acid and *N*-(3-aminopropyl)methacrylamide hydrochloride with increasing amounts of MPC were prepared by free radical copolymerization. The compositional drift of charged monomers in polyampholytes was minimized by controlling the degree of ionization of the methacrylic acid, and copolymerizations were tracked by ^{1}H NMR, while the rate of incorporation of MPC was monitored. Macroscopic phase separation of a series of charge-balanced complexes with different degrees of charge separation was examined by both potentiometric and thermal turbidimetry as well as UV-visible spectroscopy to explore pH-, salt-, and temperature-

responsive properties. MPC incorporation was found to affect the stimuli-responsiveness of all complexes, particularly in single-component charge-balanced polyampholytes. The intramolecular charge compensation in fully charge-balanced polyampholytes, compared to pairs of partially balanced polyampholytes or polyelectrolytes, is known to reduce the driving force for phase separation. Additionally, incorporation of MPC reduces the net complex charge density and disrupts localized charge runs, which weaken the associative interactions involved in complexation and destabilize the resulting coacervates. This allows for multifaceted tuning of the stimuli-responsive and physical properties of the derived complexes, which are dependent on both charge density and charge arrangement. The different coacervate compositions different degrees of stability and resistance to various stimuli, making them suitable models for, i.a., intrinsically disordered proteins and underwater adhesives.

3.2. Introduction

Self-assembly of water-soluble macromolecules is a pertinent concept in biomaterial technologies. A wide range of desirable properties can be achieved by both natural and synthetic (co)polymers that can be modified with respect to chain length, composition, and architecture. Charged polymers, known as polyelectrolytes, and their associative interactions with other charged species can be designed to generate polyelectrolyte complexes (PECs) that exhibit specific responsiveness to external stimuli including ionic strength, temperature, or pH, which has led to technologies in drug delivery,[1] tissue scaffolds,[2] self-healing materials,[3,4] and wearable electronics.[5]

Polyelectrolyte architecture, including charge sequence or arrangement, has significant effects on the stability of the ionic associations involved in polyelectrolyte composition as illustrated by Perry for both sequence-controlled polyampholytes, and other complex coacervates.[6-14] Others have shown the effects of changes in polymer architecture on solution properties, including distribution effects in random polyelectrolyte sequences.[7-11] This leads to notable changes in the physical properties of stimuli-responsive PECs. We recently explored the physical properties of polyelectrolyte complexes using polymers composed of methacrylic acid (MAA) and *N*-(3-aminopropyl)methacrylamide (APM), demonstrating the effects of charge separation and intramolecular charge neutralization on both stimuli-responsiveness and the physical characteristics of formed complexes based on underlying ionic association strength.[15]

In addition to charge distribution, complex charge density can also be used to tune responsive properties in such materials.[16-21] Alteration of charge density in polyelectrolytes has proven useful in applications such as the design of polycation-alginate capsules for cell encapsulation,[22,23] and may serve as synthetic models for proteins in terms of the range of achievable charge densities and charge distributions.[24,25] Recently, Huang et al. demonstrated that charge density can affect the viscoelastic properties of complex coacervates, using a library of polyanions and polycations with varying amounts of charge-neutral hydrophilic or hydrophobic groups introduced by post-polymerization modification.[26] Interestingly, while this study showed that hydrophobicity of the neutral functional group does not impact complexation, others have demonstrated that the

hydrophobicity of termonomer has substantial effects on the coacervation window and salt resistance.[9,17]

Our group previously incorporated non-ionic *N*-(2-hydroxyethyl)acrylamide (HEA) into charge-balanced polyampholytes of MAA and APM to explore the effect of charge density on stimuli-responsive properties.[27] Similarly, 2-hydroxyethyl methacrylate and *N,N*-dimethylacrylamide were introduced into polyampholyte hydrogels to weaken the associative ionic interactions, effectively softening the gels and enhancing skin adhesion.[28] Hence, charge-neutral comonomers can be very useful in adjusting different physical and mechanical properties in polyelectrolyte systems.

Hydrophilic monomers such as 2-methacryloyloxyethyl phosphorylcholine-based (MPC) are known to disrupt interactions between oppositely charged macromolecules,[29] and have been used to prevent protein fouling in biomaterials.[30-33] Though zwitterionic MPC contains both positive and negative charged groups, the monomer has a neutral net charge and possesses inherent hydration properties that are often used to prevent hydrophobic interactions and to impede ionic associations involved in polyelectrolyte complexation. This makes MPC an interesting candidate in reducing the effective charge density[*] of polyelectrolyte coacervates.

[*] *Effective charge density refers to the neutral nature of MPC and its incorporation into charged polyelectrolytes. MPC is a charged, zwitterionic monomer but we do not expect these charges to actively participate in polyelectrolyte complexation and, hence, reduces the number of charged groups used in associative interactions during coacervation.*

Here, we explore the effects of the highly hydrophilic, charge-neutral termonomer MPC on the stimuli-responsive properties of charge-balanced coacervates based on MAA and APM. The different PEC compositions explored range from single polyampholytes capable of self-coacervation to complex coacervates formed from pairs of polyelectrolytes; this includes pairs of complementary, nonstoichiometric polyampholytes and polyanion-polycation pairs with no intramolecular charge compensation (Scheme 3.1).

Scheme 3.1. Compositional map of the different charge arrangements explored, including polyanion-polycation pairs (bottom), complementary nonstoichiometric polyampholyte pairs (middle) and charge-balanced polyampholytes (top), with additional incorporation of MPC increasing left to right.

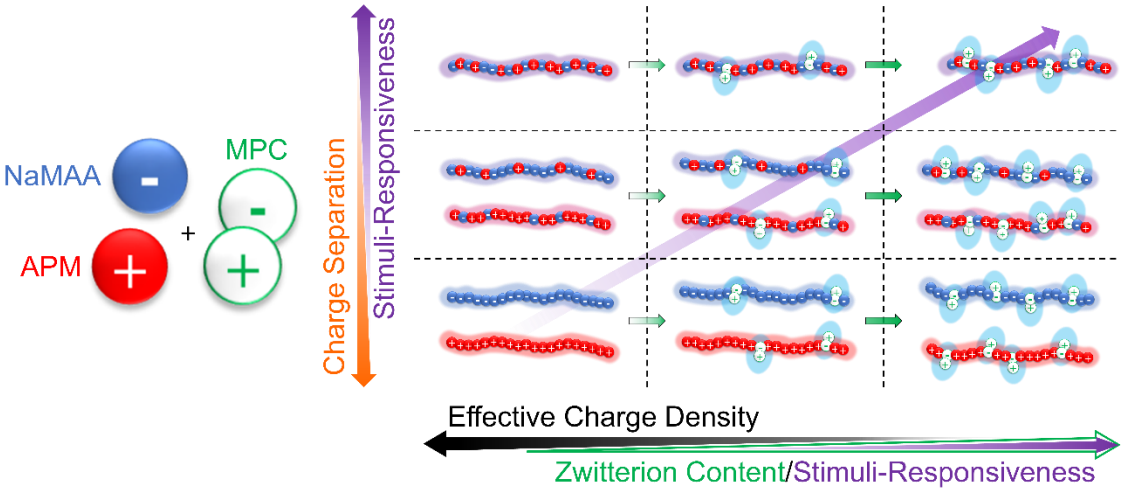

The diagonal arrow (purple) indicates the expected increase in stimuli-responsiveness and decrease in coacervate stability.

3.3. Experimental

3.3.1. Materials

2,2''-Azobis(2-methylpropionamidine)dihydrochloride (97%, Vazo-56), deuterium chloride (99% D), D_2O (>99%), methacrylic acid, sodium methacrylate, fluorescein

isothiocyanate isomer I (>90%), 2-methacryloyloxyethyl phosphorylcholine (97%), cysteamine hydrochloride, and ethylene carbonate (98%) were purchased from Sigma-Aldrich and used as received. *N*-3-(Aminopropyl)methacrylamide hydrochloride (98%) and poly(methacrylic acid) 100 kDa were purchased from PolySciences Inc. and used as received. Cellulose dialysis tubing (3.5 kDa) was purchased from Spectrum Laboratories and used as received.

3.3.2. Effective Reactivity Ratios of (MAA/APM) and MPC in Charge-Balanced Polyampholytes

Copolymerizations were followed in-*situ* by ^{1}H NMR spectroscopy using a 600 MHz Bruker Avance spectrometer. NMR scale (100 mg) polymerizations of varying MPC ratios were performed to determine the NaMAA:MAA molar feed ratios required to achieve comparable reactivities of MAA and APM, as reported previously.[34] A NaMAA:MAA ratio of 3:1 in 1 M NaCl results in stoichiometric MAA/APM incorporation. Additional NMR scale polymerizations were then carried out with different amounts of MPC, to 60-80 % conversion. ^{1}H NMR spectra were recorded at roughly 10-25 % conversion steps at 10 wt % total monomer loading in D_2O with 1 M NaCl, 1 mol % Vazo-56, and 5 mol % potassium hydrogen phthalate (KHP) as an internal standard. Initial (MAA+APM):MPC molar feed ratios were 90:10, 80:20, 64:36, 43:57, 31:69, 20:80, and 10:90. The reaction temperatures were limited to 45 °C to maintain a low rate of polymerization and facilitate tracking by ^{1}H NMR. Monomer conversion was monitored using the distinct vinyl signals of MPC, APM, and MAA with respect to the KHP aromatic signals as an internal standard. Given their stoichiometric incorporation across different MPC contents, MAA and APM were treated

as a single species [MAA + APM] to facilitate modelling as a binary copolymerization with MPC. Effective reactivity ratios for [MAA + APM] and MPC were estimated by least-squares fitting of the terminal model of the instantaneous copolymer composition equation to comonomer conversion data as previously reported[23,27] based on a procedure by Aguilar et al[35], and confirmed by the Fineman-Ross method.[36]

3.3.3. Preparation of Polymers

3.3.3.1 Binary Polyampholytes

Binary polyampholytes comprised of MAA and APM were prepared according to our previous work.[15,27,34] Polymers are denoted as poly(MAA-*co*-APM)$_x$ (PMA$_x$), where x represents the mol % of APM in the copolymer. PMA$_{75}$ is used here as an example: using an 8 mL screw cap vial, NaMAA (84 mg, 0.778 mmol), APM (416 mg, 2.33 mmol), and Vazo-56 (8.4 mg, 0.031 mmol) were dissolved in 5 mL of deionized water (10% w/v total monomer loading). The vial was submerged in a 45 °C water bath and monitored using ^{1}H NMR spectroscopy at 30 min intervals, before halting at about 60% conversion after about 3 h of cumulative heating. All polymers were purified by dialysis, lyophilized, and characterized post-purification by ^{1}H NMR spectroscopy and by gel permeation chromatography (GPC).

Scheme 3.2. Copolymerization of NaMAA/MAA, APM, and MPC using Vazo-56.

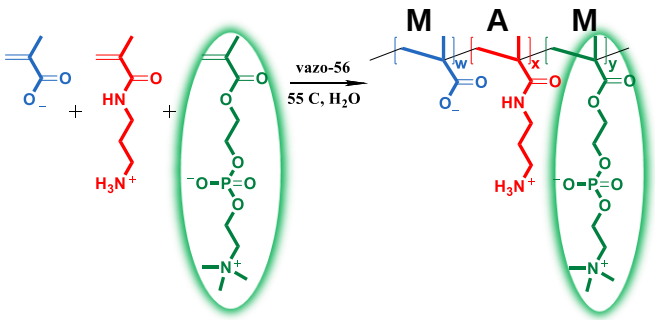

Poly[**M**AA-*co*-**A**PM$_x$-*co*-**M**PC$_y$]

$$x = \frac{[APM]}{[APM]+[MAA]} * 100$$

y = mol % MPC

3.3.3.2. Stoichiometric Ternary Polyampholytes with MPC

Charge-balanced polyampholytes of MAA and APM with MPC are denoted as PMA$_x$M$_y$, where x represents the mole fraction APM relative to total charged monomer (MAA+APM), and y represents the mol % MPC incorporated (Scheme 3.2), as determined by ^{1}H NMR of the isolated polymer. A 1:1 polyampholyte with 10% MPC was prepared at a 1 g scale as follows: to a 20 mL screw cap vial, NaMAA (234 mg, 2.16 mmol), MAA (62 mg, 0.721 mmol), APM (515 mg, 2.88 mmol), MPC (189 mg, 0.641 mmol), and vazo-56 (17.4 mg, 64.1 μmol) were added and dissolved in 10 mL of 1 M NaCl. The reaction was purged with nitrogen for 30 min and was followed by ^{1}H NMR spectroscopy using a 600 MHz Bruker Avance spectrometer by diluting aliquots of the reaction solution in D_2O at estimated intervals for spectrum acquisition. The vial was then submerged in a 45 °C water bath and halted at roughly 50% conversion to ensure minimal monomer drift. The final copolymer was dialyzed against water at pH 3 using 3.5 kDa MW cut-off cellulose tubing and freeze-dried to yield solid white polymer (> 90% yield). Lower MW polyampholytes

were prepared in a similar manner, incorporating 0.7 mol % cysteamine hydrochloride as a chain transfer agent.

3.3.3.3. Nonstoichiometric Polyampholyte Terpolymers

Using previously reported procedures, nonstoichiometric polyampholytes including 1:3 and 3:1 MAA/APM charge ratios were prepared with different amounts of MPC. Polymers are denoted as PMA_xM_y, where *x* represents the mole fraction APM relative to total charged monomer (MAA+APM) and *y* represents the mol % MPC. $PMA_{25}M_5$ is listed here as an example. Using an 8 mL screw cap vial, NaMAA (123 mg, 1.14 mmol), MAA (147 mg, 1.71 mmol), APM (170 mg, 0.952 mmol), MPC (59 mg, 0.200 mmol), vazo-56 (11 mg, 40.5 μmol), and ethylene carbonate (20 mg, 0.227 mmol) were dissolved in 5 mL of a 1:1 mixture of dimethylformamide (DMF) and water (10% w/v total monomer loading). The vial was then placed in a UVP Laboratory Products HB-1000 hybridizer oven at 60 °C, and the polymerization was followed by ^{1}H NMR spectroscopy at 30 min intervals. During polymerization, precipitation of insoluble polymer was observed; copolymer vials were centrifuged and aliquots of the supernatant containing the internal standard were diluted in D_2O and used to track comonomer consumption. Polymerizations were halted at roughly 60% conversion after about 1 h of heating. 5 mL of 1 M NaOH was added to dissolve the precipitated polymer, followed by purification by dialysis against water at pH 11 for 1 day and against deionized water for 2 days. The polymer was lyophilized to yield solid white polymer (> 90% yield). Lower MW $PMA_{25}M_y$ and $PMA_{75}M_y$ were prepared using 0.5 and 0.75 mol % CTA, respectively.

Preliminary ^{1}H NMR experiments of nonstoichiometric polyampholytes of 3:1 and 1:3 MAA/APM by using low amounts of MPC were also used to briefly show how the polyampholyte charge ratio and different polymerization conditions for low compositional drift impact the incorporation of (MAA+APM) versus MPC.

3.3.3.4. P(APM-co-MPC)$_y$

Copolymers of APM and MPC were prepared using feed ratios chosen based on reactivity ratios previously determined to achieve particular MPC incorporations.[23] PAM$_{13}$ is listed here as an example: APM (445 mg, 2.49 mmol), MPC (55 mg, 0.186 mmol), and vazo-56 (7.3 mg, 26.8 μmol) were dissolved in deionized water at 10% monomer loading. The solutions were purged with nitrogen for 30 min before being submerged in a 45 °C water bath. The reaction was monitored by ^{1}H NMR and final polymers are denoted as PAM$_y$, where *y* represents the mol % of MPC. Polymerizations were run to an estimated total conversion of > 60%. The polymer was dialyzed against 1 M NaCl for 1 day, followed by deionized water for 2 days and lyophilized to yield solid white polymer. Lower MW polymers were prepared using 1-1.15 mol % CTA.

3.3.3.5. P(MAA-co-MPC)$_y$

P(NaMAA) was prepared by dissolving 1 g of P(MAA) in deionized water, adjusting pH to 7 with 1 M NaOH and dialyzing in distilled water for 3 days, changing baths every 12 h. Copolymers of MAA and MPC were prepared using similar procedures to work for high MW methacrylic acid polymers.[37] MAA, MPC, vazo-56, and ethylene carbonate were dissolved in deionized water at 10% total monomer loading. The mixtures were heated in a 45 °C water bath and run to approximately >50% conversion. Polymerizations of various

feed ratios of MAA and MPC were followed by ^{1}H NMR spectroscopy. To purify final polymer, 1 M NaOH was added to increase the pH (>10) and polymers were dialyzed against deionized water for 4 days and lyophilized to yield solid white polymer. Lower MW polymers were prepared in an analogous manner but with 0.5 mol % CTA.

3.3.4. Polymer Characterization

Polymers with predicted pH(*I*) above 6 (amine-rich) were analyzed using a Waters GPC consisting of a 717plues autosampler, a 515 HPLC pump, Ultrahydrogel (120, 250, and 500) columns (30 cm x 7.8 mm i.d.; 6 μm particles) and a 2414 refractive index detector, using a 1 M acetate buffer (pH 4.76) with a flow rate of 0.8 mL/min at 30 °C as the mobile phase. This GPC system was calibrated with poly(ethylene glycol) (PEG) standards (Waters Inc.) ranging in MWs from 106 Da to 881 kDa.

Polymers with pH(*I*) below 6 (acid-rich) were analyzed using an Agilent 1260 infinity II GPC system equipped with an Agilent 1260 infinity RI detector and a GE Healthcare Superose 6 Increase 10/300 GL with 100 mM borate running buffer (pH 9.4). The column was calibrated using PEG standards (M_n of 3,000 to 60,000).

3.3.5. Fluorescent Labeling of Copolymers

50-60 mg of amine-rich copolymer was dissolved in 6 mL of deionized water and the pH was raised to 8.8-9.0 using 1 M NaOH. While stirring, appropriate volumes of 10 mg/mL FITC dissolved in DMF were added to each solution to target 0.1 mol % labeling relative to total monomer. The mixtures were stirred for 1 h in the absence of light before pH was decreased to 3 for $PMA_{50}M_y$ or 7 for $PMA_{75}M_y$ and PAM_y. Polymers were then dialyzed

against deionized water for 3 days (pH 3 for PMA_{50}), filtered and lyophilized to yield yellow-orange solid polymer in > 85% yield.

3.3.6. Turbidimetric/Potentiometric Titration

Turbidimetric titrations were carried out, as previously reported, at 22 °C on 25 mL solutions of polymer in deionized water.[38] Using a VWR SympHony pH probe and a Mitsubishi GT-LD photometric detector equipped with an optical fibre turbidity probe (λ > 620 nm), the pH and turbidity of the solution were monitored after 30 s of stabilization after addition of each aliquot. The concentrations of NaOH (5 mM to 1 M) additions were selected to achieve pH changes of roughly 0.05-0.15 per injection of 25 μL aliquots. The resulting high pH solutions were subsequently titrated back to low pH using 25 μL aliquots of 5 mM to 1 M HCl, again monitoring turbidity as a function of pH. Because of the pronounced shoulders following maximal phase separation at pH(*I*), the pH(*I*) was determined as the midpoint between the leading edges of the forward and reverse titration curves at the estimated half-minimum transmittance detected.

For charge-balanced combinations of complementary polyanion-polycation pairs, weight ratios required to achieve a charge-balanced solution were calculated. The titration of $PMA_{25}M_{10}$-$PMA_{75}M_{10}$ is given as an example: 1.1 mL of $PMA_{25}M_{10}$ solution (0.1% w/v) at pH 3 was diluted into 22.5 mL of deionized water in a 30 mL beaker. The solution was adjusted to pH 3 before 1.4 mL of $PMA_{75}M_{10}$ solution (0.1% w/v) at pH 3 was added to achieve a 0.1 mg/mL total polymer loading. The mixture was then titrated as described above up to pH 11.

The pH range over which complexes are stable, remaining insoluble during turbidimetric titration, is a distinct feature of each coacervate.[15] First-derivative plots of turbidity versus pH were used to identify the pH values corresponding to steepest reductions in turbidity following the pH(*I*), which were taken as points of dissolution for forward (toward high pH) and reverse titrations. The difference between these two pH values was taken as measure of the relative strength of the underlying associative interactions.

3.3.7. Phase Separation Efficiency

To determine the phase separation efficiency of polyampholytes, 3.5 mg of FITC-labeled PMA_{50} was dissolved at 0.1% w/v in screw cap glass vials in water of varying ionic strength. The pH of the sample was raised to 10 using 0.1 M NaOH to fully dissolve the polymer. The pH was then adjusted to the pH(*I*) to induce phase separation, and the cloudy polymer solution was centrifuged at 2360 g for 5 min. The supernatant was removed, adjusted to pH 10, and absorbance of FITC remaining (495 nm) was analyzed by UV-visible spectroscopy (Varian Cary 50Bio Spectrometer) to determine the concentration of polymer remaining, according to equation **3.1**.

$$\%\, Efficiency = \frac{A(initial) - A(final)}{A(initial)} \times 100\% \qquad \textbf{(3.1)}$$

Complementary polyelectrolytes – In screw cap vials, samples of polyanion and polycation were separately dissolved at 0.1% w/v in solutions of varying ionic strength. Only the amine-rich copolymer was FITC-labeled as described above. The pH values of the polyanion and polycation solutions were adjusted to pH 7.0, and calculated volumes were combined to prepare 3 mL of charge-balanced complex solutions. $PMA_{25}M_{23}$ – $PMA_{75}M_{30}$-

f is here listed as an example: 1.30 mL of $PMA_{25}M_{23}$ and 1.70 mL of $PMA_{75}M_{30}$-*f* solution were mixed in a separate vial. The pH of the mixed solution was adjusted, the combined solution was centrifuged as described, the supernatant removed, and the pH adjusted to 11 for analysis by UV-visible spectroscopy. The absorptions of the complex supernatants were compared with standard solutions of FITC-labeled polycation (0.057% w/v $PMA_{75}M_{30}$-*f*) in deionized water at pH 11. The above procedures were repeated for all $PC^{25/75}$ and $PC^{0/100}$ combinations at different MPC composition with increasing [NaCl]. Procedures here were adapted from Spruijt et al.[39]

3.3.8. Optical Microscopy of Polymer Phase Separation at pH(I)

Polymer complexes were imaged with a Nikon Eclipse T_i optical microscope equipped with a pco.panda 4.2 monochrome sCMOS camera. Copolymer solutions were prepared at 10 mg/mL with varying NaCl concentrations. The pH values of $PMA_{50}M_y$ solutions at 0 M NaCl were adjusted to 7.0-7.2 to induce phase separation. The pH of premixed polyanion/polycation solutions were adjusted separately to pH 7.0 before mixing at [NaCl] corresponding to an estimated 50% of maximal phase separation efficiency. A drop of the resulting mixture was placed on a clean glass microscope slide for imaging.

3.3.9. Temperature Response of Aqueous Solutions

Cloud point measurements were carried out using a Varian 3E spectrophotometer with a temperature controlled 12-sample holder. Polymer solutions of 1 mg/mL were heated at 1 °C/min from 23 to 87 °C and the transmittance at 500 nm was measured at 0.5 °C intervals. Prepared from stock NaCl solutions, polymers were dissolved in different ionic strengths. For two-polymer coacervates, both polyanion and polycation were separately dissolved in

the appropriate ionic strength. The solution pH was adjusted to pH 7.0 for each polyampholyte/polyelectrolyte combination. Cloud point temperatures approximating lower critical solution temperatures (LCST) were taken as the value halfway between 100% and minimal transmittance for the curve with the lowest [NaCl]. For example, PMA_{50} at 950 mM NaCl showed a minimum transmittance value of 10%, therefore the cloud point temperature was taken as the temperature at which the transmittance value was roughly 55%.

3.4. Results and Discussion

3.4.1. Preparation of Polymers

A series of binary (MAA/APM) and ternary (MAA/APM/MPC) copolymers were prepared by aqueous free radical copolymerization. ^{1}H NMR was used to quantify consumption of all three monomers during the copolymerizations. Comonomer ratios and copolymer compositions are described in Table 3.1.

Specific empirically determined NaMAA/MAA ratios and solvent conditions were used to equate reactivity ratios and suppress compositional drift between MAA and APM in both binary and ternary copolymerizations, as described previously.[34] For example, a 3:1 molar ratio of NaMAA/MAA in 1 M NaCl gave low-drift, 1:1 incorporation of MAA and APM into both binary (MAA/APM) copolymers, and ternary (MAA/APM/MPC) copolymers (Figure 3A.1). Notably, incorporation of MPC is favoured over the charged monomers; Figure 3.1 (A) shows the depletion of MPC in the comonomer pool during a series of seven PMA_{50} copolymerizations with 10-90 mol % MPC. The effective reactivity

ratios for r_1(MAA+APM) = 1.03 and r_2(MPC) = 0.45 were estimated by fitting NMR data of comonomer consumption to the Mayo-Lewis instantaneous copolymer equation by a least-squares method (Figure 3.1 (B)), while Figure 3A.2 shows comparable reactivity ratios obtained using the Fineman-Ross method.

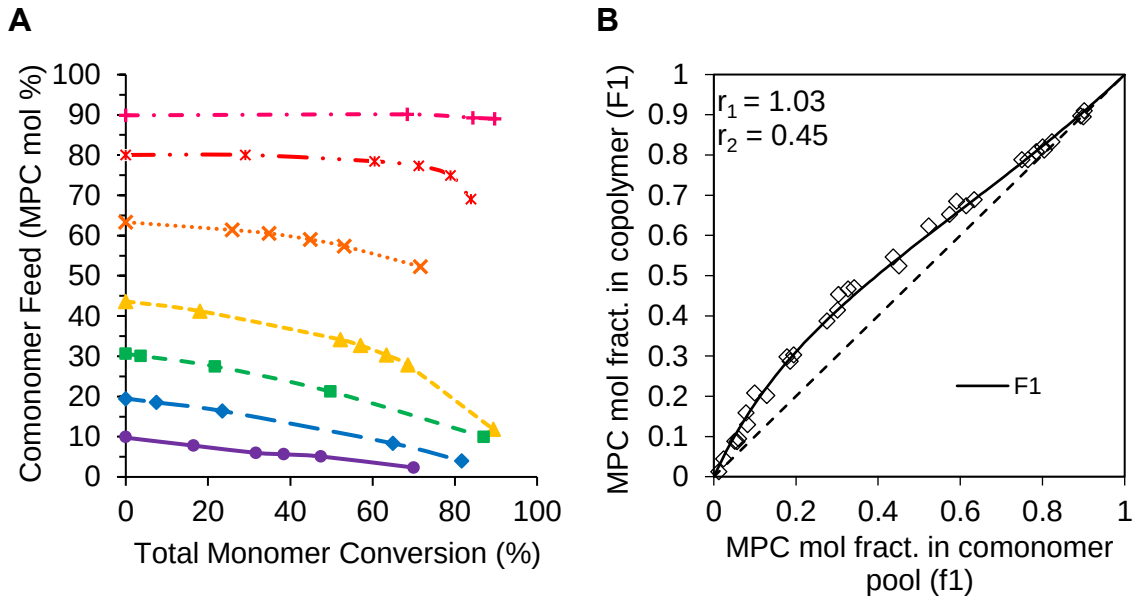

Figure 3.1. (A) Fraction of MPC in ternary copolymerization feeds with equimolar amounts of MAA/APM in 1 M NaCl, monitored by 1H NMR (3:1 molar ratio of NaMAA/MAA used for the methacrylic acid component). **3.1. (B)** Effective reactivity ratios of MPC versus the charged comonomer pool by least-squares fitting of monomer consumption to the instantaneous copolymerization equation.

Similar low-drift incorporation of MAA and APM in nonstoichiometric binary polyampholytes PMA_{25} (25% APM) and PMA_{75} (75% APM), and in their respective ternary MPC-containing analogs, was achieved with empirically determined MAA/NaMAA ratios of 3:2 and 0:1, respectively (Table 3.1, Figure 3A.3). MPC is again incorporated preferentially, especially at higher APM:MAA ratios (as shown in reactivity

ratio estimates in Figures 3A.4-3A.5), and this is attributed to the higher inherent reactivity of methacrylates over methacrylamides.

Table 3.1. Composition, predicted pH(I), and M_p of polyampholytes (* compositions for which aliquots were FITC-labeled post-polymerization).

MAA: NaMAA	Polymer	Composition (MAA:APM:MPC)[a]	Predicted pH(*I*)[b]	Experimental pH(*I*)	M_p (kDa)	Est. Charge (pH 7)
3:2	**PMA_{25}**	75:25:0	4.34	4.55	448	-50
3:2	**$PMA_{25}M_6$**	71:23:6	4.34	--	452	-48
3:2	**$PMA_{25}M_{17}$**	67:22:17	4.34	--	465	-44
3:2	**$PMA_{25}M_{23}$**	60:17:23	4.23	--	481	-43
1:3	**PMA_{50}***	49.5:50.5:0	7.58	7.51	362	+1
1:3	**$PMA_{50}M_7$***	46.3:46.5:7.2	6.98	7.01	458	0
1:3	**$PMA_{50}M_{17}$***	40.8:42.0:17.2	7.61	7.57	414	+1
1:3	**$PMA_{50}M_{25}$***	37.1:37.7:25.2	8.15	8.02	456	+1
1:3	**$PMA_{50}M_{31}$***	32.0:36.5:31.4	8.25	8.15	449	+4.5
0:1	**PMA_{75}***	24:76:0	9.41	N/A	329	+52
0:1	**$PMA_{75}M_8$***	24:68:8	9.45	--	316	+44
0:1	**$PMA_{75}M_{17}$***	21:62:17	9.40	--	332	+41
0:1	**$PMA_{75}M_{30}$***	17:53:30	9.41	--	348	+36

[a]Compositions were determined by ^{1}H-NMR of isolated polymer. [b]pH(*I*) predicted based on ^{1}H NMR determined compositions.

Minimization of MAA/APM drift was thus achieved across a wide range of MAA/APM ratios, which is considered key to this study. The moderate drift of MPC content observed was considered acceptable and was limited by halting ternary copolymerizations at ~60% conversion.

A series of MAA-MPC and APM-MPC binary copolymers were prepared as well. MAA-MPC copolymerizations showed minimal drift, while APM-MPC copolymers again showed preferential MPC incorporation (Table 3A.11).[23]

Most of the copolymers studied elute at the exclusion limit of the GPC columns used (GPC traces found in Figures 3A.6-3A.10). As MW can affect polyelectrolyte complexation,[40,41] high-MW polymers (> 500 DP) were used here for all complex studies to minimize the effects of polymer chain lengths. Separately, a group of low-MW polymers (M_n - 16-31 kDa) were prepared and are described in Table 3A.12.

Ternary copolymers are denoted as PMA_xM_y where *x* represents the mol % APM with respect to total ionizable monomer (MAA+APM) and *y* represents the mol % of MPC relative to total monomer. Polyanion/polycation two-component complexes $PC^{a/b}$ (where *a* represents the cationic mole fraction in polyanion and *b* represents the cationic mole fraction in polycation in equations **3.2** and **3.3**) are denoted additionally with M_y where *y* represents the total amount of MPC in the PEC. The amount of MPC in complex coacervates was determined from the calculated mole ratio of polyanion:polycation required to form a charge-balanced complex and the MPC mol % in of each polymer.

$$a = [\frac{APM}{(MAA+APM)} * 100] \text{ of polyanion} \quad \textbf{(3.2)}$$

$$b = [\frac{APM}{(MAA+APM)} * 100] \text{ of polycation} \quad \textbf{(3.3)}$$

For example, 1.0 mg of $PMA_{25}M_6$ (23% APM overall, given the presence of 6% MPC) and 1.4 mg of $PMA_{75}M_8$ (68% APM overall, 8% MPC) combine to give a 1:1 charge ratio complex termed $PC^{25/75}M_7$ (46.5% MAA, 46.5% APM, and 7% MPC).

3.4.2. Turbidimetric Titrations: pH-Responsiveness

Polyampholytes (PA) - Forward (low to high pH) and reverse (high to low pH) potentiometric titrations monitored by a turbidity probe were used to study the pH-induced phase separation into self- and complex coacervates as a function of both polymer charge distribution and MPC content. Experimental pH(*I*) values for both single polyampholytes and multicomponent complex mixtures were obtained by averaging the pH values for half-maximum turbidity during sequential forward and reverse titrations. These values are very close to the theoretical pH(*I*) values calculated according to equation 3.4 using the ^{1}H NMR determined composition, as shown in Table 3.1.

$$pH(I) = pK_a - \log\left\{\frac{R}{2} * \left[-\frac{(1-R)}{R} + \sqrt{\left(\frac{1-R}{R}\right)^2 + \frac{4}{R} * 10^{(pK_a - pK_b)}}\right]\right\} \qquad \textbf{(3.4)}$$

While MAA/APM ratios drift only minimally in the present copolymers, even small variations in comonomer composition can significantly affect the pH(*I*).[42] This is exemplified in the titration curves of five charge balanced $PMA_{50}M_y$ polyampholytes (Figure 3.2 (A)). The plots show features previously noted in such copolymers: sharp onsets of coacervation in both forward towards higher pH) and reverse titrations, and shoulders indicating slow re-dissolution of the complex.[15,34]

Addition of hydrophilic MPC reduces the overall turbidity of these polyampholyte coacervate suspensions at their pH(*I*) as well as the pH range in which coacervates are observable by turbidimetry. Previous studies have found that water molecules interact more strongly with betaines such as MPC compared with charge neutral groups such as hydroxyethyl acrylate or ethylene glycol repeat units.[30,43-46] These water molecules provide

an energy barrier that is useful in preventing ionic associations in the PEC. Hence, the consequent weakening of ionic associations and strong solvation together make the resulting coacervate droplets less distinct as well as more sensitive to small pH changes.

Complex Coacervates - The isoelectric points of complex coacervates depend on both the individual copolymer compositions and mixing ratio of the separate components. Charge-balanced polymer complexes were formed here by mixing binary anionic (MAA-MPC) and cationic (APM-MPC) polyelectrolyte copolymers, and similarly by mixing anionic ($(MAA_{75}\text{-}APM_{25})\text{-}MPC_y$) with cationic ($(MAA_{25}\text{-}APM_{75})\text{-}MPC_y$) ternary polyampholytes, with mixing ratios calculated using the ^{1}H NMR-determined compositions shown in Table 3.1. Titration curves of the resulting charge-balanced $PC^{25/75}M_y$ and $PC^{0/100}M_y$ complexes incorporating different amounts of MPC are shown in Figures 3.2 (B) and (C), respectively.

We previously described the effect of charge distribution in different complexes on the exhibited turbidimetric titration curves, shown in Figure 3. Complexes with stronger associative interactions can form more stable complexes with plateaus in transmittance after onset of complexation over a range of pH. Notably strong complexes can range from strong coacervates to solid precipitates that can adhere to beaker walls, reducing the amount of suspended complex measured in solution turbidity. Further investigation is necessary to fully describe the shapes of forward and reverse titration curves for various arrangements of high MW polymers, with careful consideration of charge ratio and complex phase behaviour, as these criteria play a notable role in the observed solution turbidimetric titration curves.

Both multicomponent complex arrangements show pH(*I*) values very close to that expected for such charge-balanced polyelectrolyte complexes and polyampholytes according to equation 3.4. The two sets of complexes also show notably broader pH windows of insolubility than the stoichiometric polyampholytes shown in Figure 3.2, suggesting that progressive charge separation onto distinct polymers (from single stoichiometric polyampholytes through paired nonstoichiometric polyampholytes to singly charged polyelectrolyte complexes) strongly increases the stability of the PEC, even in the presence of zwitterionic MPC. The transmittance at pH(*I*) of both $PC^{25/75}M_y$ and $PC^{0/100}M_y$ complexes increases with increasing MPC content, though much less than observed in the charge-balanced polyampholytes $PMA_{50}M_y$.

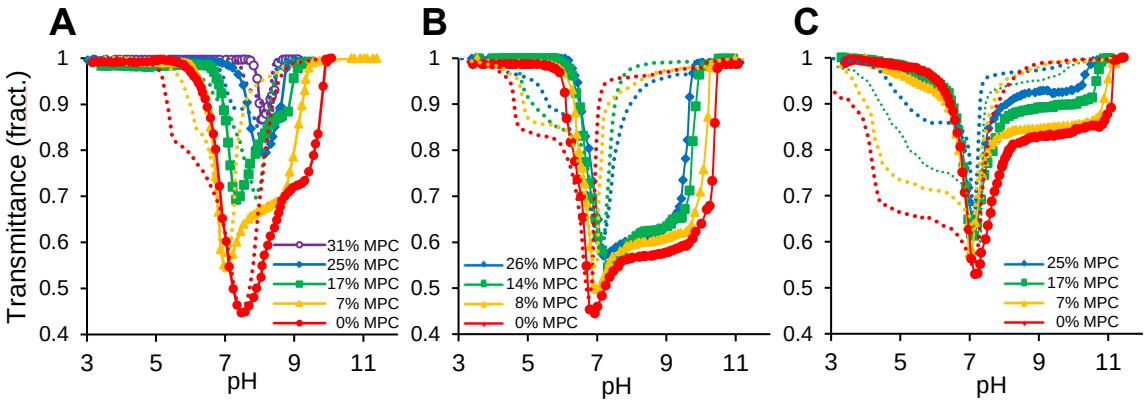

Figure 3.2. (A) Turbidimetric titration curves for PA-M_y (forward – solid; reverse – dashed). **3.2. (B)** Turbidimetric titration curves for $PC^{25/75}M_y$. **(C)** Turbidimetric titration curves for $PC^{0/100}M_y$.

Analogous effects have been seen in comb-type polycations that could form coacervates with linear polyanions having up to 90% sulfobetaine pendent groups; spatial separation of charged groups enhances coacervation even in the presence of hydrating zwitterions[47] Hence, while MPC significantly weakens ionic interactions in polyampholyte self-coacervates, this effect is highly dependent on polyelectrolyte structure and is notably

reduced in systems with stronger ionic interactions. Figure 3.3 summarizes these observations in the form of plots of the pH range of insolubility as a function of charge distribution and MPC content.

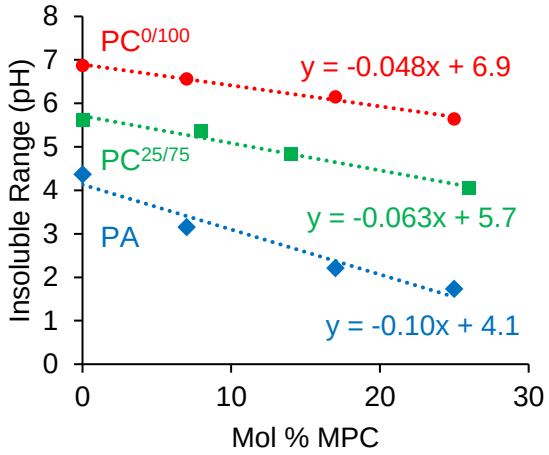

Figure 3.3. Stability of different PECs with changing pH as a function of increasing MPC mol %.

Macroscopic effects of phase behaviour and precipitation effects on titration curve shapes are not observed at lower MW, and hence the pH responses are more easily compared. The trends regarding pH sensitivity, insoluble ranges, and transmittance minima for the different complexes remain consistent in lower MW polyelectrolytes of ca. 16-31 kDa (Figures 3A.13-3A.15). PAs are highly sensitive to MPC introduction, with transmittance increasing and insoluble pH range decreasing as MPC is introduced. The complex coacervates of $PC^{25/75}$ and $PC^{0/100}$ show little change in max. turbidity but do demonstrate the increased sensitivity to pH, as MPC is added.

Coacervation is a thermodynamic process, driven primarily by the release of counterions and water molecules from the swollen polyelectrolytes.[48] With zwitterionic MPC added to these PECs, the effective charge density is reduced, and water is drawn into

the complexes. As charged groups are replaced by MPC, fewer ionic associations are possible and the macroscopic complexes become weaker. Notably, the effects of hydration do not appear to be significant in complex coacervates composed of more favourably interacting polyelectrolytes, supporting that counterion localization and release are the predominant factors in the stability of these coacervates. The response of weak acid/base groups as pH deviates from the pH(*I*) is often seen as another way to alter charge density in polyelectrolyte complexes.[49]

In the different complex coacervate charge arrangement, similar increases in pH sensitivity with comparable MPC content are observed; larger *Δ*pH is required to destabilize PECs with larger statistical charge runs, whereas complexes with increasing self-neutralization are more easily disrupted by the changing degree of ionization of either weak acid or base groups.

Single polyampholyte coacervates offer relatively lower stability and because of significant self-neutralization, are therefore more effectively destabilized by the decreased number of charged species (charge dilution). This makes the ionic associations more easily impeded by the higher water content or presence of hydration barriers between charges provided by MPC between charges; polyampholyte self-coacervates are more effectively destabilized by charge density reduction with respect to salt shielding and hydration by the zwitterionic termonomer.

3.4.3. Coacervation Efficiency: Ionic Strength Responsiveness

Here we explore the effect of [NaCl] on phase separation efficiencies of different charge-balanced coacervates incorporating different amounts of MPC. Amine-rich polymer was

FITC-labeled, and the phase separation efficiencies of self- and complex coacervates at their pH(*I*) are plotted in Figure 3.4 as a function of [NaCl]. The full UV-vis spectra corresponding to PMA_{50}-*f* coacervation efficiency are shown in Figure 3A.16, as an example.

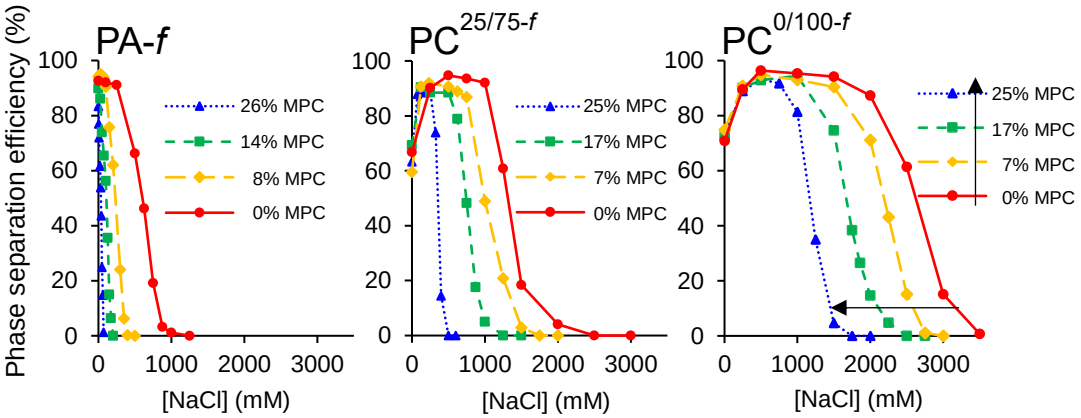

Figure 3.4. Phase separation efficiency determined by UV-vis of PA-*f*, $PC^{25/75\text{-}f}$ and $PC^{0/100\text{-}f}$ with increasing MPC, as a function of [NaCl].

In general, ionic associations within or between polymer chains are subject to screening by NaCl,[39,48,49] which can hamper macroscopic phase separation or lead to complete dissolution of coacervates. In each of the single polyampholytes studied, phase separation is near quantitative at zero or low [NaCl]. Salt ions form extrinsic pairs with polymeric charges, interfering with polymer-polymer intrinsic ionic associations and subsequent coacervation. This leads to an increase in the amount of FITC-labeled, soluble polymer detectable by UV-vis after sedimentation. Incorporation of MPC destabilizes the PECs, lowering the amount of salt for required for significant charge shielding and narrowing the coacervation window: for example, while $PMA_{50}M_0$ coacervation efficiency

only begins to decrease at about 250 mM NaCl, $PMA_{50}M_{17}$ is already fully soluble at 125 mM NaCl.

Polyampholyte coacervates are destabilized due to inherent self-neutralization and limited counterion localization during complexation, thus further sensitivity to stimuli is observed upon MPC introduction. The zwitterionic MPC reduces overall effective charge density, and hence the number of charged groups capable of association during coacervation. Additionally, MPC draws significant amounts of water into the coacervates by dipole-dipole interactions, providing a solvation barrier that weakens ionic and hydrophobic associations, a property commonly exploited in non-fouling applications.[29-33]

Complex coacervates of $PC^{25/75}M_y$ also show heightened sensitivity to ionic strength with increasing MPC mol %. Complexes with 0% MPC are fully solubilized only at 2 M NaCl, whereas complexes with 25% MPC are solubilized at 0.5 M NaCl, respectively. Polyanion-polycation complexes of $PC^{0/100}M_y$ show only moderately higher salt sensitivity in the presence of MPC: 0% MPC coacervates have a critical salt concentration (C_s) of >3 M NaCl, while only 1.5 M is required for complete dissociation of complexes with 25% MPC. It is noted that in complex coacervates, an apparent increase in phase separation efficiency at low [NaCl] is attributed to the formation of colloidally stable PEC that are not separated effectively by sedimentation, resulting in artificially lower efficiencies, as previously reported.[15] On the basis of phase separation efficiency, it is clear the ability of MPC to increase salt sensitivity declines as charges are segregated into larger runs on separate chains. Similar conclusions were drawn using random polyelectrolytes to

discern the differences in charge distribution[7] and can be further supported by systems using sequence-control and specific block separation.

As polyelectrolyte compositions shift from charge-balanced polyampholytes to polyanion-polycation complexes, charges are separated into larger domains or runs of charges. Perry and Sing have shown that larger runs of charges lead to better localization of counterions and hence a larger entropic gain through counterion release during coacervation,[6-13,50] in agreement with other experimental results.[51] We have previously demonstrated these principles using series of charge arrangements in responsive binary polyelectrolyte coacervates.[15] polyampholytes, by definition, incorporate oppositely charged groups along the polymer chain that are capable of intramolecular charge-neutralization, but also disrupt localization of charges. Hence, charge-balanced polyampholytes and to some extent pairs of complementary nonstoichiometric polyampholyte complexes are held together by weaker interactions. In these PECs, the deficient stability allows relatively lower amounts of incorporated MPC, or added [NaCl], to prevent complexation.

By separating charges to generate larger runs of similar charges (PA → $PC^{25/75}$ → $PC^{0/100}$), coacervates are more stabilized and the relative effects of MPC are expected to diminish progressively. Two-component polyampholyte coacervates ($PC^{25/75}$) possess longer charge runs than single polyampholytes but do have a degree of self-neutralization, whereas $PC^{0/100}$ are composed of two polymers with a single type of charged group on each chain, offering greater charge localization and longer charge runs. This is demonstrated clearly in Figure 3.4, signifying the diminished the coacervation window and, concurrently,

the reduction in critical salt concentration by MPC addition is more pronounced in PAs compared to $PC^{25/75}$, and especially compared to $PC^{0/100}$ complexes. For example, the incorporation of 17% MPC reduced the C_s in PA by a factor of 5, in $PC^{25/75}$ by a factor of 3 and in $PC^{0/100}$ by less than a factor of 2. The [NaCl] needed to reduce coacervate efficiency to 50 and 0% as a function of mol % MPC for each complex is plotted in Figure 3.5 and Figure 3A.18. The corresponding MPC required for coacervation efficiency of each complex as a function of salt is shown in Figure 3A.19.

MPC destabilizes ionic associations in these coacervates by simultaneously reducing effective charge density, decreasing charge localization, and increasing complex hydration. We previously found that statistical incorporation of MPC into polycations can reduce the strength of the ionic associations during complexation with calcium alginate hydrogels, leading to greater in-diffusion and thicker polycation membranes at the surface.[22,23] Others have also previously described that the critical salt concentration is markedly decreased by charge dilution of the polyelectrolytes.[17,26] As seen in Figure 3.5, $PC^{0/100}$ coacervates gradually become more salt responsive with reduced effective charge density by MPC addition.

With charge distribution and termonomer incorporation as controllable parameters, phase behaviours can be mapped by using the determined critical salt concentration (Figure 3.5). This approach may prove useful in designing a range of achievable complex charge arrangements with specific sensitivities to various stimuli.

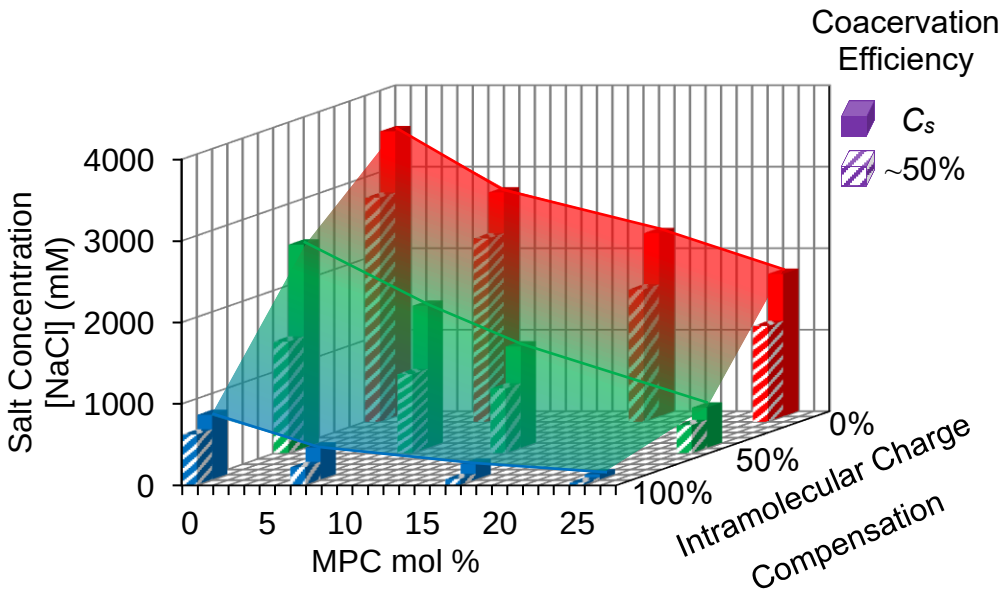

Figure 3.5. 3D map of MAA/APM PEC critical salt concentrations as a function of MPC content and charge arrangement (intramolecular compensation: PA – 100%; $PC^{25/75}$ – 50%; $PC^{0/100}$ – 0%).

Our findings are consistent in lower MW PECs (Figure 3A.17). It is observed that 15% MPC decreases the critical salt concentration for PAs to 6% of those seen in PAs with no MPC, whereas the same amount of MPC addition reduces the critical salt concentration to about 45% in $PC^{25/75}$ and only 80% in $PC^{0/100}$ compared to the respective complex arrangements with no MPC. Additionally, with no added salt, 15% MPC incorporation limits the coacervation efficiency of polyampholytes to 40% but did not substantially impede the coacervation of pure polyanion-polycation complexes. This indicates that the effects of MPC on different polyelectrolyte charge distributions hold consistent at both high and low MW.

3.4.4. Microscopy of Complexes

Using bright field microscopy, binary and ternary polyampholyte self-coacervates were imaged at 0 M added NaCl, at their respective isoelectric points (Figure 3.6). Complexes with 0% MPC show well-defined coacervate droplets capable of fusion and smearing by physical disturbance. As MPC incorporation increases, the corresponding spherical droplets become progressively less distinct and less viscous, reflecting increased hydration. At 25% MPC, only droplets fusing with the settled polymer-dense layer of coacervate liquid can be seen. The liberation of weaker ionic associations in polyampholytes with fewer charged groups by MPC addition leads to hydrated coacervate networks and with mobile polymer acting to fuse individual coacervates. The coacervate networks are more swollen, offering enhanced chain mobility between and within separate polymer-rich domains.

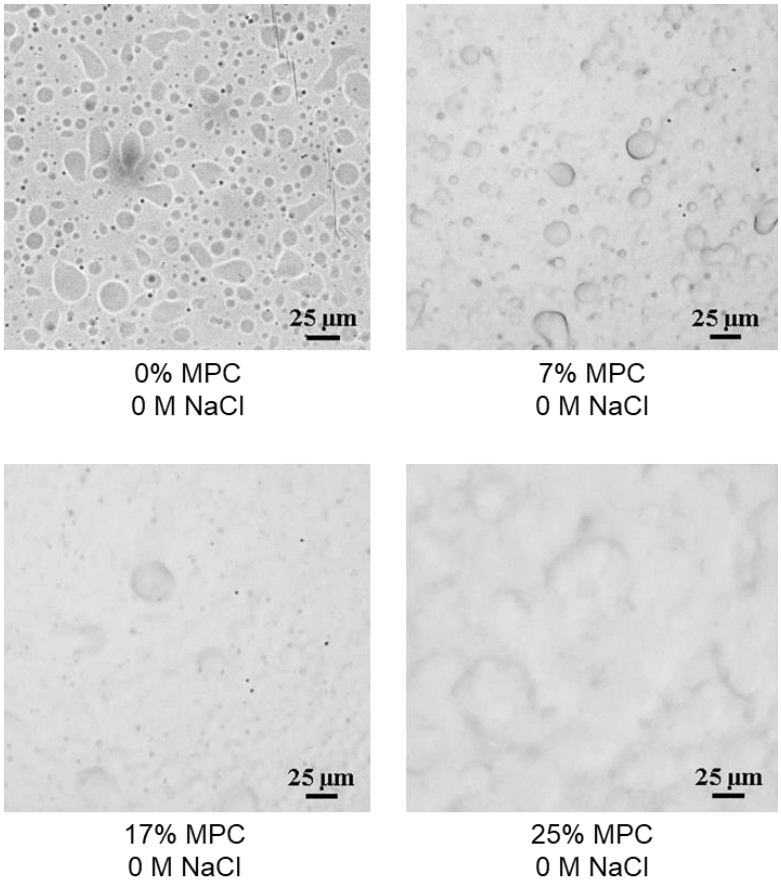

Figure 3.6. Bright field microscope images (20X) of PMA_{50} coacervates with increasing amounts of zwitterionic termonomer.

For complex coacervates, images were taken at [NaCl] required for efficient coacervation. $PC^{25/75}$ complexes appear as spherical coacervate droplets. At each amount of MPC mol %, the amount of salt required to shield and swell coacervates decreases, and larger coacervate droplets are observed. $PC^{25/75}$ complexes with 0 and 14% MPC show comparable coacervate hydration and morphology at different optimal [NaCl], a behaviour similarly observed in $PC^{0/100}$ complexes (Figure 3A.20).

This supports that charge dilution and disruption of charge runs predominantly dictate the increase in stimuli-responsiveness for these PECs. The ionic associations formed

from larger runs of charged groups provide sufficient entropic gain during coacervation to generate more stable complexes, whereas PA coacervates are considerably destabilized by self-neutralization such that added MPC hydration or NaCl can more drastically impact the resulting coacervates.

3.4.5. Temperature Responsive Behaviour and Cloud Point Measurements

Polyampholytes and PECs are known to undergo thermally-induced macroscopic phase separation in aqueous solutions, with cloud point temperatures (CPTs) increasing with increasing NaCl. [15,34,38,52] Figure 3.7 summarizes the cloud point behaviour of the three different coacervate arrangements, separately, as a function of MPC and [NaCl]. Charge-balanced PMA_{50} polyampholytes (PA) show steep transmittance vs. temperature curves, with transmittance decreasing to minima of roughly 10% in the absence of MPC. As MPC is introduced, the curves broaden and the transmittance minima increase, reflecting the increased chain heterogeneity due to reactivity differences between MPC and the charged monomer pool and hydration of these complexes, respectively.

In agreement with phase separation efficiency data, the amount of salt required to raise the cloud point temperature by a given amount is notably reduced with increasing MPC content. This was previously seen in HEA terpolymer polyampholytes[27] and in terpolymer polyampholytes containing hydrophobic groups.[53] Both the $PC^{25/75}M_y$ and the $PC^{0/100}$ transmittance curves show less significant effects of MPC on slope and transmittance minima and less dramatic effects of [NaCl], again in agreement with determined coacervation efficiency trends. It is noted that temperature-induced phase

separation for all complexes appear to be reversible, as solutions became transparent upon cooling (Figure 3A.21).

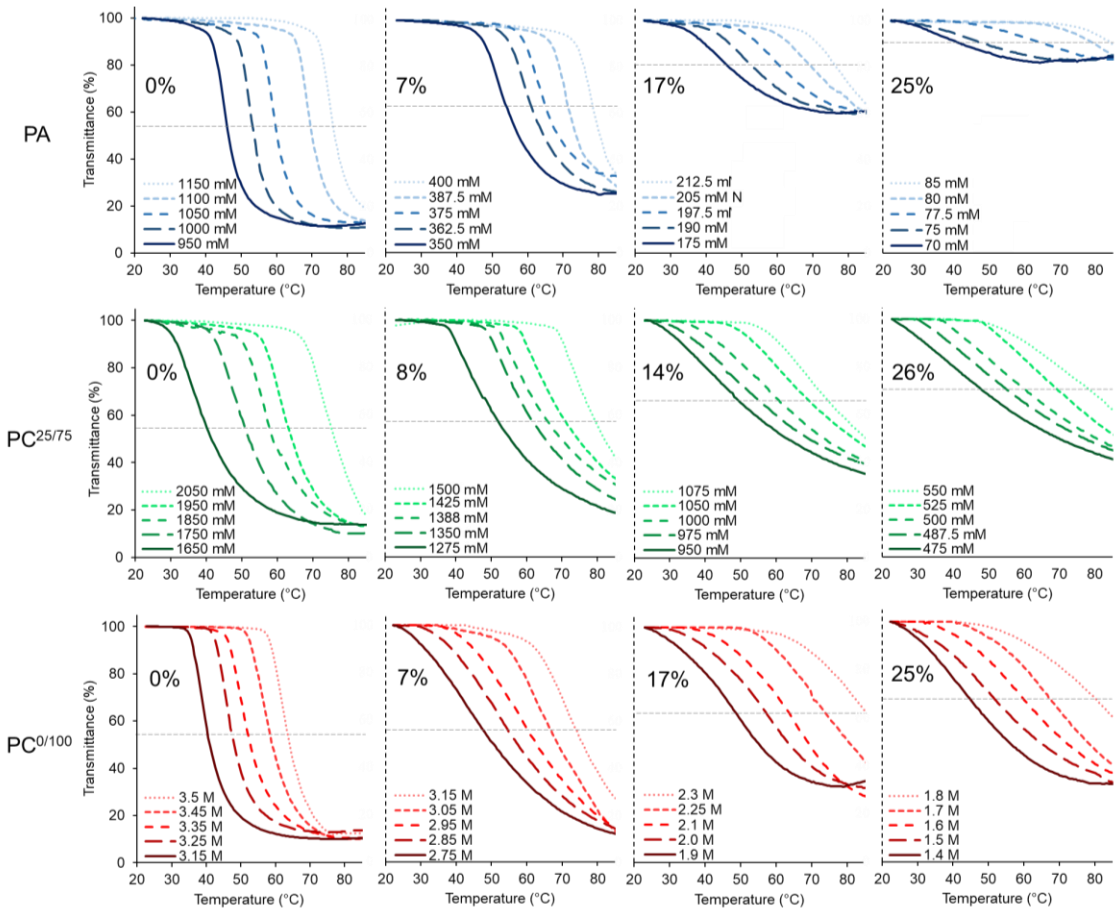

Figure 3.7. Transmittance curves of each PEC arrangement at different [NaCl] and MPC mol % as a function temperature (PA – top; $PC^{25/75}$ – middle; $PC^{0/100}$ – bottom). Dashed lines represent the half-max. turbidity point at which CPTs are determined for each data set.

Figure 3.8 shows plots of the cloud point temperatures of the polyampholytes $PMA_{50}M_y$ against increasing [NaCl] for different MPC mol %. The effect of [NaCl] on cloud points for each polyampholyte is quite linear, with slopes (sensitivity of CPT to NaCl) increasing with increasing MPC. Semilog plotting these slopes against MPC content for all

three complex types studied here (Figure 3.8 (B)) shows that cloud point temperature sensitivity to [NaCl] and % MPC increases with increased intramolecular charge neutralization, specifically in single polyampholytes (full data set in Figure 3A.22). Conversely, $PC^{25/75}M_y$ coacervates gradually increase in sensitivity with MPC and salt (Figure 3A.23), and $PC^{0/100}$ cloud points appear to be relatively insensitive to MPC effects (Figure 3A.24). Raw slopes of CPTs in each complex arrangement are shown in Figure 3A.25.

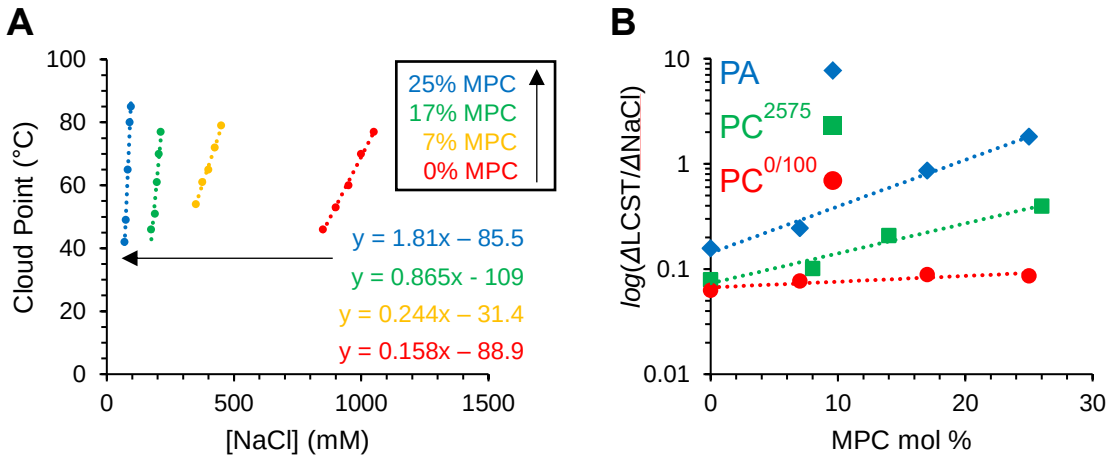

Figure 3.8. (A) Plotted CPTs vs. [NaCl] for $PMA_{50}M_y$ with increasing MPC content. **3.8. (B)** Semilog plot of cloud point response to ΔNaCl vs. MPC mol % for each complex composition.

The coacervation efficiency for the three PEC arrangements illustrates that lowering of the critical salt concentration for all coacervate compositions is achieved by decreasing the effective charge density, impeding ionic associations, and enhancing polymer solubility by MPC incorporation. Heating at [NaCl] above this critical salt concentration can re-establish a favourable entropic gain via the release of counterions and polymer collapse at the respective cloud points. Both coacervation efficiency and cloud point temperatures

hence become more sensitive to [NaCl] with increasing charge separation and with increasing MPC mol %.

In future work, it may be useful to investigate complex coacervate systems at higher levels of MPC with different termonomers and systematically at different molecular weights to further explore the differences between these complex coacervate arrangements.[15,54-56]

3.5. Conclusions

An exploration of various terpolymerizations of MPC with APM and MAA showed that MAA/APM drift can be minimized through use of specific, empirically determined MAA/NaMAA ratios, while a slight favourability toward MPC incorporation can be mitigated by limiting conversion to 60%.

The effects of incorporating MPC on PEC sensitivity to pH, ionic strength, and temperature were determined through turbidimetric titrations, UV-vis determination of coacervation efficiencies and cloud point measurements; the relative impact was found to depend strongly on charge separation, decreasing with greater charge separation from single polyampholytes PMA_{50}, through pairs of complementary nonstoichiometric polyampholytes $PC^{25/75}$, to fully charge-separated polyanion-polycation $PC^{0/100}$ complexes.

Charge-balanced combinations of nonstoichiometric polyampholytes and polyanion/polycation polyelectrolytes do offer simpler pH(*I*) control and a wider range of isoelectric points compared to single, composition-dependent polyampholytes. Therefore, it may be useful to explore other charge arrangements between single-component

polyampholytes and the nonstoichiometric polyampholyte complex coacervates, to better map the phase behaviour and responsive properties as charge compensation is increased.

For future work, it may be useful to prepare copolymers with defined MW and further limit residual MPC compositional drift using, e.g., controlled radical copolymerization combined with either semi-batch addition of MPC, use of different betaine comonomers, or post-polymerization modification. It may also be useful to explore less costly cationic monomers such as *N*,*N*-(dimethylaminoethyl) methacrylate (DMAEMA) to allow for larger scale polymerizations needed for rheological studies and generation of a binodal phase diagram, as previously described.[39] The coacervate arrangements offer themselves as potential responsive underwater adhesives and scalable models for intrinsically disordered proteins used in the formation of so-called membraneless organelles. Additionally, these different coacervates may be crosslinked to form macro and microgels with tunable swelling behaviour and binding/release properties in drug delivery systems. Finally, it may be interesting to similarly investigate polymers that exhibit upper critical solution temperatures in solution, as MPC may also be capable of tuning their stimuli-responsive properties toward conditions useful in biomedicine.

Supporting Information

^{1}H NMR tracking of monomer reactivities in PMA_{50} with MPC; Fineman-Ross plot of reactivity ratios for the charged monomer pool and MPC in PMA_{50}; ^{1}H NMR tracking of MPC feed in different polyampholytes; instantaneous copolymer equation plots of NMR data for different polyampholytes with MPC; GPC traces of polymers; characterization of binary polyelectrolytes with MPC; characterization of low-MW polymers; forward/backward titrations of low MW charge-balanced solutions of PMA_{50}, $PC^{25/75}$, and $PC^{0/100}$ with increasing MPC; UV−vis absorbance curves of PMA_{50} for phase separation efficiency; phase separation efficiency for low MW complexes; raw data expected MPC required to achieve specific critical salt concentrations; images of optimal [NaCl] coacervates of $PC^{25/75}$ and $PC^{0/100}$ at different MPC mol %; lower critical solution temperatures plotted against ionic strength for PA, $PC^{25/75}$, and $PC^{0/100}$ with increasing MPC mol %; raw slopes of cloud point temperatures for different complexes as a function of MPC mol %; images of reversible coacervation with cooling below LCST.

Author Information

Corresponding Author

Email: stoverh@mcmaster.ca, Ph.: 1-905-525-9140 ext. 24983.

Notes:

The authors declare no competing financial interest.

3.6. Acknowledgements

The authors would like to thank the Natural Sciences and Engineering Research Council of Canada funding for this research through its Discovery Grant program (RGPIN89661-11), and through the CGS-D award held by D. E. Hastings. In addition, the authors thank Ryan Wylie for allowing the use of the Agilent GPC and Alex Jesmer for assisting in the experiments involved. The authors also thank Alex Adronov for allowing the use of his UV-vis Spectrophotometer and Dialia Ritaine for assisting with equipment setup. Finally, the authors thank Carl Ellis for his assistance with general equipment maintenance and operation.

3.7. References

1. Luo, Y.; Wang, Q. Recent development of chitosan-based polyelectrolyte complexes with natural polysaccharides for drug delivery. *Int. J. Bio. Macromol.* **2014**, *64*, 353-367.

2. Hamad, F. G.; Chen, Q.; Colby, R. H. Linear Viscoelasticity and Swelling of Polyelectrolyte Complex Coacervates. *Macromolecules* **2018**, *51*, 5547-5555.

3. Zhang, H.; Wang, C.; Zhu, G.; Zacharia, N. S. Self-Healing of Bulk Polyelectrolyte Complex Material as a Function of pH and Salt. *ACS Appl. Mater. Interfaces* **2016**, *8*, 26258-26265.

4. Chen, D.; Wu, M.; Li, B.; Ren, K.; Cheng, Z.; Ji, J.; Li, Y.; Sun, J. Layer-by-Layer-Assembled Healable Antifouling Films. *Adv. Mater.* **2015**, *27*, 5885-5888.

5. Liao, M.; Wan, P.; Wen, J.; Gong, M.; Wu, X.; Wang, Y.; Shi, R.; Zhang, L. Wearable, Healable, and Adhesive Epidermal Sensors Assembled from Mussel-Inspired Conductive Hybrid Hydrogel Framework. *Adv. Funct. Mater.* **2017**, *27*, 1703852.

6. Chang, L.-W.; Lytle, T. K.; Radhakrishna, M.; Madinya, J. J.; Vélez, J.; Sing, C. E.; Perry, S. L. Sequence and entropy-based control of complex coacervates. *Nat. Commun.* **2017**, *8*, 1273.

7. Rumyantsev, A. M.; Jackson, N. E.; Yu, B.; Ting, J. M.; Chen, W.; Tirrell, M. V.; de Pablo, J. J. Controlling Complex Coacervation via Random Polyelectrolyte Sequences. *ACS Macro Lett.* **2019**, *8*, 1296-1302.

8. Pak, C. W.; Kosno, M.; Holehouse, A. S.; Padrick, S. B.; Mittal, A.; Ali, R.; Yunus, A. A.; Liu, D. R.; Pappu, R. V.; Rosen, M. K. Sequence Determinants of Intracellular Phase Separation by Complex Coacervation of a Disordered Protein. *Mol. Cell* **2016**, *63*, 72-85.

9. Tabandeh, S.; Leon, L. Engineering Peptide-Based Polyelectrolyte Complexes with Increased Hydrophobicity. *Molecules* **2019**, *24*, 868.

10. Hazra, M. K.; Levy, Y. Charge pattern affects the structure and dynamics of polyampholyte condensates. *Phys. Chem. Chem. Phys.* **2020**, *22*, 19368-19375.

11. Luo, F.; Sun, T.-L.; Nakajima, T.; Kurokawa, T.; Zhao, Y.; Sato, K.; Ihsan, A. B.; Li, X.; Guo, H.; Gong, J. P. Oppositely Charged Polyelectrolytes Form Tough, Self-Healing, and Rebuildable Hydrogels. *Adv. Mater.* **2015**, *27*, 2722-2727.

12. Madinya, J. J.; Chang, L.-W.; Perry, S. L.; Sing, C. E. Sequence-Dependent Self-Coacervation in High Charge-Density Polyampholytes. *Mol. Sys. Des. Eng.* **2020**, *5*, 632-644.

13. Lytle, T. K.; Chang, L.-W.; Markiewicz, N.; Perry, S. L.; Sing, C. E. Designing Electrostatic Interactions via Polyelectrolyte Monomer Sequence. *ACS Cent. Sci.* **2019**, *5*, 709-718.

14. Radhakrishna, M.; Basu, K.; Liu, Y.; Shamsi, R.; Perry, S. L.; Sing, C. E. Molecular Connectivity and Correlation Effects on Polymer Coacervation. *Macromolecules* **2017**, *50*, 3030-3037.

15. Hastings, D. E.; Bozelli, J. C.; Epand, R. M.; Stöver, H. D. H. Investigating the Effects of Charge Arrangement in Stimuli-Responsive Polyelectrolytes. *Macromolecules* **2021**, *54*, 11427-11438.

16. Mattison, K. W.; Dubin, P. L.; Brittain, I. J. Complex Formation between Bovine Serum Albumin and Strong Polyelectrolytes: Effect of Polymer Charge Density. *J. Phys. Chem. B* **1998**, *19*, 3830-3836.

17. Neitzel, A. E.; Fang, Y. N.; Yu, B.; Rumyantsev, A. M.; de Pablo, J. J.; Tirrell, M. V. Polyelectrolyte Complex Coacervation across a Broad Range of Charge Densities. *Macromolecules* **2021**, *54*, 6878-6890.

18. Hugerth, A.; Caram-Lelham, N.; Sunfelöf, L.-O. The effect of charge density and conformation on the polyelectrolyte complex formation between carrageenan and chitosan. *Carbohydr. Polym.* **1997**, *34*, 149-156.

19. Dautzenberg, H.; Jaeger, W. Effect of Charge Density on the Formation and Salt Stability of Polyelectrolyte Complexes. *Macromol. Chem. Phys.* **2002**, *203*, 2095-2102.

20. Kayitmazer, A. B.; Koksal, A. F.; Iyilik, E. K. Complex Coacervation of Hyaluronic Acid and Chitosan: Effect of pH, Ionic Strength, Charge Density, Chain Length and Charge Ratio. *Soft Matter* **2015**, *11*, 8605-8612.

21. Seručnik, M.; Podlipnik, Č.; Hribar-Lee, B. DNA-Polyelectrolyte Complexation Study: The Effect of Polyion Charge Density and Chemical Nature of the Counterions. *J. Phys. Chem. B* **2018**, *122*, 5381-5388.

22. Kleinberger, R. M.; Burke, N. A. D.; Zhou, C.; Stöver, H. D. H. Synthetic polycations with controlled charge density and molecular weight as building blocks for biomaterials. *J. Biomater. Sci. Polym. Ed.* **2016**, *27*, 351-369.

23. Hastings, D. E.; Stöver, H. D. H. Crosslinked Hydrogel Capsules for Cell Encapsulation Formed Using Amino/Betaine Dual-Functional Semibatch Copolymers. *ACS Appl. Polym. Mater.* **2019**, *1*, 2055-2067.

24. Barlow, D. J.; Thornton, J. M. The Distribution of Charged Groups in Proteins. *Biopolymers* **1986**, *25*, 1717-1733.

25. Collins, K. D. Charge Density-Dependent Strength of Hydration and Biological Structure. *Biophys. J.* **1997**, *72*, 65-76.

26. Huang, J.; Morin, F. J.; Laaser, J. E. Charge-Density-Dominated Phase Behaviour and Viscoelastic Properties of Polyelectrolyte Complex Coacervates. *Macromolecules* **2019**, *52*, 4957-4967.

27. Abdilla, A.; Shi, S.; Burke, N. A. D.; Stöver, H. D. H. Multistimuli responsive ternary polyampholytes: Formation and crosslinking of coacervates. *J. Polym. Sci. A Polym. Chem.* **2016**, *54*, 2109-2118.

28. Lee, J. H.; Lee, D. S.; Jung, Y. C.; Oh, J.-W.; Na, Y. H. Development of a Tough, Self-Healing Polyampholyte Terpolymer Hydrogel Patch with Enhanced Skin Adhesion via Tuning the Density and Strength of Ion-Pair Associations. *ASC. Appl. Mater. Interfaces* **2021**, *13*, 8889-8900.

29. Ahmed, M.; Bhuchar, N.; Ishihara, K.; Narain, R. Well-Controlled Cationic Water-Soluble Phospholipid Polymer-DNA Nanocomplexes for Gene Delivery. *Bioconjugate Chem.* **2011**, *22*, 1228-1238.

30. Ye, S. H.; Watanabe, J.; Iwasaki, Y.; Ishihara, K. Antifouling blood purification membrane composed of cellulose acetate and phospholipid polymer. *Biomaterials* **2003**, *24*, 4143-4152.

31. Lin, X.; Boit, M. O.; Wu, K.; Jain, P.; Liu, E. J.; Hsieh, Y.-F.; Zhou, Q.; Li, B.; Hung, H.-C.; Jiang, S. Zwitterionic carboxybetaine polymers extend the shelf-life of human platelets. *Acta Biomater.* **2020**, *109*, 51-60.

32. Jiang, S.; Cao, Z. Ultralow-Fouling, Functionalizable and Hydrolyzable Zwitterionic Materials and Their Derivatives for Biological Applications. *Adv. Mater.* **2010**, *22*, 920-932.

33. Wu, J.; Lin, W.; Wang, Z.; Chen, S. Investigation of the Hydration of Nonfouling Material Poly(sulfobetaine methacrylate) by Low-Field Nuclear Magnetic Resonance. *Langmuir* **2012**, *28*, 7436-7441.

34. Dubey, A.; Burke, N. A. D.; Stöver, H. D. H. Preparation and Characterization of Narrow Compositional Distribution Polyampholytes as Potential Biomaterials: Copolymers of *N*-(3-Aminopropyl)methacrylamide Hydrochloride and Methacrylic Acid (MAA). *J. Polym. Sci. A Polym. Chem.* **2015**, *53*, 353-365.

35. Aguilar, M.; Gallardo, A.; Fernández, M.; Román, J. In-Situ Quantitative 1H NMR Monitoring of Monomer Consumption: A Simple and Fast Way of Estimating Reactivity Ratios. *Macromolecules* **2002**, *35*, 2036-2041.

36. Fineman, M.; Ross, S. D. Linear method for determining monomer reactivity ratios in copolymerization. *J. Polym. Sci.* **1950**, *5*, 259-262.

37. Buback, M.; Hesse, P.; Hutchinson, R. A.; Kasák, P.; Lacik, I.; Stach, M.; Utz, I. Kinetics and Modelling of Free-Radical Batch Polymerization of Nonionized Methacrylic Acid in Aqueous Solution. *Ind. Eng. Chem. Res.* **2008**, *47*, 8197-8204.

38. Zhao, J.; Burke, N. A. D.; Stöver, H. D. H. Preparation and study of multi-responsive polyampholyte copolymers of *N*-(3-aminopropyl)methacrylamide hydrochloride and acrylic acid. *RCS Adv.* **2016**, *6*, 41522-41531.

39. Spruijt, E.; Westphal, A. H.; Borst, J. W.; Stuart, M. A. C.; van der Gucht, J. Binodal Compositions of Polyelectrolyte Complexes. *Macromolecules* **2010**, *43*, 6476-6484.

40. Zhang, R.; Shklovskii, B. I. Phase diagram of solution of oppositely charged polyelectrolytes. *Phys. A* **2005**, *352*, 216-238.

41. Wang, Q.; Schlenoff, J. B. The Polyelectrolyte Complex/Coacervate Continuum. *Macromolecules* **2014**, *47*, 3108-3116.

42. Patrickios, C. S. Polypeptide amino acid composition and isoelectric point: 1. A closed-form approximation. *J. Colloid Interface Sci.* **1995**, *175*, 256-260.

43. Leng, C.; Huang, H.; Sun, S. W.; Wang, D. Y.; Li, Y. T.; Jiang, S.; Chen, Z. Probing the Surface Hydration of Nonfouling Zwitterionic and PEG Materials in Contact with Proteins. *ACS Appl. Mater. Interfaces* **2015**, *7*, 16881-16888.

44. Ishihara, K.; Nomura, H.; Mihara, T.; Kurita, K.; Iwasaki, Y.; Nakabayashi, N. Why Do Phospholipid Polymers Reduce Protein Adsorption? *J. Biomed. Mater. Res.* **1998**, *39*, 323-330.

45. He, Y.; Hower, J.; Chen, S.; Bernards, M. T.; Chang, Y.; Jiang, S. Molecular Simulation Studies of Protein Interactions with Zwitterionic Phosphorylcholine Self-Assembled Monolayers in the Presence of Water. *Langmuir* **2008**, *24*, 10358-10364.

46. Morisaku, T.; Watanabe, J.; Konno, T.; Takai, M.; Ishihara, K. Hydration of Phosphorylcholine Groups Attached to Highly Swollen Polymer Hydrogels Studied by Thermal Analysis. *Polymer* **2008**, *49*, 4652-4657.

47. Johnston, B. M.; Johnston, C. W.; Letteri, R. A.; Lytle, T. K.; Sing, C. E.; Emrick, T.; Perry, S. L. The effect of comb architecture on complex coacervation. *Org. Biomol. Chem.* **2017**, *15*, 7630-7642.

48. Srivastava, S.; Tirrell, M. V. Polyelectrolyte Complexation. *Adv. Chem. Phys.* **2016**, *161*, 499-543.

49. Neitzel, A. E.; De Hoe, G. X.; Tirrell, M. V. Expanding the structural diversity of polyelectrolyte complexes and polyzwitterions. *Curr. Opin. Solid State Mater. Sci.* **2021**, *25*, 100897.

50. Sing, C. E.; Perry, S. L. Recent Progress in the Science of Complex Coacervation. *Soft Matter* **2020**, *16*, 2885-2914.

51. Patrickios, C. S.; Hertler, W. R.; Abbott, N. L.; Hatton, T. A. Diblock, ABC Triblock, and Random Methacrylic Polyampholytes: Synthesis by Group Transfer Polymerization and Solution Behavior. *Macromolecules* **1994**, *27*, 930-937.

52. Ali, S.; Bleuel, M.; Prabhu, V. M. Lower Critical Solution Temperature in Polyelectrolyte Complex Coacervates. *ACS Macro. Lett.* **2019**, *8*, 289-293.

53. Das, E.; Matsumura, K. Tunable Phase-Separation Behavior of Thermoresponsive Polyampholytes Through Molecular Design. *J. Polym. Sci. A Polym. Chem.* **2017**, *55*, 876-884.

54. Zhao, J. Synthesis and Properties of Polyampholyte and Their Application to Cell Cryoprotection. Ph.D. Dissertation, McMaster University, Hamilton, ON, **2018**.

55. Sharker, K. K.; Ohara, Y.; Shigeta, Y.; Ozoe, S.; Yusa, S.-I. Upper Critical Solution Temperature (UCST) Behavior of Polystyrene-Based Polyampholytes in Aqueous Solution. *Polymers* **2019**, *11*, 265.

56. Ieong, N. S.; Hasan, M.; Phillips, D. J.; Saaka, Y.; O'Reilly, R. K.; Gibson, M. I. Polymers with molecular weight dependent LCSTs are essential for cooperative behaviour. *Polym. Chem.* **2012**, *3*, 794-799.

3.8. Appendix

Figure 3A.1. ^{1}H NMR tracking of MAA:APM ratio in comonomer feed during terpolymerization with MPC in NMR scale polymerizations of PMA_{50}.

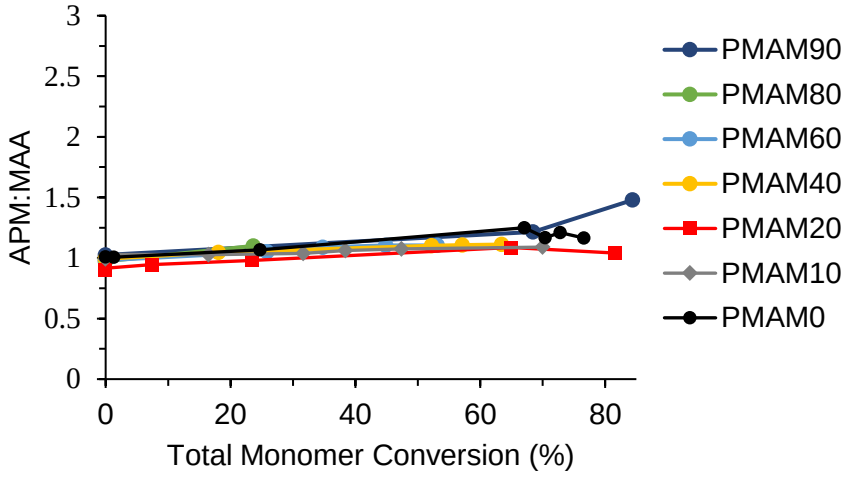

Suppression of APM/MAA drift during ternary copolymerizations, across MPC loadings ranging from 10 to 90 mol %. A 3:1 molar ratio of APM:MAA was used in all ternary PMA_{50} polymerizations, resulting in essentially 1:1 molar incorporation of APM and MAA to relatively high conversion for all MPC ratios.

Figure 3A.2. Fineman-Ross plot of reactivity ratios for MPC with (MAA/APM).

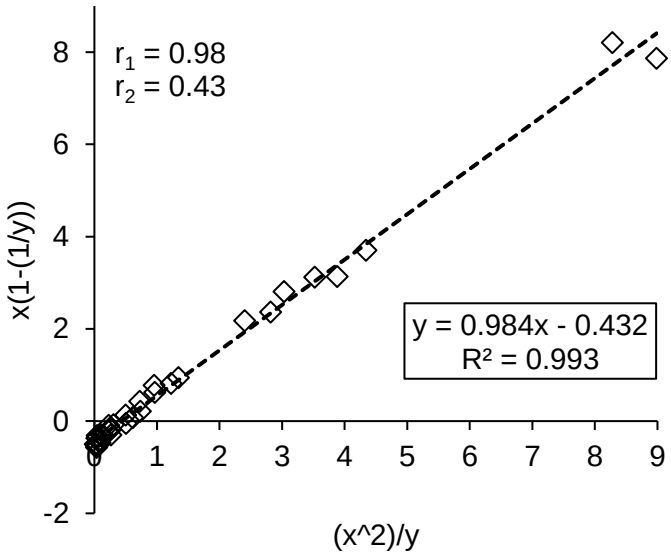

Figure 3A.3. ^{1}H NMR tracking in different polyampholytes shows the ratio of charged monomers in the comonomer feed are stable through terpolymer conversion with MPC.

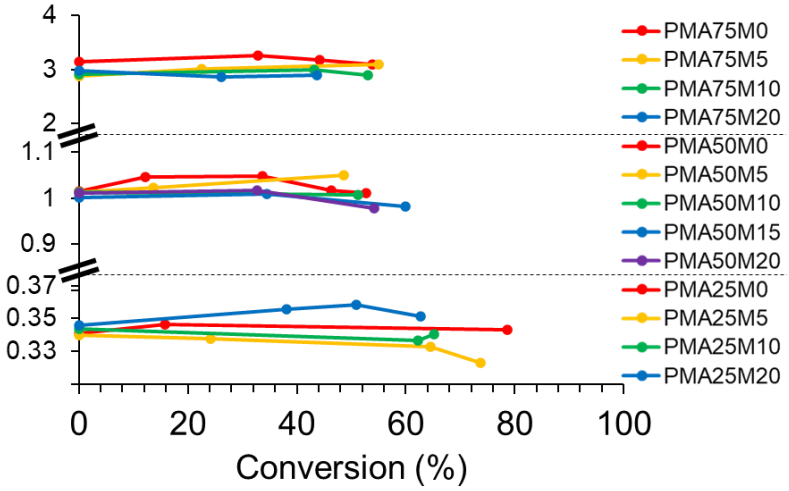

Figure 3A.4. Mol fraction of MPC in termonomer feed through conversion, tracked using ^{1}H NMR.

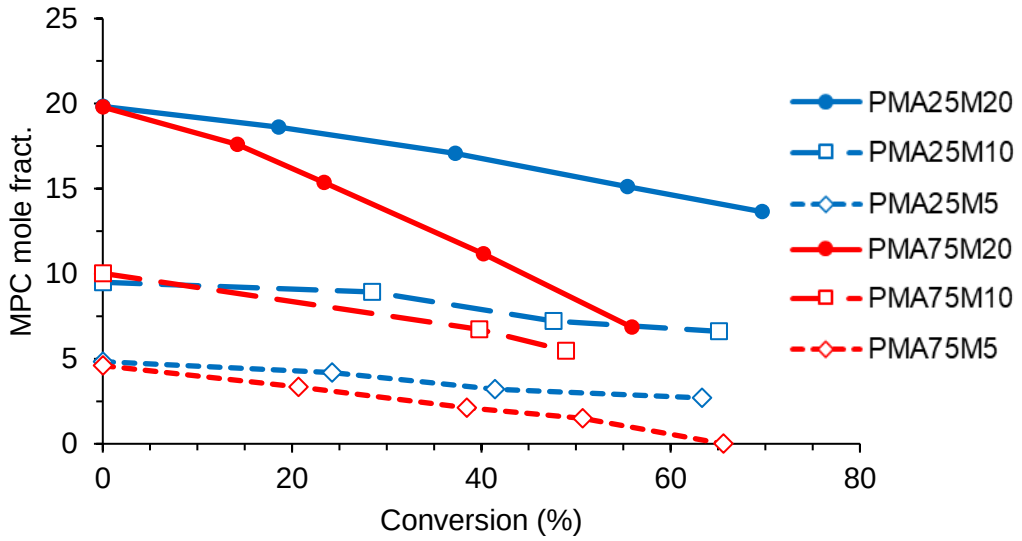

Figure 3A.5. MPC incorporation plotted for PMA_{25}, PMA_{50}, and PMA_{75} polyampholytes up to 20% monomer feed.

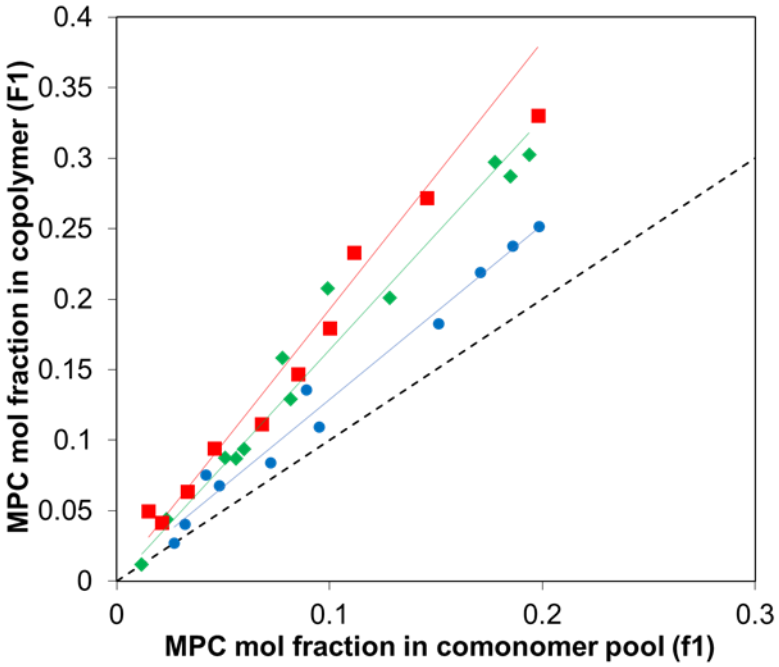

Figure 3A.6. GPC traces for $PMA_{50}M_y$ terpolymers using Waters aqueous GPC (pH 4.7).

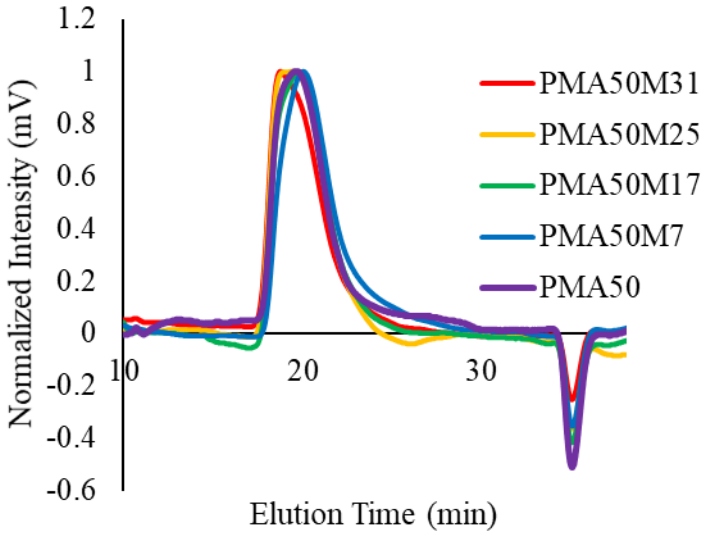

Figure 3A.7. GPC traces for $PMA_{75}M_y$ terpolymers using Waters aqueous GPC (pH 4.7).

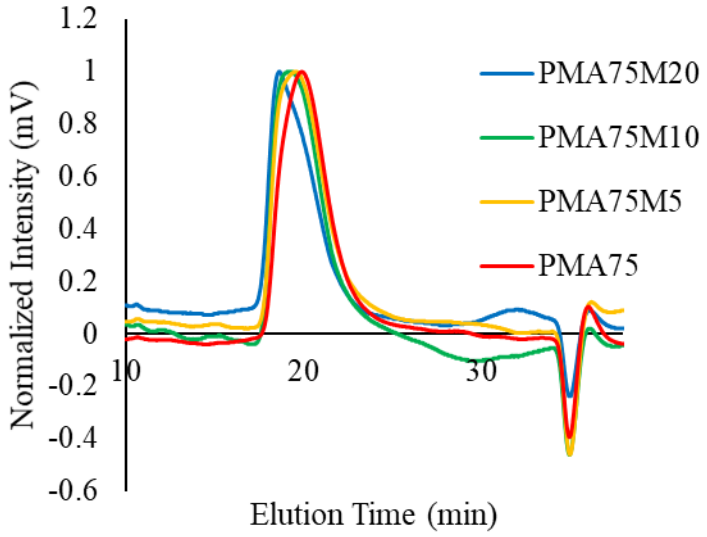

Figure 3A.8. GPC traces for PAM_y copolymers using Waters aqueous GPC (pH 4.7).

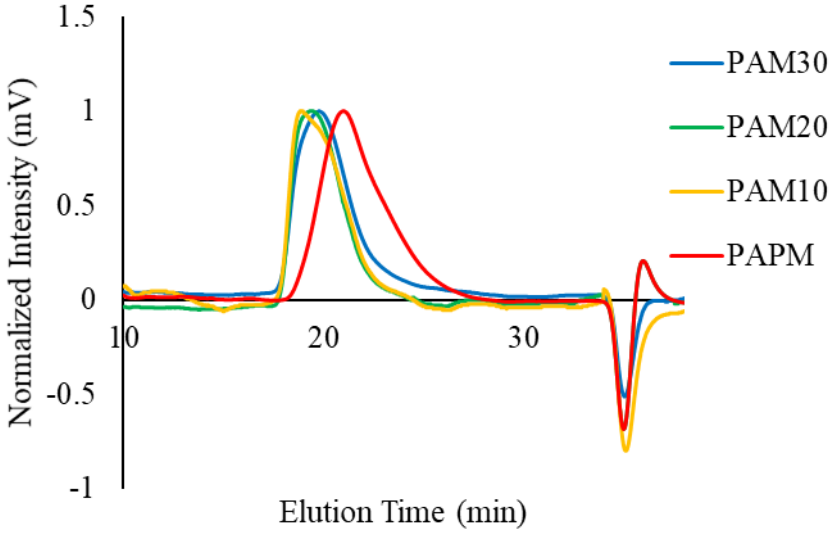

Figure 3A.9. GPC traces for $PMA_{25}M_y$ terpolymers using Agilent aqueous GPC (pH 9.4).

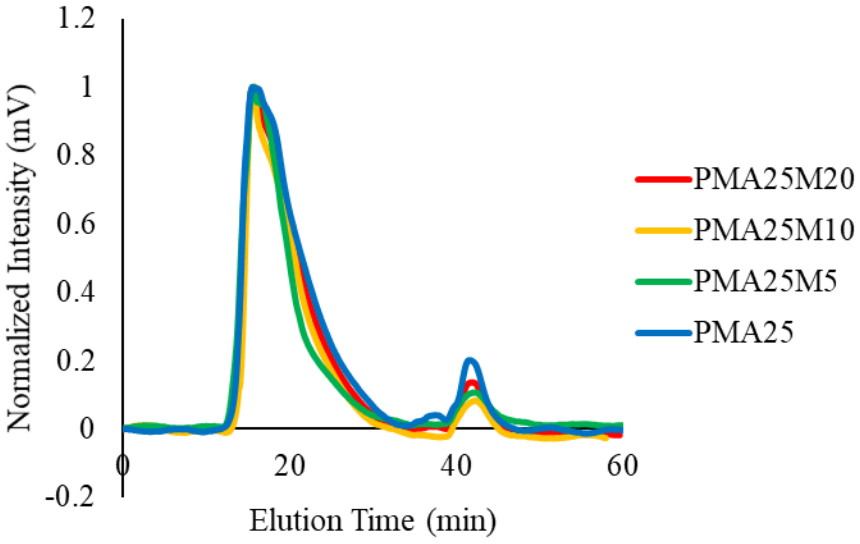

Figure 3A.10. GPC traces for PMM_y copolymers using Agilent aqueous GPC (pH 9.4).

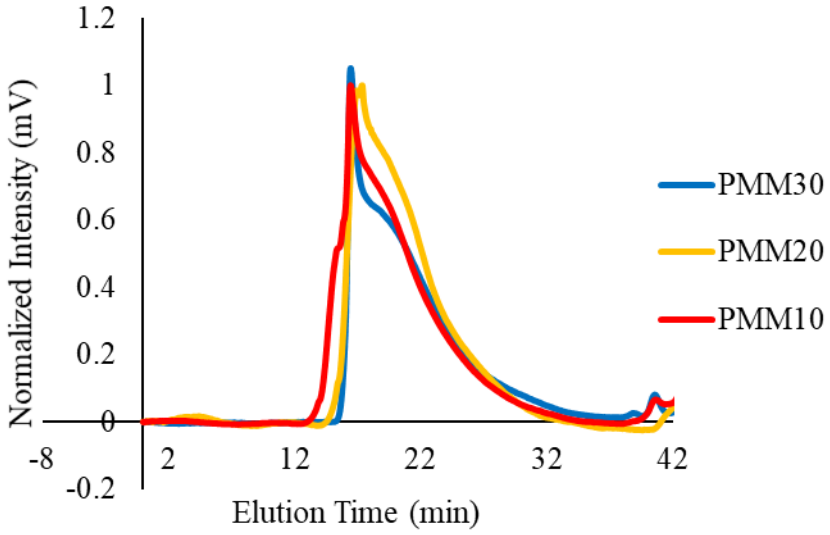

Table 3A.11. Characterized copolymers of MAA-MPC (PMM_y) and APM-MPC (PAM_y).

MAA: Na^+MAA	Polymer	Composition (MAA/APM:MPC)*	M_p (kDa)	Est. Charge at pH 7
1:0	**P(NaMAA)**	100:0	412	-100
1:0	**PMM_{10}**	90:10	428	-90
1:0	**PMM_{22}**	78:22	422	-88
1:0	**PMM_{26}**	74:26	450	-73
N/A	**P(APM)***	100:0	251	+100
N/A	**PAM_5***	95:5	301	+91
N/A	**PAM_{13}***	87:13	332	+87
N/A	**PAM_{24}***	77:23	338	+77

*FITC-labelled post-polymerization. M_p are listed here as the high MW polymers exceed the exclusion limit of the GPC columns used.

Table 3A.12. Characterized lower MW polymers.

MAA: Na^+MAA	Polymer	Composition (MAA:APM:MPC)	Measured pH(*I*)	M_p (kDa)	M_n (kDa)	*Đ*	Est. Charge (pH 7)
3:2	**PMA_{25}**	76:24:0	4.55	37	27	1.8	-52
3:2	**$PMA_{25}M_6$**	76:24:6	--	36	27	1.9	-52
3:2	**$PMA_{25}M_{13}$**	65:22:13	--	40	31	1.8	-43
1:3	**PMA_{50}**	49:51:0	7.95	39	28	1.6	+2
1:3	**$PMA_{50}M_8$**	46:46:8	6.86	25	16	1.5	0
1:3	**$PMA_{50}M_{15}$**	42:43:15	7.6	27	18	1.7	+1
0:1	**PMA_{75}**	25:75:0	N/A	26	19	1.7	+50
0:1	**$PMA_{75}M_5$**	24:71:5	N/A	25	18	1.7	+50
0:1	**$PMA_{75}M_{12}$**	23:65:12	N/A	28	20	1.6	+42
N/A	**P(NaMAA)**	100:0:0	N/A	28	18.5	--	-100
N/A	**PMM_{10}**	90:0:10	N/A	31	20	1.8	-90
N/A	**PMM_{21}**	79:0:21	N/A	36	24	1.8	-79
N/A	**P(APM)**	0:100:0	N/A	38	26	1.6	+100
N/A	**PAM_6**	0:94:6	N/A	38	25	1.6	+94
N/A	**PAM_{10}**	0:90:10	N/A	40	29	1.7	+90

*FITC-labelled post-polymerization.

Figure 3A.13. Titration curves for low MW $PMA_{50}M_y$.

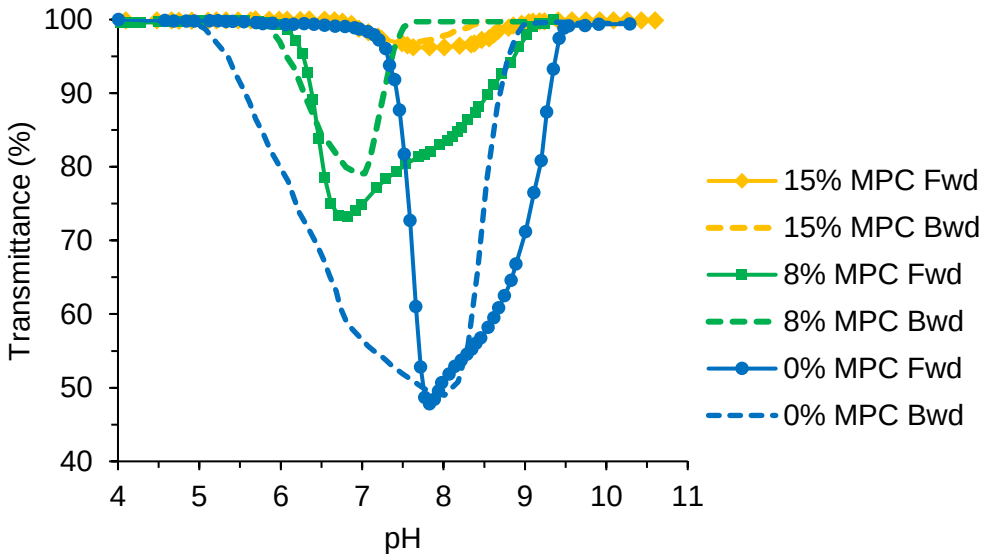

Figure 3A.14. Titration curves for low MW $PC^{25/75}M_y$.

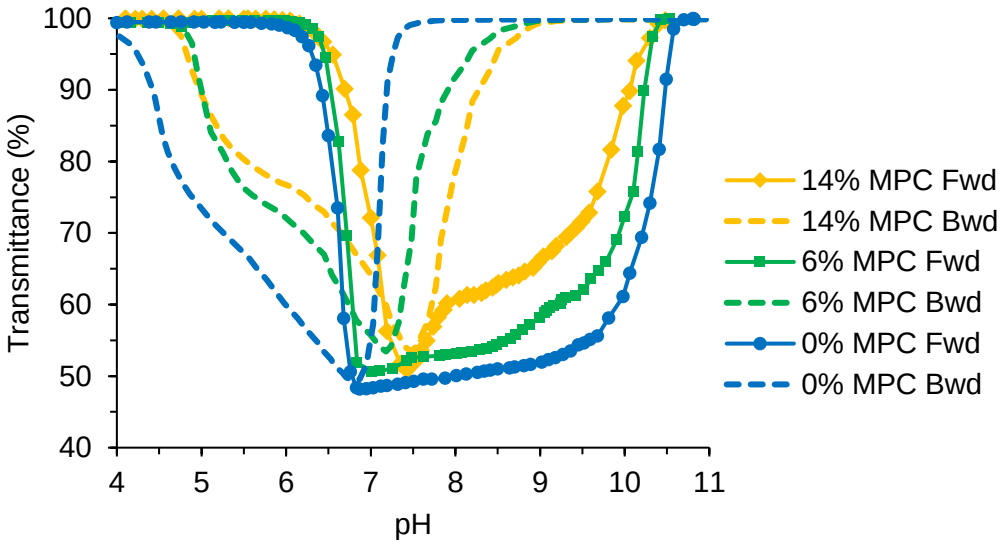

Figure 3A.15. Titration curves for low MW $PC^{0/100}M_{y.}$

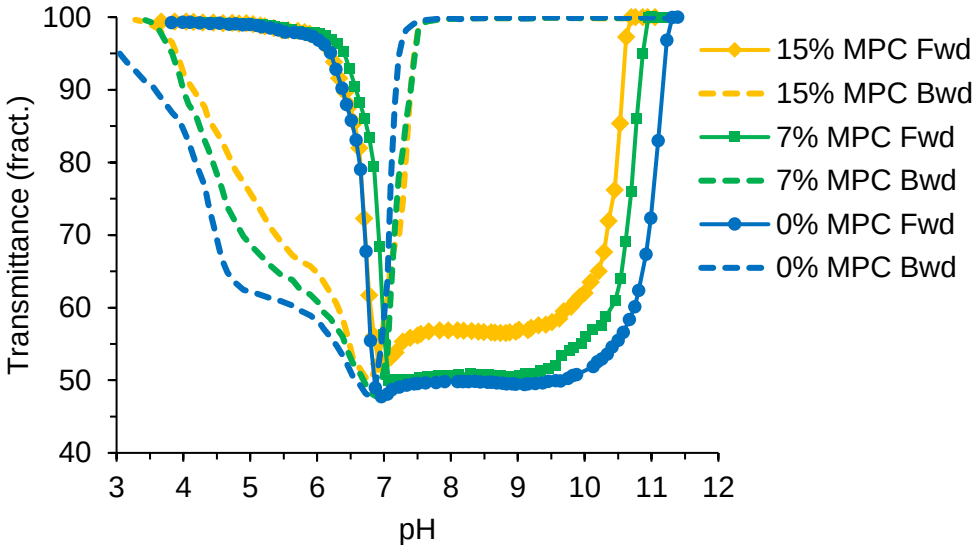

Figure 3A.16. UV-vis absorbance curves for PMA_{50}-*f* with increasing [NaCl].

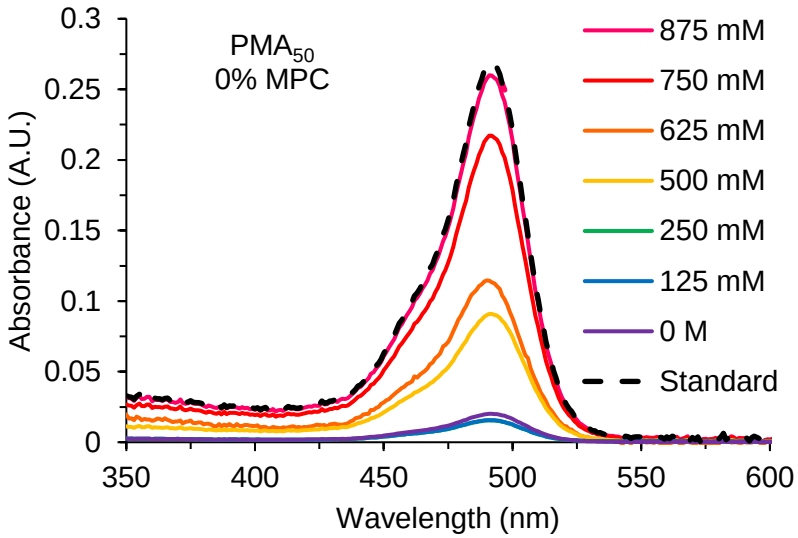

Figure 3A.17. Phase separation efficiency of low MW coacervates.

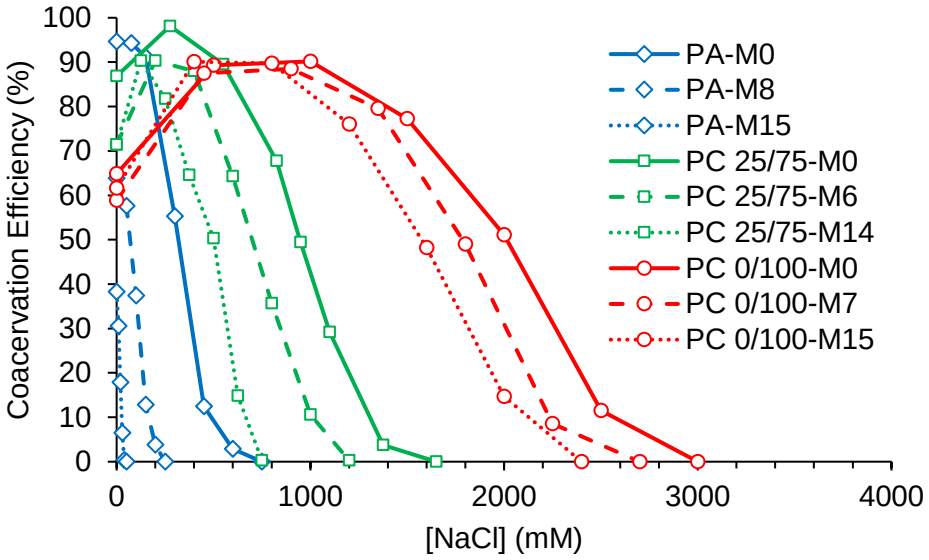

Most high MW PA systems show phase separation efficiencies of above 90%, with even the polyampholyte system $PMA_{50}M_{25}$, expected to have the weakest intermolecular interactions, showing 80% phase separation at zero [NaCl]. It is noted here that MPC prevents a significant amount of ionic association and solubilizes the polyampholyte, preventing macroscopic phase separation to roughly 40% with as little as 15% MPC. This shows that MPC hydration is highly effective in polyampholytes compared to complex coacervates.

Figure 3A.18. Relative critical salt concentration as a function of MPC (solid), and [NaCl] required for ~50% phase separation efficiency (dashed). Plot is normalized for each complex using the critical salt concentration and [NaCl] for 50% coacervation with 0% MPC. Lines are drawn to aid the eye.

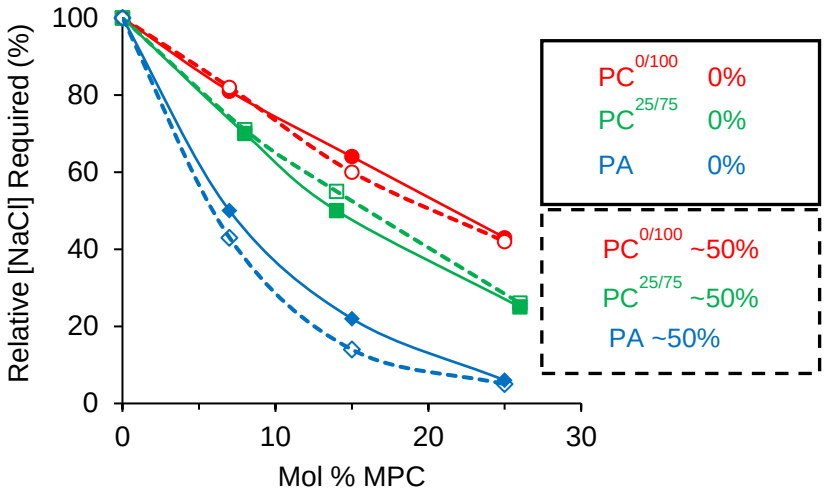

Figure 3A.19. NaCl required for estimated 0% (solid) and 50% (dashed) phase separation efficiency for PA (blue), $PC^{25/75}$ (green), and $PC^{0/100}$ (red) complexes with different amounts of incorporated MPC.

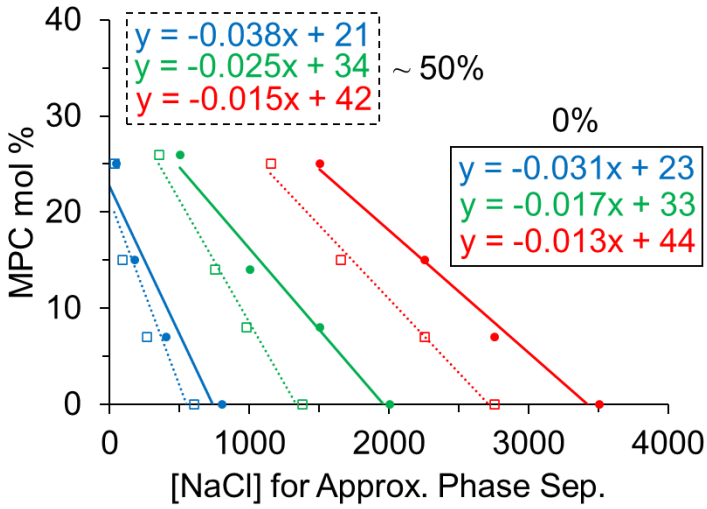

Slopes of the resulting [NaCl] required for each complex arrangement with different MPC mol % for both complete charge shielding (0% efficiency) and partial charge shielding (50%) indicate that the complexes increase in sensitivity to salt with increasing charge compensation (PA > $PC^{25/75}$ > $PC^{0/100}$). The y-intercepts indicate that $PC^{25/75}$ complexes also likely require greater MPC incorporation to fully prevent

coacervation (~33-34%), which is further exacerbated in $PC^{0/100}$ (~42-44%); further investigation may help better approximate the curve shapes in each complex.

Figure 3A.20. Bright field microscope (*20X*) images of complex coacervates $PC^{25/75}$ (left) and $PC^{0/100}$ (right) with different amounts of MPC at optimal [NaCl] for high phase separation efficiency.

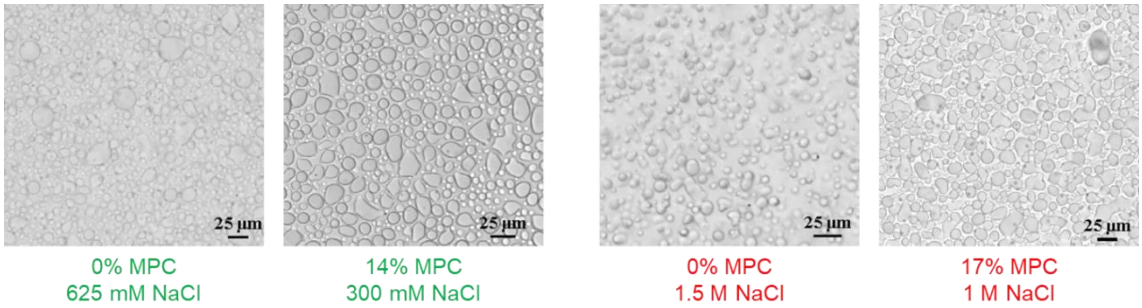

Figure 3A.21. Reversible cloud point temperatures of PMA_{50} coacervates.

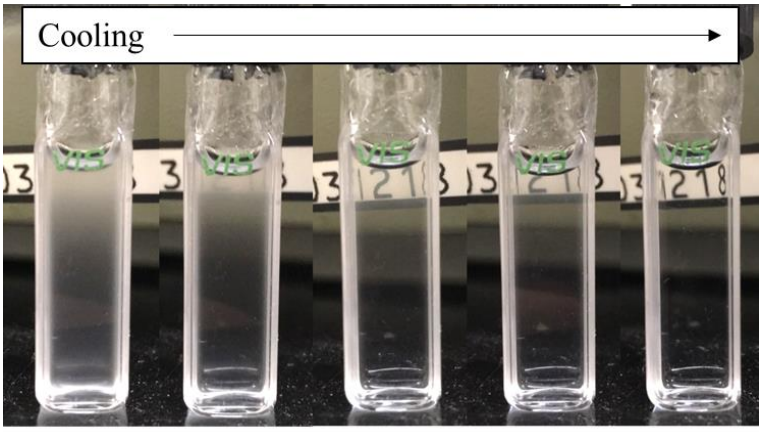

Figure 3A.22. Transmittance curves of all $PMA_{50}M_y$ solutions in LCST measurements and plotted cloud point temperatures (determined at dashed line transmittance values) vs. NaCl.

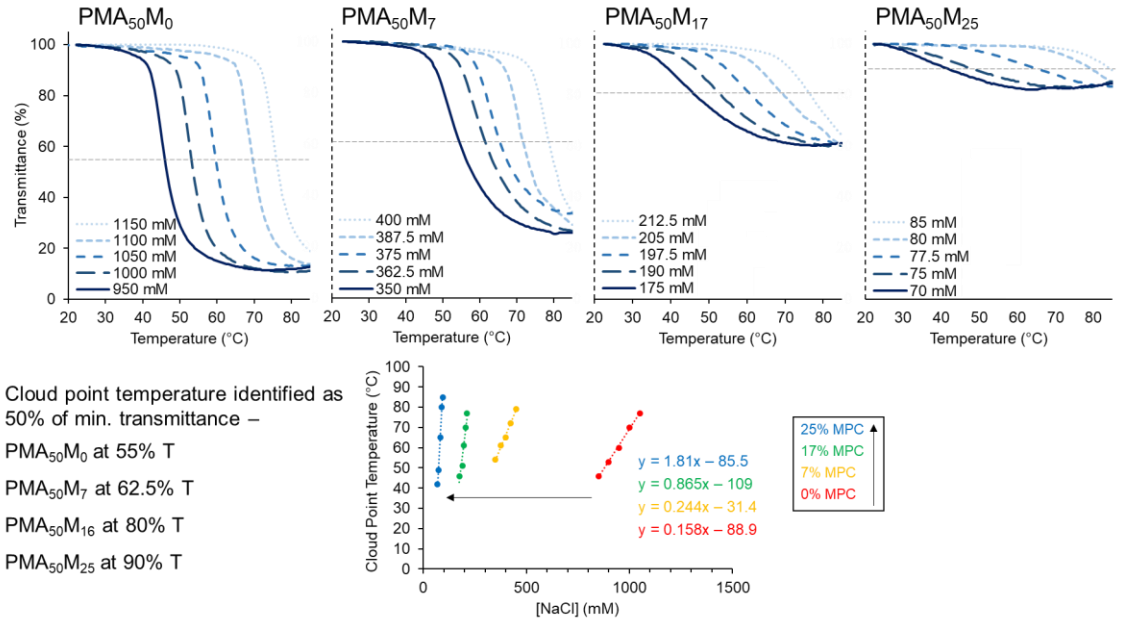

Figure 3A.23. Transmittance curves of all $PC^{25/75}M_y$ solutions in LCST measurements and plotted cloud point temperatures (determined at dashed line transmittance values) vs. NaCl.

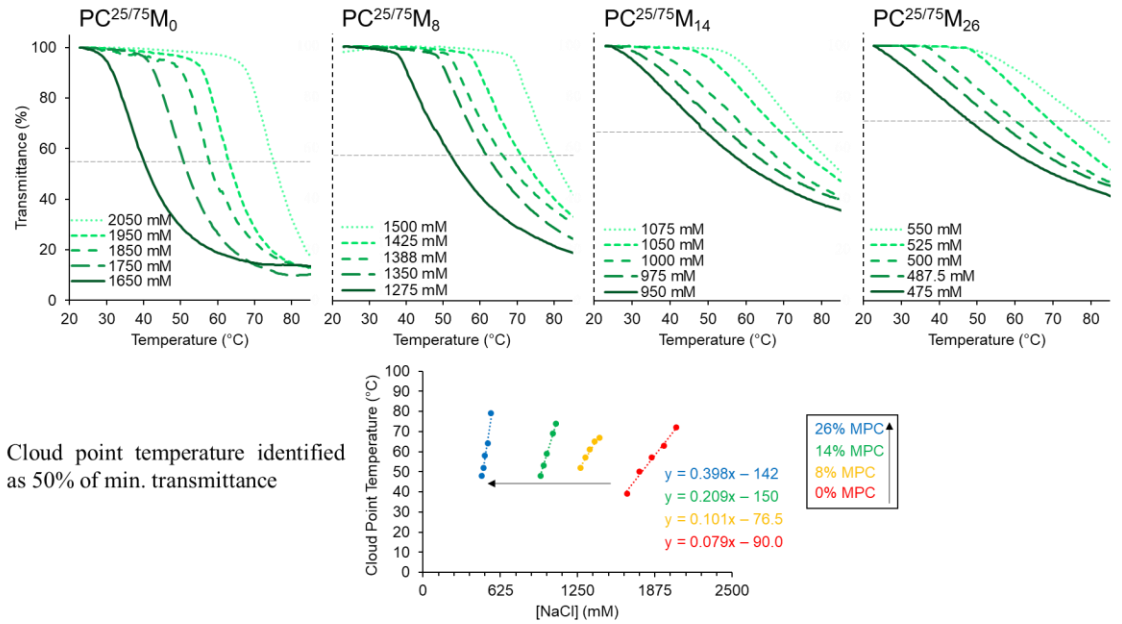

Figure 3A.24. Transmittance curves of all $PC^{0/100}M_y$ solutions in LCST measurements and plotted cloud point temperatures (determined at dashed line transmittance values) vs. NaCl.

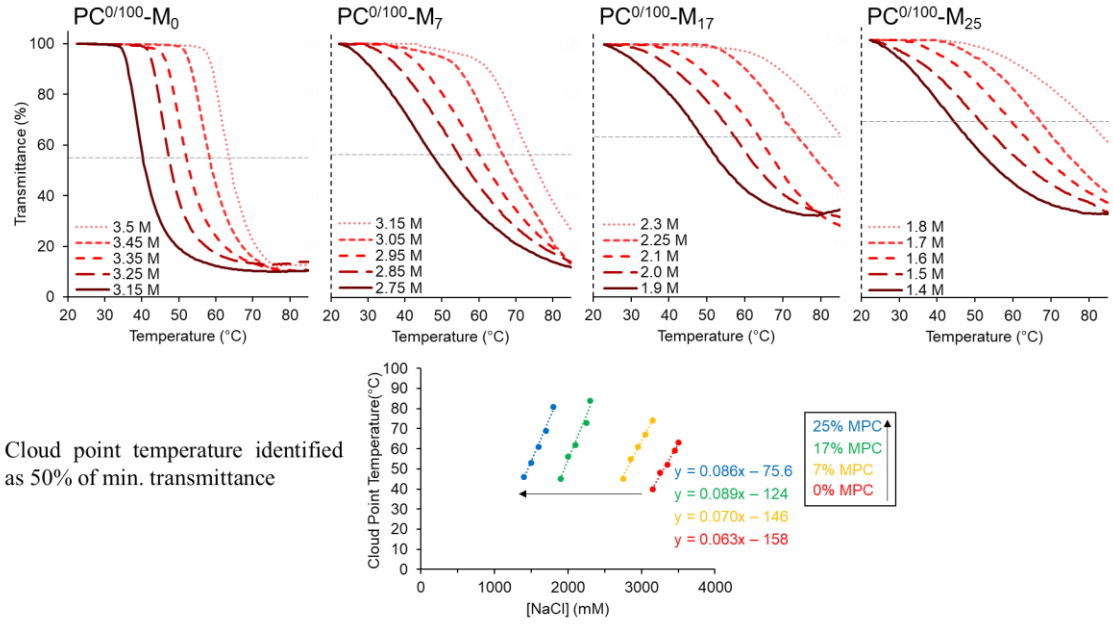

Figure 3A.25. Slopes of CPT responsiveness to NaCl for each PEC composition, as a function of MPC mol %.

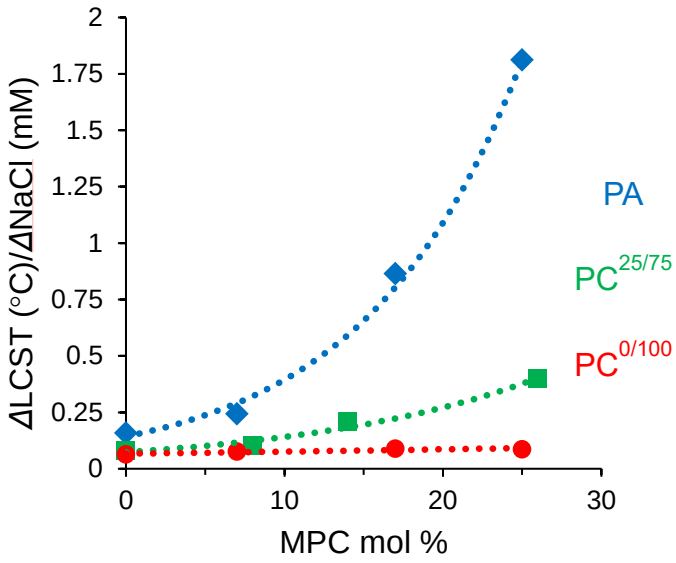

Chapter 4. Crosslinked Hydrogel Capsules Formed Using Amino/Betaine Dual-Functional Semibatch Copolymers

Derrick E. Hastings, Harald D. H. Stöver

Department of Chemistry and Chemical Biology, McMaster University, Hamilton, ON, L8S 4M1, Canada

Reprinted (adapted) with permission from Hastings, D. E. *et al.*, *ACS Appl. Polym. Mater.* **2019**, *1*, 2055-2067.

4.1. Abstract

Robust hydrogel capsules consisting of calcium alginate beads with shells reinforced via crosslinked amino/betaine copolymers of *N*-(3-aminopropyl) methacrylamide hydrochloride (APM) with 2-methacryloyloxyethyl phosphorylcholine (MPC) are described. These capsules are designed to support future use in immunoisolation of therapeutic cells for transplant purposes. The poly[APM-co-MPC] copolymers were prepared by semibatch free radical copolymerization to reduce the significant compositional drift and the resulting diffusional spread within alginate beads, observed for analogous batch copolymers. Fluorescent labeling was used to track copolymer distribution within the alginate hydrogels. Semibatch copolymers led to better shell confinement and lower cationic charge density on the capsule surface. Three reagents were used to

covalently cross-link the resulting poly(amino/betaine) shells: cationic tetrakis(hydroxymethyl)phosphonium chloride (THPC), charge-neutral genipin and anionic partially hydrolyzed poly(methyl vinyl ether-*alt*-maleic anhydride) (PM-*a*-M_{50}). Genipin-crosslinked capsules were found to be remarkably robust in pipet aspiration tests. Selected capsules were exposed to FITC-labeled bovine serum albumin to assess the relative degree of protein adhesion, as a proxy for immune recognition; genipin crosslinked capsules were found to have very low levels of BSA binding and good mechanical robustness.

4.2. Introduction

Non-specific resistance to protein is key to reducing the immune response against biomedical implants in applications such as biosensing, drug delivery and tissue engineering. Encapsulation and transplantation of allogenic cells for treatment of enzyme and hormone disorders[1,2], and of other active materials useful in biomedicine[3-6], requires minimizing protein fouling and immune response to ensure transplant survival. Calcium alginate (Ca-Alg) hydrogel beads coated with poly-L-lysine (PLL) and alginate (APA capsules)[7] can protect transplanted allogenic cells from contact with immune cells, while permitting metabolic exchange of nutrients and out-diffusion of the expressed therapeutic peptides such as insulin.[8] However, impurities in alginate and exposed patches of cationic PLL not masked by alginate have been shown to elicit host immune responses to the transplant.[9-12]

Incorporation of poly(ethylene oxide) or poly(ethylene glycol) (PEG)[13-16] as PEG-*b*-PLL di-block copolymers[17], PEG grafted onto PLL[18], and PEG microgels into PLL/alginate capsules have been shown to reduce fouling.[19] However, in a small number of people PEG evokes hyper sensitivity reactions that can trigger anaphylactic shock, attributed to both non-specific recognition as well as regeneration of PEG-specific antibodies.[14,20-25] PEG is also susceptible to oxidative damage,[26] which may promote protein adhesion and immune response. As a result, alternative anti-fouling biomedical materials are now being explored, including polyelectrolytes and polyzwitterions.

Polyzwitterions bear equal amounts of adjacent positive and negative charges, either on separate repeat units (polyampholytes) or on the same repeat unit (polybetaines). Either can gain a net positive or negative charge by incorporation of charged monomers; copolymer composition and, for weakly acidic and basic ions, the solution pH can dictate the overall charge of the copolymer.[27,28] Polyampholytes are being recognized as synthetic mimics of proteins and have shown anti-fouling properties at net neutral charge.[29,30] Similarly, polybetaines can be seen as polymeric analogues of phospholipids.[31] Typically composed of repeat units such as sulfobetaine methacrylate (SBMA), carboxybetaine methacrylate (CBMA) or 2-methacryloyloxyethyl phosphorylcholine (MPC), they are extremely hydrophilic, with hydration shells based on ion-dipole interactions that are stronger than hydrogen bonding interactions in hydrated PEG.[32,33]

MPC has shown anti-fouling properties in blood purification membranes,[34] as self-assembled monolayers (SAMs)[35], and has been used to increase protein circulation time[36] as well as coatings in artificial blood vessels.[37] Recently, Yesilyurt et al. developed anti-

fouling MPC coatings for alginate beads and polystyrene microspheres, using mussel-inspired polydopamine films and Michael addition reactions for covalent crosslinking.[38]

We propose here the use of MPC copolymers with *N*-3-(aminopropyl) methacrylamide (APM) as hydrophilic shell-formers for the calcium alginate beads. The p[APM-*co*-MPC] copolymers combine the cationic charges useful in polyelectrolyte complexation with anionic alginate hydrogels and the covalent crosslinking ability of the primary amine on APM with the excellent anti-fouling properties of MPC, and will complement copolymers of APM with either polar neutral comonomers such as *N*-(2-hydroxypropyl) methacrylamide,[39] anionic comonomers such as methacrylic acid and acrylic acid,[27,40,41] and charge-shifting comonomers such as 2-(dimethylamino)ethyl acrylate.[42] Copolymers of MPC and APM have been previously investigated in other biomedical applications[43-45] but have not yet been explored as shell formers in alginate capsules.

Scheme 4.1. Illustration of copolymers comprising cationic APM and zwitterionic MPC for Ca-Alg capsule formation with covalent crosslinking provided by various reagents.

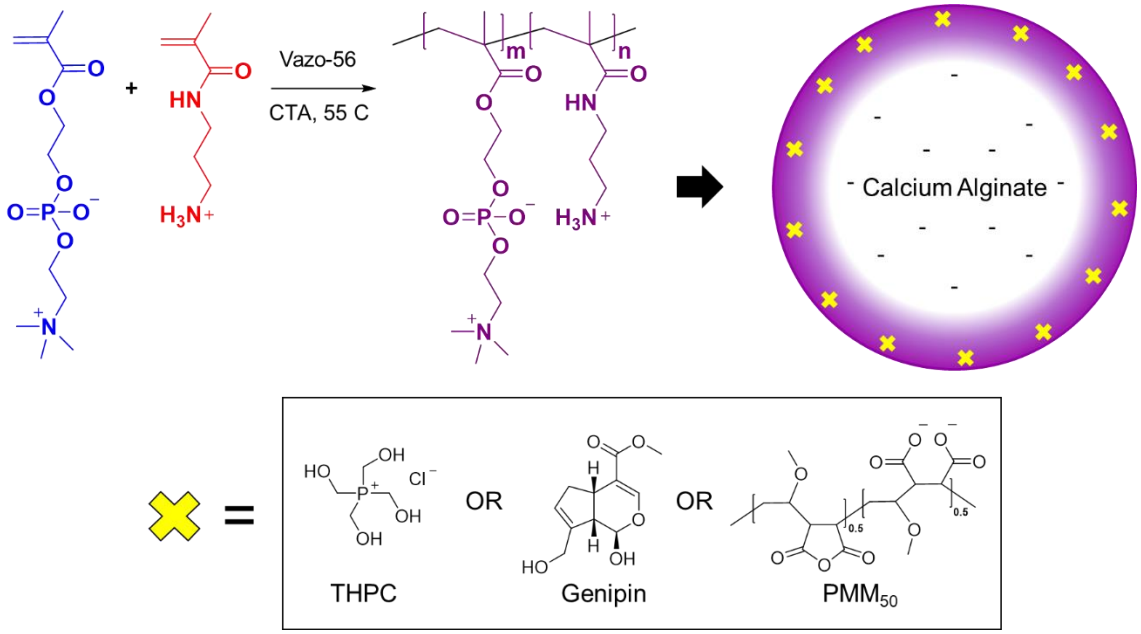

Batch copolymerization of methacrylates and methacrylamides involves significant compositional drift between chains formed at different times during copolymerization because of the monomers' different reactivities.[46-48] During alginate capsule formation, copolymer fractions rich in the cationic comonomer would preferentially bind at the outer alginate surface, affecting the antifouling and possibly the mechanical properties of the final capsules. Radical addition-fragmentation chain transfer (RAFT) copolymerization could be used to ensure each chain would contain the same, broad compositional drift imposed by batch copolymerization, while semibatch copolymerization would minimize drift both along and between chains, by approximately maintaining the initial comonomer feed ratio.[49]

We hence used a simple semibatch copolymerization involving addition of several aliquots of the more reactive comonomer, MPC, during the copolymerization. The

copolymerizations were tracked by ^{1}H NMR to adjust comonomer feeds as needed to maintain copolymer composition. A chain transfer agent was used to control the copolymer molecular weight. The copolymers were deposited onto calcium alginate beads and exposed to three different reagents used for covalent crosslinking. Capsule morphology and mechanical robustness after crosslinking were compared for batch and semibatch copolymers, and model protein adhesion was used to examine the capsule anti-fouling properties for select compositions.

4.3. Experimental

4.3.1. Materials

2,2'-Azobis(2-methylpropionamidine)dihydrochloride (97%, Vazo-56), deuterium chloride (99% D), D_2O (>99% D), *N*,*N*-dimethyl formamide (99.9%), *N*-3-(aminopropyl) methacrylamide hydrochloride (98%), 2-methacryloyloxyethyl phosphorylcholine (97%), tetrakis(hydroxymethyl)phosphonium chloride solution (80% in water), potassium hydrogen phthalate (>99.95%), cysteamine hydrochloride, fluorescein isothiocyanate isomer I (>90%) and albumin-fluorescein isothiocyanate conjugate bovine serum albumin were purchased from Sigma-Aldrich and used as received. Genipin was donated and used as received. DMSO-d_6 and acetonitrile-d_3 were purchased from Cambridge Isotope Laboratories, Inc. and used as received. Cellulose dialysis tubing (3.5 kDa) was purchased from Spectrum Laboratories and used as received. UP MVG sodium alginate (BP-1606-17) was purchased from Pronova and used as received. Poly(methyl vinyl ether-*alt*-maleic anhydride) 80 kDa was purchased from Sigma-Aldrich and was used as received.

4.3.2. Molecular Weight Control/Chain Transfer Analysis

4.3.2.1. Effect of Chain Transfer Agent on Molecular Weight

Multiple 1 mL aliquots of a 10 wt % total monomer loading APM:MPC (52:48 mol %) stock solution containing 1 mol % Vazo-56, as a thermal initiator, relative to total monomers in deionized water were placed in 4 mL screw cap vials. To each vial was added a unique amount of cysteamine chain transfer agent: 0, 0.9, 1.6, 2.4, 3.4, 4.3, 5.2 and 10.4 mol % relative to total monomer. The vials were placed in a UVP Laboratory Products HB-1000 Hybridizer oven at 55 °C for 1 h. Typical conversions were at or above 65%, determined by comparing ^{1}H integrations of vinyl signals of total monomer at t = 0 and t = 1 h using a 600 MHz Bruker Avance NMR spectrometer, with sidechain integrations of MPC acting as an internal standard. Copolymers were characterized by GPC using a Waters GPC consisting of a 717plus autosampler, a 515 HPLC pump, Ultrahydrogel (120, 250, and 500) columns (30 cm x 7.8 mm (i.d.; 6 μm particles) and a 2414 refractive index detector, using a 1 M acetate buffer (pH 4.8) with a flow rate of 0.8 mL/min at 30 °C as the mobile phase. The GPC system was calibrated with poly(ethylene glycol) (PEG) standards (Waters Inc.) ranging in molecular weights from 106 Da to 584 kDa.

4.3.2.2. Effect of Composition on Molecular Weight

Four stock solutions of APM:MPC feed ratios (0:100, 26:74, 76:24 and 100:0 mol %) containing 1 mol % Vazo-56 in deionized water were divided into four 1 mL aliquots each. Cysteamine stock solution (20 mg/mL) was added to each aliquot such that each feed ratio had four separate chain transfer agent concentrations: 0, 2, 5 and 10 mol %. The polymerizations were carried out in a hybridizer oven at 55 °C for 1-1.5 h, depending on

composition and conversion determined by ^{1}H NMR, such that all reactions reached >50% conversion. Copolymer molecular weights were analyzed by GPC as described above.

4.3.3. Determination of Reactivity Ratios of APM and MPC

Copolymerization of APM and MPC was followed in situ by ^{1}H NMR spectroscopy using a 600 MHz Bruker Avance spectrometer. Spectra were recorded at roughly 10-25 % conversion steps at 10 wt % total monomer loading in D_2O, with initial APM:MPC molar feed ratios of 90:10, 75:25, 60:40, 40:60, 30:70, 15:85, and 5:95, and 1 mol % Vazo-56. Solution pH was adjusted to about pH 3. The reactions were heated at 55 °C for the first 15-20 min through the initial lag period and then decreased to 45 °C to reduce the rate of polymerization. Monomer vinyl peaks, integrated with respect to MPC methylene sidechain signals at 4.0-4.5 ppm, were monitored throughout the polymerization. Reactivity ratios were estimated by a least-squares fitting of the terminal model of the instantaneous copolymer composition equation to comonomer conversion data as previously reported[27] based on a procedure by Aguilar et al.,[50] and compared with the reactivity ratios estimated using the Fineman-Ross method.[51] The reactivity ratios from the fitted copolymer equation were used to produce copolymers of targeted compositions.

4.3.4. Preparative Batch Free Radical Copolymerization of APM and MPC

Polymerizations of poly[APM-*co*-MPC] or PAM_x, where *x* is the average mol % of MPC, were carried out in a hybridizer oven at 55 °C. Based on determined reactivity ratios, the molar feed ratios of APM:MPC were set at 0:100, 27:73, 45:55, 52:48, 68:32, 84:16, 95:5, and 100:0 targeting final copolymers PAM_{100}, PAM_{80}, PAM_{75}, PAM_{65}, PAM_{55}, PAM_{45}, PAM_{25}, PAM_{15}, and PAM_0, respectively. The subscript denotes the average MPC content

in mole % for copolymers formed to about 65% conversion. The formation of PAM_{55} using a 52:48 (APM:MPC) feed ratio is given below as an example: Stock solutions of chain transfer agent cysteamine (20 mg/mL) and initiator Vazo-56 (10 mg/mL) were prepared in deionized water. APM (79 mg, 0.44 mmol) and MPC (120 mg, 0.41 mmol) were dissolved in 1.63 mL of deionized water in an 8 mL screw cap vial prior to addition of 130 μL of cysteamine stock solution and 230 μL of Vazo-56 stock solution, resulting in a 2 mL final volume. The pH was adjusted to 3.0 using small amounts of 1 M NaOH. The reaction vial was capped with a septum before nitrogen purging through a needle for 30 min. The comonomer conversions were analyzed by ^{1}H NMR after 1 h by taking aliquots and diluting with D_2O for spectrum acquisition. Cumulative monomer conversion was typically about 55-75% after 1.5 h of heating. Final copolymer compositions were determined by ^{1}H NMR spectroscopy in D_2O, comparing the integrations of MPC peaks from 4.1-4.5 ppm (6H) with both the backbone proton signals at 0.5-2.5 ppm (5H from MPC and 7H from APM) and sidechain proton signals at 2.8-3.5 ppm (9H from MPC and 4H from APM). Both calculations were consistent, indicating no transamidation or ester hydrolysis during polymerization.

The vials were cooled to room temperature, and the copolymer dialysed against distilled water using cellulose tubing (Spectrum Laboratories, 3.5 kDa MW cut-off) for about 3 days, changing dialysis baths twice daily until UV-vis spectroscopy of the bath water showed no absorbance of small molecules. The polymer was isolated by freeze-drying, yielding white solid polymer (PAM_{55}) in approximately 95% yield with respect to monomer conversion in the hydrochloride form. Average copolymer composition was

calculated by ^{1}H NMR, and ranges of composition were derived from the instantaneous copolymer compositions based on initial and final NMR spectra taken during polymerization. Molecular weights were estimated by GPC as described above.

4.3.5. Semibatch Copolymerization of APM and MPC

Polymerizations (300 mg scale) were set up similar to the batch copolymerizations, at 10 wt % total initial monomer loading, 1 mol % Vazo-56, 2.5-3.0 mol % cysteamine and with pH adjusted to pH 3.0 in deionized water. Additionally, 5 mol % of potassium hydrogen phthalate (KHP) was added as internal ^{1}H NMR standard. Reaction vials were capped with septa and purged with nitrogen for 30 min. Initial feed ratios 96:4, 92:8, 87:13, 80:20, 69:31 and 55:45 of APM:MPC were chosen to target copolymer compositions of PAM^{sb}_{10}, PAM^{sb}_{20}, PAM^{sb}_{30}, PAM^{sb}_{40}, PAM^{sb}_{50} and PAM^{sb}_{60} over the first ca 20 mol % conversion, which would limit compositional drift to 7-8 mol %. Separately, a stock solution containing 100 mg/mL stock solution of MPC and 2.5-2.8 mol % cysteamine relative to MPC was prepared in a screw cap vial, and degassed.

After recording initial ^{1}H NMR spectra, the reaction mixtures were submerged in a 45 °C water bath for 10-20 min, estimated to result in ca 20 % conversion. Polymerizations were halted by immersing in an ice bath and briefly opened admit air. Aliquots of 20 μL were taken and diluted with D_2O for ^{1}H NMR analysis, and integrations of the vinyl signals of MPC and APM relative to the KHP aromatic signal (4H, δ 7.4-7.7ppm) were used to estimate the volumes of MPC/CT stock solution to be added to re-establish the initial MPC/APM ratio. The vials were then purged again with nitrogen for 20-30 min and

polymerization continued. This process was repeated until cumulative conversion of APM was about 50%. Copolymer was then isolated as described above.

4.3.6. Alginate-Polymer Complexation of Batch and Semibatch Copolymers

Solutions of 0.5 wt % polycation in pH 7.4 HEPES-buffered saline (HBS) were prepared in 4 mL screw cap vials. All solutions were filtered through 0.45 μm filters before addition of varying volumes of 0.5 wt % sodium alginate in saline, prepared by mixing on a rotating wheel for 24 h, were added to establish a 1:1 charge ratio of carboxylate to primary ammonium cation. The mixtures were gently agitated for 45 s and drops of the resulting suspensions were placed on clean microscopy slides and imaged by bright field microscopy on a Nikon Eclipse LV100 ND equipped with an Andor Zyla sCMOS camera and running Nikon Elements software.

4.3.7. Fluorescent Labelling of PAM Copolymers

PAM copolymer, 50-60 mg per sample, was dissolved in 2 mL of deionized water and the solution pH adjusted to 8.6-8.8 using 1 M NaOH. While stirring, appropriate volumes of 10 mg/mL FITC dissolved in dimethylformamide were added to each solution to target a 0.2% labelling relative to total monomer. The reactions were stirred for 1 h before pH was decreased to 6.6-7 by addition of 1 M HCl. The solutions were dialyzed against deionized water using 3.5 kDa MW cut-off cellulose tubing and freeze dried to yield yellow-orange PAM-*f* solids in roughly 90% yield.

4.3.8. Preparation of Calcium Alginate Beads

A 1.0 wt % sodium alginate solution (10 mL) was prepared in 0.9 wt % saline and allowed to mix for 24 h on a rotating wheel. The homogenous solution was filtered through a 0.2

μm syringe filter before being drawn into a 10 mL polypropylene syringe set up with a 27-gauge, blunt tip needle. A volume of 2.5 mL was extruded at a rate of 8 mL/h with an external airflow rate of 3.0 L/min, into 30 mL of gelling bath solution (1.1 wt % $CaCl_2$, 0.45 wt % NaCl). The calcium alginate beads were left to gel for 10 min after extrusion (30 min total) and were stored in fresh saline solution (3.3 mL saline/ 1 mL beads). The saline supernatant was disturbed, removed, and filtered through a 0.45 μm syringe filter three times to remove small, outlying alginate particles (< 100 μm). The average diameter of the beads was then determined using optical microscopy, measured using Nikon Elements software. Alginate beads of sizes 470 ± 15 μm to 500 ± 20 μm (batch to batch variation) were recovered and stored in the absence of light at 4 °C.

4.3.9. Coating Alginate Beads with Batch/Semibatch PAM

Calcium alginate beads (0.3 mL) were coated with copolymers by addition of 1 mL of 0.1 wt % PAM solutions in 35 mM HBS (pH 7.4) and gently agitating for 6 min. The supernatant was removed with a plastic Pasteur pipet and beads were washed twice with 1 mL HBS for 2 min. The coated beads were re-suspended in 1 mL HBS and stored in absence of light at 22-24 °C. Batch copolymers PAM^{b}_{24}, PAM^{b}_{42}, PAM^{b}_{55}, PAM^{b}_{65}, and PAM^{b}_{81}, and semibatch copolymers PAM^{sb}_{12}, PAM^{sb}_{22}, PAM^{sb}_{29}, $PAM^{sb}_{38,}$ PAM^{sb}_{51}, and PAM^{sb}_{61} were examined as shell formers.

4.3.10. Microscopy of Calcium Alginate Beads and Capsules

Fluorescently labelled beads were imaged by conventional microscopy using a Nikon Eclipse T*i* optical microscope equipped with an Andor Zyla sCMOS camera and by confocal laser-scanning microscopy using a Nikon A1 Confocal Eclipse T*i* microscope

with Nikon Elements software. Capsule thicknesses (*n=15*) were given as full width at half-height of a 5 μm thick equatorial fluorescence intensity line profile across alginate beads. Shell/core fluorescence ratios were calculated by dividing the maximum surface fluorescence of the bead by the average fluorescence intensity of inner-most sections of the core using acquired line profiles (*n=10*).

4.3.11. Crosslinking of PAM Coated Capsules

4.3.11.1. THPC – After coating, PAM coated beads were exposed to 1 mL of 0.1 wt % tetrakis(hydroxymethyl)phosphonium chloride (THPC) in HBS for 2 min. Supernatant was removed, and beads were washed with 1 mL HBS for 2 min and stored in 1 mL of fresh HBS.

4.3.11.2. Genipin – After coating, PAM coated beads were exposed to 1 mL of genipin in HBS for 1 h on a rotating wheel (~42 RPM) before removing supernatant, washing once with 1 mL HBS for 2 min and storing in 1 mL of fresh HBS. Genipin/HBS concentrations of 0.1 w.t % and 0.05 w.t % were employed based on previous reports.[52,53]

4.3.11.3. PM-a-M50 – 50% hydrolyzed poly(methyl vinyl ether-*alt*-maleic anhydride) (PM-*a*-M_{50}) was prepared according to a previously reported procedure.[9] PM-*a*-M_0 (anhydride form, 100 mg, 80 kDa) was partially hydrolyzed in a 1 mL acetonitrile-d_3/D_2O mixture (9:1 v/v) in an NMR tube, with hydrolysis monitored by ^{1}H NMR. The anhydride CH signal shifts upfield as it converts to carboxylic acid; comparing integrations of the identified CH and CH_2 of methyl vinyl ether, an estimated degree of hydrolysis was determined. Reaction for 18 h at 55 °C for resulted in hydrolysis of 50% of the anhydride

groups. After cooling to room temperature, 0.1 mL of the mixture was diluted to 2.5 mL with 35 mM HBS (pH 7.4).

The resulting suspension was immediately vortexed for 15-20 s to give a clear solution containing 0.4 wt % PM-*a*-M_{50}. This solution was immediately drawn up into a syringe and 0.5 mL was quickly filtered through a 0.2 μm syringe filter directly into a suspension of PAM-coated calcium alginate beads in 0.5 mL HBS, resulting in a coating solution of 1 mL of 0.2 wt % PM-*a*-M_{50}.

4.3.12. Sodium Citrate and Sodium Hydroxide Test for PAM Capsule Crosslinking

A drop (~ 45 μL) of HBS containing PAM-*f* capsules was placed on a 35 mm polystyrene petri-dish, and a few drops (~ 250-500 μL) of 50 mM sodium citrate was added to the capsules, before gentle agitation for 15 s to chelate the divalent calcium ions and liquefy the alginate core. Supernatant was removed from the capsules and a few drops (~ 500 μL) of 0.1 M sodium hydroxide were added to deprotonate primary ammonium cations of APM and eliminate electrostatic interactions between copolymer and alginate. The capsules were monitored by conventional bright field and fluorescence microscopy through each addition.

4.3.13. Qualitative Agitation-Survival Tests of PAM^{sb} Capsules

A droplet of HBS containing PAM-*f* capsules on a polystyrene petri-dish was treated with 50 mM sodium citrate (~ 250-500 μL) and 0.1 M sodium hydroxide (~ 500 μL) before aspiration by polypropylene pipet (uptake-release: 10 times/5 s). Using optical microscopy images, an estimated survival ratio (intact capsules vs. fragmented capsule remains, *n=100*) was used to qualitatively determine the robustness of each capsule composition across the various crosslinkers. Uncertainty of robustness was estimated using the standard deviation

of survival percentages of $PAM^{sb}_{29,}$ PAM^{sb}_{38} and PAM^{sb}_{51} triplicates (n=3) for each crosslinker.

4.3.14. Bovine Serum Albumin Protein Adhesion Assay

Bovine serum albumin (BSA) protein adhesion screening was carried out following a procedure by Shen et al.[54] to investigate the effects of crosslinking methods and copolymer composition on potential compatibility. Briefly, 0.1 mL of a concentrated PAM crosslinked bead suspension was added to 1 mL of a 0.05 wt % solution of fluorescein labelled BSA (BSA-*f*) in HBS. After 24 h at room temperature in the absence of light, the capsules were washed 3 times with 1 mL of saline containing 0.1 wt % calcium chloride for 2 min before monitoring the presence and distribution of residual BSA-*f* by confocal microscopy. This was carried out for PAM compositions of interest based on crosslinking experiments, including an alginate-PLL (AP) control with each crosslinker.

4.4. Results and Discussion

4.4.1. Batch Copolymerization of MPC and APM

Copolymerizations of water soluble MPC and APM-HCl salt were carried out in aqueous media using a water-soluble initiator, Vazo-56, and water-soluble chain transfer agent, cysteamine. The pH was adjusted to 3 to ensure the primary amine of APM was protonated and to avoid base-catalyzed hydrolysis of MPC.

For biomaterial applications, the renal clearance limit of about 40 kDa commonly serves as molecular weight ceiling.[55] Polycations used as shell formers with alginate beads,

however, usually have MW between 15 and 30 kDa, to avoid excessive in-diffusion at low MW and wrinkling of the shell at higher MW.[56,57] Initial 1:1 APM:MPC copolymerization resulted in molecular weights above the 300 kDa exclusion limit of the GPC columns used, indicating the need for chain transfer agents (CTA).

The agent selected here, cysteamine, is known to undergo rapid Michael addition to acrylic monomers,[42] reducing the amount of CTA available and even affecting comonomer ratios. A 1:1 molar mixture of APM and MPC at 10 wt % in D_2O with 3 mol % cysteamine devoid of initiator was monitored by ^1H NMR for 1.5 h at 55 °C to confirm that cysteamine does not readily add to methacrylic monomers in absence of DMSO and catalysts.[58-60]

Exploratory copolymerizations were carried out with different CTA levels and comonomer ratios, indicating that roughly 2.5-3 mol % CTA led to a desirable 15-30 kDa MW range for most PAM compositions (Figure 4A.1).

The reactivity ratios for the APM/MPC comonomer pair were estimated by following a series of copolymerizations using ^1H NMR spectroscopy, according to previously reported methods.[27,42,50] The amounts of each monomer consumed in consecutive 10-25% conversion steps to a final conversion of about 75 % were determined from the changes in integration of the two monomer vinyl signals during each step, compared to MPC side-chain proton signals (6H) as an internal standard. The resulting plots of MPC mol % versus total monomer conversion (Figure 4.1 (A)) show preferential incorporation of MPC across all seven initial feed ratios. The monomer conversion steps from the seven copolymerizations were fitted to the instantaneous copolymer composition

equation using a non-linear Excel Solver routine, with the reactivity ratios as fitting parameters.

The resulting reactivity ratios of MPC and APM, of 1.47 and 0.21, respectively, resemble those obtained using the Fineman-Ross method (1.27, 0.22) (Figure 4A.2). The instantaneous copolymer equation (**4.1**) was plotted against the instantaneous comonomer feed ratio in Figure 4A.3.

$$F_1 = \frac{r_1 f_1^2 + f_1 f_2}{r_1 f_1^2 + 2 f_1 f_2 + r_2 f_2^2} \quad (\mathbf{4.1})$$

The fitted reactivity ratios 1.47 and 0.21 were used to select appropriate feed ratios required to achieve target copolymer compositions, as these values better match the experimental data when plotted using the instantaneous copolymer equation (Figure 4A.3). The favourable reactivity of methacrylates over methacrylamides has been previously reported, owing to the greater electron withdrawing character of the ester.[46-48]

A series of batch PAM copolymers were prepared by conventional free radical copolymerization in water at pH 3 (Table 4.1). They are denoted at PAM^{b}_{x}, where *x* stands for the average mol % MPC in the copolymer. MPC feed mol % were chosen to compensate for preferential MPC incorporation, and polymerizations were stopped at 65-70% conversion to limit compositional drift. Average MPC contents were close to targeted values, with the estimated compositional ranges shown in Table 4.1 reflecting determined drifts in instantaneous copolymer composition from monomer feeds at $t = 0$ and t = final, shown in Figure 4.1 (C).

Table 4.1. Molecular weight and composition of PAM batch copolymers.

Copolymer	MPC in Monomer Feed [mol %]	Average MPC in Copolymer [mol %]	Est. MPC range in Copolymer [mol %]	M_n (kDa)	M_w (kDa)	Conv. (%)	CTA [mol %]	$Đ$
PAM^b_{100}	100	100	100	24.9	43.4	83	3.0	1.7
PAM^b_{81}	80	81	85-60	23.0	42.3	92	3.2	1.8
PAM^b_{77}	73	77	82-75	26.3	46.4	71	2.2	1.7
PAM^b_{65}	55	65	71-56	22.3	36.8	67	2.8	1.6
PAM^b_{55}	48	55	66-39	21.1	39.0	76	2.4	1.8
PAM^b_{42}	32	42	54-25	16.1	27.2	70	2.9	1.7
PAM^b_{24}	16	24	38-12	13.3	22.4	62	2.6	1.7
PAM^b_{9}	5	9	18-3	11.3	17.3	55	2.8	1.5
PAM^b_{0}	0	0	0	11.0	16.4	80	2.3	1.4

GPC analysis of batch PAM copolymers indicated molecular weights near the targeted range, showing a trend of increasing apparent MW with increasing mol % MPC likely due to chain transfer efficiency toward the different monomers and strong hydration of MPC increasing the hydrodynamic radius.

4.4.2. Semibatch Copolymerization of MPC and APM

The significant compositional drift during batch copolymerization shown in Table 4.1 and Figure 4.1 (B), led us to explore simple semibatch copolymerizations to form PAM copolymers with narrower compositional distributions. Semibatch copolymerizations of MPC and APM have not yet been reported in the literature. The decreases in MPC and APM during each conversion interval were used to calculate additions of an MPC/CTA stock solution needed to re-establish initial MPC/APM ratios (Figs. 4A.4, 4A.5). Figure 4.1

(C) shows the resulting saw-toothed comonomer feed ratios versus APM conversion. These semibatch copolymerizations were limited to MPC feeds of 45 or less mol % to achieve compositions capable of sufficient binding to calcium alginate beads. Figure 4.1 (D) shows the relatively narrow compositional ranges obtained by these semibatch copolymerizations, compared with the broad, overlapping compositional ranges obtained during batch copolymerization in Figure 4.1 (B)

Table 4.2. PAM semibatch copolymers.

Copolymer	MPC in Monomer Feed [mol %]	Average MPC in Copolymer [mol %]	Est. MPC range in Copolymer [mol %]	M_n (kDa)	M_w (kDa)	[a]CTA [mol %]	$Đ$
PAM^{sb}_{61}	45-37	61	64-57	29.3	48.2	3.5	1.6
PAM^{sb}_{51}	31-24	51	53-47	23.8	37.8	3.0	1.6
PAM^{sb}_{38}	20-15	38	43-37	19.6	31.7	2.8	1.7
PAM^{sb}_{29}	13-9	29	34-27	18.4	30.2	2.6	1.6
PAM^{sb}_{22}	8-5	22	25-18	16.6	26.1	2.8	1.6
PAM^{sb}_{12}	4-2	12	15-9	12.5	20.5	2.5	1.6

[a]*Initial mol %, adjusted through addition of 2.5 mol % in MPC stock solution.*

Semibatch copolymer data (Table 4.2) show that the MPC range in comonomer feed now stays within narrow boundaries for each initial comonomer feed. As a result, the MPC ranges in the resulting copolymers denoted PAM^{sb}_{x}, estimated from the instantaneous copolymer compositions formed at low and high ends of each MPC feed band (Figure 4.1 (D)), are significantly narrower than those obtained for the batch copolymers (Table 4.1).

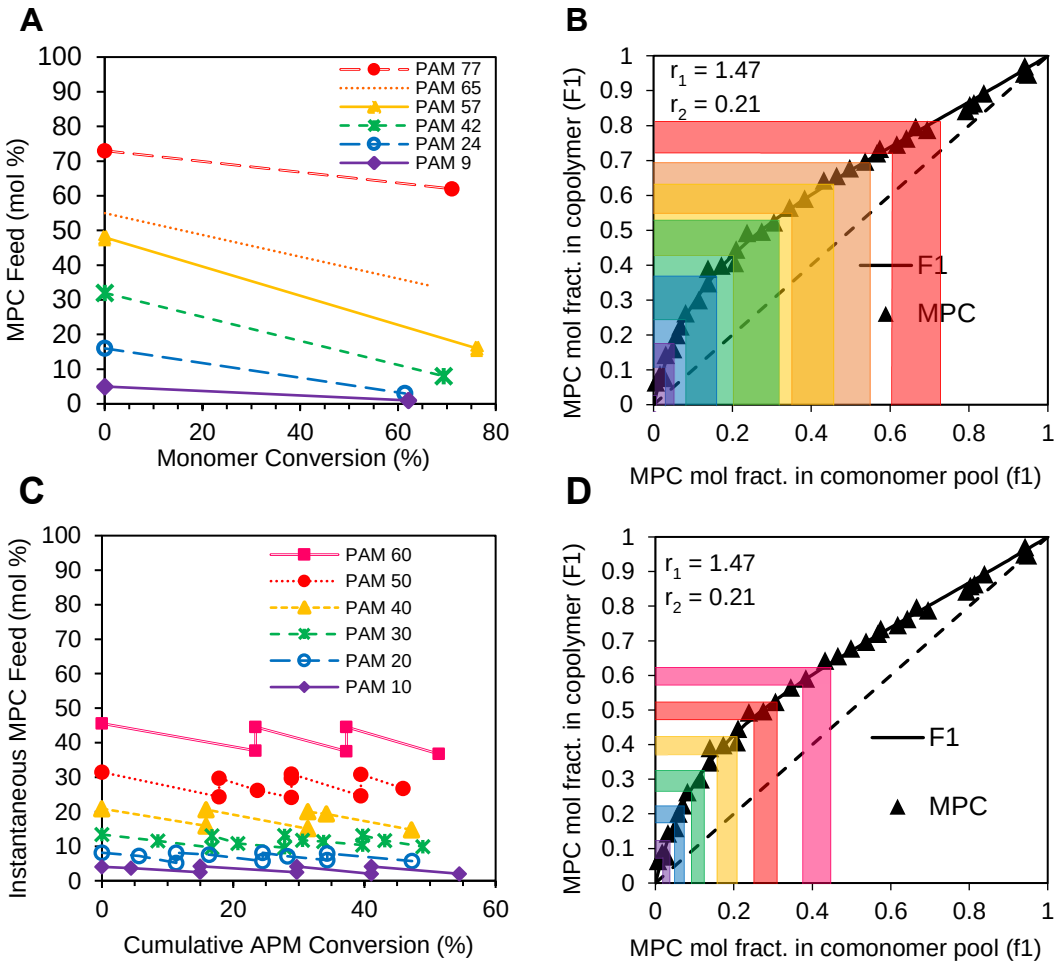

Figure 4.1. (A) MPC fraction of monomer feed remaining as a function of conversion for various batch copolymerizations of APM and MPC in reactivity ratio determination by ^{1}H NMR. **(B)** Ranges of drift in instantaneous comonomer feeds and instantaneous copolymer compositions in preparative batch copolymerization superimposed on fitted instantaneous copolymer equation using determined reactivity ratios. **(C)** Instantaneous MPC fraction of monomer feed ratios as a function of cumulative APM conversion for various semibatch copolymerizations, determined by ^{1}H NMR. **(D)** Ranges of drift in instantaneous comonomer feeds and instantaneous copolymer compositions in semibatch copolymerization superimposed on fitted instantaneous copolymer equation using determined reactivity ratios.

4.4.3. Alginate-PAM Complexation for Batch and Semibatch Copolymers

The copolymers synthesized here were coated onto preformed calcium alginate beads. Coating in this context involves diffusion of the polycations into the highly porous, polyanionic alginate beads with more cationic copolymers typically bound closer to the capsule surface, resulting in thinner shells with a higher loading of polycation. Additionally, the use of the term capsule in this field describes alginate hydrogels coated with copolymer, as the alginate core is preserved through cell encapsulation and application.

Hydrophobicity of the resulting polyelectrolyte complexes (PECs) between anionic alginate and polycations at the capsule surface is one important predictor of the foreign body response they elicit. For PECs of copolymers with different cationic charge densities, the relative hydrophobicity can be assessed by comparing the apparent opacity (refractive index contrast) in transmission optical microscopy, which is inversely related to degree of hydration. Therefore, modelling these interactions by mixing sodium alginate and copolymer solutions serves as a useful method of visually monitoring the interactions of alginate with various copolymer compositions. Microscope images and discussion of these experiments, found in Supporting Information (Figs. 4A.6-4A.8), indicate semibatch copolymers form more hydrated complexes than batch copolymers of comparable average composition; this is attributed to the narrower compositional distribution and, in particular, the absence of copolymer fractions with very high APM content. Scheme 4.2 illustrates the expected effect of narrower compositional range on alginate-polycation capsule shell thickness for batch and semibatch copolymers having similar average MPC content.

Scheme 4.2. Illustration of expected alginate capsules for batch PAM^{b}_{65} (top left), PAM^{b}_{42} (bottom left) and PAM^{sb}_{38} (bottom right) copolymers.[a]

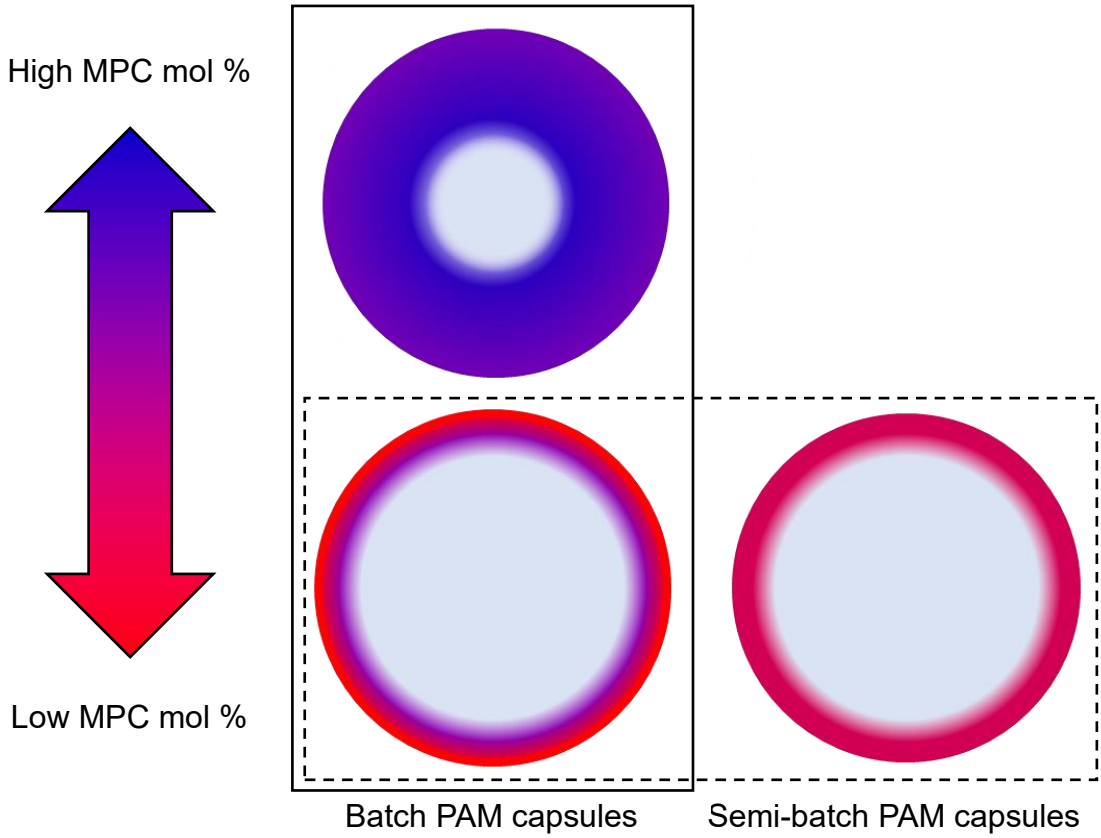

[a]Capsules in the solid box illustrate the difference in capsule morphology based on composition. Capsules in the dashed box show the difference between batch and semibatch copolymer surfaces. Capsule colour scheme is meant to illustrate the different distributions of comonomer ratio found across the shells for both copolymer types (25-75 mol % MPC).

In Scheme 4.2, expected capsules of alginate hydrogel beads with representative copolymers of similar average MPC content are shown. Semibatch copolymers are expected to result in a more MPC-rich surface due to their narrower compositional distribution, which would improve anti-fouling properties.

4.4.4. Alginate Capsules with Batch and Semibatch PAM

Calcium alginate beads were exposed to FITC-labelled batch (PAM^{b}-*f*) or semibatch (PAM^{sb}-*f*) copolymer solutions. Based on the charge, molecular weight, and backbone of the copolymers in solution, the depth of copolymer in-diffusion into porous alginate beads is representative of a copolymer shell with a particular thickness, determined by confocal microscopy. Figure 4.2 shows a side-by-side comparison of equatorial confocal images together with line-profiles of the fluorescence intensities across these sections, reflecting radial distributions of the fluorescent batch and semibatch copolymers. The values shown in brackets to the left of each line profile indicate the average MPC mol % for each copolymer, while the numbers shown over the line profiles indicate the shell/core fluorescence intensity ratios.

As seen in Figure 4.2, PAM^{b}_{65}-*f* and PAM^{b}_{55}-*f* formed polyelectrolyte complex (PEC) shells with high surface polymer concentration that falls off towards the bead centre. The thickness of these shells is in part due to their broad compositional distributions, with higher MW and APM-rich chains preferentially retained at the capsule surface. Batch copolymers with 42 mol % MPC formed thin PEC shells, reflecting quantitative capture of these copolymers at the bead surface, leading to higher cationic charge density and higher PEC hydrophobicity on the bead surface.

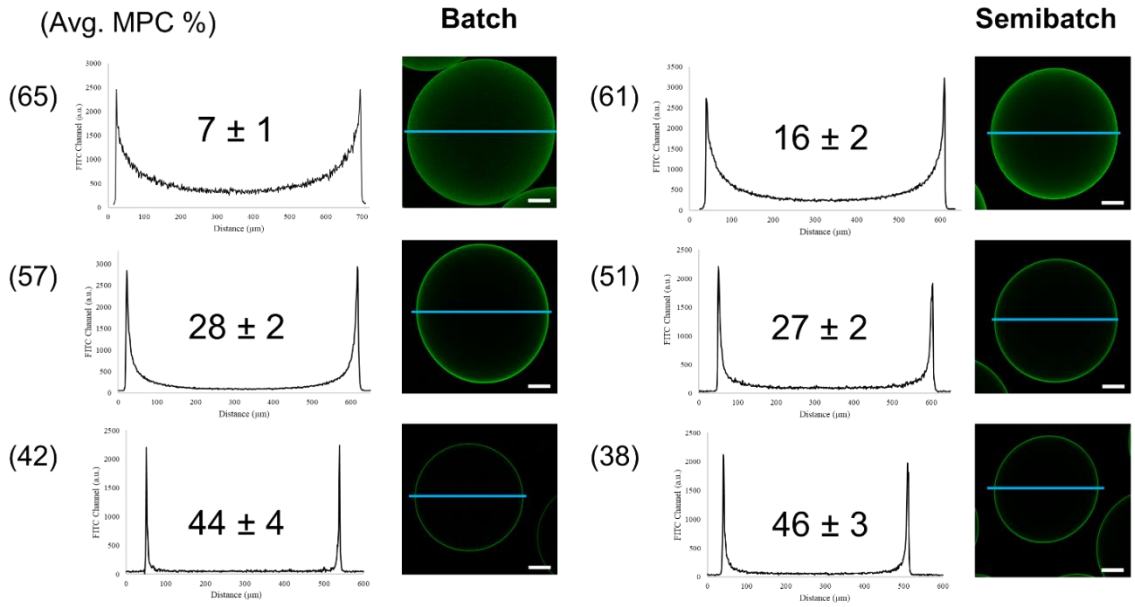

Figure 4.2. Line profiles and equatorial confocal fluorescence images of ~500 μm Ca-Alg beads coated with three batch and three semibatch copolymers. For each copolymer-coated bead, both average MPC mol % are given in round. Shell/core fluorescence ratios are shown above the line profiles (scale bars = 100 μm).

Likewise, semibatch copolymers of comparable average MPC content (Figure 4.2, right) also show thinner shells with lower MPC content but more importantly, have lower peak APM than batch copolymers with comparable average composition (see Figure 4A.9 and 4A.10 for graphical representations). This lower peak APM content for semibatch coated capsules would lead to increased surface hydrophilicity and decreased cationic charge density of the PEC at the capsule surface, both highly desirable properties.

Shell/core fluorescence intensity ratios indicate increasing shell confinement with increasing APM content for both types of capsules, as expected. Figure 4A.9 shows that shell thicknesses are roughly comparable for batch and semibatch copolymers with comparable average composition and increase from 4 to 10-15 μm with increasing average MPC content.

Batch copolymer with 82 mol % MPC diffused evenly throughout the alginate beads which prevented subsequent crosslinking, while copolymers with less than 24 mol % MPC showed increased incidence of capsule aggregation leading to patch-tear-off (Figure 4A.11). We below compare robustness after crosslinking, and protein deposition, for a subset of batch and semibatch capsules.

4.4.5. Crosslinking PAM Capsules

Given the weakening of calcium alginate cores by in-vivo exchange of divalent calcium for sodium, it is desirable to covalently crosslink a reinforcing shell or whole bead to improve long-term stability in a host. The primary amines of APM present in copolymers with MPC offer different methods for covalent crosslinking of the copolymer bound to the Ca-Alg surface. THPC, genipin, and PM-*a*-M_{50} (Figure 4.3) have each been previously evaluated as cyto-compatible crosslinkers for separate polyamine systems.[9,61,62] They represent cationic, neutral, and anionic crosslinker and are here compared with regards to their ability to crosslink PAM copolymers complexed to Ca-Alg beads. In addition to reinforcing the polymer shells, these crosslinking methods consume primary amines, decreasing the overall surface charge. This is however dependent on the crosslinker used.

After crosslinking, capsules were treated with sodium citrate to extract calcium from the hydrogel cores, followed by NaOH to break electrostatic interactions between copolymer and alginate, and were subjected to a manual pipetting assay to assess mechanical robustness of the resulting covalently crosslinked shells as illustrated in Figs. 4A.12-4A.13.

4.4.5.1. THPC

Batch and semibatch polycation capsules were crosslinked by exposure to 0.1% THPC for 2 min and were imaged by confocal laser-scanning microscopy. APM-rich capsules ($PAM^{b}_{\leq 42}$) remained largely intact after treatment with citrate and NaOH, and pipetting (Figure 4A.14). On the other hand, PAM^{b}_{55} and PAM^{b}_{65} were displaced towards the capsule cores by addition of the cationic THPC (Figure 4A.15). This displacement is analogous to similar effects observed upon introduction of calcium[39,63] and interferes with crosslinking efficiency. Indeed, only about 50% of the PAM^{b}_{55} capsules survived the pipetting assay without rupture and show notable fluorescence in the supernatant from out-diffusion of copolymer, while PAM^{b}_{65} did not form crosslinked capsules stable in citrate/NaOH.

Semibatch capsules crosslinked with 0.1 wt % THPC similarly showed good robustness for compositions up to and including PAM^{sb}_{38}. The capsules maintained their spherical shape after citrate and NaOH exposure as well as pipette aspiration, exhibiting improved crosslinking over their batch counterparts. Capsules formed using 12-38% MPC semibatch copolymer displayed high levels of capsule survival and appear suitable for further study; PAM^{sb}_{38} is particularly attractive as the capsules formed show good robustness with limited capsule aggregation and shell tearing.

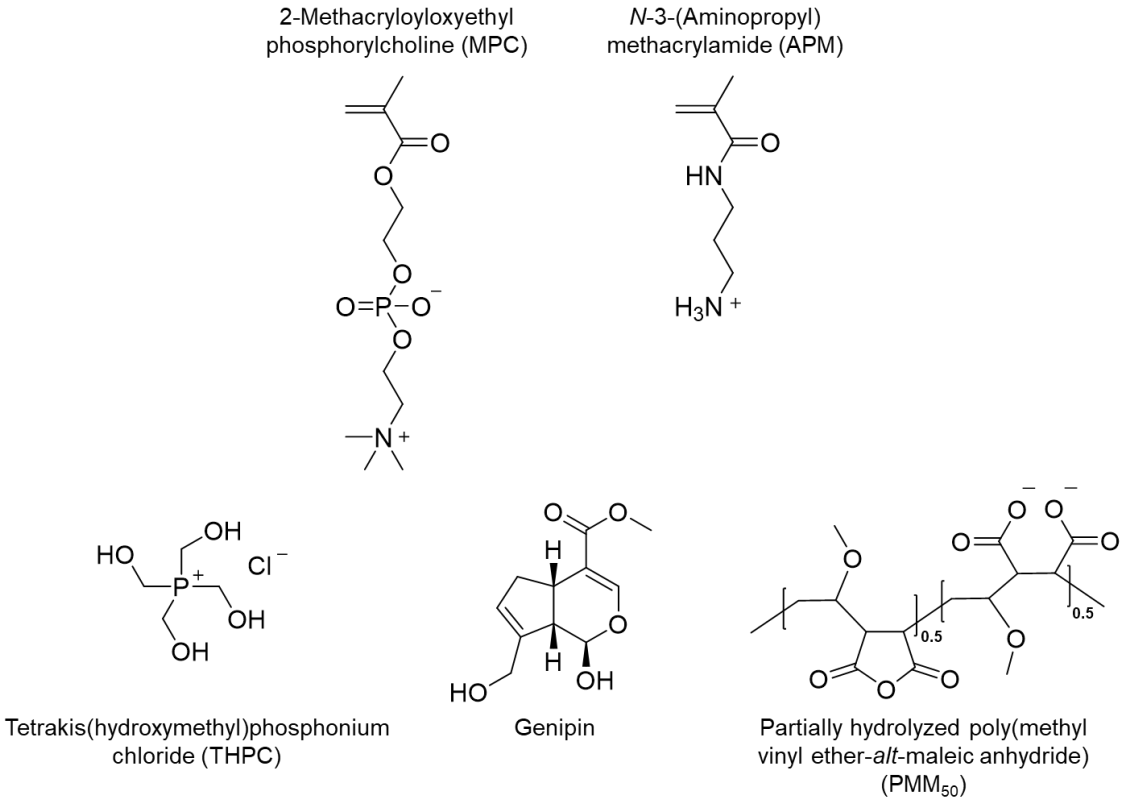

Figure 4.3. Structures of MPC and APM monomers (top) and crosslinkers (bottom) investigated for covalently enhancing capsule robustness.

4.4.5.2. Genipin

To avoid the introduction of cations during crosslinking, the orchid-derived crosslinker genipin was tested as a charge-neutral crosslinker (Figure 4A.16 shows the assigned ^{1}H NMR spectrum).[64] Genipin, used in herbal medicine and food products,[65] has shown topical anti-inflammatory activity[66] and is reported to be less cytotoxic than commonly used glutaraldehyde, by three orders of magnitude.[61] It has also been shown to improve the strength and biocompatibility of APA capsules through crosslinking and consumption of primary amines, thus reducing the cationic charge density.[52,53,67] After 1 h of exposure, the

genipin-treated capsules appear darker in colour than those seen in THPC crosslinking (Figure 4A.17), a property used in food products to introduce dark blue pigments.[65,68]

While the exact mechanism of genipin crosslinking remains under discussion[65,69] covalent crosslinking was observed for all semibatch compositions of ≤ 51 mol % MPC, with nearly all capsules surviving citrate and sodium hydroxide treatments. Results of pipette aspiration (Figure 4.4) mirrored those of THPC crosslinked capsules for PAM^{sb}_{12} to PAM^{sb}_{29}, with genipin capsules showing relatively increased survival for PAM^{sb}_{38} and, in particular, for PAM^{sb}_{51}. PAM^{sb}_{61} capsules did not survive aspiration. Confocal laser-scanning microscopy (Figure 4.5) allows parallel observation of FITC-labelled PAM and auto-fluorescing genipin (TRITC channel), respectively, showing close overlap of genipin and copolymer.

After 48 h, the capsules appear to darken further indicating an increased consumption of genipin, although capsule robustness did not appear to significantly change. To minimize in-diffusion, amine-decoration, and mobilized polymer, 0.05 wt % genipin crosslinking was also investigated and resulted in similar capsule robustness (Figure 4.6).

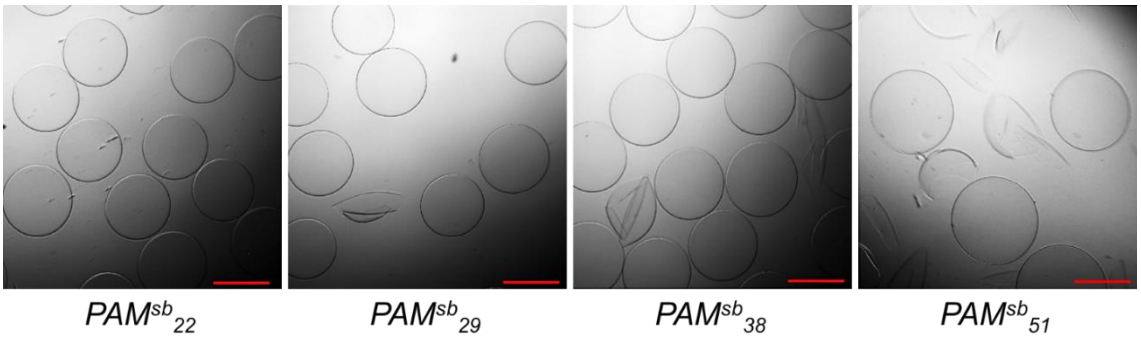

Figure 4.4. Genipin crosslinked PAM^{sb} capsules after sodium citrate, sodium hydroxide and robustness testing show decreased strength as MPC mol % increases (scale bars = 500 μm).

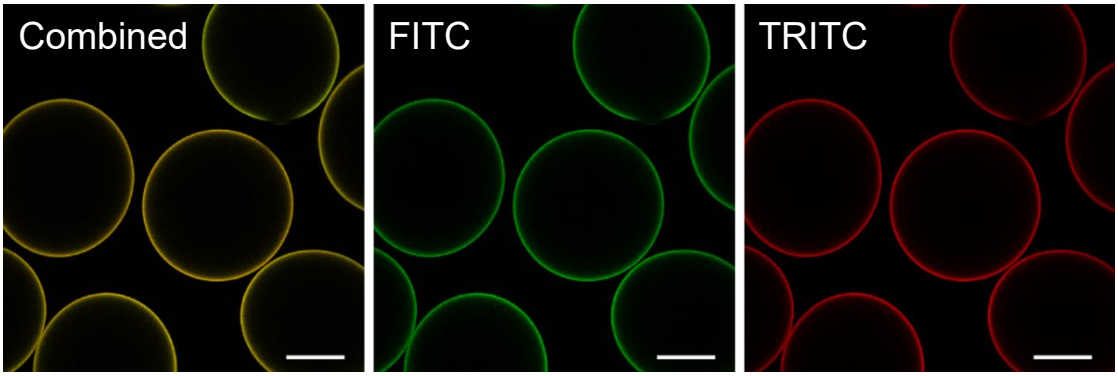

Figure 4.5. Confocal microscopy images of PAM^{sb}_{51}-f capsules crosslinked by 0.1 wt % genipin for 1 h, showing combined fluorescence channel (left), FITC channel (centre), and TRITC channel (right) (scale bars = 200 μm).

4.4.5.3. PM-a-M_{50}

PM-*a*-M_{50} is a reactive polyanion formed by 50% hydrolysis of poly(methyl vinyl ether-*alt*-maleic anhydride) (Figure 4A.18 shows NMR of PM-*a*-M hydrolysis), that was previously used to covalently crosslink poly-L-lysine coated Ca-Alg capsules. In addition to improving capsule stability, PM-*a*-M_{50} also reduced the host immune response for capsules implanted into the peritoneum of immune-competent mice, which was attributed to reduction of cationic charge-density by converting PLL-based amines and introducing additional anionic groups.[9]

The PM-*a*-M_{50} crosslinked PAM^{sb} capsules studied here were quite weak, with less than 10% surviving citrate and NaOH treatment and pipette aspiration. Part of this may be attributed to reduced binding of anionic PM-*a*-M_{50} and the charge-reduced PAM^{sb} copolymers as compared to PLL. However, we also found weak shell formation in PLL-controls, suggesting the PM-*a*-M_{50} used may have been hydrolyzed more than expected, as supported by ^{1}H NMR data (Figure 4A.18). We included the PM-*a*-M_{50} coated capsules in

subsequent comparative protein adhesion studies to explore the anti-fouling properties of these anionic crosslinkers.

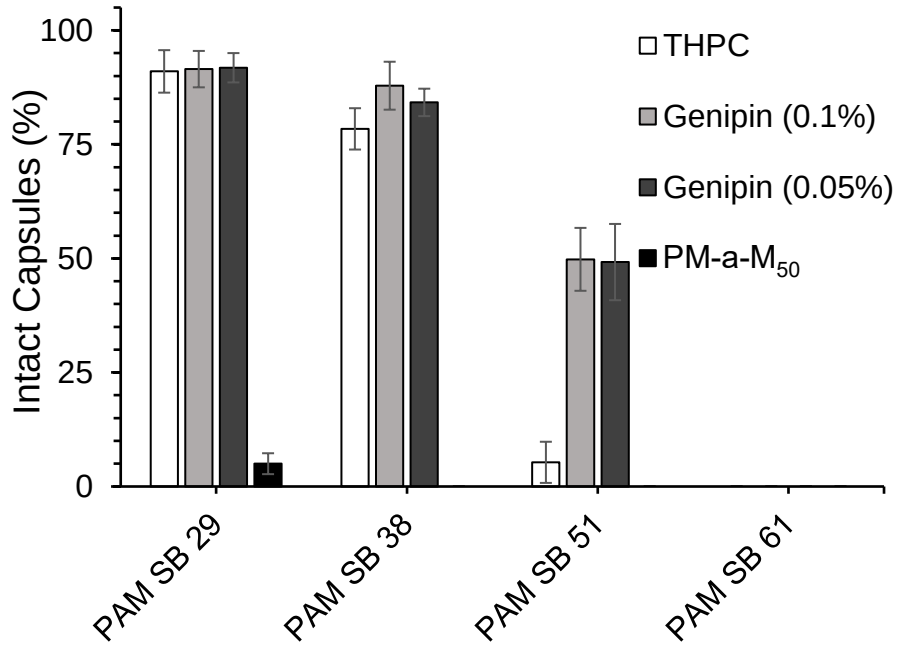

Figure 4.6. Qualitative robustness estimates of intact vs fragmented capsules (n = 100) across varying compositions and crosslinkers, using optical microscopy. For PAM^{sb}_{61} no capsules survived aspiration tests.

On the basis of the survival rates of THPC and genipin crosslinked capsules, semibatch copolymers of 22-38 mol % MPC currently appear to be promising candidates for robust capsules. Future studies of shear flow exposure and bead deformation may enable comparison of overall bead/capsule robustness with literature values.[70]

4.4.6. Bovine Serum Albumin (BSA-f) Protein Adhesion Assay

Adhesion of host proteins to the capsule surface is a key indication that the capsules will evoke an immune response upon implantation. BSA-*f* was used here as a model protein for qualitative screening for protein adherence using PLL crosslinked capsules as controls.

Un-labelled PAM^{sb} capsules crosslinked by THPC, genipin and PM-*a*-M_{50}, respectively, were exposed to a BSA-*f* solution and washed with saline containing 0.1 wt % $CaCl_2$ to remove any unbound BSA. $CaCl_2$ was added to avoid capsule swelling due to calcium loss.

Figure 4.7 shows that THPC crosslinked PAM^{sb} capsules show BSA-*f* adhesion increasing with MPC mol % from PAM^{sb}_{29} to PAM^{sb}_{38}, suggesting that BSA-*f* binding is enhanced with unreacted crosslinker. While THPC consumes primary amines, the crosslinker also introduces new phosphonium ions, hindering its ability to reduce capsule surface charge. THPC functional groups may also decorate the copolymer. As a result, PAM^{sb}_{22} and PAM^{sb}_{29} crosslinked with THPC are perhaps more promising candidates for further study as low-fouling capsule coatings. In particular, they show reduced BSA-*f* binding compared to PLL-coated capsules.

PM-*a*-M_{50} crosslinked PLL control capsules showed lowest protein adhesion across the three crosslinkers due to the charge-shielding effect of the anionic groups introduced by this crosslinker.[9] Figure 4.7 also shows very low levels of fluorescence for PM-*a*-M_{50}-crosslinked PAM^{sb} capsules, though these capsules may have weaker shells as observed in the pipet assays.

Genipin crosslinked capsules were examined before BSA-*f* exposure to assess the background fluorescence in the FITC channel from reacted genipin. Capsules were then exposed to BSA-*f* after 48 h to allow complete consumption of genipin. Side-by-side comparison of genipin capsules before and after exposure to BSA-*f* show negligible surface fluorescence attributable to BSA-*f* for copolymers with 12% to 38% MPC (Figure 4A.19).

Copolymers with 51% MPC show an increase in fluorescence after BSA-*f* exposure, which is attributed to weakened electrostatic shell interactions and reaction with available bound genipin. Hence, BSA-*f* adhesion to PAM^{sb} capsules crosslinked with genipin is minimal for PAM^{sb} of 38 or less mol % MPC, and lower than for PLL-coated capsules crosslinked with genipin (Figures 4.7 and 4A.19). Coupled with their desirable robustness, these results indicate PAM^{sb}_{29} and PAM^{sb}_{38} capsules crosslinked with genipin are promising candidates for further study.

This protein adhesion assay indicates promising compositions, but robust capsules with low BSA adhesion should be further investigated in more complex protein solutions, such as full serum, for comparison with other reported low-fouling capsules. Surface plasmon resonance offers qualitative comparison of protein adhesion and will be used to explore promising capsules in future work.

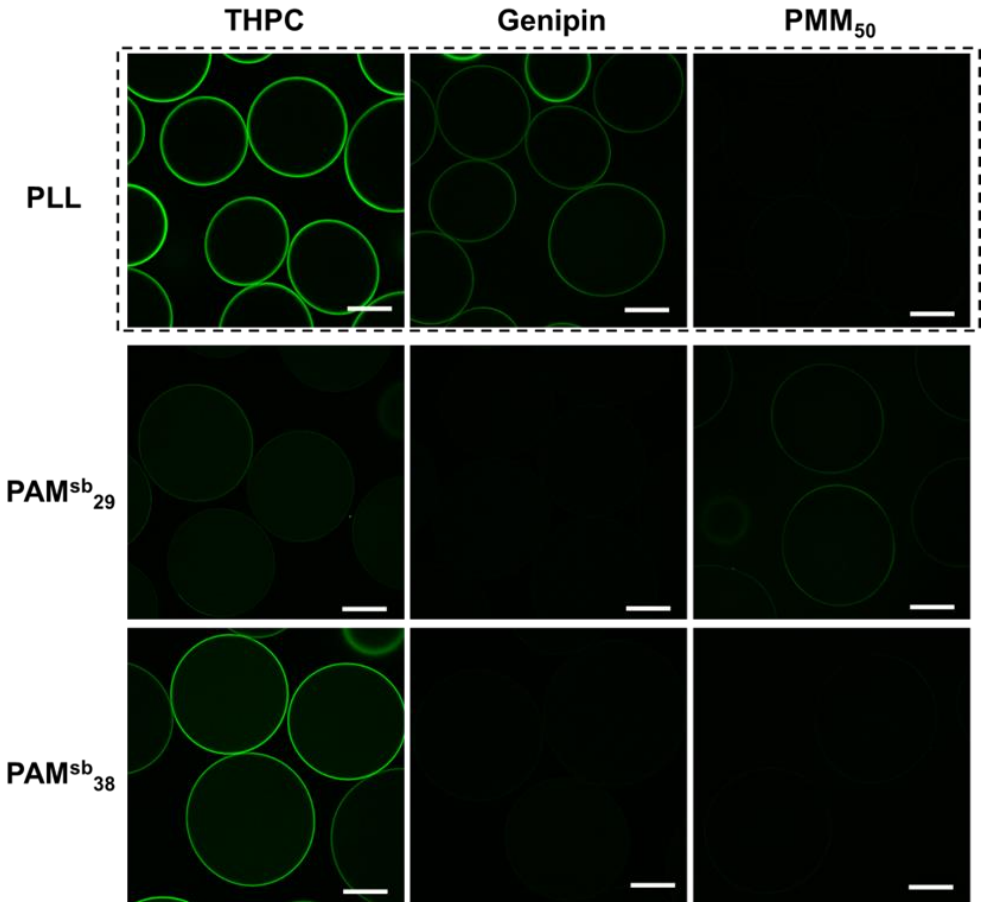

Figure 4.7. Confocal microscope images of control PLL capsules (dotted lines) and PAM^{sb} capsules exposed to BSA-*f* for 24 h with various crosslinkers, using consistent microscope and camera settings (scale bars = 200 μm).

4.5. Conclusions

This work describes a series of semibatch APM/MPC copolymers that can be coated onto Ca-Alg beads and crosslinked in place through the primary amines on the APM monomers. The reduced charge density of these copolymers compared to, for example, PLL, and incorporation of the highly hydrophilic MPC comonomer lead to low BSA-*f* binding. In

particular, APM/MPC copolymers incorporating about 22 to 38 mol % MPC permitted formation of stable, crosslinked capsules with tunable characteristics.

The molecular weight of these copolymers was controlled through addition of chain transfer agent. Reactivity ratios were determined using ^{1}H NMR and were used to generate specific copolymer compositions.

In addition, semibatch copolymerization was used to limit compositional drift during copolymerization, consequently improving copolymer hydration for comparable MPC mol % and retention of copolymer in the Ca-Alg shell without increasing peak APM content at the bead surface. This allows for formation of more robust shells without increasing the risk for non-specific protein fouling.

THPC, genipin, and PM-*a*-M_{50} were screened as cross-linkers, and the resulting capsules were studied using sodium citrate and sodium hydroxide solutions, and pipet aspiration to test for successful crosslinking and relative robustness. These tests indicate formation of robust capsules up to about 38 mol % MPC using THPC and genipin.

Using BSA-*f* to screen for protein binding showed the importance of crosslinker charge: proceeding from cationic THPC through neutral genipin to anionic PM-*a*-M_{50}, these crosslinkers allowed formation of low-BSA-*f* binding shells for PAM^{sb} containing 12-29, 12-38 and 12-51 mol % MPC, respectively. THPC gave rapid crosslinking and robust crosslinked capsules but enhanced copolymer in-diffusion at higher MPC content. Genipin did not introduce additional cationic charges and formed remarkably robust capsules, though requires longer crosslinking times at room temperature. PM-*a*-M_{50}

introduced excess anionic groups that have the potential to further repel proteins but may require additional optimization to increase robustness.

Future work will involve optimizing crosslinking procedures, exploring crosslinking kinetics, investigating other betaine monomers such as carboxybetaine methacrylate (CBMA), and applying these copolymers to cell encapsulation for use in immunoprotected transplantation of therapeutic cells.

Supporting Information

GPC chromatograms of copolymers as a function of comonomer ratio and chain transfer agent; reactivity ratios obtained from NMR data using the Fineman−Ross method; instantaneous copolymer composition graphs for reactivity ratios obtained using progressive composition analysis and Fineman−Ross; spreadsheet describing semibatch procedure; spreadsheet describing compositional spread during semibatch procedure; microscopy images comparing hydration of alginate-copolymer complexes for batch and semibatch processes; Bright field microscopy images showing increasing hydration of polyelectrolyte complexes as a function of increasing MPC content; plot of capsule thickness as a function of MPC mole fraction; plot of estimated peak APM content at capsule surface for batch and semibatch copolymers; fluorescence microscopy images of capsules; ^{1}H NMR spectrum of genipin used; photographs of color changes during genipin-mediated crosslinking; ^{1}H NMR spectra on progressive hydrolysis of PM-*a*-M during formation of PM-*a*-M_{50}; and fluorescence microscopy images of BSA-*f* deposition on capsules.

Author Information

Corresponding Author

Email: stoverh@mcmaster.ca, Ph.: 1-905-525-9140 ext. 24983.

Notes:

The authors declare no competing financial interest.

4.6. Acknowledgements

The authors would like to thank the Natural Sciences and Engineering Research Council of Canada for funding this research, including the CGS-M held by D. E. Hastings. The authors would like to thank Samantha Ros for valuable insights regarding copolymerization and reactivity ratio determination. The authors would also like to thank Jing Zhao for useful discussion of polyzwitterions as well as Alison Stewart and Mitchell Johnson for insights on alginate beads and gel properties.

4.7. References

1. Leroux, G.; Neumann, M.; Meunier, C. F.; Fattaccioli, A.; Michiels, C.; Arnould, T.; Wang, L.; Su, B.-L. Hybrid Alginate@TiO2 Porous Microcapsules as a Reservoir of Animal Cells for Cell Therapy. *ACS Appl. Mater. Interfaces* **2018**, *10*, 37865-37877.

2. Song, Y.; Chan, Y. K.; Ma, Q.; Liu Z.; Shum, H. C. All-Aqueous Electrosprayed Emulsion for Templated Fabrication of Cytocompatible Microcapsules. *ACS Appl. Mater. Interfaces* **2015**, *7*, 13925-13933.

3. Li, P.; Müller, M.; Chang, M. W.; Frettlöh, M.; Schönherr, H. Encapsulation of Autoinducer Sensing Reporter Bacteria in Reinforced Alginate-Based Microbeads. *ACS Appl. Mater. Interfaces* **2017**, *9*, 22321-22331.

4. Zhang, B.-B.; Wang, L.; Charles, V.; Rooke, J. C.; Su, B.-L. Robust and Biocompatible Hybrid Matrix with Controllable Permeability for Microalgae Encapsulation. *ACS Appl. Mater. Interfaces* **2016**, *8*, 8939-8946.

5. Fenn, S. L.; Miao, T.; Scherrer, R. M.; Oldinski, R. A. Dual-Cross-Linked Methacrylated Alginate Sub-Microspheres for Intracellular Chemotherapeutic Delivery. *ACS Appl. Mater. Interfaces* **2016**, *8*, 17775-17783.

6. Lin, N.; Gèze, A.; Wouessidjewe, D.; Huang, J.; Dufresne, A. Biocompatible Double-Membrane Hydrogels from Cationic Cellulose Nanocrystals and Anionic Alginate as Complexing Drugs Codelivery. *ACS Appl. Mater. Interfaces* **2016**, *8*, 6880-6889.

7. Shoichet, M. S.; Li, R. H.; White, M. L.; Winn, S. R. Stability of Hydrogels Used in Cell Encapsulation: An In Vitro Comparison of Alginate and Agarose. *Biotechnol. Bioeng.* **1996**, *50*, 374-381.

8. Lim, F.; Sun, A. M. Microencapsulated islets as bioartificial endocrine pancreas. *Science* **1980**, *210*, 908-910.

9. Gardner, C. M.; Burke, N. A. D.; Stöver, H. D. H. Cross-Linked Microcapsules Formed From Self-Deactivating Reactive Polyelectrolytes. *Langmuir*, **2010**, *26*, 4916-4924.

10. Rice, J.; Martino, M. M.; De Laporte, L.; Tortelli, F.; Briquez, P. S.; Hubbell, J. A. Engineering the Regenerative Microenvironment with Biomaterials. *Adv. Healthcare Mater.* **2013**, *2*, 57-71.

11. Strand, B. L.; Ryan, L.; Veld, P. I.; Kulseng, B.; Rokstad, A. M.; Skjåk-Bræk, G.; Espevik, T. Poly-L-Lysine Induces Fibrosis on Alginate Microcapsules via the Induction of Cytokines. *Cell Transplant.* **2001**, *10*, 263-275.

12. Pueyo, M. E.; Darquy, S.; Capron, F.; Reach, G. In vitro activation of human macrophages by alginate-polylysine microcapsules. *J. Biomater. Sci., Polym. Ed.* **1994**, *5*, 197-203.

13. Knop, K.; Hoogenboom, R.; Fischer, D.; Schubert, U. S. Poly(ethylene glycol) in Drug Delivery: Pros and Cons as Well as Potential Alternatives. *Angew. Chem. Int. Ed.* **2010**, *49*, 6288-6308.

14. Krishnan, S.; Weinman, C. J.; Ober, C. K. Advances in polymers for anti-biofouling surfaces. *J. Mater. Chem.* **2008**, *18*, 3405-3413.

15. Harris, J. M. Poly(Ethylene Glycol) Chemistry: Biotechnical and Biomedical Applications Springer Science+Business Media: New York, 1992; pp 1-12.

16. Leng, C.; Hung, H.-C.; Sun, S.; Wang, D.; Li, Y.; Jiang, S.; Chen, Z. Probing the Surface Hydration of Nonfouling Zwitterionic and PEG Materials in Contact with Proteins. *ACS Appl. Mater. Interfaces.* **2015**, *7*, 16881-16888.

17. Spasojevic, M.; Bhujnal, S.; Paredes, G.; de Haan, B. J.; Schouten, A. J.; de Vos, P. Considerations in binding diblock copolymers on hydrophilic alginate beads for providing an immunoprotective membrane. *J. Biomed. Mater. Res. A.* **2014**, *102*, 1887-1896.

18. Sawhney, A. S.; Hubbell, J. A. Poly(ethylene oxide)-graft-poly(L-lysine) copolymers to enhance the biocompatibility of poly(L-lysine)-alginate microcapsule membranes. *Biomaterials* **1992**, *13*, 863-870.

19. Sawhney, A. S.; Pathak, C. P.; Hubbell, J. A. Interfacial photopolymerization of poly(ethylene glycol)-based hydrogels upon alginate-poly(L-lysine) microcapsules for enhanced biocompatibility. *Biomaterials* **1993**, *14*, 1008-1016.

20. Chanan-Khan, A.; Szebeni, J.; Savay, S.; Liebes, L.; Rafique, N. M.; Alving, C. R.; Muggia, F. M. Complement activation following first exposure to pegylated liposomal doxorubicin (Doxil®): possible role in hypersensitivity reactions. *Ann. Oncol.* **2003**, *14*, 1430-1437.

21. Szebeni, K. Complement activation-related pseudoallergy: A new class of drug-induced acute immune toxicity. *Toxicology* **2005**, *216*, 106-121.

22. Verhoef, J. J. F.; Carpenter, J. F.; Anchordoquy, T. J.; Schellekens, H. Potential induction of anti-PEG antibodies and complement activation toward PEGylated therapeutics. *Drug Discov. Today* **2014**, *19*, 1945-1952.

23. Richter, A. W.; Akerblom, E. Antibodies against polyethylene glycol produced in animals by immunization with monomethoxy polyethylene glycol modified proteins. *Int. Arch. Allergy Appl. Immunol.* **1983**, *70*, 124-131.

24. Armstrong, J. K.; Hempel, G.; Koling, S.; Chan, L. S.; Fisher, T.; Meiselman, H. J.; Garratty G. Antibody against pol(ethylene glycol) adversely affects PEG-asparaginase therapy in acute lymphoblastic leukemia patients. *Cancer* **2007**, *110*, 103–111.

25. Wang, X. Y.; Ishida, T.; Kiwada, H. Anti-PEG IgM elicited by injection of liposomes is involved in the enhanced blood clearance of a subsequent dose of PEGylated liposomes. *J. Control. Release* **2007**, *119*, 236-244.

26. He, M.; Gao, K.; Zhou, L.; Jiao, Z.; Wu, M.; Cao, J.; You, X.; Cai, Z.; Su, Y.; Jiang, Z. Zwitterionic materials for antifouling membrane surface construction. *Acta Biomater.* **2016**, *40*, 142-152.

27. Zhao, J.; Burke, N. A. D.; Stöver, H. D. H. Preparation and study of multi-responsive polyampholyte copolymers of N-(3-aminopropyl)methacrylamide hydrochloride and acrylic acid. *RSC Adv.* **2016**, *6*, 41522-41531.

28. Lowe, A. B.; McCormick, C. L. Synthesis and Solution Properties of Zwitterionic Polymers. *Chem. Rev.* **2002**, *102*, 4177-4190.

29. Schroeder, M. E.; Zurick, K. M.; McGrath, D. E.; Bernards, M. T. Multifunctional Polyampholyte Hydrogels with Fouling Resistance and Protein Conjugation Capacity. *Biomacromolecules* **2013**, *14*, 3112-3122.

30. Leng, C.; Huang, H.; Zhang, K.; Hung, H.-C.; Xu, Y.; Li, Y.; Jiang, S.; Chen, Z. Effect of Surface Hydration on Antifouling Properties of Mixed Charged Polymers. *Langmuir* **2018**, *34*, 6538-6545.

31. Georgiev, G. S.; Kamenska, E. B.; Vassileva, E. D.; Kamenova, I. P.; Georgeiva, V. T.; Illiev, S. B.; Ivanov, I. A. Self-Assembly, Antipolyelectrolyte Effect, and Nonbiofouling Properties of Polyzwitterions. *Biomacromolecules* **2006**, *7*, 1329-1334.

32. Jiang, S.; Cao, Z. Ultralow-Fouling, Functionalizable and Hydrolyzable Zwitterionic Materials and Their Derivatives for Biological Applications. *Adv. Mater.* **2010**, *22*, 920-932.

33. Wu, J.; Lin, W.; Wang, Z.; Chen, S. Investigation of the Hydration of Nonfouling Material Poly(sulfobetaine methacrylate) by Low-Field Nuclear Magnetic Resonance. *Langmuir* **2012**, *28*, 7436-7441.

34. Ye, S. H. L.; Watanabe, J.; Iwasaki, Y.; Ishihara, K. Antifouling blood purification membrane composed of cellulose acetate and phospholipid polymer. *Biomaterials* **2003**, *24*, 4143-4152.

35. Bengani-Lutz. P.; Converse, E.; Cebe, P.; Asatekin, A. Self-Assembling Zwitterionic Copolymers as Membrane Selective Layers with Excellent Fouling Resistance: Effect of Zwitterion Chemistry. *ACS Appl. Mater. Interfaces* **2017**, *9*, 20859-20872.

36. Zhang, X.; Chen, W.; Zhu, X.; Lu, Y. Encapsulating Therapeutic Proteins with Polyzwitterions for Lower Macrophage Nonspecific Uptake and Longer Circulation Time. ACS Appl. Mater. Interfaces **2017**, *9*, 7972-7978.

37. Ishikara, K.; Tanaka, S.; Furukawa, N.; Kurita, K.; Nakabayashi, N. Improved blood compatibility of segmented polyurethanes by polymeric additives having phospholipid polar groups. I. Molecular design of polymeric additives and their functions. *J. Biomed. Mater. Res.* **1996**, *32*, 391-399.

38. Yesilyurt, V.; Veiseh, O.; Doloff, J. C.; Li, J.; Bose, S.; Xie, X.; Bader, A. R.; Chen, M.; Webber, M. J.; Vegas, A. J.; Langer, R.; Anderson, D. G. A Facile and Versatile Method to Endow Biomaterial Devices with Zwitterionic Surface Coatings. *Adv. Healthc. Mater.* **2018**, *6*, 160191.

39. Kleinberger, R. M.; Burke, N. A. D.; Zhou, C.; Stöver, H. D. H. Synthetic polycations with controlled charge density and molecular weight as building blocks for biomaterials. *J. Biomater. Sci.* **2016**, *27*, 351-369.

40. Dubey, A.; Burke, N. A. D.; Stöver, H. D. H. Preparation and Characterization of Narrow Compositional Distribution Polyampholytes as Potential Biomaterials: Copolymers of N-(3-Aminopropyl)methacrylamide Hydrochloride (APM) and Methacrylic Acid (MAA). *J. Polym. Sci. Part A* **2015**, *53*, 353-365.

41. Abdilla, A.; Shi, S.; Burke, N. A. D.; Stöver, H. D. H. Multistimuli Responsive Ternary Polyampholytes: Formation and Crosslinking of Coacervates. *J. Polym. Sci. Part A* **2016**, *54*, 2109-2118.

42. Ros, S.; Burke, N. A. D.; Stöver, H. D. H. Synthesis and Properties of Charge-Shifting Polycations: Poly[3-aminopropylmethacrylamide-co-2-(dimethylamino)ethyl acrylate]. *Macromolecules* **2015**, *48*, 8958-8970.

43. Ahmed, M.; Bhuchar, N.; Ishihara, K.; Narain, R. Well-Controlled Cationic Water-Soluble Phospholipid Polymer-DNA Nanocomplexes for Gene Delivery. *Bioconjugate Chem.* **2011**, *22*, 1228-1238.

44. Yu, K.; Lo, J. C. Y.; Mei, Y.; Haney, E. F.; Siren, E.; Kalathottukaren, M. T.; Hancock, R. E. W.; Lange, D.; Kizhakkedathu, J. N. Toward Infection-Resistant Surfaces: Achieving High Antimicrobial Peptide Potency by Modulating the Functionality of Polymer Brushes and Peptide. *ACS Appl. Mater. Interfaces.* **2015**, *7*, 28591-28605.

45. Lollmahomed, F. B.; Narain, R. Photochemical Approach toward Deposition of Gold Nanoparticles on Functionalized Carbon Nanotubes. *Langmuir* **2011**, *27*, 12642-12649.

46. Kucharski, M.; Lubczak, R. Copolymerization of Hydroxyalkyl Methacrylates with Acrylamide and Methacrylamide I. Determination of Reactivity Ratios. *J. Appl. Polym. Sci.* **1997**, *7*, 1259-1265.

47. Saini, G.; Leoni, A.; Franco, S. Solvent Effects in Radical Copolymerization III. Methacrylamide. *Macromol. Chem.* **1971**, *147*, 213-218.

48. Crauwels, K.; Smets, G. Polymers of Methacrylamide. *Bull. Soc. Chim. Belg.* **1950**, *59*, 182-192.

49. Wang, R.; Luo, Y.; Li, B.; Zhu, S. Control of Gradient Copolymer Composition in ATRP Using Semibatch Feeding Policy. *AIChE J.* **2007**, *53*, 174-186.

50. Aguilar, M.; Gallardo, A.; Fernández, M.; Román, J. In-Situ Quantitative 1H NMR Monitoring of Monomer Consumption: A Simple and Fast Way of Estimating Reactivity Ratios. *Macromolecules* **2002**, *35*, 2036-2041.

51. Fineman, M.; Ross, S. D. Linear Method for Determining Monomer Reactivity Ratios in Copolymerization. *J. Polym. Sci.* **1950**, *5*, 259-262.

52. Hillberg, A. L.; Kathirgamanathan, K.; Lam, J. B. B.; Law, L. Y.; Garkavenko, O.; Elliot, R. B. Improving alginate-poly-L-ornithine-alginate capsule biocompatibility through genipin crosslinking. *J. Biomed. Mater. Res. B, Appl. Biomater.* **2013**, *2*, 258-268.

53. Chen, H.; Ouyang, W.; Lawuyi, B.; Prakash, S. Genipin Cross-Linked Alginate-Chitosan Microcapsules: Membrane Characterization and Optimization of Cross-Linking Reaction. *Biomacromolecules*, **2006**, *7*, 2091-2098.

54. Shen, F.; Mazumder, M. A. J.; Burke, N. A. D.; Stöver, H. D. H., Potter, M. A. Mechanically Enhanced Microcapsules for Cellular Gene Therapy. *J. Biomed. Mater. Res. B, Appl. Biomater.* **2009**, *90B*, 350-361.

55. Asgeirsson, D.; Venturoli, D.; Rippe, B.; Rippe, C. Increased glomerular permeability to negatively charged Ficoll relative to neutral Ficoll in rats. *Am. J. Physiol. Renal. Physiol.* **2006**, *291*, 1083-1089.

56. Thu, B.; Bruheim, P.; Espevik, T.; Smidsrød, O.; Soon-Shiong, P.; Skjâk-Bræk, G. Alginate polycation microcapsules: I. Interaction between alginate and polycation. *Biomaterials* **1996**, *17*, 1031-1040.

57. Goosen, M. F. A.; O'Shea, G. M.; Gharapetian, H. M.; Chou, S. Optimization of Microencapsulation Parameters: Semipermeable Microcapsules as a Bioartificial Pancreas. *Biotechnol. Bioeng.* **1985**, *27*, 146-150.

58. Li, G.-Z.; Randev, R. K.; Soeriyadi, A. H.; Rees, G.; Boyer, C.; Tong, Z.; Davis, T. P.; Remzi Beer, C.; Haddleton, D. M. Investigation into thiol-(meth)acrylate Michael addition reactions using amine and phosphine catalysts. *Polym. Chem.* **2010**, *1*, 1196-1204.

59. Mather, B. D.; Viswanathan, K.; Miller, K. M.; Long, T. E. Michael addition reactions in macromolecular design for emerging technologies. *Prog. Polym. Sci.* **2006**, *31*, 487-531.

60. Nair, D. P.; Podgorski, M.; Chatani, S.; Gong, T.; Xi, W.; Fenoli, C. R.; Bowman, C. N. The Thiol-Michael Addition Click Reaction: A Powerful and Widely Used Tool in Materials Chemistry. *Chem. Mater.* **2014**, *26*, 724-744.

61. Sung, H.-W.; Huang, R.-N.; Huang, L. L. H.; Tsai, C.-C. In vitro evaluation of cytotoxicity of a naturally occurring cross-linking reagent for biological tissue fixation. *J. Biomater. Sci. Polym. Ed.* **1999**, *10*, 63-78.

62. Chung C.; Lampe, K. J.; Heilshorn, S. C. Tetrakis(hydroxymethyl) Phosphonium Chloride as a Covalent Cross-Linking Agent for Cell Encapsulation within Protein-Based Hydrogels. *Biomacromolecules* **2012**, *13*, 3912-3916.

63. Kleinberger, R. M.; Burke, N. A. D.; Dalnoki-Veress, K.; Stöver, H. D. H. Systematic study of alginate-based microcapsules by micropipette aspiration and confocal fluorescence microscopy. *Mater. Sci. Eng. C* **2013**, *33*, 4295-4304.

64. Di Tommaso, S.; David, P.; Picolet, K.; Gabant, M.; David, H.; Morançais, J.-L.; Gomar, J.; Leroy, F.; Adamo, C. Structure of genipin in solution: a combined experimental and theoretical study. *RSC Adv.* **2013**, *3*, 13764-13771.

65. Park, J.-E. J., Lee, J.-Y.; Kim, H.-G.; Hahn, T.-R.; Paik, Y.-S. Isolation and Characterization of Water-Soluble Intermediates of Blue Pigments Transformed from Geniposide of Gardenia jasminoides. *Agric. Food Chem.* **2002**, *50*, 6511-6514.

66. Koo, H-J.; Lee, S.; Shin, K.-H.; Kim, B.-C.; Lim, C.-J.; Park, E.-H. Geniposide, an Anti-Angiogenic Compound from the Fruits of Gardenia jasmioides. *Planta Medica* **2004**, *70*, 467-469.

67. Paul, A.; Cantor, A.; Shum-Tim, D.; Prakash, S. Superior Cell Delivery Features of Genipin Crosslinked Polymeric Microcapsules: Preparation, In Vitro Characterization and Pro-Angiogenic Applications Using Human Adipose Stem Cells. *Mol. Biotechnol.* **2011**, *48*, 116-127.

68. Sundararaghavan, H. G.; Monteiro, G. A.; Lapin, N. A.; Chabal, Y. J.; Miksan, J. R.; Schreiber, D. I. Genipin-induced changes in collagen gels: Correlation of mechanical properties to fluorescence. *J. Biomed. Mater. Res. A* **2008**, *87A*, 308-320.

69. Touyama, R.; Inoue, K.; Takeda, Y.; Yatsuzuka, M.; Ikumoto, T.; Moritome, N.; Shingu, T.; Yokoi, T.; Inouye, H. Studies on the Blue Pigments Produced from Genipin and Methylamine. II. On the Formation Mechanisms of Brownish-Red Intermediates Leading to the Blue Pigment Formation. *Chem. Pharm. Bull.* **1994**, *42*, 1571-1578.

70. David, B.; Barbe, L.; Barthès-Biesel, D.; Legallais, C. Mechanical properties of alginate beads hosting hepatocytes in a fluidized bed bioreactor. *Int. J. Artif. Organs* **2006**, *29*, 756-763.

4.8. Appendix

Figure 4A.1. (A) Normalized GPC Chromatograms of PAM_{48} with different amounts of cysteamine relative to total monomer.

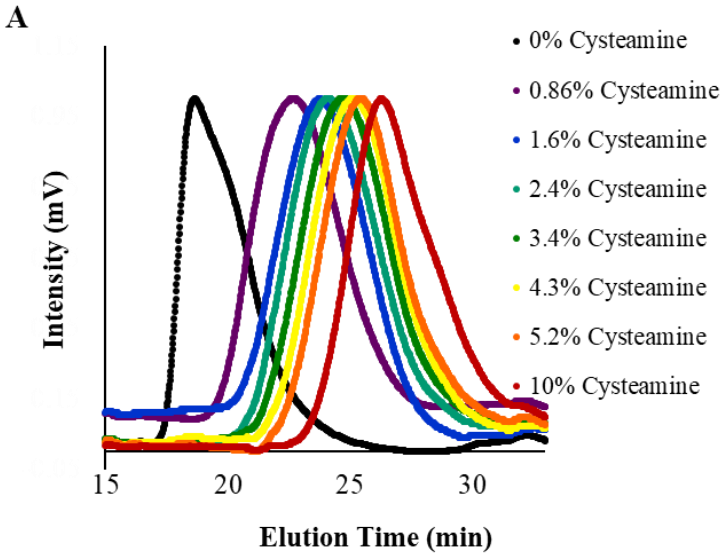

Figure 4A.1. (B) Comparison of molecular weights across different PAM compositions with different amounts of cysteamine.

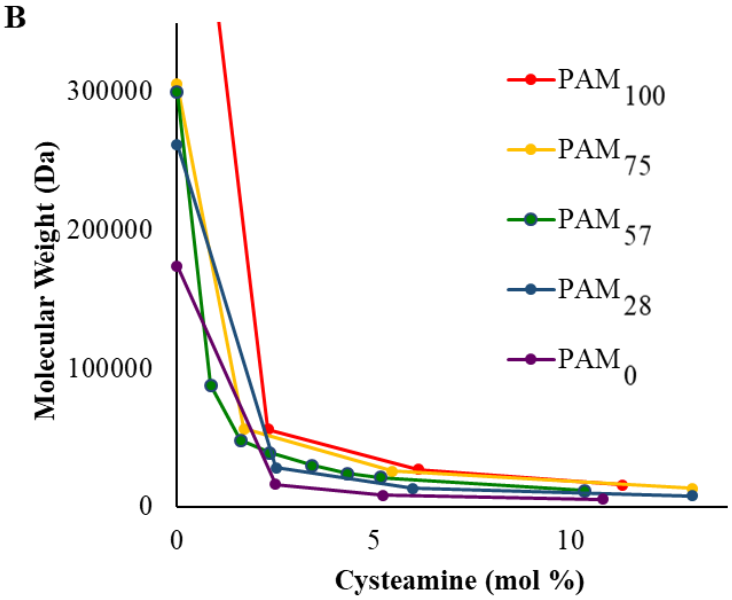

Figure 4A.2. Reactivity ratios determined using NMR data via the Fineman-Ross method, where r_1 is the linear slope and r_2 is the y-intercept.

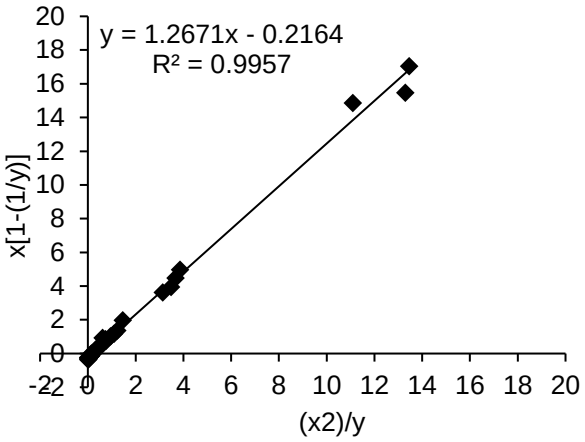

Figure 4A.3. Instantaneous copolymer equation using MPC and APM reactivity ratios of 1.47 and 0.21, respectively, determined by our previously reported method (*left*) and of 1.27 and 0.22, respectively, determined using the Fineman-Ross method (*right*) superimposed on reactivity data collected by ^{1}H NMR.

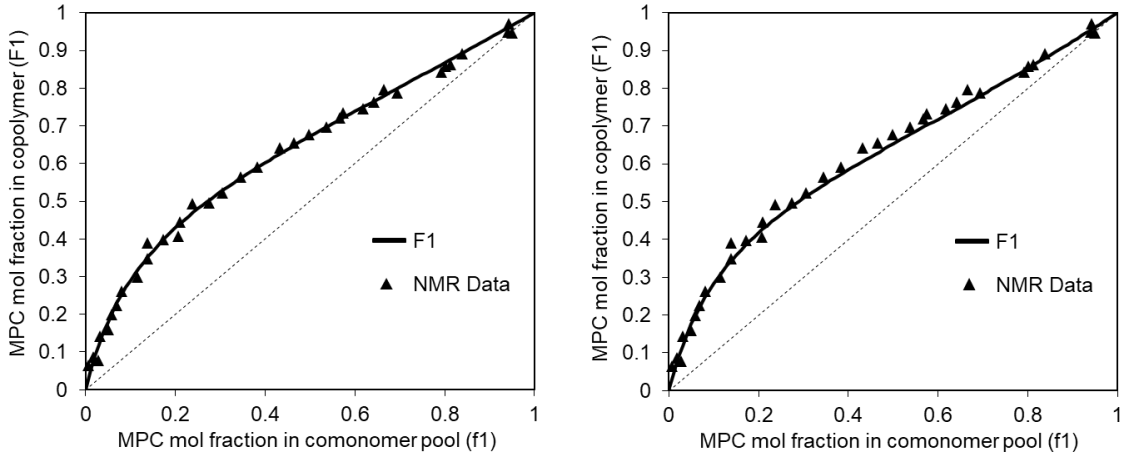

Figure 4A.4. Spreadsheet representation targeting of semibatch copolymer PAM^{sb}_{61} using the instantaneous copolymer composition at specific monomer feed ratios from experimentally determined reactivity ratios (1.47, 0.21). As copolymerization decreases the MPC feed ratio from 45%-36%, calculated additions of MPC stock solution, containing roughly 2.5% CTA, re-establishes initial monomer feed ratio in solution for continued polymerization.

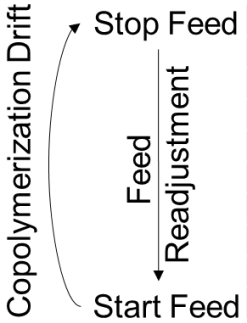

Monomer MPC mol Fraction (f1)	Monomer APM mol Fraction (f2)	$r_1f_1*f_1$	f_1f_2	$r_2f_2*f_2$	Polymer MPC mol Fraction F_1	Polymer APM mol Fraction F_2
0.300	0.700	0.133	0.210	0.102	0.523	0.477
0.310	0.690	0.142	0.214	0.099	0.532	0.468
0.320	0.680	0.151	0.218	0.097	0.540	0.460
0.330	0.670	0.160	0.221	0.094	0.548	0.452
0.340	0.660	0.170	0.224	0.091	0.556	0.444
0.350	0.650	0.181	0.228	0.088	0.564	0.436
0.360	0.640	0.191	0.230	0.086	0.572	0.428
0.370	0.630	0.202	0.233	0.083	0.580	0.420
0.380	0.620	0.213	0.236	0.080	0.587	0.413
0.390	0.610	0.224	0.238	0.078	0.594	0.406
0.400	0.600	0.236	0.240	0.075	0.602	0.398
0.410	0.590	0.248	0.242	0.073	0.609	0.391
0.420	0.580	0.260	0.244	0.070	0.616	0.384
0.430	0.570	0.272	0.245	0.068	0.623	0.377
0.440	0.560	0.285	0.246	0.065	0.630	0.370
0.450	0.550	0.298	0.248	0.063	0.637	0.363
0.460	0.540	0.312	0.248	0.061	0.644	0.356
0.470	0.530	0.326	0.249	0.059	0.651	0.349
0.480	0.520	0.340	0.250	0.056	0.658	0.342
0.490	0.510	0.354	0.250	0.054	0.665	0.335
0.500	0.500	0.368	0.250	0.052	0.672	0.328
0.510	0.490	0.383	0.250	0.050	0.679	0.321

$$\left[\left(\frac{MPC_i}{APM_i} * APM_n\right) - MPC_n\right] * \left[\frac{\left(\frac{m_{IS}}{M_{IS}}\right)}{Int_{IS}}\right] = moles\ of\ MPC \qquad (4.2)$$

where MPC_i is the initial average integration of vinyl MPC peaks, APM_i is the initial average integration of vinyl APM peaks, MPC_n is the average integration of vinyl MPC peaks at time n, APM_n is the average integration of vinyl APM peaks at time n, m_{IS} is the mass of internal standard in the polymerization, M_{IS} is the molecular weight of the internal standard and Int_{IS} is the reference integration of the internal standard, held at a constant value of 1.0. The calculated moles of MPC were used to determine appropriate additions of a 100 mg/mL MPC stock solution, containing roughly 2.5% CTA, to re-establish the initial comonomer feed ratio.

Equation **4.2** was used to analyze ^{1}H NMR spectra and calculate appropriate volumes of MPC stock additions in order to re-establish initial comonomer feed ratios.

Figure 4A.5. Acquired data of PAM^{sb}_{61} showing copolymerization and appropriate adjustments calculated using Equation 4A.1, polymerization halt points are highlighted.

Time (min)	MPC Addition (mg)	MPC Avg. Int.	APM Avg. Int.	KHP Mass (mg)	KHP Int.	KHP mol %	APM Conversion (%)	MPC mole ratio	APM mole ratio	F1
0	0	2.3039	2.7569	13.3	1.0	4.940	0	45.524	54.476	64
25	0	1.2787	2.1115	13.3	1.0		23.412	37.717	62.283	58
25	37	1.7800	2.2364	13.3	1.0		23.412	44.591	55.409	63
51	0	1.0362	1.7288	13.2	1.0		37.294	37.476	62.524	58
51	31	1.4012	1.7458	13.2	1.0		37.294	44.525	55.475	63
78	0	0.7862	1.3544	13.2	1.0		48.188	36.727	63.273	57

Vinyl Signal Adj.	moles MPC Required	mg MPC Required
0.4858	0.000126	37.119
0.4085	0.000106	31.209

Figure 4A.6. PAM-sodium alginate complexes imaged using bright field optical microscopy (batch top; semibatch bottom) as compared by average MPC content (images were used from Figure 4A.5). The range (distribution) of instantaneous MPC incorporation during the batch and semibatch copolymerizations are listed in Tables 1 and 2, respectively.

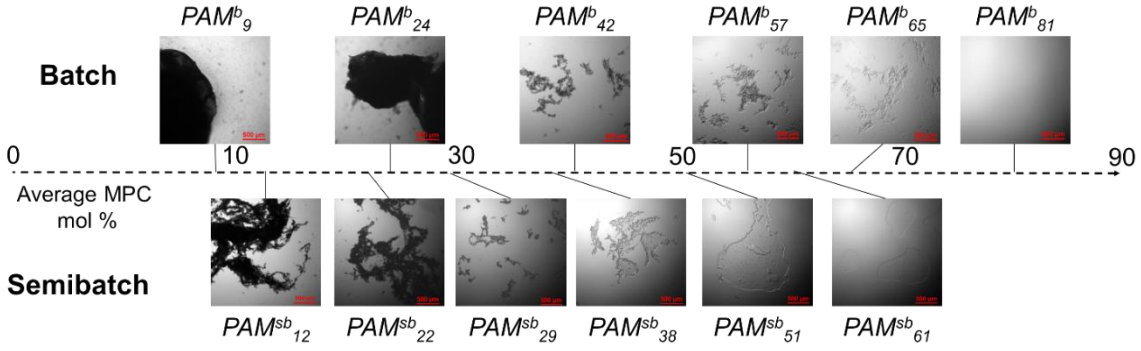

Figure 4A.7. PAM-sodium alginate complexes imaged using bright field optical microscopy show decreased contrast with increased hydrophilicity (batch top; semibatch bottom) as compared by estimated peak APM content. The numbers in brackets give the range (distribution) of instantaneous MPC incorporation during the batch and semibatch copolymerizations, as listed in Tables 1 and 2, respectively.

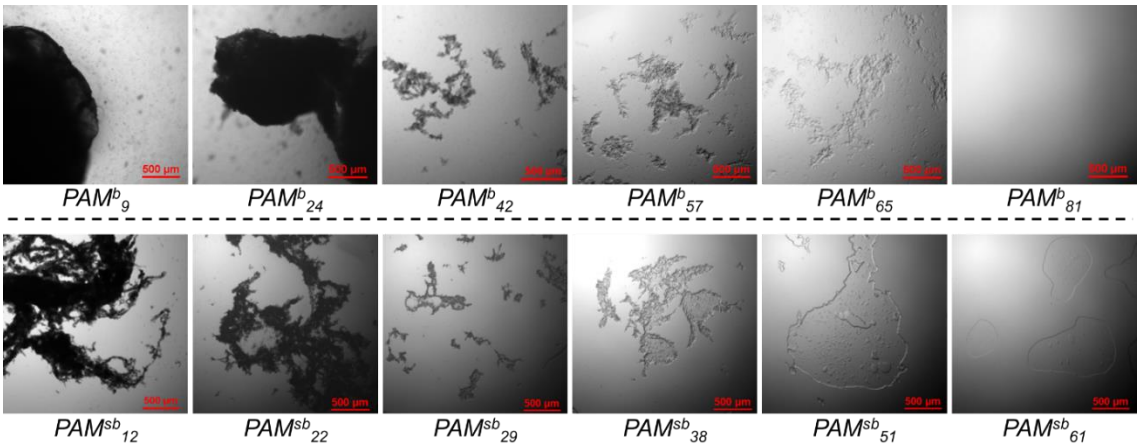

Comments: Model complexes between both batch and semibatch PAM polycations and sodium alginate were prepared by mixing dilute alginate and PAM solutions at a 1:1 charge ratio and were investigated by optical microscopy. Batch and semibatch copolymers as shell formers may be compared according to average MPC mol % or estimated peak APM content, i.e. the APM content of the most APM-rich fraction of the copolymer. We find comparison of average MPC more useful as it is the hydrophilic component incorporated to minimize protein adhesion. When compared according to betaine content, semibatch copolymer complexes appear more hydrated (more translucent) than their batch counterparts due to narrowed composition range and lowered maximum charge density in APM rich fractions. Such model experiments help illustrate the nature of the capsule surface as a function of copolymer composition, a helpful tool to explore promising compositions that balance PEC strength with PEC hydration.

It may be useful to also examine comparable peak APM content with respect to capsule formation, as these fractions of copolymers form the capsule surface by strong electrostatic binding and are of concern regarding immune system exposure and response; when compared according to estimated peak APM content, the complexes formed by batch and semibatch copolymers are very similar at notably different average MPC content. In both cases, hydration increases with MPC resulting in more translucent complexes.

Figure 4A.8. Conventional bright field microscope images (20X) of PAM^{b} supernatant show smaller particles increasing in hydration towards coacervate-like particles (PAM^{b}_{65}).

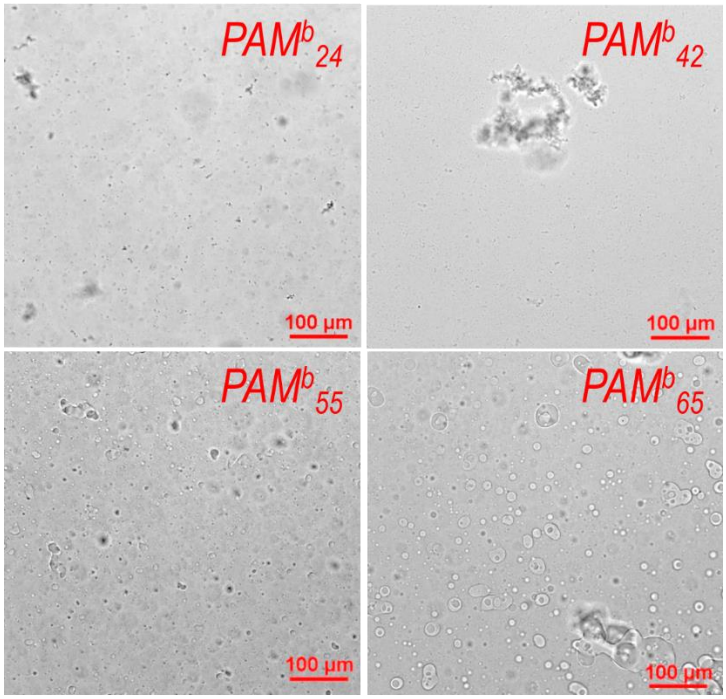

Figure 4A.9. Connected scatter plot shows capsule thicknesses of PAM^{b} (grey) and PAM^{sb} (black) (at 95% CI) (*n=15*).

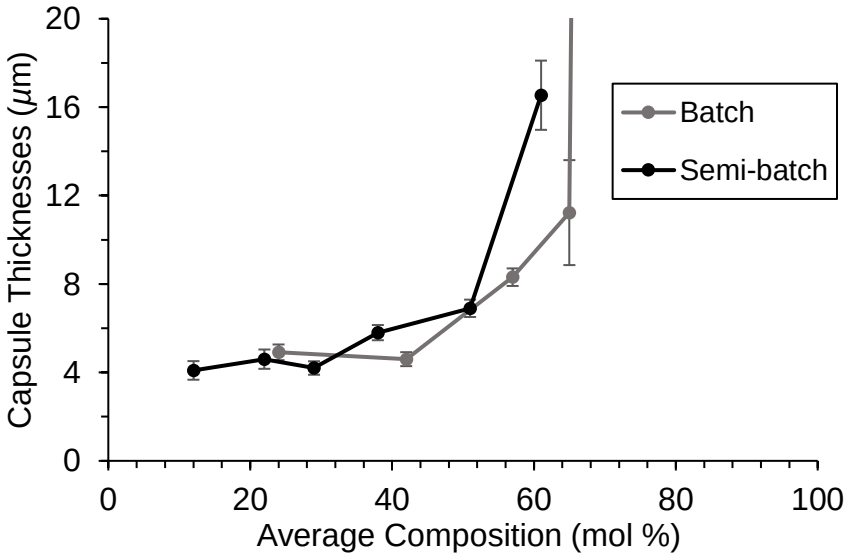

Figure 4A.10. Scatter plot shows estimated peak APM content of PAM^{b} (grey) and PAM^{sb} (black).

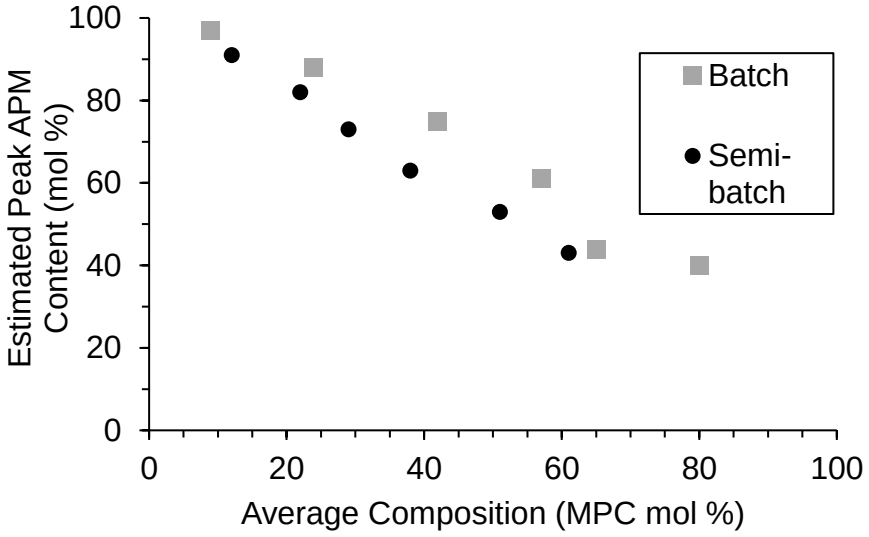

Comments: Capsules with comparable MPC mol % show similar capsule thicknesses and shell/core fluorescence ratios. It is noted that when copolymers are compared based on their estimated maximum charge density (peak APM content), the semibatch copolymers show much larger shell/core fluorescence ratios. This is likely a result of an increased number of chains with high cationic charge due to the compositional narrowing of semibatch copolymerization; a larger fraction of the isolated copolymer consists of chains having compositions near the estimated peak APM content as a result of compositional narrowing. For example, PAM^{sb}_{38} and PAM^{b}_{42} have comparable shell/core fluorescence intensity ratios at comparable average MPC mol %. However, PAM^{sb}_{38} and PAM^{b}_{55} have comparable peak APM content containing chains. The semibatch PAM^{sb}_{38} has a significantly higher shell/core ratio indicating improved shell confinement. This is an additional benefit of semibatch copolymerization for capsule shell formers to limit compositional spread within a sample.

Figure 4A.11. Fluorescent microscope images of A) PAM^{sb}_{12}, B) PAM^{sb}_{22}, C) PAM^{sb}_{29}, and D) PAM^{sb}_{38} show decreased number of surface patches (bright patches) and tears, with less capsule-capsule adhesion as MPC mol % increases.

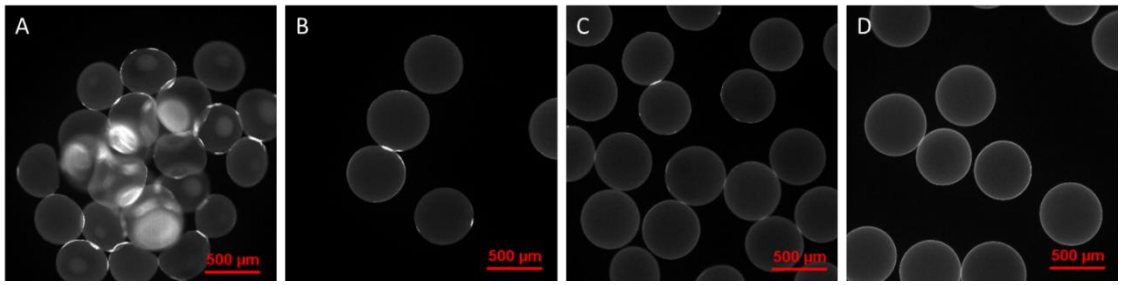

Comments: It was observed that for both semibatch and batch capsules, an increased MPC content reduced capsule aggregation and capsule-capsule adhesion. This is advantageous in shell formation as capsule-capsule interactions can lead to rips and tears of individual shells as well as areas of excess polymer, affecting the shell smoothness or uniformity and negatively impacting the ability of the capsules to act as a functioning cell containers.

The slight decrease in robustness of PAM^{sb}_{12} is attributed to pre-existing tears in capsules resulting from its strong complex with alginate. Capsules coated with PAM^{sb}_{51} swelled upon THPC treatment, and largely fragmented during aspiration, which is again attributed to the cationic nature of THPC, displacing calcium.

Figure 4A.12. PAM^{b}_{55} capsules without crosslinking dissolve in supernatant after sodium citrate and sodium hydroxide exposure, images by conventional fluorescence microscopy.

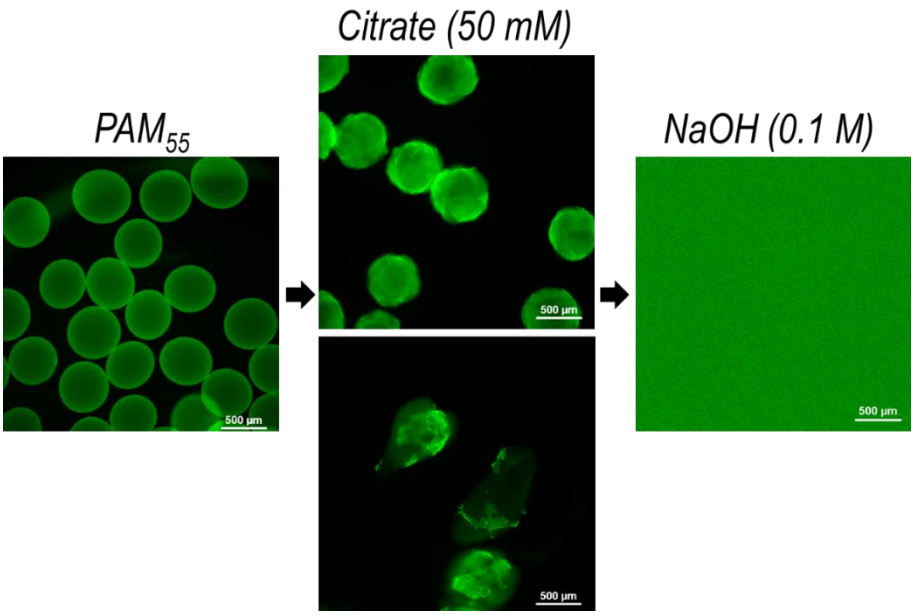

Figure 4A.13. PAM^{b}_{55} capsules crosslinked by 0.1 wt % THPC show successful covalent crosslinking, with weak robustness (capsule fragments or tea-bags) after sodium citrate and sodium hydroxide exposure, images by conventional fluorescence microscopy. Background fluorescence increases as diffuse, non-crosslinked copolymer is released during capsule fracture.

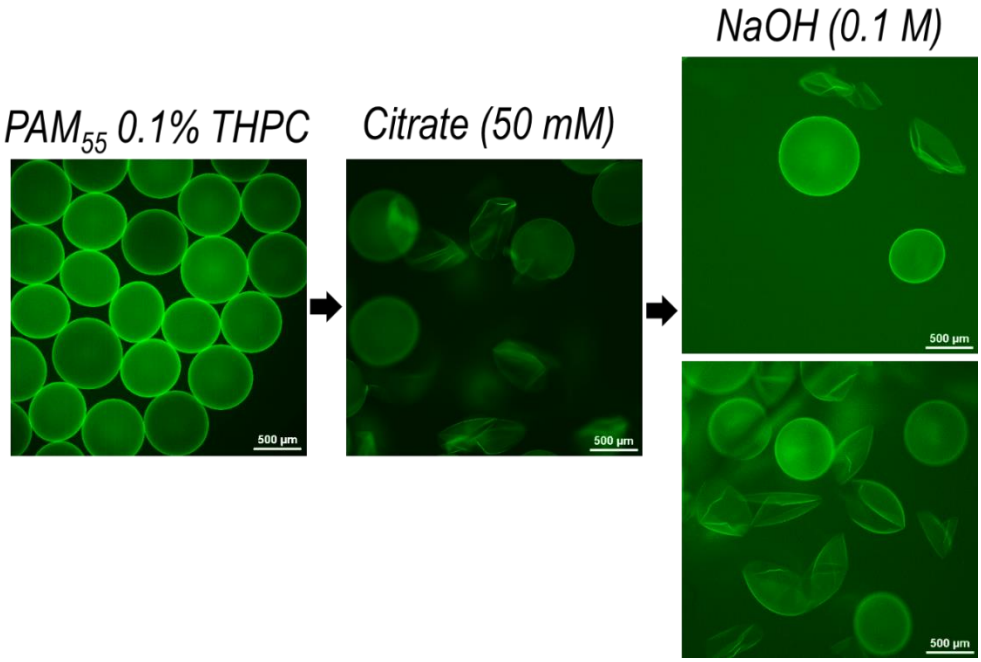

Figure 4A.14. PAM^{b}_{42} capsules crosslinked by 0.1% THPC show no broken capsules from pipette aspiration (left) but were physically pierced using a 19-gauge needle (right) (scale bars = 500 μm).

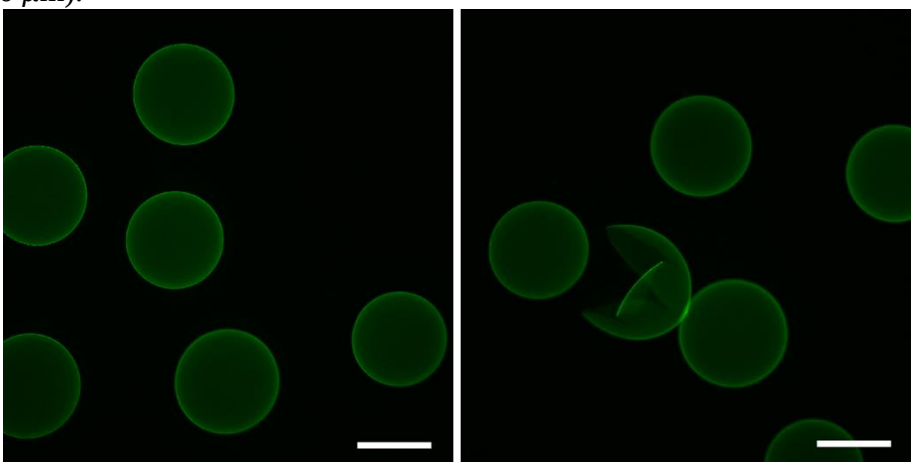

Figure 4A.15. Confocal microscope images comparing in-diffusion from THPC addition of batch copolymers PAM^{b}_{55} and PAM^{b}_{42} (left) and semibatch copolymers PAM^{sb}_{51} and PAM^{sb}_{38} shows decreased core fluorescence and decreased bead swelling after THPC addition for copolymers of narrowed compositional distribution (brightness increased for all images). Scale bars = 250 μm.

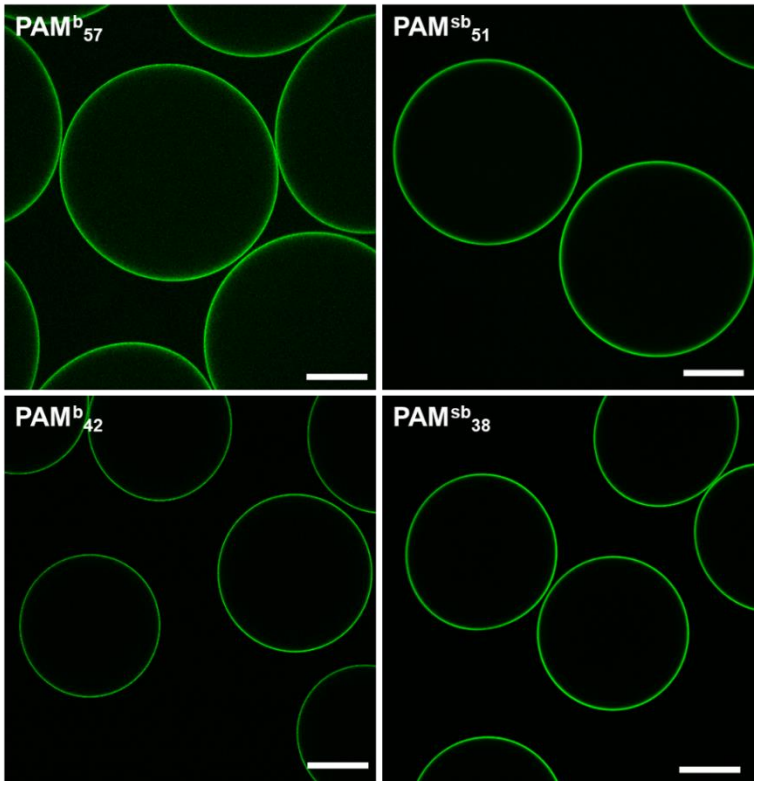

Figure 4A.16. Assigned ^{1}H NMR Spectrum of genipin using a 600 MHz Bruker Avance NMR Spectrometer in D_2O.

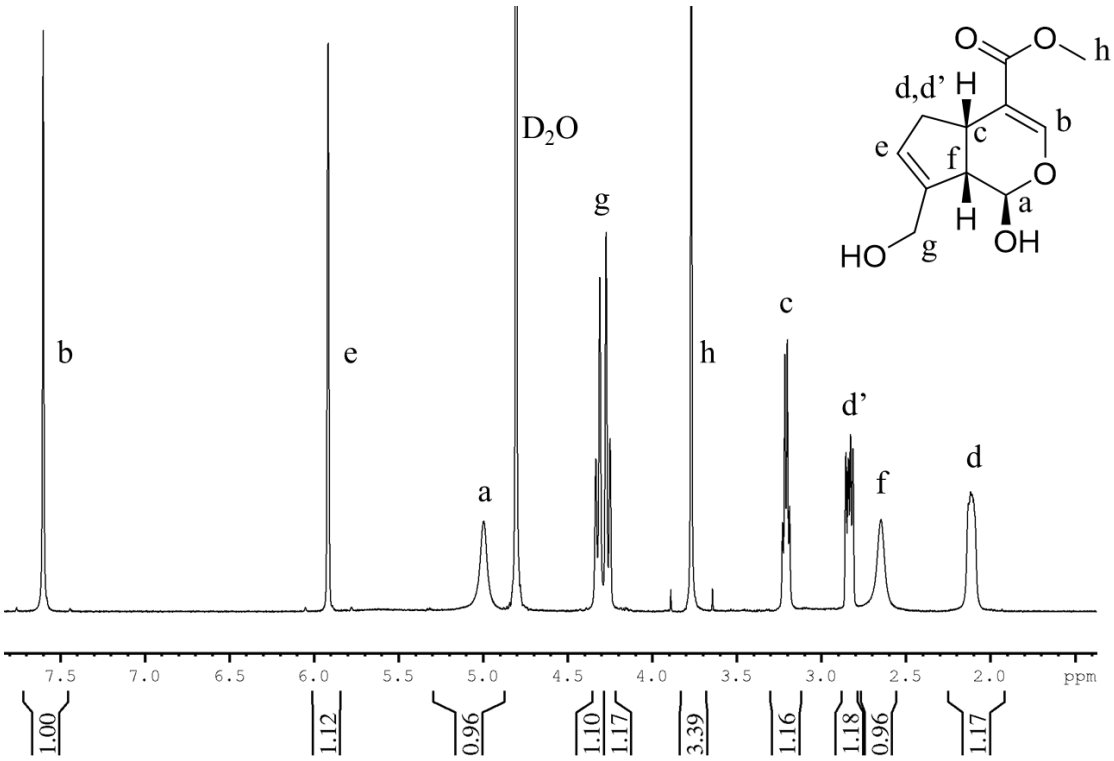

Figure 4A.17. PAM$^{sb}_{22}$-*f* capsules crosslinked by 0.1 wt % genipin over time show darkening capsule colour, as a result of the prolonged reaction of genipin.

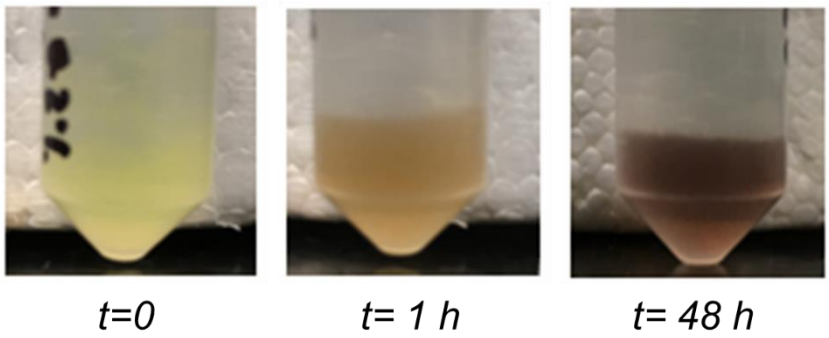

Figure 4A.18. ^{1}H NMR spectra of PM-*a*-M hydrolysis at A) *t* = 0, B) *t* = 15 h and C) *t* = 18 h, resulting in PM-*a*-M_{50} (50% hydrolysed) in a 9:1 mixture of ACN-d_3/D_2O (adapted from Gardner *et al.*).[10]

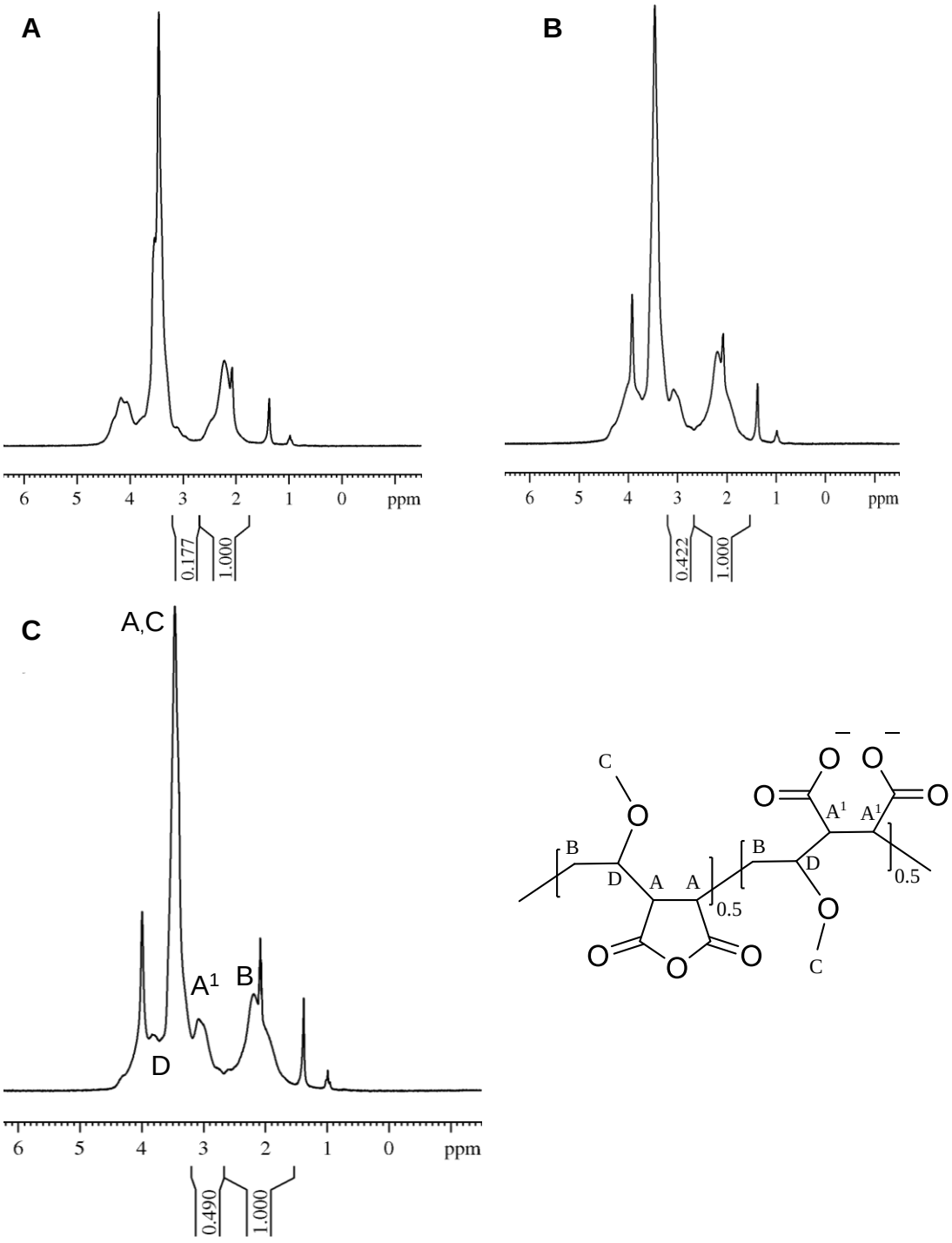

Figure 4A.19. Confocal microscope images of genipin crosslinked capsules comparing genipin background fluorescence intensities to capsules exposed to BSA-*f*. Excluding trapped BSA within the core, surface fluorescence does not increase for compositions of 12-38 mol % MPC.

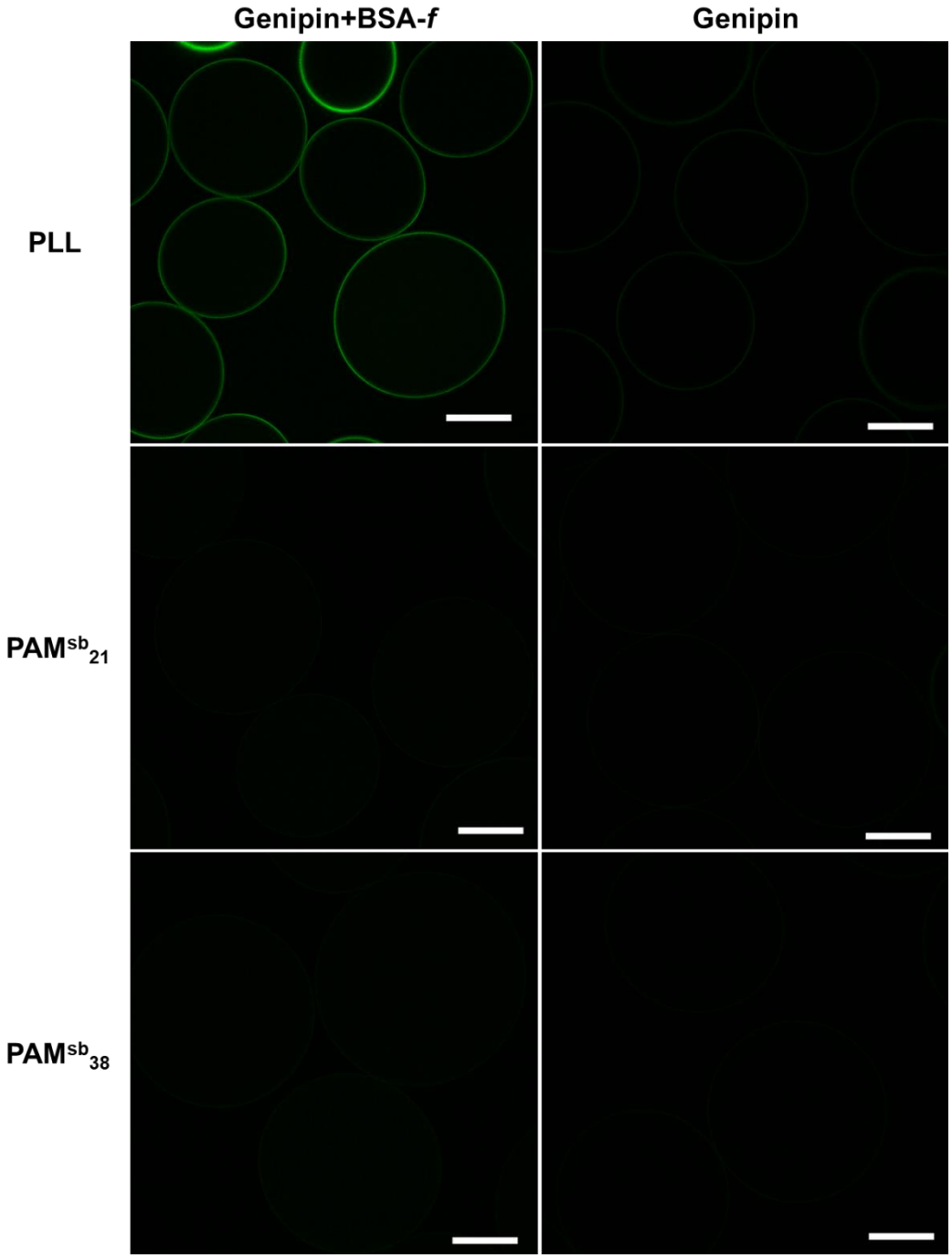

Figure 4A.20. Confocal microscope images of control PLL capsules (dotted lines) and PAM^{sb} capsules, including PAM^{ab}_{51} and PAM^{sb}_{22}, exposed to BSA-*f* for 24 h with various crosslinkers (scale bars = 200 μm).

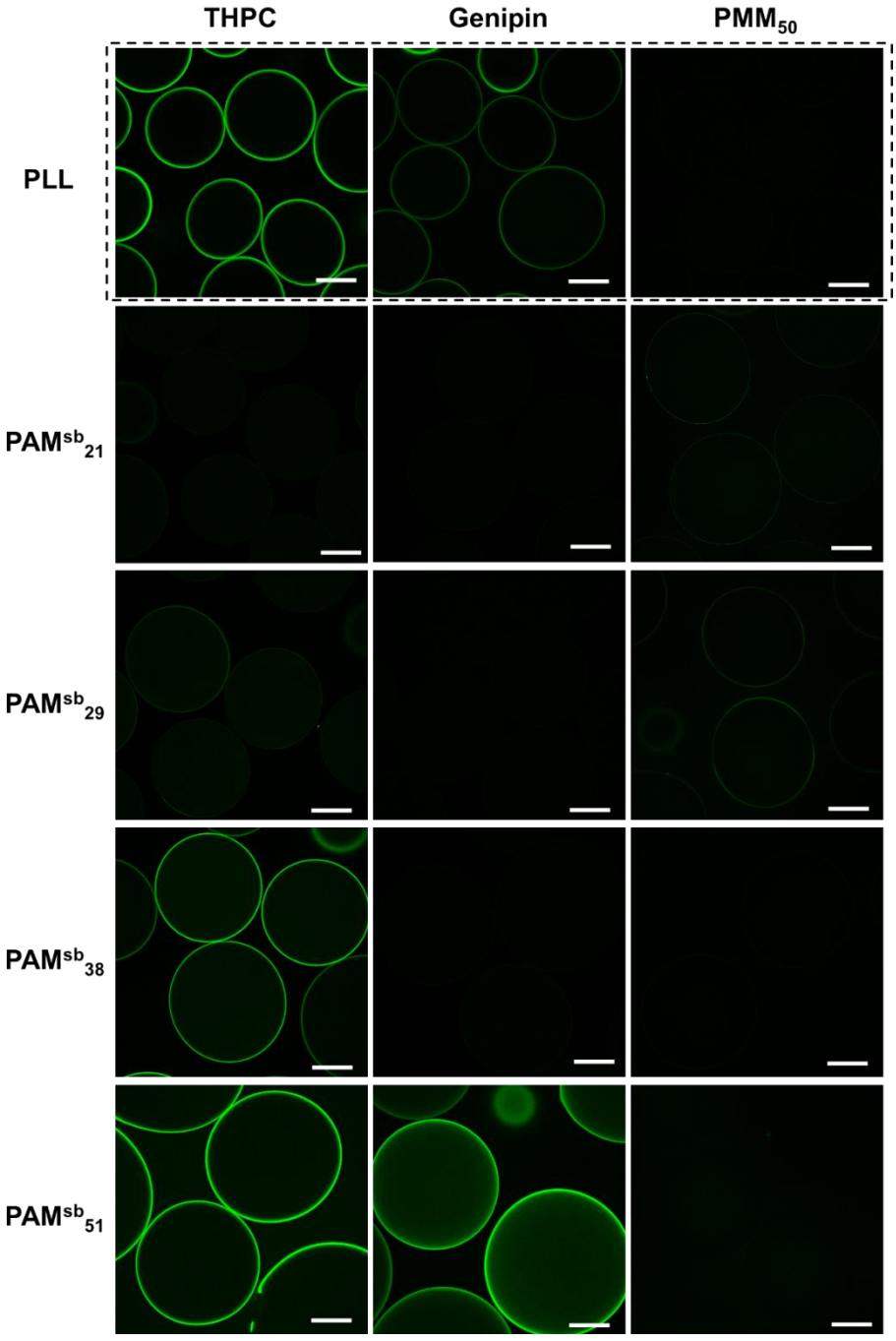

Chapter 5. Polyampholyte Physical Hydrogels of *p*-Sodium styrenesulfonate and *p*-(Vinylbenzyl)trimethylammonium chloride and the Effects of Charge Density by Termonomer Addition

Derrick E. Hastings, Harald D.H. Stöver*

Department of Chemistry and Chemical Biology, McMaster University, Hamilton, ON,

L8S 4M1, Canada

To be submitted.

5.1. Abstract

Polyampholytes formed by copolymerization of sodium *p*-styrenesulfonate (NaSS) with cationic *p*-(vinylbenzyl)trimethylammonium chloride (VBTA) were shown by in-situ ^{1}H NMR spectroscopy to have a highly alternating sequence. Polyampholyte physical hydrogels composed of NaSS and VBTA were then prepared by redox copolymerization and characterized by elemental analysis. Charge-balanced, binary polyampholyte gels were evaluated as possible stimuli-responsive materials to salt and temperature. Furthermore, hydrogel mechanical properties were explored using tensile testing, demonstrating the impact of monomer loading and charge shielding by salt.

To tune the responsive and mechanical properties, charge-neutral termonomers 2-hydroxyethyl methacrylate (HEMA) and 2-methacryloyloxyethyl phosphorylcholine

(MPC) were incorporated by ternary copolymerization to evaluate the effects of charge dilution and hydration of different structures on the physical properties of the polyampholyte gels. Tracking of these polymerizations shows that the charged comonomers are incorporated at a higher rate than the methacrylate termonomers, but do not show significant drift in the NaSS/VBTA comonomer pool. The polyampholyte responsive properties were explored using swelling ratios of binary gels and terpolymer gels under different salt and temperature conditions.

Hydrogels containing even small amounts of termonomer showed more swelling than binary PA gels, in particular where the termonomer was the zwitterionic MPC. Additionally, MPC-containing gels swelled more at elevated temperatures, which was attributed to the ability of MPC to shield ionic interactions and impede hydrophobic interactions. HEMA gels showed evidence of a lower critical solution temperature (LCST) behaviour at higher temperatures. In general, MPC had a stronger impact on the responsive properties of the material, with less impact on the elasticity of the material; conversely, HEMA can be incorporated at much higher levels leading to materials with greater malleability, fatigue resistance, and strain hardening, and with less notable changes in the responsive properties. Preliminary experiments show these terpolymer gels are capable of self-healing at higher termonomer mol % as a result of weakened ionic interactions, though further optimization will be necessary to yield more effective self-healing materials.

5.2. Introduction

Hydrogels are swollen networks of polymers with high water content that can be designed to exhibit a range of functional and mechanical properties depending on cross-linking and polymer composition. Strong hydrogels have drawn a great deal of interest in research areas such as soft robotics,[1] smart actuators, and biomaterials[2] due to their potential as load-bearing materials in, e.g., artificial cartilage.[3,4] Polyelectrolyte hydrogels are particularly useful with respect to their compositional variability and tunable properties.

Recently, polyelectrolyte hydrogels with reversible adhesion in underwater environments have been developed, which may be useful in materials for tissue engineering and wound dressings.[5] Similar work demonstrated that comonomer structure has a significant impact on the physical properties of the resulting gels such as mechanical strength, self-healing capabilities, and response to external stimuli.[6] It has also been highlighted that the arrangement of charged monomers can impact the physical properties of polyelectrolyte species.[7-9]

Physical polyampholyte hydrogels typically comprise anionic sodium *p*-styrenesulfonate (NaSS) and different cationic monomers. The associative electrostatic interactions of the charged groups in the polymer networks provide physical cross-links and are the basis for the material properties. This offers the ability to generate tough, stretchable materials with highly responsive properties to external stimuli, offering impressive self-healing abilities under specific conditions.[6,7] Throughout the study of numerous polyampholyte and polyelectrolyte materials, different monomers have been explored and demonstrate different relative strengths of ionic associations.[10,11] Hence,

compositional parameters such as selection of charged comonomer, for example, can impact the inherent physical properties of polyelectrolyte complexes.

The strength of the associative ionic interactions in polyelectrolyte complexes are also tunable by altering charge density via addition of charge-neutral monomers. The effects of introducing hydroxyl sidechains, such as 2-hydroxyethyl acrylate (HEA)[12], and betaines, such as 2-methacryloyloxyethyl phosphorylcholine (MPC)[13], have previously been explored. These monomers reduce the number and strength of the associative interactions and, consequently, increase the polymer responsiveness to external stimuli. Recently, charge-neutral termonomer was incorporated into tough polyampholyte hydrogels to impede ionic associations to improve transdermal adhesion strength by enhanced compliance of the material.[14] Therefore, the incorporation of neutral termonomers with different structures are capable of enhancing stimuli response and altering the mechanical properties of tough hydrogels.

Scheme 5.1. Reaction process for binary PNV_{50} and ternary $PNV_{50}H_y$/$PNV_{50}M_y$ hydrogels.

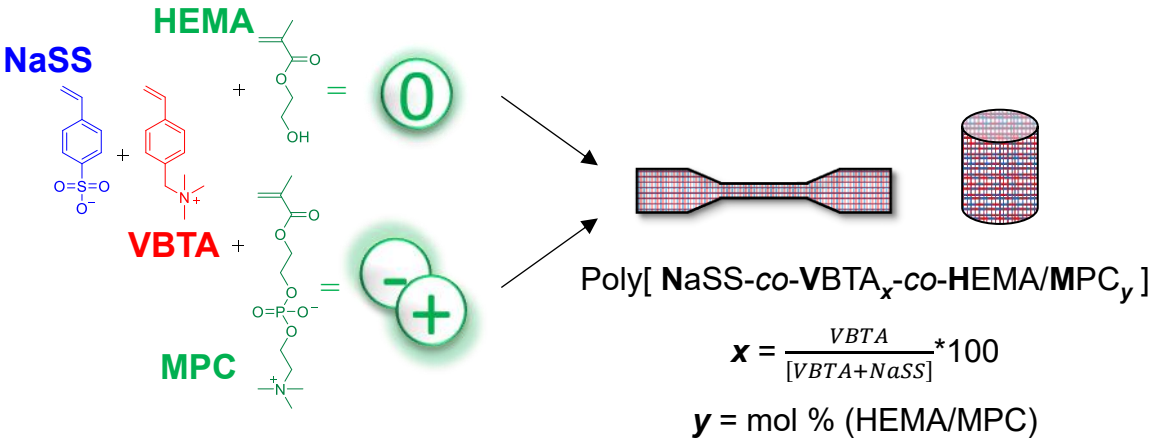

Here, we describe the preparation and study of polyampholyte hydrogels of charged monomers *p*-(vinylbenzyl)trimethylammonium chloride VBTA and NaSS. This work first

explores the responsive and mechanical properties of these binary styrenic polyampholyte hydrogels. These gels are expected to have high tensile strength with very limited sensitivity to salt and temperature, due to polymer chain rigidity and the hydrophobic nature of the selected monomers. As a result, we further explore these hydrogels and the effects of incorporating two charge-neutral termonomers, 2-hydroxyethyl methacrylate (HEMA) and MPC, into NaSS-VBTA to form ternary polyampholyte hydrogels (Scheme 1). Reduced charge density due to the incorporation of hydrophilic monomers is meant to impede ionic associations underlying the physical hydrogel structures, ultimately weakening the material and increase responsiveness to various stimuli such as ionic strength. We expect that the difference in termonomer structures will offer different effects on the underlying physical interactions and, hence, on hydrogel properties. These impacts may facilitate stimuli-responsive self-healing, making these cost-effective, scalable materials interesting candidates for load-bearing biomaterial applications.

5.3. Experimental

5.3.1. Materials

Deuterium oxide (>99%), ammonium persulfate (APS), *N,N,N',N'*-tetramethylethylenediamine (TEMED) (99%), ethylene carbonate, 2-oxoglutaric acid, *p*-(vinylbenzyl)trimethylammonium chloride, sodium *p*-styrenesulfonate (90%), 2-hydroxyethyl methacrylate (99%), 2-methacryloyloxyethyl phosphorylcholine (97%), potassium bromide and brilliant blue G were purchased from Sigma-Aldrich and used as

received. 150 kDa fluorescently labelled dextran (Dextran-*f*) was purchased from PolySciences and used as received.

5.3.2. NaSS-VBTA/Terpolymerization Monomer Reactivities

^{1}H NMR scale polymerizations were prepared at 10% w/v total monomer loading in D_2O. 200 mg scale polymerizations of NaSS:VBTA were set up at mole ratios of 15:85, 30:70, 45:55, 60:40, 75:25, and 90:10 as follows, using P(NaSS-co-VBTA)$_{50}$ (PNV_{50}) as an example: NaSS (106 mg) and VBTA (101 mg) were dissolved in 0.5 M NaCl in D_2O containing 2.5 mol % oxoglutaric acid as UV-initiator, 6 mol % methanol relative to moles of monomer as an internal standard. Polymerizations were equipped with rubber septa, purged with nitrogen gas for 30 minutes, and monitored by ^{1}H NMR spectroscopy using a 600 MHz Bruker Avance spectrometer. Spectra were collected at roughly 7-15% conversion as polymerizations were irradiated at small time intervals and aliquots were diluted with D_2O. The aliquot containing D_2O vials were then centrifuged to sediment precipitated polymer before filtering using a 0.45 μm syringe filter and monomer vinyl signals were compared to internal standard signals to estimate the relative reactivities of the two styrenic monomers. Reactivity ratios were estimated by a least-squares fitting of the terminal model of the instantaneous copolymer composition equation to comonomer conversion data as previously reported[15] based on a procedure by Aguilar et al.[16]

Terpolymerizations were also tracked as described above, to estimate the relative rate of incorporation for different termonomers (HEMA, MPC) in PNV_{50} polyampholytes. Terpolymerizations with MPC $\geq$ 40% used ethylene carbonate as the internal standard. Reactivity ratios were then modelled as a binary system, treating the charged monomer

pool (NaSS+VBTA) as a single monomer and the termonomer as a second monomer, as previously reported.[9]

5.3.3. Polyampholyte Hydrogel Preparation – P(NaSS-VBTA)$_{50}$ Hydrogel

Using 20 mL screw cap vials, monomer was weighed and dissolved such that a 1:1 mole ratio of NaSS:VBTA was achieved at different monomer concentrations from 1-3.5 M. The monomer was dissolved in 0.5 M NaCl and separately solutions of APS initiator and TEMED accelerator were prepared. 1.83 mol% initiator relative to total monomer was added to the monomer solution and 10% w/w TEMED relative to initiator mass. The monomer solution was cast into modified 1 mL polypropylene syringes and into 3D printed thermoplastic polyurethane (polylactic acid PLA) moulds with dumbbell wells (35 x 6 x 2 mm; 0.35 mL). Dumbbell moulds were sealed with plastic wrap and syringes were plugged with a second plunger and left to polymerize for > 8 hours. Final gels were carefully removed from the moulds and dialyzed against large amounts of deionized water for 7 days with solution refreshed twice daily. Gels were stored in deionized water for and use within 2-4 weeks.

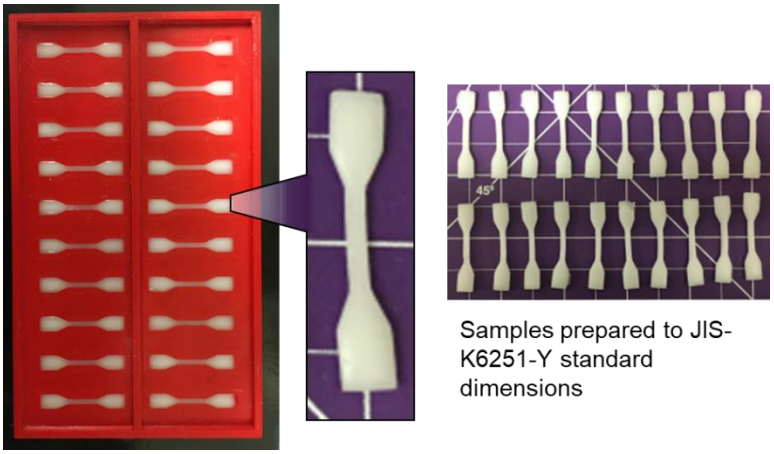

Figure 5.1. Prepared dumbbells of PNV_{50} in 3D printed mould for JIS-K6251-Y standard gels.

5.3.4. Termonomer Hydrogels: P(NaSS-VBTA)$_{50}$X$_y$ (PNV$_{50}$X$_y$)

Monomer solutions were prepared as described. Separately, different amounts of termonomer (X = HEMA or MPC) were added such that total monomer concentration was 1.5 M, with a constant 1:1 ratio of NaSS:VBTA. Polymerization solutions were cast into molds, covered as described above, and left for 8 hours to polymerize. Hydrogels were then extracted and dialyzed against deionized water for at least 5 days.

5.3.5. Elemental Analysis

Dialyzed cylindrical gels were lyophilized and ground into a powder for characterization by combustion elemental analysis using a Simultaneous Thermal Analyzer (STA) 6000 from PerkinElmer (Waltham, MA). In each experiment, 2-5 mg of dried material was placed in the instrument pan and loaded under argon atmosphere. The chamber was heated from 30 to 600 °C at a rate of 10 °C/min under argon. Using the elemental makeup of the gels, compositions were estimated for various terpolymer gels containing either HEMA or MPC.

5.3.6. Confocal Laser-Scanning Microscopy

Sections of syringe moulded cylindrical hydrogels (~5 mm length) were cut and placed in 0.1% wt solutions of 150 kDa dextran-*f* to permit in-diffusion of the polysaccharide into the pores of the gel. The gels were then dabbed dry using a KimWipe and placed in a 96 well plate for imaging. Gel surface morphologies were explored by confocal laser-scanning microscopy using a Nikon A1 Confocal Eclipse T*i* microscope with Nikon Elements software.

5.3.7. Responsive Hydrogel Swelling

Cylinders of syringe-moulded hydrogels were cut (~5 mm long) and soaked in 20 mL salt solutions for 7 days. The swelling volume ratio, Q_v, was characterized by the volume ratio of the swollen gels at equilibrium in NaCl solution (V_{salt}) to the initial volume ratio in water (V_{water}) using digital calipers. Swelling ratios were calculated for different hydrogels, including different monomer loadings and termonomer compositions, at 25 °C. Swelling ratio measurements were also used to monitor the temperature responsive behaviour of PA hydrogels; using a hybridizer oven to maintain elevated temperature conditions for 7 days, gels were soaked in salt solution and Q_v was recorded for different PA gels.

5.3.8. Tensile Testing

Tensile tests were carried out on an Instron Model 3366 benchtop universal mechanical testing machine at a stretch velocity of 100 mm/min. Gels were prepared in the dumbbell-shaped moulds (gauge length of 12 mm and 2 mm width) using the standard JIS-K6251-Y size. Grips were equipped with fine grit sandpaper to prevent slippage during extension. The Young's moduli were determined from the initial slope (less than 15% strain) of the

curve, while elongation was determined as the break point of the sample. Tensile tests were performed at room temperature in air, dried by KimWipe within 60 s of testing. All samples were tested in triplicate (n = 3).

5.3.9. Self-Healing

The self-healing of different hydrogel compositions at 1 M monomer concentration were evaluated by cutting a dumbbell into two equal pieces by a scalpel before the two ends were dipped in 5 M KBr solution for 30 minutes. Pieces were then brought together for 12 hours in air sealed with plastic wrap, before dialyzing for 7 days in against deionized water. These gels were then subjected to tensile testing as described above. Each test sample was repeated in triplicate (n = 3) and were compared to virgin reference samples exposed to identical KBr soaking and dialysis conditions.

5.4. Results and Discussion

5.4.1. Binary Polyampholytes of NaSS and VBTA

5.4.1.1. Copolymerization Tracking by ^{1}H NMR

Using ^{1}H NMR tracking methods as described by Aguilar et al.[16], relative conversions of NaSS and VBTA during copolymerization at various feed ratios were monitored and used to estimate the reactivity ratios of the two charged monomers. As seen in similar copolymer systems[17,18], the monomers copolymerize in a near-alternating fashion, with minimal drift from the initial 1:1 comonomer ratio across a wide range of instantaneous comonomer feeds. This limits compositional drift in the polymer, which has been reported to impact the

underlying ionic associations in polyampholyte gels incorporating acrylate, methacrylate or methacrylamide cationic monomers with NaSS.[6,7,19]

This offers the generation of charge-balanced polyampholytes with limited variability in material composition. Polyampholyte charge ratio has a significant impact on the inherent properties[20-22], making these polymers interesting for cost-effective, responsive material applications. Additionally, intramolecular charge neutralization and ionic associations within charge-balanced polyampholytes interactions facilitate increased responsiveness to stimuli such as salt, temperature, and pH (in weak acid/base containing polyampholytes), according to our recent work.[8,9]

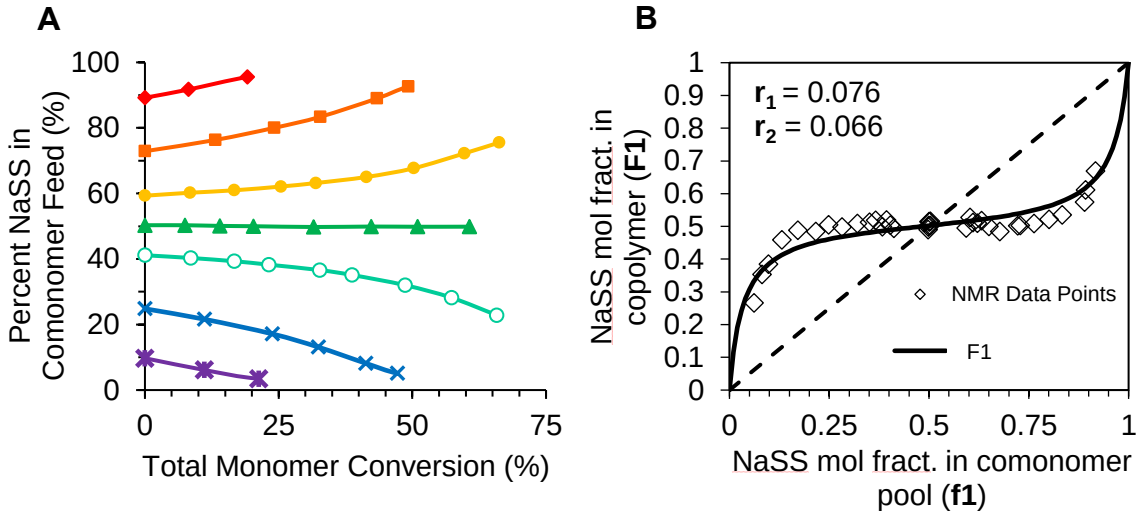

Figure 5.2. (A) ^{1}H NMR tracking of NaSS remaining in the monomer mixture as a function of conversion. **(B)** Estimated reactivity ratios generated for NaSS (r_1) and VBTA (r_2) show near alternating copolymerization.

5.4.1.2. Hydrogel Preparation and Characterization

To prepare hydrogels for stimuli-responsive and mechanical property testing, redox-initiated polymerization using APS initiator and TEMED accelerator was adapted from literature and employed.[23,24] This method does not require air-sensitive conditions,

although polymerizations were sealed to prevent evaporation during gelation. After 8 h of polymerization, hydrogels were equilibrated by salt exchange in deionized water for 7 days and combustion elemental analysis confirmed a near 1:1 composition of NaSS:VBTA for the different monomer loadings.

The resulting hydrogels appear opaque below 3 M loading, while monomer concentrations ≥ 3 M lead to increasingly translucent gels. This has been reported for other polyampholyte systems,[6,25] attributed to higher chain lengths and decreased polymer chain mobility preventing macroscopic phase separation during polymerization at the critical monomer concentration, confirmed by the lowering of the C_m when covalent cross-linker is introduced. Polyampholyte gels are formed strictly by physical associations, confirmed here by the complete dissolution and dissociation of PNV_{50} hydrogels at high ionic strength and elevated temperatures (i.e., 2 M KBr at 65 °C).

Cylindrical gel segments (~5 mm height x 4.5 mm diameter) were soaked in 1 mg/mL solution of 150 kDa dextran-*f*. In domains of greater porosity as a result of inhomogeneous physical crosslinking, in-diffusion of the labelled dextran is more effective and exhibits greater fluorescence. Confocal laser-scanning microscopy was used to examine the surface characteristics of the prepared hydrogels, showing observable surface roughness suggesting phase separation leads to a physically cross-linked network up to 2.5 M monomer loading. Above 2.5 M loading, the gels appear more uniform with no significant surface features. Confocal images of the dextran-*f* soaked gels can be found in Figures 5A.1 and 5A.2.

5.4.1.3. Hydrogel Swelling: Response to Ionic Strength

Concentration effects also arise during dialysis equilibration of hydrogels after polymerization, as hydrogels swell or shrink after polymerization, depending on total monomer loading and composition. Here, the PNV_{50} gels appear to undergo slight collapse at all concentrations, with higher monomer loadings (>1.5 M) showing less notable effects (>90% initial volume). This could be due to a high degree of polymerization (DP) or, in part, due to the potential hydrophobic and pi-stacking interactions restricting the reorientation of polymer chains during removal of salt ions. It is interesting, therefore, to explore these underlying interactions and test their response to stimuli that may facilitate chain mobility or via disruption of ionic and hydrophobic interactions.

Salt-induced plasticization or charge shielding has previously been described[26] and manifests as volumetric changes in polyelectrolyte-based materials.[6,22,27] Hence, the effect of salt ions on the underlying ionic associations were examined using volumetric ratios before and after soaking in salt solution as a function of monomer loading. Diameter and height of equilibrated hydrogel cylinders were measured using digital calipers. Swelling ratios, Q_v, of the gels were calculated as the volume of the gel swollen in salt solution versus the volume of the gel at equilibrium in deionized water (equation **5.1**). These swelling ratios are indicative of the responsiveness of the material to salt-induced charge-shielding and chain plasticization.

$$Q_v = \frac{Volume\ in\ salt\ solution\ (V_{salt})}{Volume\ in\ water\ (V_{water})} \quad \textbf{(5.1)}$$

PNV_{50} gels were not drastically swollen when soaked in NaCl solution. Previously explored polyampholyte gels with more hydrophilic cationic monomers show significant swelling using NaCl, and their mechanical properties could be manipulated by soaking in relatively low [NaCl] solutions (0.05 to 1 M).[6,7] Here, however, the ionic associations formed between NaSS and VBTA sidechain groups are coupled with strong hydrophobic interactions and, potentially, pi-stacking interactions; consequently, these gels may require salts that better solvate hydrophobic polyelectrolytes based on the Hofmeister series.[28,29] Previous reports of NaSS-VBTA and similar polyelectrolyte systems show that using salts such as NaBr or KBr can better impede the interactions of these structures, consequently improving polymer solvation.[30,31] Therefore, KBr soaking was used alongside NaCl to better examine hydrogel swelling.

Hydrogels of 1.5 and 2 M loading appear to be relatively resistant to charge shielding effects, showing the least significant relative change from 0 M to 3 M KBr (Figure 5A.3). The effect of KBr on the swelling ratio of these gels appears to be most significant in lower monomer loadings (1 M) and in relatively higher monomer loadings (3 and 3.5 M). On the lower end of monomer loading, the material has fewer ionic associations and physical cross-links which may be more easily impeded by fewer K^+ and Br^- ions. As a result, lower salt concentrations are required to permit hydrogel swelling.

However, the higher concentrations (> 2 M) may lead to frustrations between oppositely charged groups or along polymer chains as conformations are kinetically trapped during polymerization and dialysis; the increased density of polymer charges and groups can create unfavourable crowding in the material that are alleviated by salt swelling to an

equilibrium solids loading volume. At 1.5-2 M loading, strong gels are formed but do not introduce frustrations. Above this concentration, KBr charge shielding facilitates chain rearrangement and swelling to alleviate unfavourable polymer conformations. For example, 2 M hydrogel contains ~400 mg/mL solids loading, and 3 M hydrogels contain ~600 mg/mL. The gels swell to 1.15x and 2x the equilibrium volume in 3 M KBr, respectively, which reduces the effective solids loading of both gels to ~300-350 mg/mL.

5.4.1.4. Hydrogel Swelling: Response to Temperature

To explore the effect of temperature, 1.5 M loading PNV_{50} gels were equilibrated in salt solutions of NaCl and KBr. The gels were left at elevated temperatures in a hybridizer oven for 7 days and Q_v were recorded.

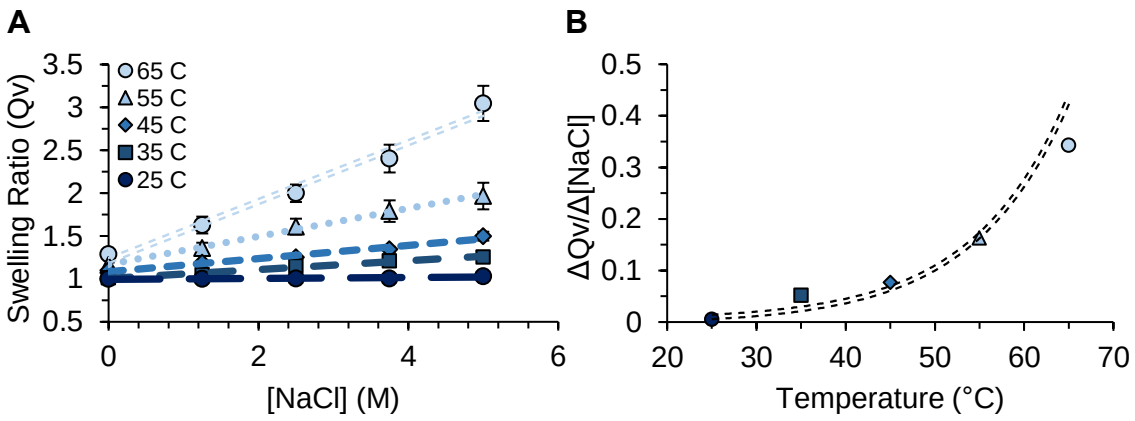

Figure 5.3. (A) Temperature-dependent hydrogel swelling of PNV_{50} (1.5 M) gels in NaCl. **(B)** PA hydrogel swelling with increase in [NaCl] plotted as a function of temperature.

Polyampholytes are known to elicit temperature responses representative of lower critical solution temperatures (LCSTs) or upper critical solution temperatures (UCSTs). A UCST-type behaviour, denoted in polyampholyte material studies as the softening temperature,[14,32,33] involves the solvation of polymer that becomes miscible in solution

above a critical temperature toward a one phase system. At T > UCST, the polymer-polymer interactions are broken and, due to the charged nature of polyampholytes, can be manipulated by tuning the relative entropy of mixing.[34] UCSTs in polyelectrolytes are salt-dependent and can be lowered by the addition of salt counterions to enhance the entropy of mixing.

Polyampholytes of NaSS and VBTA exhibit a UCST in aqueous solution as demonstrated specifically in temperature dependent turbidimetry[18] and in temperature-dependent adsorption behavior compounds, with higher temperatures favouring release or desorption.[35,36] Here, we explore the UCST-type behavior with respect to hydrogel swelling.

At 25 °C, NaCl solution does not notably swell the hydrogels. However, as the temperature is increased, the polymer ionic associations weaken and are more easily shielded by salt ions. As temperature is raised from 25 to 65 °C (Figure 5.3), the responsiveness of the polymers to salt shielding appears to increase exponentially. It is also noted that the weakening of the polymer-polymer interactions by salt and/or temperature is critical in self-healing processes, which are contingent on the plasticization of polymer chains and charged groups for reforming ionic associations.

5.4.1.5. Tensile Strength

Dumbbell shaped gels were prepared at different monomer loading and dialyzed in deionized water. Using an Instron Mechanical Analyzer, PNV_{50} polyampholyte gel stress-strain curves were generated for samples based on monomer loading (Figure 5.4 (B)). The

elongation at break, or fracture strain (ε_b), and Young's modulus (E) of different monomer loadings are plotted in Figure 5A.4.

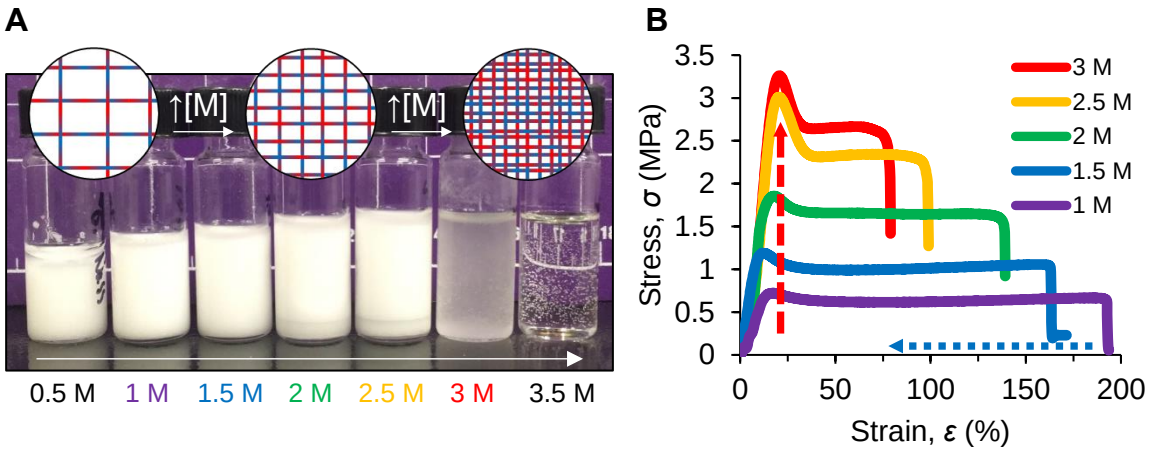

Figure 5.4. (A) Images of PNV_{50} polyampholyte gels with increasing monomer loadings. **(B)** Stress-strain curves of PNV_{50} hydrogels show stiffening and strengthening with increased monomer loading.

As the [M] increases from 1 to 3 M, the dumbbells become stiffer and stronger; the stress at break and Young's moduli increase substantially, due to the increasing numbers of ionic cross-links and greater chain entanglement associated with polymer loading.[6,7] The effect of polymer loading on mechanical properties has also been demonstrated in polyampholyte gels and in double network gels of polyzwitterions.[37]

Conversely, as the strength of the material increases, the fracture strain (ε_b) decreases. At 1 M monomer loading, the dumbbells have some mechanical flexibility but become more rigid toward 3 M loading. In agreement, these materials do not exhibit significant strain hardening and do not significantly recover after deformation as seen in other polyampholyte gels likely due to the limited flexibility in the polymer chains through cumulative effects of high cross-link density, hydrophobic interactions, and potential pi-

stacking interactions. The structure of VBTA compared to more hydrophilic cationic monomers adds substantial rigidity to the polymer network. As chain mobility and flexibility is reduced, the network becomes less forgiving and does not recover, showing poor fatigue resistance. However, these materials appear to offer impressive tensile strength which is desirable for high load-bearing materials.[38,39] Hence, we observe materials that are highly resistant to deformation under significant stress, showing poor recovery and fatigue resistance.

PNV_{50} gels require weakening of either ionic or hydrophobic interactions to exhibit properties comparable to softer polyampholyte materials. As demonstrated with Q_v values, charge shielding with salt counterions can be an effective way of liberating ionic associations and facilitating polymer mobility in the material. In agreement with Q_v data, the stiffness of PNV_{50} hydrogels decreases with charge shielding by NaCl. Figure 5A.5 shows the effect of weakening of physical cross-links, which facilitates chain mobility and softens the material. This manifests in both an increase in ε_b and a decrease in both E and σ_b. This mechanical responsiveness to salt has been previously observed, but PNV_{50} gels require substantially larger amounts of salt to induce charge shielding than in PA materials with more hydrophilic cationic comonomer.[6] While KBr was found to improve the swelling ratios of the hydrogels relative to NaCl, dumbbells soaked in comparable concentrations of KBr became too soft for our Instron clamp setup and were subject to notable elastic deformation leading to slippage during pull tests.

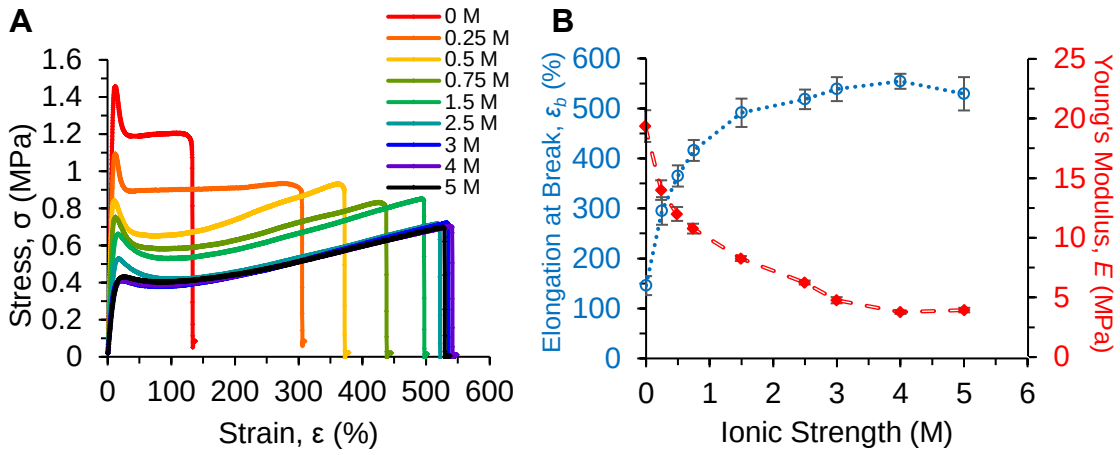

Figure 5.5. (A) Stress-strain curves of PNV_{50} at 1.5 M monomer loading after equilibration in different salt solutions of NaCl. **(B)** Summarized data of tensile testing for ε_b and E.

The effect of NaCl on the Young's modulus and stretchability of the material appears to be more pronounced at lower ionic strength; weaker ionic interactions are disrupted by Na^+ and Cl^- at moderate salt concentrations (<2.5 M), whereas domains higher crosslink density and better alignment of oppositely charged polymeric groups provide the basis for mechanical elasticity as "permanent" crosslinks appear to persist past 2.5 M. This gives rise to a plateau in both the ε_b and moduli of the materials. PA materials, generally, are comprised of strongly associating domains of polyampholyte, intertwined with weaker ionic interactions. At low tensile strain, the modulus of the material is representative of strong and weak interactions is observed before weaker associations are broken and polymers begin, giving rise to the very brief elastic region. As the material is further deformed, stronger crosslinked regions are broken until complete fracture occurs.

Interestingly, the strain-hardening and different strengths of ionic interactions in polyampholyte materials are often attributed to differences in comonomer reactivities.[6,7,33] In PNV_{50} polyampholytes, the alternating polymerization does not allow for significant

compositional gradients that could facilitate regions of highly localized anionic or cationic charged segments for stronger interactions. However, it is possible that the alternating nature of the chains might allow for a zipper-type arrangement of oppositely charged groups to form intermolecular interactions between chains and are the primary source of "permanent" cross-links between polymer domains. Conversely, intramolecular associations, misaligned charges, or domains of limited polymer entanglement may be the source of "sacrificial" bonds within the material.

With no salt, the hydrogels appear to be broken down at a near constant tensile stress. However, as weaker ionic bonds are liberated by salt screening, the chains having more flexibility allow for the materials become more stretchable and elastic. As the gels are further strained with increasing salt, regions of greater chain entanglement and stronger ionic associations become the primary source of mechanical strength and allow the material to withstand greater force as at increasing strain while chain mobility becomes increasingly limited, resulting in strain-hardening. This was also found to be true for 2 M loading samples of PNV_{50}, found in Table 5A.6.

These results indicate that the PNV_{50} polyampholytes possess tunable properties with respect to both monomer loading and ionic strength. In previous work, we demonstrated that charge dilution and polyelectrolyte hydration can have a significant impact on the responsive[9,12] and mechanical properties[13] of polyelectrolyte complexes. Therefore, charge dilution by neutral termonomers such as HEMA or zwitterionic MPC might provide additional tunability of PNV_{50} materials and offer a strategy for increasing stimuli-responsiveness and mechanical properties of these tough hydrogels.

5.4.2. Terpolymer hydrogels: The Effect of HEMA and MPC Termonomer

5.4.2.1. Terpolymerization Tracking by ^{1}H NMR

Given the utility of the alternating copolymerization to form PNV_{50} polyampholytes, two different terpolymer systems containing either MPC or HEMA with PNV_{50} were then monitored over small conversion steps to model the reactivity ratios. These ^{1}H NMR experiments indicate that the ratio of NaSS and VBTA does not appear to deviate from the 1:1 ratio with added termonomer (Figure 5.6), which allows the pair to be considered as a single moiety in these terpolymerizations with methacrylate termonomer in a binary model.

As shown in Figure 5.6 (C), the comonomer feed of termonomer gradually increases as the charged monomers are consumed. The alternating-type copolymerization has a tendency to exclude the termonomer, leading to drift in comonomer feed in both methacrylate monomers (Figure 5.6 (B)). While the differences in reactivity ratios for physical hydrogels have been previously reported, it has been assumed that the early and later chains formed exist as a homogeneous mix of polymer chains.[6]

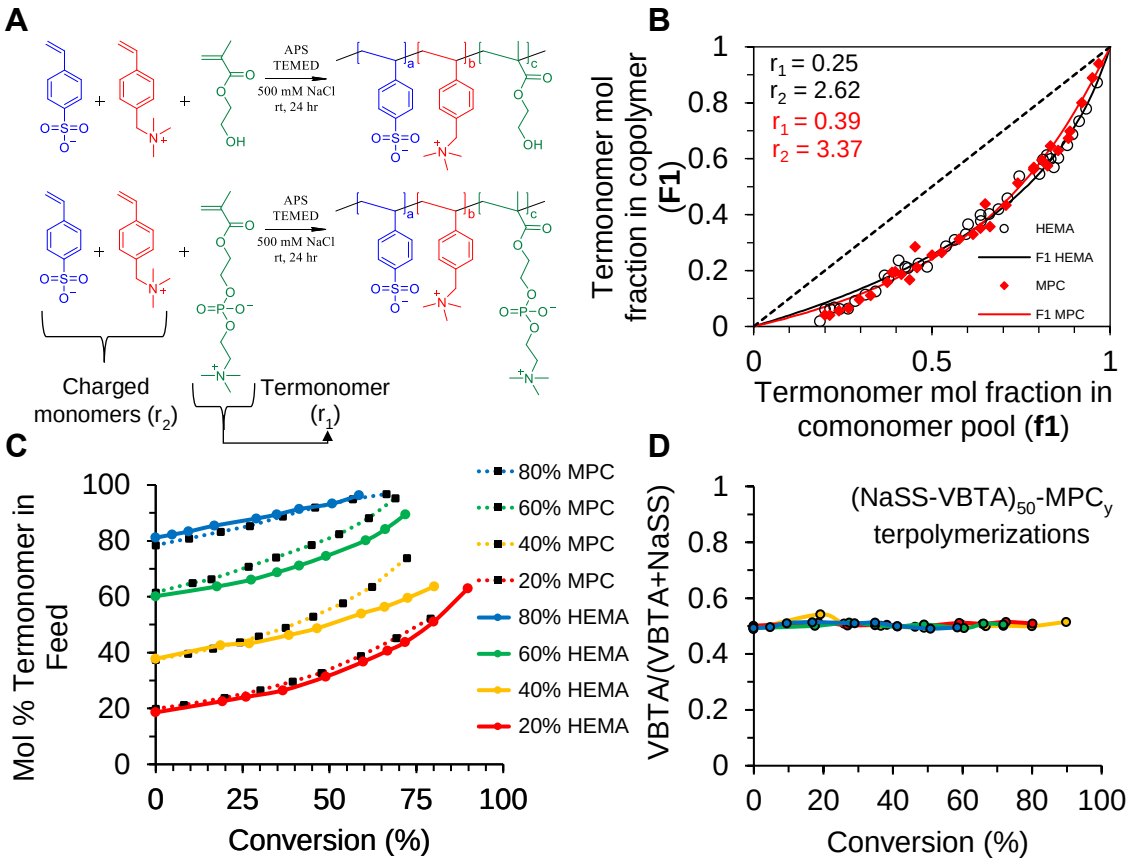

Figure 5.6. (A) Scheme of $PNV_{50}H_y$ and $PNV_{50}M_y$ redox gel preparation. **(B)** Plotted reactivity ratio data for both HEMA and MPC show comparable incorporation rates. **(C)** Termonomer pool tracking shows an increase in HEMA and MPC through total conversion, indicating favourable incorporation of styrenic comonomers NaSS+VBTA. **(D)** VBTA fraction of charged monomers in MPC terpolymerizations show minimal drift, demonstrating the alternating tendency of the NaSS-VBTA polymerization.

5.4.2.2. Terpolymer Gel Preparation

Hydrogel characterization was done by combustion elemental analysis, confirming that the termonomer feed ratio are roughly achieved (Table 5A.7). Each gel appears to be lacking a small percentage of termonomer, which may be due to out-diffusion of a small fraction of termonomer-rich chains during dialysis. Gels are denoted using the mol % termonomer in the comonomer pool before polymerization.

Hydrogels prepared with different termonomer mol % appear to offer different mechanical properties before dialysis. Up to 50 % HEMA can be incorporated gels that can still be handled and removed from both syringe and dumbbell moulds. These gels become increasingly flexible and soften with HEMA content but appear to stiffen after dialysis. Conversely, only 8% of MPC can be introduced before the polymers begin to flow and the gels become too soft for handling; this demonstrates the difference in hydration resulting from zwitterions compared to neutral HEMA, and points to a limitation of these monomers in physical hydrogels. Interestingly, $PNV_{50}M_y$ gels show mechanical properties comparable to HEMA gels with 5x less termonomer before equilibration. Images were taken of syringe moulded gels that were clamped and left for 60 seconds to hang horizontally (Figure 5A.8-5A.10). After equilibrium is achieved through out-diffusion of salt ions, both sets of termonomer gels appear to stiffen. $PNV_{50}H_y$ gels stiffen but still offer some observable flexibility due to a substantial decrease in charge density; conversely, $PNV_{50}M_y$ gels stiffen dramatically and resemble the mechanical properties of the equilibrium gels of ≤ 10% HEMA. These early observations suggest that at equilibrium, the mechanical properties of the material are dependent more on the degree of charge dilution than the functional group of the neutral termonomer.

5.4.2.3. Hydrogel Swelling: Response to Ionic Strength

Combustion elemental analysis used to confirm the final composition of the gels agrees with the monomer feeds tracking data, although the gels appear to be slightly lower in incorporated termonomer, likely due to the less favourable incorporation.

In general, KBr was able to increase swelling ratios as the ionic associations were more effectively shielded by K^+ and Br^- ions, while NaCl addition led to less significant swelling (Figure 5A.11-5A.12). As the charge density of the gels was reduced by incorporation of termonomer, Q_v consequently increases and gels become softer and slightly more translucent. The increase in stimuli-responsiveness with a reduction in charge density has previously been reported for liquid coacervates[9,40-42], and recently in solid, physically cross-linked polyampholyte hydrogels.[14] As the number of charges decreases with the addition of neutral termonomer, the entropy of mixing underlying polyelectrolyte complexation is diminished, resulting in less favourable interactions that are more susceptible to charge shielding effects.[43-45]

Termonomer selection has a notable impact on the responsiveness of the polyampholyte to salt. While HEMA charge dilution greatly increases the responsivity to salt, significantly lower amounts of incorporated MPC can increase the observable Q_v values that are achieved; MPC hydration drastically weakens the physical cross-links formed between the charged NaSS-VBTA and increases the response to salt-shielding (Figure 5.7). Betaines such as MPC are highly hydrophilic, interacting strongly with water molecules while maintaining high degree of mobility of water molecules surrounding the zwitterionic group[46-49]; this property has been exploited in non-fouling applications, as the monomers create hydration energy barriers used in preventing ionic associations and hydrophobic interactions between proteins and various surfaces.[50-52] Some betaines are also known to elicit anti-polyelectrolyte effects and the response of poly(MPC) brushes to salts has been previously demonstrated.[53] Hence, the notable increase in response to salt

and swelling as a result of hydration and solvation effects by MPC correspond with literature reports.

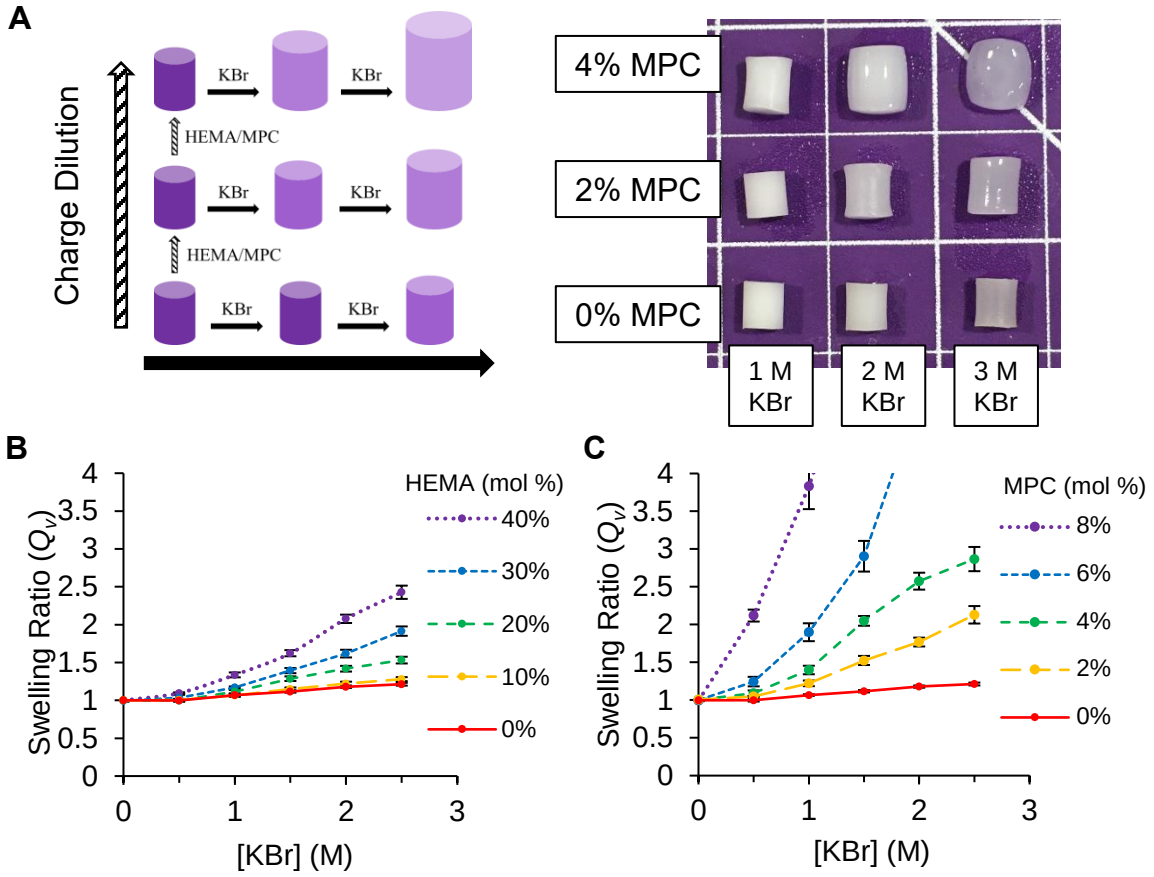

Figure 5.7. (A) Illustration of expected responsive swelling and images of swollen hydrogels at equilibrium (7 days) with addition of termonomer and salt. **(B)** Swelling ratios of 1.5 M HEMA terpolymer hydrogels as a function of [KBr]. **(C)** Swelling ratios of 1.5 M MPC terpolymer hydrogels as a function of [KBr].

5.4.2.4. Hydrogel Swelling: Response to Temperature

Temperature effects are prevalent in both hydrophilic and hydrophobic polyampholytes, and can be tuned by altering the ionic interactions in the material by tuning, for example, charge density.[9,14,54,55] As seen in binary PNV_{50}, elevated temperatures enhance the effects

of charge shielding on $PNV_{50}M_y$ hydrogels. These gels have fewer associative interactions due to a decrease in charge density and by hydration via zwitterionic MPC, such that the energy required to mobilize chains is significantly lowered. Coupled with salt shielding effects of NaCl, the increasing betaine composition significantly raises the responsiveness of the chains to temperature. As a demonstration, the sensitivity of swelling ratio to salt at 4% MPC is significantly higher than that of 2% and 0% (Figure 5.8, Figure 5A.14). In KBr at elevated temperature, these terpolymer gels can melt or flow with more notable dissociation by both UCST and salt effects (Figure 5A.16).

In HEMA-containing polyampholytes, elevated temperatures do not appear to significantly enhance swelling; although charge shielding leads to salt-dependent swelling, the impact of temperature on hydrogel swelling is diminished with additional HEMA (Figure 5A.13). Rather, $PNV_{50}H_y$ swelling becomes less responsive to temperature with increasing HEMA. HEMA containing copolymers with hydrophobic components have been shown to elicit an LCST-type behaviour at elevated temperatures.[56-59] As HEMA-rich portions facilitate polymer collapse with increasing temperature, they enhance hydrophobic effects in polyampholytes inhibiting chain mobility and limiting swelling at elevated temperatures. This temperature response may be competing with the weakening of the ionic interactions in the material, resulting in a less effectively swollen hydrogel. As HEMA content is increased, as these gels do not dissolve or flow significantly at high KBr and high temperature (3 M KBr at 65 °C).

Interestingly, at 0 M NaCl, the ternary gels show drastic swelling at elevated temperatures (45 °C). MPC hydrogels swell significantly and become translucent, while

HEMA hydrogels swell to a slightly lesser extent but remain relatively opaque (Figure 5A.14). In the absence of charge shielding, there may be charged patches within the material trapped near like charges. With an increase in temperature, the weakening of polymer-polymer interactions allow the chains to alleviate the unfavourable interactions. With the addition of a small amount of salt, some of the unfavourable interactions are shielded and hydrogel swelling resumes the expected salt- and temperature-dependence (Figure 5A.15).

The multi-responsive properties of PNV_{50} polyampholytes may be of interest in self-healing materials. For polyampholytes, hydrogels are soaked in salt solution to plasticize the ionic interactions and facilitate chain rearrangement as well as reforming of ionic associations; the enhanced salt responsiveness with less monomer required, in the case of MPC, could be very attractive in these types of applications.

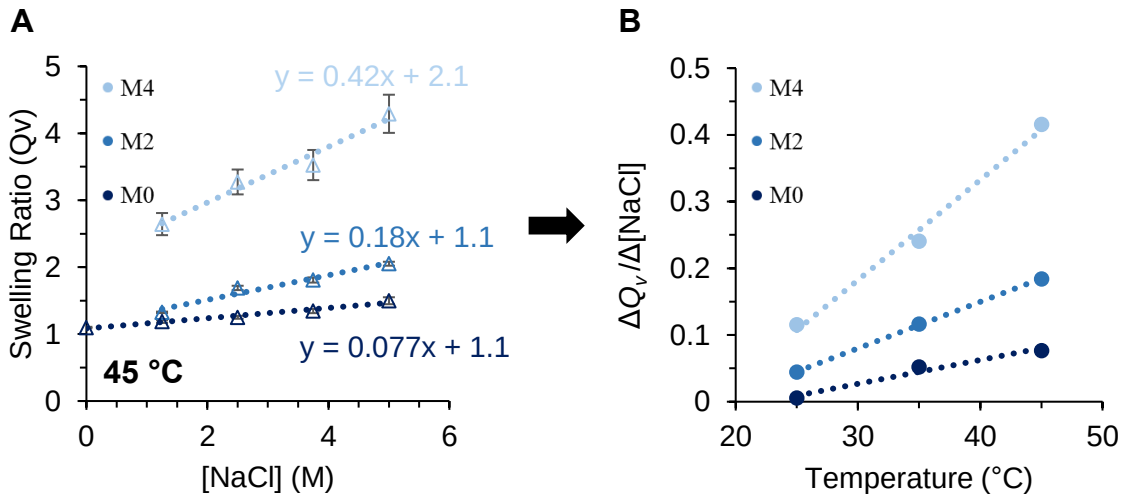

Figure 5.8. (A) Temperature-dependent swelling of $PNV_{50}M_y$ hydrogels in NaCl salt solution. **(B)** Responsive $PNV_{50}M_y$ hydrogel swelling with Δ[NaCl] plotted as a function of temperature.

5.4.2.5. Tensile Strength

Sample testing for MPC terpolymer gels was limited by the hydration of prepared gels before dialysis; above 8% MPC, the pre-dialyzed gels are too soft and deform upon removal from syringes and dumbbell moulds. On the other hand, gels of up to 50% HEMA were achievable, but tensile testing was limited by the mechanical setup; above 30% HEMA, dumbbells were found to undergo extensive elastic deformation at the grips causing slippage during pulling.

Using 1.5 M monomer loading, tensile testing of dumbbells of $PNV_{50}H_y$ indicates that as termonomer was introduced the gels become weaker and more stretchable, in agreement with previous reports.[14] PNV_{50}-$HEMA_x$ gels appear more deformable and stretchable as a result of higher termonomer incorporation; fracture stress increases by a factor of 5 with 20% incorporated termonomer. Interestingly, while the Young's modulus decreases slightly due to fewer ionic cross-links and improved chain mobility, the strain at break of the dumbbells appears relatively constant between 0.8 and 1 MPa due to strain hardening of the material; this suggests that higher amount of termonomer introduced reduces the number of strongly interacting domains that provide the basis for elastic behaviour and facilitates a degree of chain mobility in areas of weaker interactions (HEMA-rich) leading to a stretchable material while chain entanglement and domains of high charge density are the primary source of the mechanical strength (Figure 5.9). It has previously been reported that an increase in ε_b is relatively constant as termonomer is added while the σ_b and modulus decreases are more significantly impacted at lower termonomer additions, plateauing with increased termonomer in softer hydrogels of NaSS and MPTC.[14]

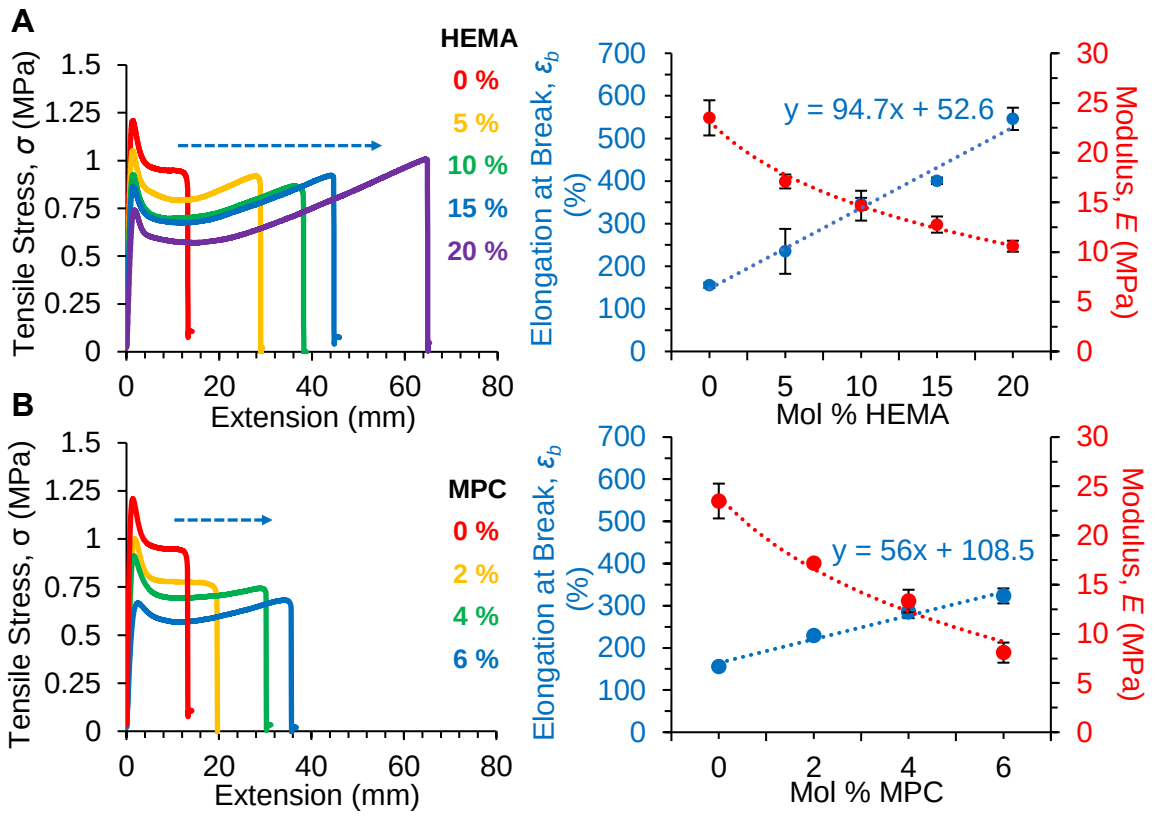

Figure 5.9. (A) Stress-strain curves of $PNV_{50}H_y$ (1.5 M) hydrogels with ε_b and Young's modulus plotted as a function of termonomer mol %. **(B)** Stress-strain curves of $PNV_{50}M_y$ (1.5 M) hydrogels with ε_b and E plotted as a function of termonomer mol %.

Comparatively, MPC significantly reduces the mechanical stiffness of the dumbbells, decreasing the Young's modulus to roughly 50% of that of PNV_{50} with 6% termonomer incorporation. MPC as a hydrating zwitterion can prevent hydrophobic and ionic interactions in the local environment, weakening the material in the elastic region. At the yield point, the material deformation becomes plastic and the strength of the material relies on domains of stronger complex interactions. The strength at break of these materials appears to be roughly comparable with the same amount of HEMA introduced (4% MPC and 5% HEMA), indicating that the fracture strain and stretchability is likely a function of charge density effects from termonomer mol % rather than functional group hydration. In

these gels, the stress at break appears to decrease with higher MPC, although at 4-6% MPC the material begins to show strain hardening, as seen in stretchable HEMA gels. The complete set of Instron data can be found in Table 5A.17. Trends in mechanical properties were also demonstrated in 2 M hydrogels, Table 5A.18.

5.4.3. Self-healing Assays

Polyampholyte materials offer themselves as self-healing, stimuli-responsive materials, with previous work illustrating the ability to self-heal to form a number of different shapes in response to salt, temperature, and pH.[6,7,14,60]

After the cut-swell-heal process, the dumbbells appear to shrink to smaller sizes. Salts such as KBr impedes the ionic association and facilitates chain mobility and allows them to reorient, after which dialysis was used to remove excess salt, allowing the polymers to form stronger, more compact materials.[30]

Early observations indicate that binary polyampholyte gels of PNV_{50} show little to no mechanical integrity after the healing procedure, with no detectable self-healing capacity. The "healed" dumbbells are easily broken at the scar during moderate stirring of the dialysis bath or changing of dialysate. As the amount of termonomer increases, the healing processes become more effective, and the hydrogels become more mechanically stable (Figure 5A.19). Termonomer addition enhances the mobility of polymer chains and ability to shield ionic associations, which can be reformed during dialysis. Stress-strain curves show that while HEMA allows gradual improvement of self-healing, the materials are still quite weak about the scar point in the gauge, with limited recovery of tensile strength and

stretchability. Qualitatively, $PNV_{50}H_{50}$ dumbbells can be successfully cut and healed using KBr soaking and dialysis to form strong interactions (Figure 5.10).

On the other hand, very low amounts of MPC appear to enhance the self-healing abilities of the hydrogels. At just 4% MPC incorporation, the recovered strength due to reformed ionic interactions is notably increased over the weakly healed binary PNV_{50} polyampholyte, while the stretchability of the materials is notably more recovered than in HEMA ternary hydrogels (Figure 5.10). Hence, zwitterionic functional groups are better candidates for improving the stimuli-responsiveness and self-healability of polyampholyte materials comprising ionic and hydrophobic interactions. These preliminary results demonstrate that these polyampholytes are capable of self-healing but require significantly higher amounts of HEMA or MPC to weaken the ionic cross-links.

While the overall self-healing ability are limited compared to those explored previously, these experiments support the hypothesis that charge dilution and improving the ability to shield charges in polyampholyte materials leads to improved self-healing capabilities; this extends to polyampholytes with more effective self-healability and could allow for the development of materials that require more moderate conditions.

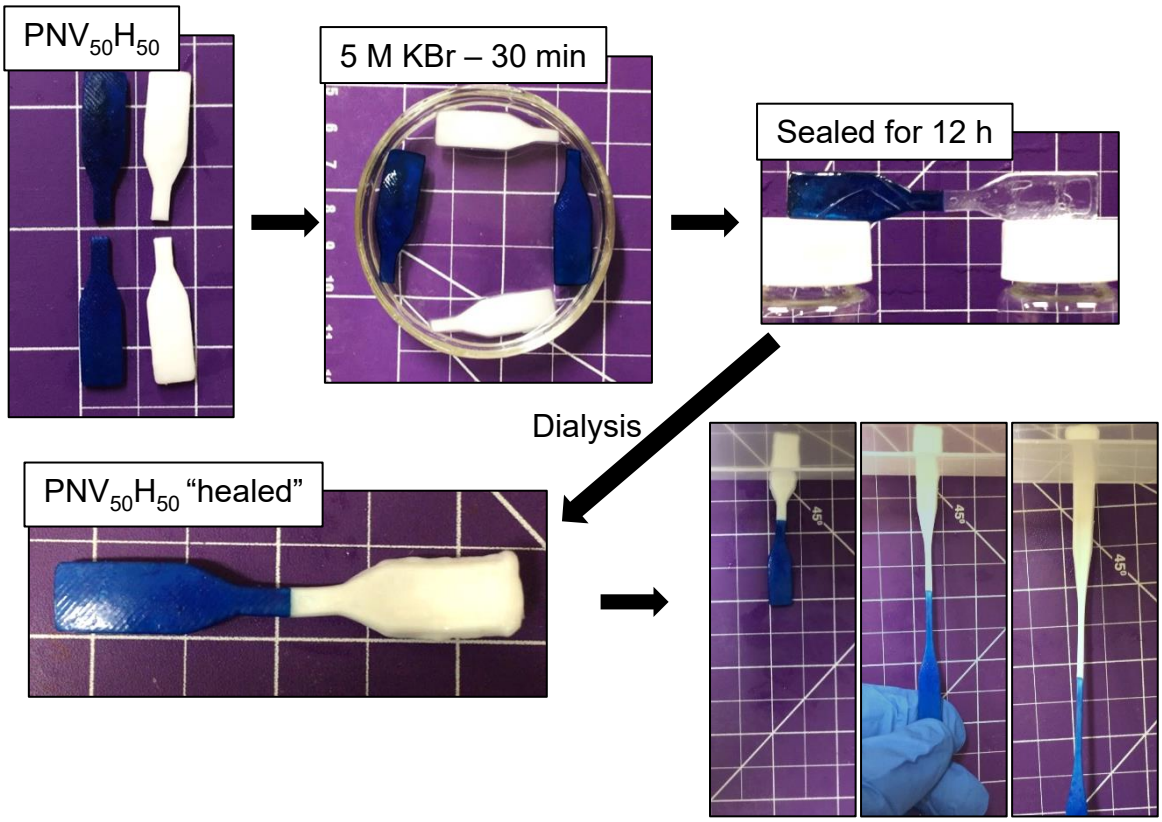

Figure 5.10. $PNV_{50}H_{50}$ (1.5 M) large dumbbells cutting and healing process (dyed with BBG and as prepared). Dumbbells show good mechanical strength and stretchability after reformation of ionic associations before and after dialysis equilibration.

As previously demonstrated, elevated temperature can be used to soften or weaken the ionic interactions holding PNV_{50} material together, specifically for MPC ternary polyampholytes, and has been used to accelerate self-healing processes.[60] Initial results in this work demonstrate that self-healing is less efficient than other polyampholyte systems, however, conditions for liberation and reformation of associative interactions in these materials may be further explored and optimized.

5.5. Conclusions and Future Work

The styrenic NaSS-VBTA copolymer system is a robust, near alternating polymerization that can offer access to polyampholyte materials in a wide range of shapes and dimensions. This system simplifies the preparation of charge-balanced polyampholytes but brings about substantial challenges in preparing polyampholytes with different charge ratios. The incorporation rate of NaSS-VBTA remains unchanged in terpolymerizations with methacrylate termonomers, favouring copolymerization over the introduction of either charge neutral termonomer.

PNV polyampholyte hydrogel mechanical and physical properties appear to be dependent on monomer loading. In general, these gels are also responsive to salts and temperature, although the total monomer loading and salt type dictate the sensitivity of the material.

To improve the stimuli responsive properties, terpolymer polyampholyte hydrogels were prepared by introducing MPC and HEMA. MPC increases stimuli-response to salt and temperature with very low amount of termonomer required to weaken the ionic associations. MPC also appears to weaken the mechanical strength of the ternary gels after equilibration by dialysis. Conversely, HEMA is less effective at weakening ionic associations in salt and appears to give rise to an LCST-type behavior that suppresses swelling at elevated temperatures. This monomer can be incorporated in much higher percentage in the gels than MPC, and thus can be used to both weaken the mechanical strength and improve the elasticity of the gels via substantial charge dilution.

Future work should explore the effects of elevated temperature to identify the change in mechanical properties by rheology.[14] Further optimization of self-healing parameters of these materials and exploring the effects of betaines on other, more capable self-healing polyampholyte gels is also of great interest. In more responsive polyampholytes, small amounts of both MPC and HEMA may both improve salt response allowing for more moderate healing conditions; HEMA appears to have less effect on the gel formation and can be incorporated at higher amounts. It might also be interesting to explore the more stretchable, responsive materials with respect to self-recovery and fatigue resistance, as these properties are desirable in long-term biomedical applications such as articular cartilage.[38]

Author Information

Corresponding Author

Email: stoverh@mcmaster.ca, Ph.: 1-905-525-9140 ext. 24983.

Notes:

The authors declare no competing financial interest.

5.6. Acknowledgements

The authors would like to thank the Natural Sciences and Engineering Research Council of Canada for funding this research through its Discovery Grant program (RGPIN89661-11 and RGPIN-2018-05585), and through the CGS-D award held by D. E. Hastings. The authors would like to thank Todd Hoare (Elemental Analyzer) and Michael Thompson (Instron) for the use of their equipment and facilities. The authors would also like to thank Afshin Abrishamkar for his assistance with combustion elemental analysis, Heera Marway for his assistance and expertise on mechanical testing, as well as Robert Bui for his insight on mechanical testing and material preparation. Finally, the authors would like to thank Cole Elford for his assistance in 3D printing custom poly(lactic acid) moulds for dumbbell preparation.

5.7. References

1. Costa, A. M. S.; Mano, J. F. Extremely strong and tough hydrogels as prospective candidates for tissue repair – a review. *Euro. Polym. J.* **2015**, *72*, 344-364.

2. Ahmed, E. M. Hydrogel: Preparation, characterization, and applications: A review. *J. Adv. Res.* **2013**, *6*, 105-121.

3. Dai, X.; Zhang, Y.; Gao, L.; Bai, T.; Wang, W.; Cui, Y.; Liu, W. A Mechanically Strong, Highly Stable, Thermoplastic, and Self-Healable Supramolecular Polymer Hydrogel. *Adv. Mater.* **2015**, *27*, 3566-3571.

4. Kitamura, N.; Yasuda, K.; Ogawa, M.; Arakaki, K.; Kai, S.; Onodera, S.; Kurokawa, T.; Gong, J. P. Induction of Spontaneous Hyaline Cartilage Regeneration Using a Double-Network Gel. *Am. J. Sports Med.* **2011**, *39*, 1160-1169.

5. Rao, P.; Sun, T. L.; Chen, L.; Takahashi, R.; Shinohara, G.; Guo, H.; King, D. R.; Kurokawa, T.; Gong, J. P. Tough hydrogels with Fast, Strong, and Reversible Underwater Adhesion Based on a Multiscale Design. *Adv. Mater.* **2018**, *30, 1801884.*

6. Sun, T. L.; Kurokawa, T.; Kuroda, S.; Ihsan, A. B.; Akasaki, T.; Sato, K.; Haque, M. A.; Nakajima, T.; Gong, J. P. Physical hydrogels composed of polyampholytes demonstrate high toughness and viscoelasticity. *Nat. Mater.* **2013**, *12*, 932-937.

7. Luo, F.; Sin, T. L.; Nakajima, T.; Kurokawa, T.; Zhao, Y.; Sato, K.; Ihsan, A. B.; Li, X.; Guo, H.; Gong, J. P. Oppositely Charged Polyelectrolytes Form Tough, Self-Healing, and Rebuildable Hydrogels. *Adv. Mater.* **2015**, *27*, 2722-2727.

8. Hastings, D. E.; Bozelli, J. C.; Epand, R. M.; Stöver, H. D. H. Investigating the Effects of Charge Arrangement in Stimuli-Responsive Polyelectrolytes. *Macromolecules* **2021**, *54*, 11427-11438.

9. Hastings, D. E.; Stöver, H. D. H. Exploring the Impact of Zwitterions in Discrete Charge Arrangements of Stimuli-Responsive Polyelectrolyte Complexes. *ACS Appl. Polym. Mater.* **2022**, *4*, 5035-5046.

10. Fu, J.; Fares, H. M.; Schlenoff, J. B. Ion-Pairing Strength in Polyelectrolyte Complexes. *Macromolecules* **2017**, *50*, 1066-1074.

11. Zhao, J. Synthesis and Properties of Polyampholyte and Their Application to Cell Cryoprotection. Ph.D. Dissertation, McMaster University, Hamilton, ON, **2018**.

12. Abdilla, A.; Shi, S.; Burke, N. A. D.; Stöver, H. D. H. Multistimuli Responsive Ternary Polyampholytes: Formation and Crosslinking of Coacervates. *J. Polym. Chem. A Polym. Chem.* **2016**, *54*, 2109-2118.

13. Hastings, D. E.; Stöver, H. D. H. Crosslinked Hydrogel Capsules for Cell Encapsulation Formed Using Amino/Betaine Dual-Functional Semibatch Copolymers. *ACS Appl. Polym. Mater.* **2019**, *1*, 2055-2067.

14. Lee, J. H.; Lee, D. S.; Jung, Y. C.; Oh, J.-W.; Na, Y.H. Development of a Tough, Self-Healing Polyampholyte Terpolymer Hydrogel Patch with Enhanced Skin Adhesion via Tuning the Density and Strength of Ion-Pair Associations. *ACS Appl. Mater. Interfaces* **2021**, *13*, 8889-8900.

15. Zhao, J.; Burke, N. A. D.; Stöver, H. D. H. Preparation and study of multi-responsive polyampholyte copolymers of N-(3-aminopropyl)methacrylamide hydrochloride and acrylic acid. *RSC Adv.* **2016**, *6*, 41522-41531.

16. Aguilar, M.; Gallardo, A.; Fernández, M.; Román, J. In-Situ Quantitative 1H NMR Monitoring of Monomer Consumption: A Simple and Fast Way of Estimating Reactivity Ratios. *Macromolecules* **2002**, *35*, 2036-2041.

17. Salamone, J. C.; Tsai, C.-C.; Watterson, A. C. Polymerization of Vinylpyridinium Salts. XI. Charge-Transfer Polymerization of 4-Vinylpyridinium p-Styrenesulfonate. *J. Macromol. Sci., Chem.* **1979**, *13*, 665-672.

18. Kanta Sharker, K.; Shigeta, Y.; Ozoe, S.; Damsongsang, P.; Hoven, V. P.; Yusa, S. Upper Critical Solution Temperature Behavior of pH-Responsive Amphoteric Statistical Copolymers in Aqueous Solutions. *ACS Omega* **2021**, *6*, 9153-9163.

19. Wang, L.; Wang, J.; Yu, H.; Luo, F.; Li, J.; Tan, H. Structure and properties of tough polyampholyte hydrogels: effects of a methyl group in the cationic monomer. *RSC Adv.* **2016**, *6*, 114532-114540.

20. Toleutay, G.; Su, Kudaibergenov, S.; Okay, O. Highly stretchable and thermally healable polyampholyte hydrogels via hydrophobic modification. *Colloid Polym. Sci.* **2020**, *298*, 273-284.

21. Patrickios, C. S. Polypeptide amino acid composition and isoelectric point: 1. A closed-form approximation. *J. Colloid Interface Sci.* **1995**, *175*, 256-260.

22. Nisato, G.; Munch, J. P.; Candau, S. J. Swelling, Structure and Elasticity of Polyampholyte Hydrogels. *Langmuir* **1999**, *15*, 4236-4244.

23. Bai, T.; Liu, S.; Sun, F.; Sinclair, A.; Zhang, L.; Shao, Q.; Jiang, S. Zwitterionic Fusion in Hydrogels and Spontaneous and Time-Independent Self-Healing Under Physiological Conditions. *Biomaterials* **2014**, *35*, 3926-3933.

24. Wang, H.; Zhan, J.; Xiao, K.; Luo, F.; Li, J.; Tan. H. Thermoresponsive Three-Stage Optical Modulation of a Self-Healing Composite Hydrogel. *Macromol. Chem. Phys.* **2018**, *219*, 1800329.

25. Ihsan, A. B.; Sun, T. L.; Kuroda, S.; Haque, M. A.; Kurokawa, T.; Nakajima, T.; Gong, J. P. A phase diagram of neutral polyampholyte – from solution to tough hydrogel. *J. Mater. Chem. B* **2013**, *1*, 4555-4562.

26. Zhang, R.; Zhang, Y.; Antila, H. S.; Lutkenhaus, J. L.; Sammalkorpi, M. Role of Salt and Water in the Plasticization of PDAC/PSS Polyelectrolyte Assemblies. *J. Phys. Chem. B* **2017**, *121*, 322-332.

27. Ogawa, Y.; Ogawa, K.; Kokufuta, E. Swelling-Shrinking Behavior of a Polyampholyte Gel Composed of Positively Charged Networks with Immobilized Polyanions. *Langmuir* **2004**, *20*, 2546-2552.

28. Salomäki, M.; Tervasmäki, P.; Areva, S.; Kankare, J. The Hofmeister anion effect and the growth of polyelectrolyte multilayers. *Langmuir* **2004**, *20*, 3679-3683.

29. Fu, J.; Schlenoff, J. B. Driving forces for oppositely charged polyion association in aqueous solutions: enthalpic, entropic, but not electrostatic. *J. Am. Chem. Soc.* **2016**, *138*, 980-990.

30. Meng, S.; Ting, J. M.; Wu, H.; Tirrell, M. V. Solid-to-Liquid Phase Transition in Polyelectrolyte Complexes. *Macromolecules* **2020**, *53*, 7944-7953.

31. Liu, Y.; Momani, B.; Winter, H. H.; Perry, S. L. Rheological Characterization of Liquid-to-Solid Transitions in Bulk Polyelectrolyte Complexes. *Soft Matter* **2017**, *13*, 7332-7340.

32. Zhang, Y.; Hu, Q.; Yang, S.; Wang, T.; Sun, W.; Tong, Z. Unique Self-Reinforcing and Rapid Self-Healing Polyampholyte Hydrogels with a pH-Induced Shape Memory Effect. *Macromolecules* **2021**, *54*, 5218-5228.

33. Luo, F.; Sun, T. L.; Nakajima, T.; King, D. R.; Kurokawa, T.; Zhao, Y.; Ihsan, A. B.; Li, X.; Guo, H.; Gong, J. P. Strong and Tough Polyion-Complex Hydrogels from Oppositely Charged Polyelectrolytes: A Comparative Study with Polyampholyte Hydrogels. *Macromolecules* **2016**, *49*, 2750-2760.

34. Seuring, J.; Agarwal, S. Polymers with Upper Critical Solution Temperature in Aqueous Solution. *Macromol. Rapid Commun.* **2012**, *33*, 1898-1920.

35. Morisada, S.; Suzuki, H.; Emura, S.; Hirokawa, Y.; Nakano, Y. Temperature-swing adsorption of aromatic compounds using polyampholyte gel. *Adsorption* **2008**, *14*, 621-628.

36. Morisada, S.; Suzuki, H.; Hirokawa, Y.; Nakano, Y. Investigation of Temperature-Swing Adsorption of Aromatic Compounds in Water Using Polyampholyte Gels with Hydrophilic Nonionic Groups. *J. Appl. Polym. Sci. 119*, 2968-2973.

37. Yin, H.; King, D. R.; Sun, T. L.; Saruwatari, Y.; Nakajima, T.; Kurokawa, T.; Gong, J. P. Polyzwitterions as a Versatile Building Block of Tough Hydrogels: From Polyelectrolyte Complex Gels to Double-Network Gels. *ACS Appl. Mater. Interfaces* **2020**, *12*, 50068-50076.

38. Liu, M.; Ishida, Y.; Ebina, Y.; Sasaki, T.; Hikima, T.; Takata, M.; Aida, T. An anisotropic hydrogel with electrostatic repulsions between cofacially aligned nanosheets. *Nature* **2015**, *517*, 68-72.

39. Porter, J. R.; Ruckh, T. T.; Popat, K. C. Bone tissue engineering: a review in bone biomimetics and drug delivery strategies. *Biotechnol. Prog.* **2009**, *6*, 1539-1560.

40. Kleinberger, R. M.; Burke, N. A. D.; Zhou, C.; Stöver, H. D. H. Synthetic polycations with controlled charge density and molecular weight as building blocks for biomaterials. *J. Biomater. Sci., Polym. Ed.* **2016**, *27*, 351-369.

41. Huang, J.; Morin, F. J.; Laaser, J. E. Charge-density-dominated phase behavior and viscoelasticity of polyelectrolyte complex coacervates. *Macromolecules* **2019**, *52*, 4957-4967.

42. Huang, J.; Laaser, J. E. Charge Density and Hydrophobicity-Dominated Regimes in the Phase Behavior of Complex Coacervates. *ACS Macro Lett.* **2021**, *10*, 1029-1034.

43. Srivastava, S.; Tirrell, M. V. Polyelectrolyte Complexation. *Adv. Chem. Phys.* **2016**, *161*, 499-543.

44. Lounis, F. M.; Chamieh, J.; Leclercq, L.; Gonzalez, P.; Geneste, A.; Prelot, B.; Cottet, H. Interactions between Oppositely Charged Polyelectrolytes by Isothermal Titration Calorimetry: Effect of Ionic Strength and Charge Density. *J. Phys. Chem. B.* **2017**, *121*, 2684-2694.

45. Mattison, K. W.; Dubin, P. L.; Brittain, I. J. Complex Formation between Bovine Serum Albumin and Strong Polyelectrolytes: Effect of Polymer Charge Density. *J. Phys. Chem. B* **1998**, *102*, 3830-3836.

46. Ishihara, K.; Nomura, H.; Mihara, T.; Kurita, K.; Iwasaki, Y.; Nakabayashi, N. Why do phospholipid polymers reduce protein adsorption? *J. Biomed. Mater. Res.* **1998**, *39*, 323-330.

47. Wu, J.; Lin, W.; Wang, Z.; Chen, S. Investigation of the Hydration of Nonfouling Material Poly(sulfobetaine methacrylate) by Low-Field Magnetic Resonance. *Langmuir* **2012**, *28*, 7436-7441.

48. Leng, C.; Hung, H.-C.; Sun, S. W.; Wang, D. Y.; Li, Y. T.; Jiang, S. Y.; Chen, Z. Probing the Surface Hydration of Nonfouling Zwitterionic and PEG Materials in Contact with Proteins. *ACS Appl. Mater. Interfaces* **2015**, *7*, 16881-16888.

49. Shao, Q.; He, Y.; White, A. D.; Jiang, S. Difference in Hydration between Carboxybetaine and Sulfobetaine. *J. Phys. Chem. B* **2010**, *114*, 16625-16631.

50. Zhang, Z.; Finlay, J. A.; Goa, Y.; Callow, J. A.; Callow, M. E.; Jiang, S. Polysulfobetaine-Grafted Surfaces as Environmentally Benign Ultralow Fouling Marine Coatings. *Langmuir* **2009**, *25*, 13516-13521.

51. Ye, S. H.; Watanabe, J.; Iwasaki, Y.; Ishihara, K. Antifouling blood purification membranes composed of cellulose acetate and phospholipid polymer. *Biomaterials* **2003**, *24*, 4143-4152.

52. Lin, X.; Boit, M. O.; Wu, K.; Jain, P.; Liu, E. J.; Hsieh, Y.-F.; Zhou, Q.; Li, B.; Hung, H.-C.; Jiang, S. Zwitterionic carboxybetaine polymers extend the shelf-life of human platelets. *Acta Biomater.* **2020**, *109*, 51-60.

53. Zhang, Z.; Moxey, M.; Alswieleh, A.; Morse, A. J.; Lewis, A. L.; Geoghegan, M.; Leggett, G. J. Effect of Salt on Phosphorylcholine-based Zwitterionic Polymer Brushes. *Langmuir* **2016**, *32*, 5048-5057.

54. Das, E.; Matsumura, K. Tunable Phase-Separation Behavior of Thermoresponsive Polyampholytes Through Molecular Design. *J. Polym. Sci. A, Polym. Chem.* **2016**, *55*, 876-884.

55. Huang, J.; Morin, F. J.; Laaser, J. E. Charge-density-dominated phase behavior and viscoelasticity of polyelectrolyte complex coacervates. *Macromolecules* **2019**, *52*, 4957-4967.

56. Zhang, H.; Kim, J.-C. Hydroxethyl Acrylate-Based Polymeric Amphiphiles Showing Lower Critical Solution Temperature. *J. Macromol. Sci., Part A: Pure Appl. Chem.* **2015**, *52*, 128-146.

57. Longenecker, R.; Mu, T.; Hanna, M.; Burke, N. A. D.; Stöver, H. D. H. Thermally Responsive 2-Hydroxyethyl Methacrylate Polymers: Soluble-Insoluble and Soluble-Insoluble-Soluble Transitions. *Macromolecules* **2011**, *44*, 8962-8971.

58. Khutoryanskaya, O. V.; Mayeva, Z. A.; Mun, G. A.; Khutoryanskiy, V. V. Designing Temperture-Responsive Biocompatible Copolymers and Hydrogels Based on 2-Hydroxyethyl(meth)acrylates. *Biomacromolecules* **2008**, *9*, 3353-3361.

59. Nikdel, M.; Salami-Kalajahi, M.; Hosseini, M. S. Dual thermo- and pH-sensitive poly(2-hydroxyethyl methacrylate-*co*-acrylic acid)-grafted graphene oxide. *Coll. Polym. Sci.* **2014**, *292*, 2599-2610.

60. Ihsan, A. B.; Sun, T. L.; Kurokawa, T.; Karobi, S. N.; Nakajima, T.; Nonoyama, T.; Roy, C. K.; Luo, F.; Gong, J. P. Self-Healing Behaviors of Tough Polyampholyte Hydrogels. *Macromolecules* **2016**, *49*, 4245-4252.

5.8. Appendix

Figure 5A.1. Confocal laser-scanning microscope images (20X) of PNV_{50} hydrogels at 1.5 and 3 M loading.

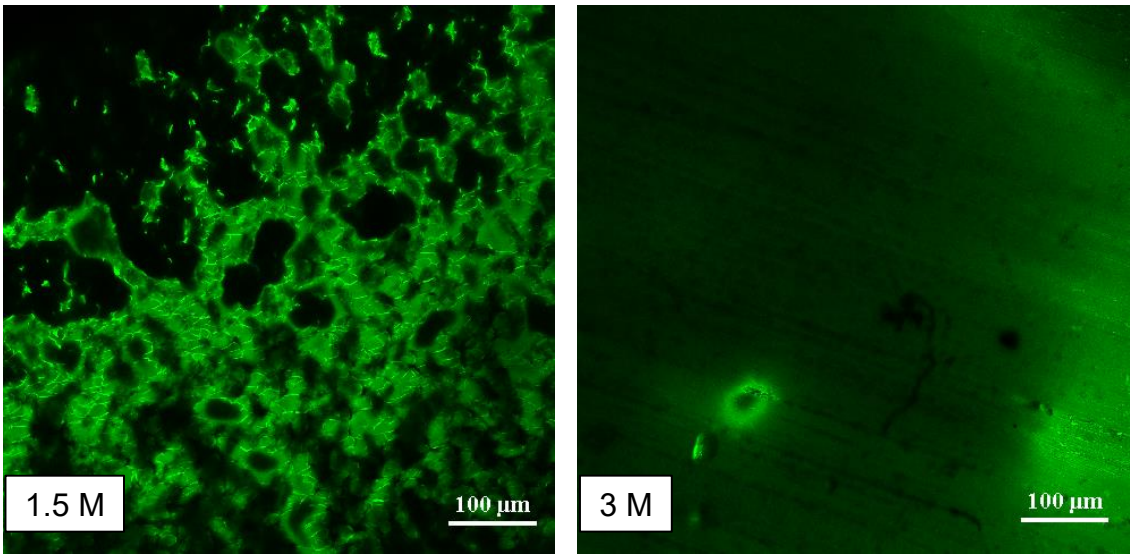

Figure 5A.2. Z-series images (20X) of PNV_{50} at 1.5 and 3 M monomer loading, taken by confocal microscopy.

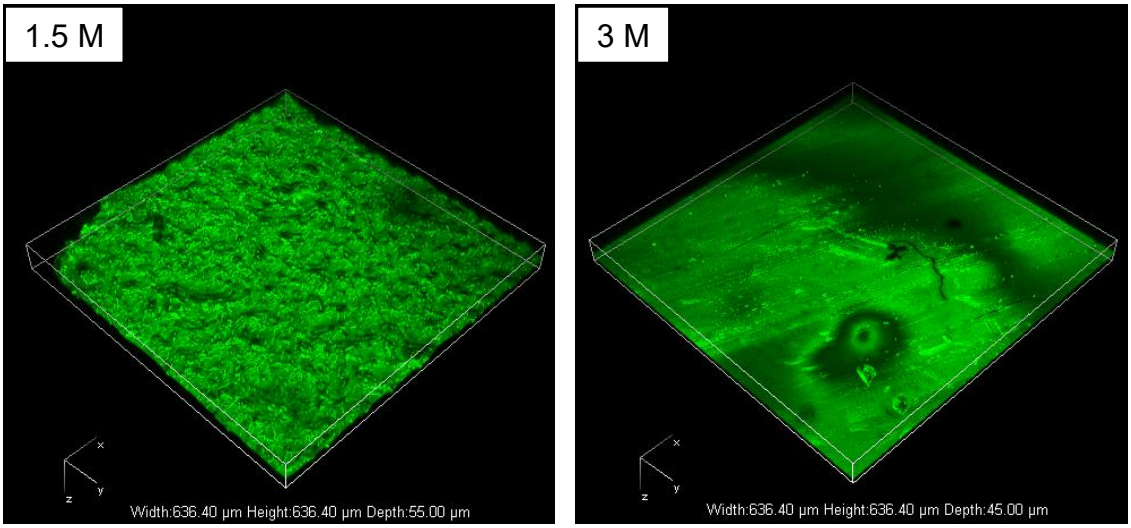

Figure 5A.3. Swelling ratios of PNV_{50} polyampholyte hydrogels in NaCl and KBr at different monomer loadings.

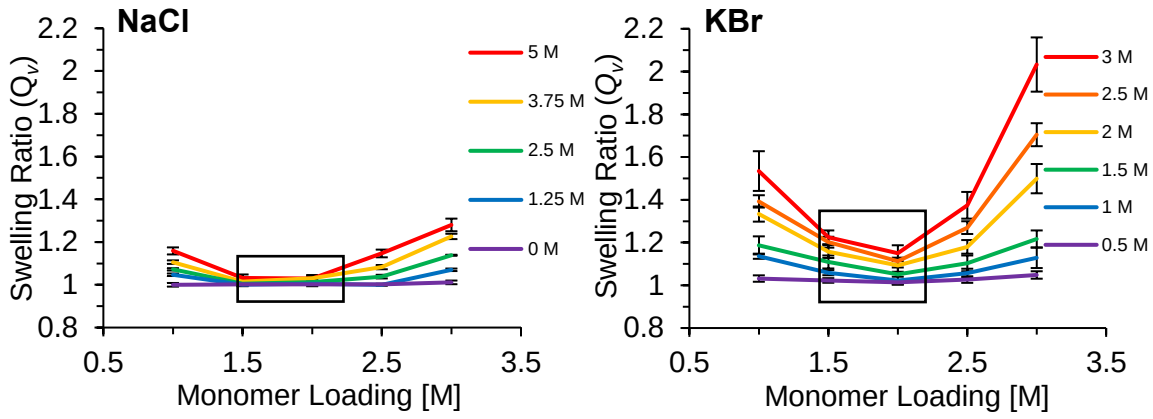

Figure 5A.4. Instron data of increasing Young's modulus and decreasing elongation with increasing PNV_{50} loadings.

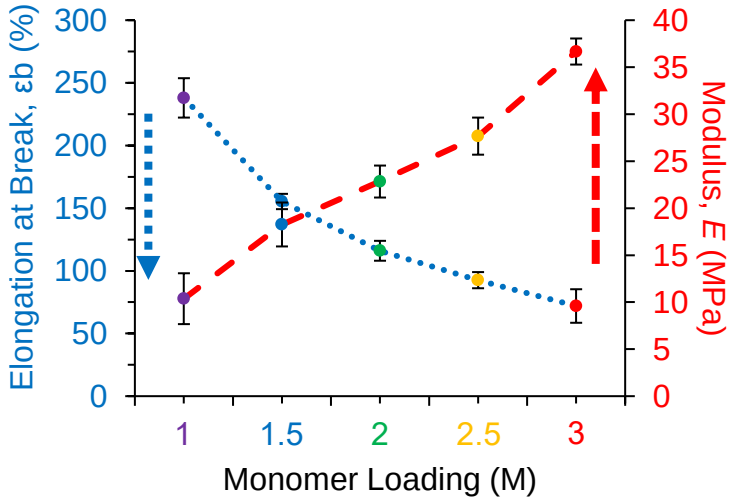

Figure 5A.5. (A) Stress-strain curves of PNV_{50} at 1.5 M monomer loading after equilibration in different salt solutions of NaCl. **(B)** Summarized data of tensile testing for ε_b and E.

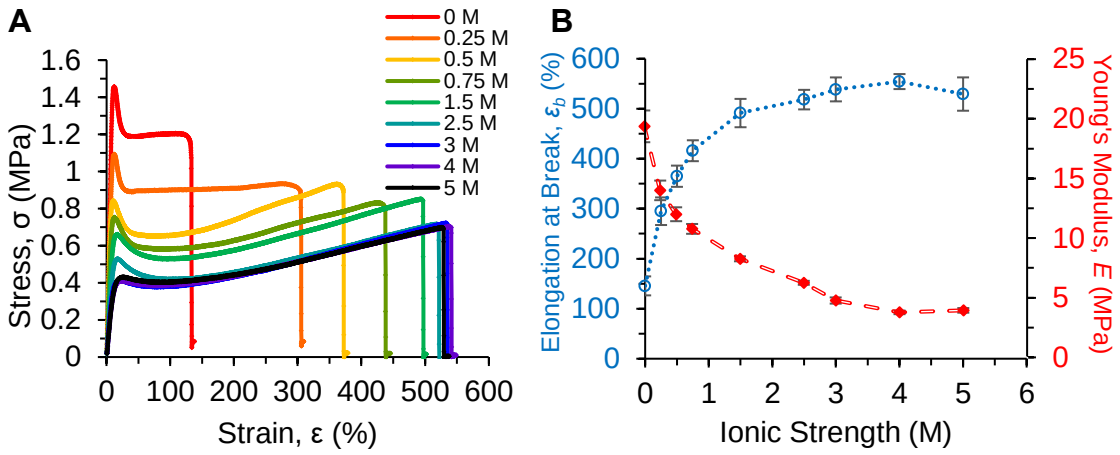

Table 5A.6. Response of mechanical properties to NaCl (2 M loading PNV_{50}).

[NaCl] (M)	Tensile Strength at Yield (MPa)	Modulus, E (MPa)	Fracture Strain, ε_b (%)	Tensile Strength at Break, σ_b (MPa)
0	1.83 ± 0.058	22.8 ± 1.70	116 ± 7.94	1.33 ± 0.13
0.25	1.43 ± 0.032	19.9 ± 1.01	214 ± 92.4	1.07 ± 0.056
0.5	1.22 ± 0.076	15.7 ± 1.92	393 ± 35.2	1.09 ± 0.12
1.0	1.01 ± 0.025	13.3 ± 0.69	498 ± 32.5	1.07 ± 0.095
1.5	0.86 ± 0.0	10.5 ± 0.30	573 ± 32.8	1.06 ± 0.031
2.0	0.78 ± 0.018	9.15 ± 0.73	573 ± 9.17	1.11 ± 0.061
3.0	0.64 ± 0.037	7.42 ± 0.64	587 ± 39.1	1.03 ± 0.091
4.0	0.59 ± 0.039	6.01 ± 0.093	567 ± 46.5	0.94 ± 0.085

Table 5A.7. $PNV_{50}H_y$ and $PNV_{50}M_y$ (1.5 M) hydrogels characterized by ^1H NMR and combustion elemental analysis.

Sample PNV_{50}__ (HEMA/ MPC)	NaSS (g)	VBTA (g)	HEMA (g)	MPC (g)	APS/ TEMED (mg)	^1H NMR Termonomer Feed (mol %)	Elemental Analysis Termonomer (mol %)
--	1.653	1.582	0	0	62.6/6.26	0	-0.87
H_{10}	1.488	1.424	0.195	0	62.6/6.26	9.19	8.09
H_{20}	1.323	1.266	0.390	0	62.6/6.26	19.8	17.2
H_{30}	1.157	1.108	0.586	0	62.6/6.26	30.78	26.8
H_{40}	0.992	0.950	0.781	0	62.6/6.26	39.98	35.1
M_2	1.620	1.551	0	0.089	62.6/6.26	1.68	0.86
M_4	1.587	1.519	0	0.177	62.6/6.26	3.47	2.35
M_6	1.554	1.488	0	0.266	62.6/6.26	5.34	4.48
M_8	1.521	1.456	0	0.354	62.6/6.26	6.98	5.94

Figure 5A.8. Syringe gels of $PNV_{50}M_y$ before dialysis show elastic properties increasing with MPC mol %.

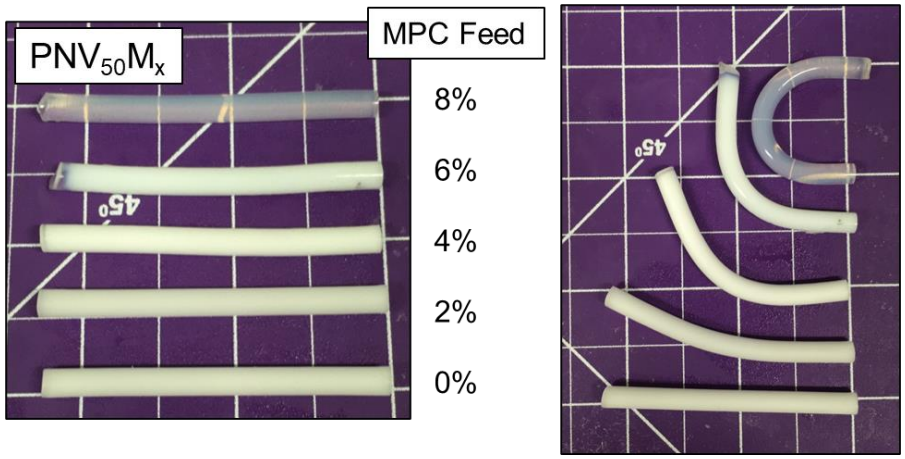

Figure 5A.9. Images of $PNV_{50}H_y$ and $PNV_{50}M_y$ hydrogels before dialysis after 60 s of hanging.

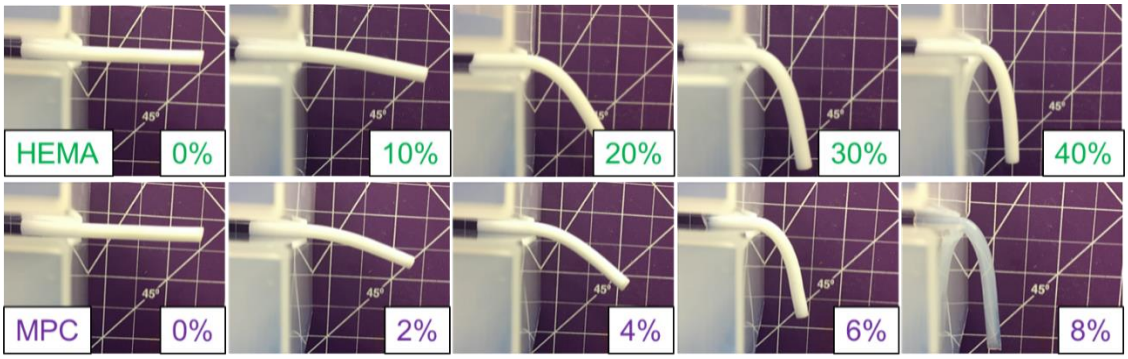

Figure 5A.10. Images of equilibrated syringe gels of HEMA and MPC termonomer incorporation after 60 s of hanging.

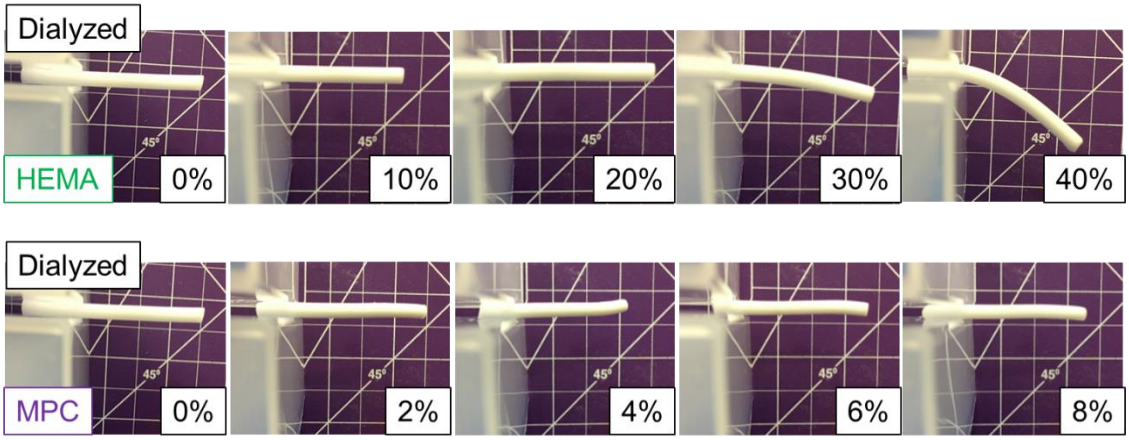

Figure 5A.11. Swelling ratios of $PNV_{50}H_y$ terpolymer gels in NaCl.

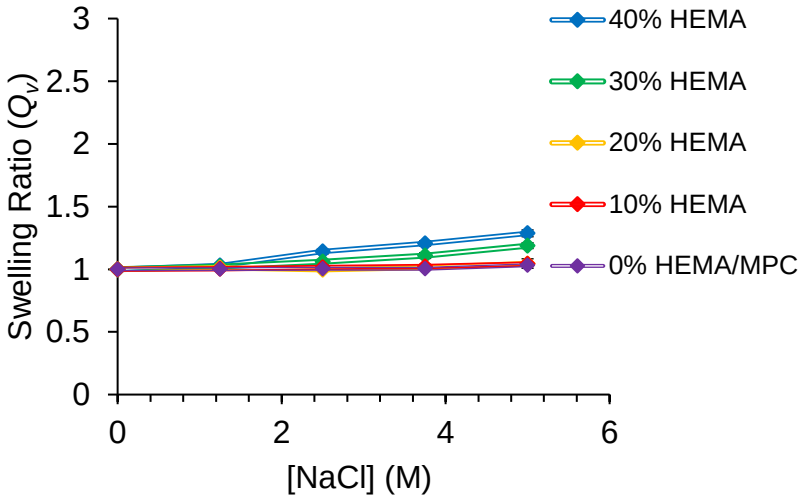

Figure 5A.12. Swelling ratios of $PNV_{50}M_y$ terpolymer gels in NaCl.

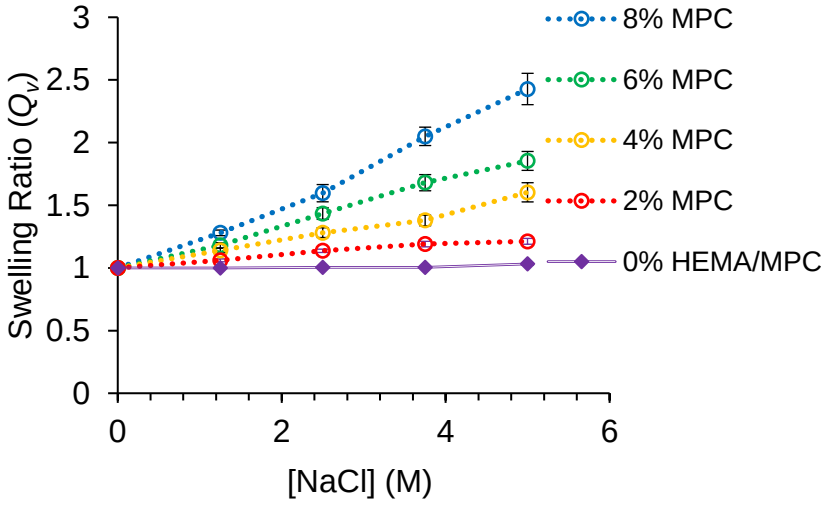

Figure 5A.13. Swelling ratios of $PNV_{50}H_y$ as a function of [NaCl] at increasing temperature.

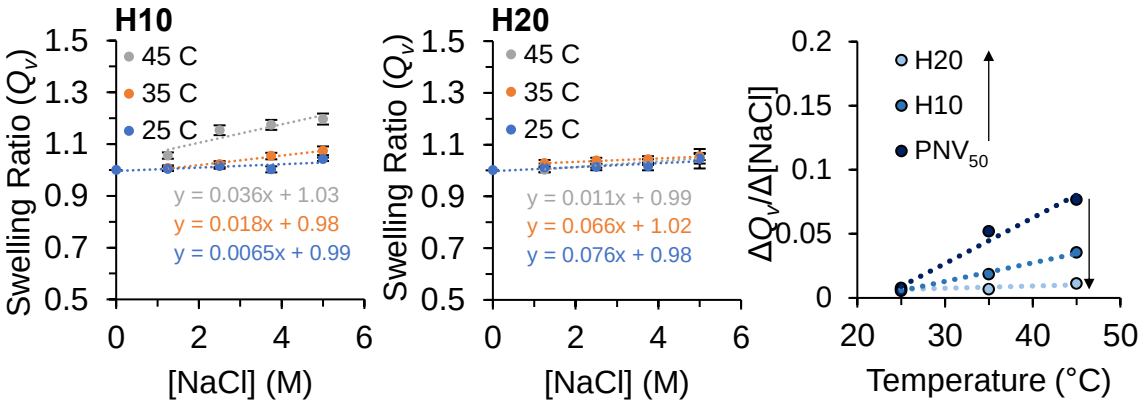

Figure 5A.14. Equilibrated swollen hydrogels in 0 M NaCl at 45 °C.

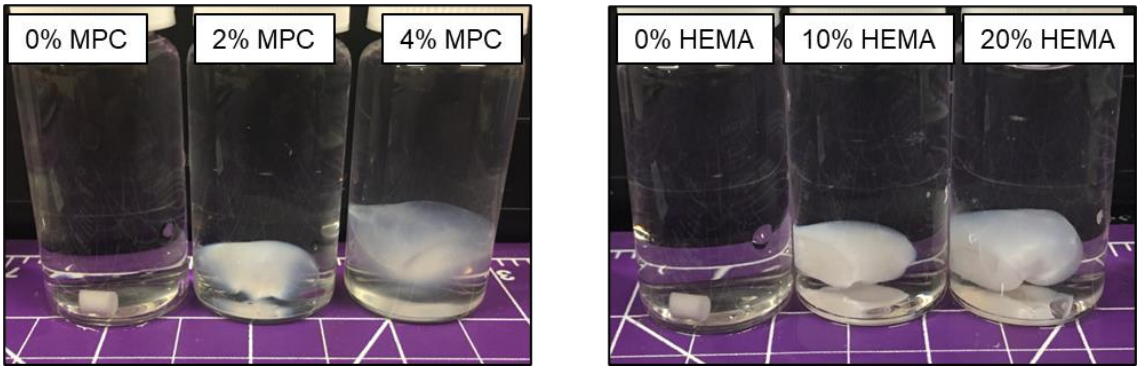

Figure 5A.15. $PNV_{50}M_4$ hydrogels at 45 °C in 0 M and 0.5 M NaCl.

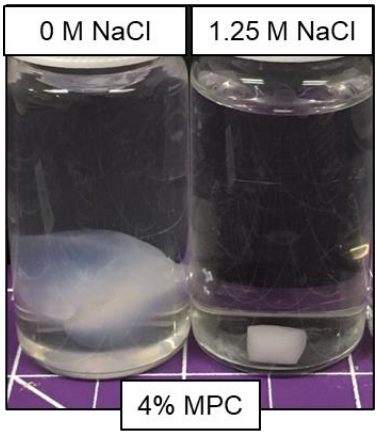

Addition of a small amount of salt shields unfavourable interactions and prevents significant swelling by temperature alleviation.

Figure 5A.16. $PNV_{50}M_y$ hydrogels in 1 M KBr at 45 °C.

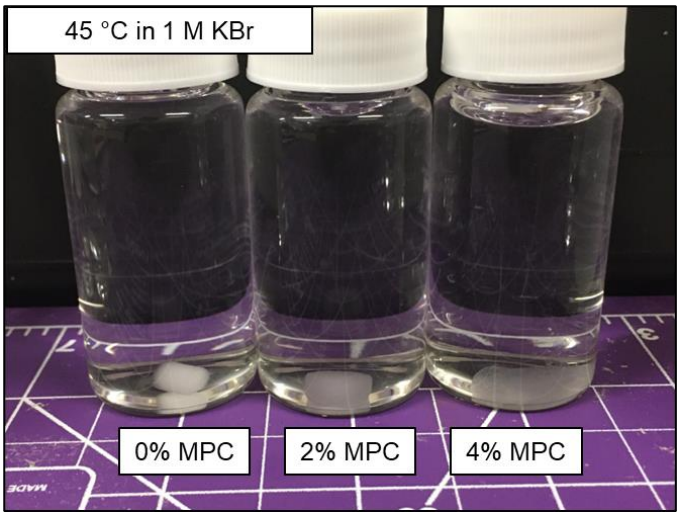

Table 5A.17. Tensile strength data for 1.5 M monomer loading $PNV_{50}H_y$ and M_y.

Specimen (PNV_{50} __)	Tensile Strength at Yield (MPa)	Modulus, *E* (MPa)	Fracture Strain, ε_b (%)	Tensile Strength at Break, σ_b (MPa)
--	1.26 ± 0.05	19.5 ± 1.77	155 ± 6	0.94 ± 0.038
H_5	1.06 ± 0.015	17.1 ± 0.70	235 ± 53	0.90 ± 0.021
H_{10}	0.92 ± 0.003	14.7 ± 1.50	347 ± 14	0.89 ± 0.043
H_{15}	0.83 ± 0.027	12.8 ± 0.81	401 ± 8	0.93 ± 0.023
H_{20}	0.75 ± 0.021	10.6 ± 0.55	546 ± 26	0.94 ± 0.055
M_2	1.01 ± 0.021	17.2 ± 0.35	230 ± 4	0.75 ± 0.040
M_4	0.90 ± 0.012	13.3 ± 1.15	286 ± 15	0.72 ± 0.023
M_6	0.67 ±0.026	8.09 ± 1.02	323 ± 18	0.67 ± 0.024

Rate of deformation was constant at 100 mm/min. Clamps were equipped with fine grit sandpaper to prevent slippage.

Table 5A.18. Tensile strength data for 2 M monomer loading $PNV_{50}H_y$ and M_y.

Specimen (PNV_{50} __)	Tensile Strength at Yield (MPa)	Modulus, *E* (MPa)	Fracture Strain, ε_b (%)	Tensile Strength at Break, σ_b (MPa)
--	1.83 ± 0.058	22.8 ± 1.70	116 ± 7.94	1.33 ± 0.13
H_5	1.55 ± 0.055	19.9 ± 0.48	179 ± 38.6	1.19 ± 0.050
H_{10}	1.42 ± 0.087	16.7 ± 1.11	273 ± 29.9	1.2 ± 0.035
H_{15}	1.36 ± 0.035	15.2 ± 0.81	354 ± 22.6	1.22 ± 0.051
H_{20}	1.19 ± 0.030	13.3 ± 0.64	438 ± 18.4	1.35 ± 0.091
H_{25}	1.04 ± 0.025	10.6 ± 0.55	570 ± 28.9	1.57 ± 0.042
M_1	1.76 ± 0.017	19.6 ± 0.87	185 ± 62.9	1.19 ± 0.031
M_2	1.5 ± 0.050	17.8 ± 1.10	250 ± 17.6	1.17 ± 0.035
M_3	1.36 ± 0.050	16.4 ± 0.45	335 ± 74.9	1.18 ± 0.13
M_4	1.14 ± 0.021	15.6 ± 0.71	413 ± 52.4	1.16 ± 0.12
M_5	1.01 ± 0.059	14.4 ± 1.28	472 ± 44.8	1.18 ± 0.076

Figure 5A.19. Stress-strain curves of self-healed dumbbells.

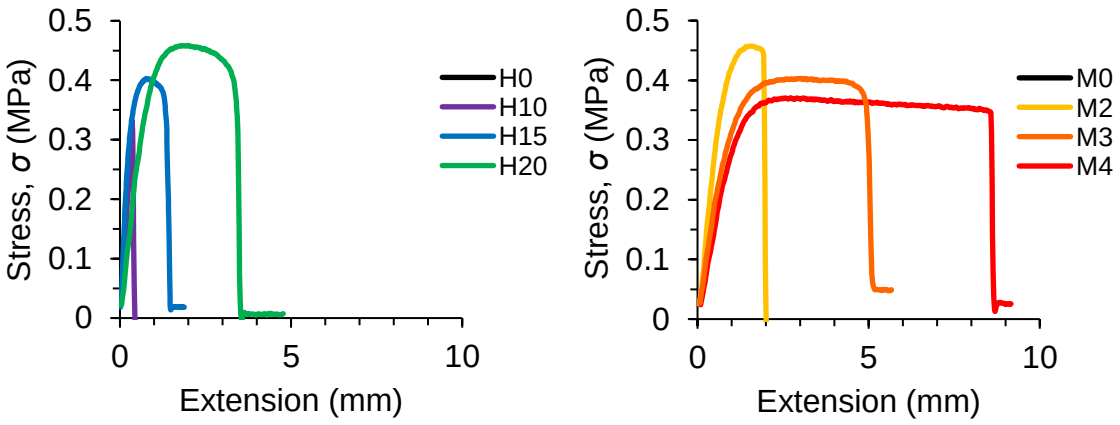

Binary PNV_{50} (H_0/M_0) tensile curves are not visible as these gels do not show detectable mechanical properties by pull testing.

Chapter 6. Summary and Future Work

6.1. Summary

Synthetic polyelectrolytes can be carefully tailored with respect to composition, architecture, charge density, and other aspects. The range of available polymer components used in polyelectrolyte complexes offers different strengths of the ionic associations which dictate the stability of their PECs and their responsive properties. Polyelectrolytes, including polyampholytes of various charge ratios and different charge densities, can be used in different stimuli responsive complexes including coacervates and precipitates.

This thesis explores the relationship of ionic associations with the charge arrangement in polyelectrolyte complexes ranging from charge-balanced polyampholytes to complex coacervates using homopolymer polyelectrolytes. This thesis also explores the effects of charge density in different polyelectrolyte-based systems, with a particular focus on the incorporation of zwitterionic monomers and their pronounced contribution to hydration. This includes their effect on stimuli-responsive properties of coacervates as well as their use in shell-forming polycations for low-fouling alginate microcapsules and as components in tough, self-healing hydrogels capable of salt-mediated self-healing.

The following summarizes the results of each chapter in this thesis:

6.2. Chapter 2

A series of polyampholytes were prepared using pH-controlled reactivity ratios of MAA/NaMAA and APM, to achieve different compositions with minimal comonomer drift at high and low molecular weights. These polymers were characterized and used as components in different polyelectrolyte complexes that result in liquid coacervates. The structure-property relationship of charge arrangement, or intramolecular charge compensation, with complex strength and stimuli responsiveness was explored with respect to pH, ionic strength, and temperature.

Using turbidimetric/potentiometric titration, isoelectric points of charge-balanced complexes were determined and the pH response of each charge arrangement was assessed, showing an increase in sensitivity to solution pH with increased intramolecular charge neutralization. UV-vis was used to monitor fluorescently-labeled polymer in self- and complex coacervates, to evaluate the coacervation efficiency as a function of ionic strength; as [NaCl] increases, charge-shielding impedes the polymeric associations and macroscopic coacervation. This further demonstrates that as charges are separated on polymer backbones with higher net charge densities, the strengths of the overall ionic associations increase and become more resistant to charge shielding by added salt. These complexes also exhibit reversible cloud point temperatures that represent LCST behaviour, dependent on NaCl, pH, charge arrangement, and molecular weight.

The coacervate physical characteristics were mapped using optical microscopy at different [NaCl], showing the range of possible complexes from viscous liquid coacervates to solid precipitates, based on composition, MW, pH, and ionic strength. The

thermodynamics of coacervation processes were briefly explored, in agreement with theoretical predictions and previous work by Perry and Tirrell; polyelectrolyte complexation is dominated by an entropic gain in the release of salt and water molecules. Discerning specific trends with highly sensitive ITC, with respect to charge separation, were limited by compositional and size distributions achieved using scalable polymers.

Finally, self-coacervates of polyampholytes and complex coacervates of non-stoichiometric polyampholytes were shown to crosslink in the presence of genipin, resulting in microgels, and were also capable of binding model ionic dyes.

6.3. Chapter 3

The third chapter uses a series of polyampholytes based on MAA and APM to explore the impact of betaine incorporation on the stimuli responsive properties of different polyelectrolyte complex arrangements. Novel terpolymer polyampholytes of various MAA:APM charge ratios were prepared incorporating zwitterionic MPC as a strongly hydrating and charge-diluting component. Turbidimetric titration of the resulting coacervates show that the isoelectric point of the complexes depend on the overall charge ratio (e.g., composition for simple coacervates, mixing ratio for complex coacervates) and that the sensitivity of each polyelectrolyte complex to pH increases with MPC content for polyampholyte self-coacervates and complex coacervates.

Similarly, the salt-sensitivity increases with MPC incorporation, with more significant effects on simple (polyampholyte) coacervates than on complex (mixed

polyampholytes and polyanion-polycation) coacervates. Temperature-responsive cloud points, representative of LCST behaviour, for the various complexes were observed, although MPC hydration decreased the turbidity of the resulting coacervate suspension for each complex arrangement. While the effects of MPC on the complexes appear to depend slightly on molecular weight, the relative trends of increased stimuli sensitivity with increased charge compensation and MPC content are consistent.

Introducing a betaine functionality had more pronounced effects on the coacervate properties of self-coacervates compared to complex coacervates, as associations were destabilized via intramolecular neutralization and disruption of charge runs for counterion localization. The addition of a hydrating termonomer, MPC, gives another variable that can be used to control the responsive properties of any given complex. Therefore, we show that these coacervates are tunable based on charge arrangement, as well as charge density using MPC and plausibly other neutral, hydrating comonomers.

6.4. Chapter 4

This chapter evaluates the use of dual-functional polycations consisting of *N*-(3-aminopropyl)methacrylamide hydrochloride (APM) and zwitterionic 2-methacryloyloxyethyl phosphoryl choline (MPC) to carefully balance electrostatic binding with anti-fouling, hydration properties. The reactivity ratios of the two monomers were determined to be 1.47 (MPC) and 0.21 (APM), by using ^{1}H NMR to directly monitor relative monomer consumption during copolymerization. This significant preference for

MPC incorporation leads to large compositional drifts in batch copolymerizations, and hence a broad range of ionic association strengths in each sample. Therefore, a semibatch technique was developed, and validated by ^{1}H NMR, to decrease the compositional distribution spread about a selected target composition.

Calcium alginate hydrogel beads were formed by jetting sodium alginate droplets into calcium chloride gelling baths. The resulting anionic gel beads were then coated with the cationic APM-MPC copolymers. The purpose of this work was to explore if the incorporation of MPC could reduce protein fouling of the resulting capsules, without undue interference with the electrostatic shell formation. Maintaining a balance of electrostatic binding with the non-fouling hydration properties of the introduced zwitterionic MPC, required careful exploration and investigation. The narrowed composition achieved by semibatch copolymerization led to better surface confinement with lowered cationic charge density, compared to corresponding batch copolymers.

Finally, the formed polycation-coated alginate capsules were treated with different covalent crosslinkers. Cationic tetrakis(hydroxymethyl)phosphonium chloride (THPC), charge-neutral genipin, and partially hydrolyzed, anionic poly(methyl vinyl ether-*alt*-maleic anhydride) (PMM_{50}) were used in attempts to improve capsule longevity and mechanical strength through crosslinking. Genipin-crosslinked capsules demonstrated the highest mechanical strength, surviving vigorous pipette aspiration compared to THPC and PMM_{50}. Additionally, these capsules showed the least amount of protein adhesion when exposed to fluorescently-labelled bovine serum albumin (BSA-*f*).

6.5. Chapter 5

This chapter describes the preparation and investigation of physical polyampholyte hydrogels based on NaSS and VBTA as well as ternary polyampholyte gels incorporating HEMA or MPC. Copolymerization of these monomers favours alternating incorporation of anionic and cationic charged monomers while the incorporation of methacrylate termonomers is highly unfavourable, leading to compositional drift in termonomer-polyampholyte chains. Alternating incorporation of NaSS-VBTA is consistent through high termonomer incorporation, illustrating the robustness of the polyampholyte copolymerization.

Binary and ternary gels were then prepared in various shapes and dimensions to explore the impact of charge density and termonomer functional group on the mechanical and responsive properties of the resulting materials. The physical properties and mechanical properties are dependent on both monomer loading and composition. As termonomer is introduced, hydrogels become more responsive to salt and temperature, manifested as increased swelling ratios, in both cases. Zwitterionic MPC has a greater impact on the response to both salt and temperature, weakening ionic interactions and facilitating chain solvation through the anti-polyelectrolyte effect and UCST-type behaviour of hydrophobic polyampholytes. Charge-neutral HEMA proved effective in increasing sensitivity to salt, however, these gels exhibit an interesting response to temperature as increasing termonomer mol % did not substantially increase the hydrogel swelling and demonstrate an LCST-type behaviour preventing significant swelling and dissolution.

Finally, mechanical properties were also explored in ternary polyampholyte gels. Very small amounts of MPC lead to weaker gels before dialysis equilibration, but all gels stiffen as salts are removed and associative interactions are stabilized. Incorporation of MPC decreases the materials' Young's moduli but does not drastically improve the stretchability of the material. Conversely, HEMA can be incorporated in substantially higher amounts to reduce mechanical strength and improve the stretchability of the gels through charge dilution rather than hydration. Therefore, both termonomers introduce unique functionality into the hydrogels and may each be more suitable for specific applications, i.e. responsive, high load-bearing versus responsive, flexible materials. These materials also have the capacity to break and reform ionic associations under different conditions and might be further optimized to develop polyampholytes for non-covalent, responsive self-healing technologies.

6.6. Future Work

6.6.1. Viscoelasticity of Coacervate Phases for Different Charge Arrangements

Chapters 2 and 3 showed that polyelectrolyte complexes of different charge arrangements have ionic association strengths that improve with charge separation. While the stimuli-responsive phase changes were described, the viscoelastic properties of the polymer-dense coacervate phase were not evaluated in this thesis. Future work with these materials should include rheological evaluation of the different coacervate arrangements and exploration of the salt-, temperature-, and composition-dependent viscoelastic properties. This technique

has been used to investigate coacervates with different charge densities[1] but has yet to be applied to different complex arrangements. It may also be interesting to explore the differences between symmetric and asymmetric coacervates with comparable intramolecular charge compensation; from Chapter 2, an equimolar (net charge neutral) mixture of PMA_{36}-PMA_{84} has comparable net intramolecular charge compensation to asymmetric, charge-balanced mixtures of PMA_{25}-P(APM) or P(NaMAA)-PMA_{75}.

It may also be possible to functionalize polyanions and polycations separately for Diels-Alder crosslinking in the coacervate form after mixing. Previous work has explored Diels-Alder crosslinking in hydrogels for cell immunoisolation[2], demonstrating the utility of D-A functional groups requiring longer reaction times. Installing this type of covalent crosslinking functionality into liquid coacervates could be used as a synthetic mimic of the glue of sandcastle worms that take advantage of catechol-type crosslinking after coacervation for covalent "curing".[3] The rheology of the curing process in different arrangements and the application of such scalable systems would be very interesting as potential surgical glues or underwater adhesive technologies.

Therefore, future work may involve developing a polyelectrolyte system using cost-effective cationic and anionic monomers to facilitate the scaling up of different polyelectrolytes and polyampholytes needed to evaluate the physical properties of the polymer-dense phase. Large scale coacervation may be also used to better depict the binodal salt-polymer phase diagram for different charge arrangements, as described in Chapter 2, and develop functional and responsive underwater adhesives.

6.6.2. Charge Arrangements within Tough, Self-Healing Hydrogels

Based on Chapter 2, charge arrangement has notable impacts on the physical properties of ionic associations in polyelectrolyte complexes. It has also been previously shown that the charge arrangement based on reactivity ratios of comonomers can have a significant effect on the properties of physical hydrogels. This has been briefly demonstrated in the distinct mechanical properties of polyampholyte gels versus polyion complex gels, composed of ([3-(methacryloylamino)propyl]trimethylammonium chloride) (MPTC) and NaSS.[4] However, a range of compositions that lie between charge-balanced polyampholytes and homopolymer polyelectrolytes have not yet been mapped. Early experiments show that homopolymer p(NaSS) in the presence of polymerizing VBTA monomer produces hydrogels very quickly that are very brittle with poor physical crosslinking. However, as mixed monomer feeds are employed, the gels become tougher; this is counterintuitive to prior work exploring charge arrangement in hydrogels. While a favourable polymerization can occur as cationic monomers template along the p(NaSS) chain, as observed in vastly higher rates of polymerization and gel phase separation than in polyampholytes, this provides a basis for strong electrostatic interaction between the two polyelectrolytes and likely generates a zipper-type complex formation. This may prevent physical crosslinking between domains of polyelectrolytes, although further study is necessary to discern the nature of these PEC gels.

Therefore, future work may investigate symmetric or asymmetric polyion complex hydrogels that incorporate different polyampholytes as components in the physical hydrogels formed using NaSS and VBTA, as well as other monomers. This could further

describe a means of mechanical tunability that is not highly dependent on monomer reactivity. It is expected that these gels will not only possess a tunable range of mechanical and responsive properties, but that they may be used in the binding/release of ionic dyes with distinct release profiles under different ionic strengths and temperatures. Additionally, these principles can be applied to monomer pairs even more capable of self-healing, to generate materials of varying responsiveness and strength.

6.6.3. Self-Healing, Shape-Memory Polyampholyte Materials

Based on Chapter 5, physical hydrogels composed of NaSS and VBTA can be quite tough and show sensitivity to salt and temperature in solution, however these quenched polyampholytes are insensitive to pH. Physical hydrogels with shape-memory have been recently developed using MPTC and NaSS, while introducing pH-responsive 2-(dimethylamino)ethyl methacrylate (DMAEMA) as a moiety for dynamic ionic associations with shape-memory capacity.[5] Therefore, there may be an opportunity to develop a robust hydrogel based on a styrenic backbone using weak acid/base groups such as 4-vinylbenzoic acid and 4-(vinylbenzyl) dimethylamine with NaSS and VBTA.

Additionally, NaSS-VBTA type hydrogels are very robust materials that require a significant reduction in charge density or enhanced hydration to offer efficient self-healing. Prior materials with more flexible methacrylate/methacrylamide backbones have demonstrated a greater response to NaCl and, hence, higher self-healing efficiency under more moderate conditions.[6] However, in Chapter 5, it was shown that betaines have a strong impact on the salt response of polyampholyte hydrogels without notable compromise of the mechanical properties. Therefore, it may be interesting to explore the effect of

termonomer structure on self-healing properties in more responsive hydrogels; it may also be useful to facilitate self-healing under significantly low salt conditions (i.e., the ionic strength of seawater) for biomedical applications.

Furthermore, the development of a carboxybetaine hydrogel based on (4-vinylbenzyl) dimethylamine might allow for high tensile strength zwitterionic materials, with interaction tunability based on spacer length and composition according to work by Jiang.[7] Incorporating NaSS and VBTA might further allow for the capture/release of target molecules in drug delivery technologies. Hence, there are many opportunities for new monomer designs and polymer compositions for useful hydrogel-based materials.

6.6.3. NaSS-VBTA Polyampholyte Block Copolymer Micelles

Alternating polyampholytes of NaSS-VBTA offer simple means of generating salt and temperature-responsive materials with no need for reactivity ratio control. The monomer pair provide strong ionic associations and form hydrophobic domains as the polymer phase separates out of aqueous solution. According to work demonstrated in this thesis and otherwise,[8] polymer architecture has a significant impact on the ionic associations and consequent complexes formed leading to unique technologies. Low molecular weight polyampholytes based on NaSS and VBTA have been prepared previously using radical addition-fragmentation chain-transfer polymerization (RAFT)[9], which is a convenient method in the development of block copolymers.

These polyampholytes form insoluble phases at low ionic strengths and below the upper critical solution temperature, making them potentially useful hydrophobic components in, for example, amphiphilic block copolymers for micelles or nanoparticles.

Prior work has explored micelles comprising individual block copolymers of poly(ethylene oxide) (PEO) including p(PEO-*b*-NaSS) and p(PEO-*b*-VBTA).[10] Compared to the two-component PEC core, an alternating polyampholyte might offer an easier means of preparation with more responsive ionic interactions. The stimuli-responsive triggers of a hydrophobic, polyampholyte block might provide interesting controlled-release properties when prepared with a hydrophilic, zwitterionic block used to stabilize the micelles and prevent protein adhesion. Furthermore, the polyampholytes are physically crosslinked in the precipitated phase, which eliminates the need for crosslinkable components during polymerization or additional crosslinking reagents for long-term stability. Hence, the design and development of block copolymers of p[(NaSS-*alt*-VBTA)-*b*-(MPC)], for instance, for drug delivery applications would be of great interest.

6.7. References

1. Huang, J.; Morin, F. J.; Laaser, J. E. Charge-density-dominated phase behavior and viscoelasticity of polyelectrolyte complex coacervates. *Macromolecules* **2019**, *52*, 4957-4967.

2. Stewart, S. A.; Backholm, M.; Burke, N. A. D.; Stöver, H. D. H. Cross-Linked Hydrogels Formed through Diels-Alder Coupling of Furan- and Maleimide-Modified Poly(methylvinyl ether-*alt*-maleic acid). *Langmuir* **2016**, *32*, 1863-1870.

3. Stewart, R. J.; Wang, C. S.; Song, I. T.; Jones, J. P. The role of coacervation and phase transitions in the sandcastle worm adhesive system. *Adv. Colloid Interface Sci.* **2017**, *239*, 88-96.

4. Luo, F.; Sun, T. L.; Nakajima, T.; Kurokawa, T.; Zhao, Y.; Sato, K.; Ihsan, A. B.; Li, X.; Guo, H.; Gong, J. P. Oppositely Charged Polyelectrolytes Form Tough, Self-Healing, and Rebuildable Hydrogels. *Adv. Mater.* **2015**, *27*, 2722-2727.

5. Zhang, Y.; Hu, Q.; Yang, S.; Wang, T.; Sun, W.; Tong, Z. Unique Self-Reinforcing and Rapid Self-Healing Polyampholyte Hydrogels with a pH-Induced Shape Memory Effect. *Macromolecules* **2021**, *54*, 5218-5228.

6. Sun, T. L.; Kurokawa, T.; Kuroda, S.; Ihsan, A. B.; Akasaki, T.; Sato, K.; Haque, A.; Nakajima, T.; Gong, J. P. Physical hydrogels composed of polyampholytes demonstrate high toughness and viscoelasticity. *Nat. Mater.* **2013**, *12*, 932-937.

7. Sinclair, A.; O'Kelly, M. B.; Hung, H.-C.; Jain, P.; Jiang, S. Self-Healing Zwitterionic Microgels as a Versatile Platform for Malleable Cell Constructs and Injectable Therapies. *Adv. Mater.* **2018**, *30*, 1803087.

8. Johnston, B. M.; Johnston, C. W.; Letteri, R. A.; Lytle, T. K.; Sing, C. E.; Emrick, T.; Perry, S. L. The effect of comb architecture on complex coacervation. *Org. Biomol. Chem.* **2017**, *15*, 7630-7642.

9. Kanta Sharker, K.; Ohara, Y.; Shigeta, Y.; Ozoe, S.; Yusa, S. Upper critical solution temperature (UCST) behavior of polystyrene-based polyampholytes in aqueous solution. *Polymers* **2019**, *11*, 265.

10. Ting, J. M.; Wu, H.; Herzog-Arbeitman, A.; Srivastava, S.; Tirrell, M. V. Synthesis and Assembly of Designer Styrenic Diblock Polyelectrolytes. *ACS Macro Lett.* **2018**, *7*, 726-733.